NOTE TO USERS

EXPERIMENTAL AND NUMERICAL STUDIES OF A NOVEL TECHNIQUE FOR ABATEMENT OF TOXIC METALS FROM AQUEOUS STREAMS

by

Avijit Basu

Submitted
in partial fulfillment of the requirements
for the degree of

DOCTOR OF PHILOSOPHY

Major Subject: Chemical Engineering
at

DALHOUSIE UNIVERSITY

Halifax, Nova Scotia March, 2005

Your file Votre référence
ISBN: 0-494-13047-4
Our file Notre référence
ISBN: 0-494-13047-4

DALHOUSIE UNIVERSITY

To comply with the Canadian Privacy Act the National Library of Canada has requested that the following pages be removed from this copy of the thesis:

Preliminary Pages
- Examiners Signature Page
- Dalhousie Library Copyright Agreement

Appendices
- Copyright Releases (if applicable)

DEDICATION

To The Almighty,

The Most Merciful

&

Babai

&

Baba

TABLE OF CONTENTS

LIST OF TABLES

LIST OF FIGURES

LIST OF SYMBOLS

A	Cross-sectional area of the column (cm^2)
AA	Atomic Absorption
c_0	Concentration at the outlet (ppm)
c_e	Concentration of the metal in the solution at equilibrium (ppm)
c_i	Initial concentration (ppm)
Ds	Surface diffusivity cm^2 per sec
Dp	Pore diffusivity cm^2 per sec
Da	Apparent diffusivity cm^2 per sec
F	Fraction of pore spaces containing pluggable pathways
H^+	Total amount of protons available at equilibrium (ppm)
Js	Solute Flux (ppm per unit time per unit surface area)
Jv	Permeate flux(ppm per unit time per unit surface area)
k_I	Kinetic constant of adsorption (I=1) or desorption (i=2)
k_1^{int}	Intrinsic acidity constants
k_2^{int}	Intrinsic acidity constant
k_p	Absolute permeability of the pluggable pathway (cm^2)
k_{pi}	Initial absolute permeability of the pluggable pathway (cm^2)
K	Sorption Coefficient (L per mmole)
K_F	Freundlich adsorption capacity indicator constant
m_1	Monolayer coverage for the contaminant (mg/g)
m_2	Monolayer coverage for the solvent (mg/g)
W	Amount of contaminant adsorbed in 1/19 mass of adsorbent in column (moles)
m_1	Mass of sorbate in dynamic test or initial mass in static test (mg)
m_2	Effluent mass in dynamic test or mass in solution at equilibrium (mg)
n'	Amount adsorbed per unit mass of adsorbent (mg/g)

n_i^e	Equilibrium surface excess of component i per unit mass of adsorbent (mg/g)
n_1^{ea}	Actual surface excess of contaminant per unit mass of adsorbent (mg/g)
n_o	Amount of liquid per unit mass of adsorbent (mg/g),
Ns	Total number of active sites in moles per g
ppm	Parts per million
pk_1(intrinsic)	-log K_1^{int}
pk_2(intrinsic)	-log K_2^{int}
q'_{exp}	Experimental capacity of Cod scale in the batch or column test (mg/gm)
q'_{th}	Theoretical capacity of Cod scale in the batch or column test (mg/g)
Qm	Ultimate adsorption Capacity of a contaminant on fish scale (mg/g)
Q	Flow rate of solution injection (ml/hr)
q_f	Flow rate (ml/min)
R^2	Correlation coefficient of the linear regression
R_L	Hall's separation factor
S	Selectivity
$S\text{-}H_2^+$	Protonated sites on adsorbent, moles per g
S^-	Negative charged sites, moles per g
t	Time (hours)
T	Duration of the experiment in batch or column test (min)
U	Local speed (cm/s)
u_c	Critical speed required to mobilize heavy metal contaminant (cm/s)
u_{np}	Local speed in the non-pluggable pathways (cm/s)
W	Amount adsorbed (gmole /g dry adsorbent)
z	Height of column (cm)
u_p	Local speed in the pluggable pathways (cm/s)
v	Pore velocity of a contaminant in column (cm/s)
V	Entrapment of the contaminant (mg/gm)

Vp	Total Molar flow rate per unit time (in pores)
Vv	Total Molar flow rate per unit time (in voidages)
Vp_l	Total molar flow through internal pore
Vv_l	Total molar flow through voids
X'_l	Adsorbed phase fraction of component i (mole fraction)
X	Fluid phase concentration in pore, mole fraction
x_l	Bulk phase mass fraction of component i (mole fraction)
X_l	Bulk phase mass fraction of solute (mole fraction)
Y	Fluid phase concentration in external voids
Z	Distance along the column height (cm)
α	Entrainment rate constant (cm^{-1})
E	External voidage
α	Internal porosity
β	Deposition rate constant (mg/g/s)
δ	Deposition rate constant for pluggable pathways (mg/gm/cm)
ρ	Deposition rate constant for pluggable pathways (cm^{-1})
ρ_l	Liquid density (gmol/ml)
ρ_r	Density of adsorbent or fish scale (g/cc) of adsorbent
φ	Porosity
λ	Dispersion parameter (cm)

ACKNOWLEDGEMENTS

I would like to express my sincere gratitude and thanks to Dr. Rafiqul Islam for his kind supervision and guidance throughout the period of this study. His creativity, interest, and inspiration contributed tremendously towards the successful completion of this study. I am also very grateful to Dr. Steve Butt for all the useful help. My appreciation also goes to Dr. Amyl Ghanem and Dr. Pak Yuet. Special thanks to Dr. Paul Bishop, in helping me with the SEM for characterization the adsorbent. I always feel excited to speak of Dr. Robert White and Dr. Mike Lumsden from Department of Chemistry, Dalhousie University. One of the major accomplishments of the research (proposed molecular structure of the adsorbent) was partially due to their efforts.

Appreciation goes to Bill Landen for providing all sorts of help during experimental pHases with Cod scale. I would like to thank my colleagues Saifur Rahaman and Shabbir Mustafiz. They helped me in setting the experiment layout and sometimes were by my side until early hours of the morning. I am pleased for the fact that they are the true pioneers of this research. I collaborated some of the experimental Runs conducted by them as members of EEC research group. Shabbir was again present in formatting the thesis. In the end, I intend to thank my wife Maneesha, who patiently encouraged me through all the turbulent times.

I would like to give thanks to NSERC and ACPI for providing the financial assistance necessary for conducting this research.

ABSTRACT

The objective of this project is to study the adsorption characteristics of fish scales that ensure efficient removal of toxic metals from wastewater. Removal of lead, cobalt and arsenic ions from both industrial and municipal water is of extreme importance prior to disposal to aqueous streams. The processes related to the removal of the ions include mainly adsorption and precipitation although flocculation, membrane separation and leaching are some of the viable alternative technologies. Materials such as granular activated carbon, metal oxides and synthetic resins are being extensively employed as adsorbent materials but the high cost of the products limits their large-scale usage.

In order to understand the mechanism of adsorption on fish scale, characterization of its substrate with Scanning Electron Microscope and Nuclear Magnetic Resonance techniques were carried out to evaluate the components on its surface that are related to the adsorption of metal ions. Applications of SEM and NMR techniques have proven that the fish scales are composites in nature. Static and dynamic experimental models were utilized to study the adsorption behavior at a pH range from 2-11. It is important to consider that given the unknown parameters of the substrate, the experimental runs are conducted to study the adsorption behavior in a qualitative approach. The quantitative approach is supplement by numerical studies based on surface excess and pore diffusion theories.

Using fish scales as an adsorbent, 95% of the lead ions, 70% of the cobalt ions and 80% of arsenic ions were removed. The effect of precipitation of the lead ions in an alkaline medium (with no adsorbent) was analyzed to be insignificant for remediation levels. As sorption dictates the interactions between the bulk and adsorbed phases, it is the most important factor that influences the transport of the chemical species through the medium. The process of adsorption includes ion exchange, chemisorption and electrostatic attraction mechanisms for specific species in interaction with specific sites on the adsorbent. A series of multi-component experimental runs indicate that the degree of adsorptivity of a specific species is dependent on the estimated equilibrium sorption coefficients of all the components and the concentration of the specific adsorbate and all the interfering ions in the bulk phase. The number of the adsorption sites available on the adsorbent is also a very sensitive parameter for competitive adsorption phenomena. However it is observed that the presence of arsenic ions at low concentrations did not adversely affect the adsorption behavior of lead ions. Conversely, the adsorption process of As (III) and As (V) anions is significantly reduced by the interfering lead ions.

To investigate the nature of the sorption mechanism, a series of experimental Runs were conducted using fish scales of the *Gadus Morhua* (Atlantic Cod) and *Lethrinus nebulosus* (Spangled Emperor or Shouairi) species as substrates. Numerical simulation results demonstrate reasonable agreements with the experimental results. This study illustrates that variation of flow rates and pH of the bulk phases bear a significant impact on breakthrough time intervals. Contrary to expectations, in certain cases at laminar flow

zones, an increase in the flow rate contributed to a delayed contaminant breakthrough. However, variance of the ion concentrations did not have a dominant effect on some of the corresponding breakthrough values. The effect of porosity of the adsorbents was observed to have a profound impact on adsorption phenomena. A decrease in porosity of the adsorbent results in an increase of the retardation factor of the contaminant in bulk phase and an equivalent delay in the breakthrough interval.

A serious drawback observed with respect to the nature of the adsorbent is the limitation in reproducibility of the un-scaled experimental runs. The characterization of the substrate (Chapter 7) displayed that the material is a composite with a random variance in its chemical components. At bench level, the reproducibility of the experimental runs is hindered by lack of a large sampling size. It is thus concluded that by only increasing the mass of the adsorbent for every experimental run, the variance of the physical parameters of the adsorbent may be reduced. It is therefore imperative to conduct scaled up experimental runs and correlate the observations with an appropriate numerical model.

Chapter 1

1 INTRODUCTION

1.1 Background

Environmental pollution by toxic metals has become a subject of interest especially since the establishment of the EPA (Environmental Protection Agency) in 1970. The problem of water quality degradation of both surface and sub-surface streams has been evident for a long time. Achieving an acceptable quality of surface water focuses on reducing emissions of known pollutants to within safe industrial and drinking standards. In developing nations, many of today's industrial projects are environmentally hostile. As a result of inadequate pollution regulations, impacts of ozone-layer depletion, of air pollution and of neglect of drinking water standards are everywhere and rampant. Islam and Wellington (2001) have charted a path for developing environmentally appealing research projects. Significantly, as far as engineering research of environmental projects is concerned, they highlight the importance of novel methods, many of which carry tremendous impact in heightening the effectiveness of green technologies. Increasingly, in environmental studies, a 'double-fold aim' (Apak *et al.*, 1998), focused on both pre- and post-problems, is especially desired. "Double-fold aim" implies both abatement of contaminants by an *in situ* technique and recovery of these contaminants for industrial usage. In broad terms, such an approach aims at accomplishing the "three R's": *Remediation*, *Recovery* and *Reuse*.

Toxic heavy metals and organic wastes are the main culprits when it comes to pollution of the environment from aqueous streams. Heavy metals are present in downstream effluents of industries, mines and geological activities such as volcanic actions and weathering of rocks. Eckenfelder (2000) reported that sources of lead pollution in wastewater include storage batteries, chrome etch cleaning processes and leaded brass. Cadmium can intrude into the waste streams from metallurgical, ceramics and electroplating industries. Metal process plating baths and pickling baths can

contribute to the wastewater with copper (Cu) as the major pollutant. Zinc (Zn) may seep into wastewaters from steelworks, rayon yarn, fiber manufacture and ground wood-pulp production. Dissolved metals including lead, zinc, copper etc. and highly acidic effluents can cause a severe problem at metal mining industries (Environment Canada, 1998). Barium is present in waste streams from the paint and pigment industry, the metallurgical industry, glass, ceramic and dye manufacturers and the vulcanization of rubber. Barium contamination in wastewater has been reported from explosive manufacturing industry. Chromium salts are used as tanning agents. Chromium concentrations in the effluents from such factories can peak to 2.9g/Kg and are often disposed of directly into the environment (Greenpeace, 2000). Also, Chromium has been utilized for protective and aesthetic plating as well as to protect against corrosion in natural gas water-cooling systems. Apart from industrial pollution, sources such as agriculture and sewage disposal also contribute significantly to waste streams. Also, the petroleum industry generates wastes that are often high in heavy metal concentration. Sources of such high concentrations of metals are geological, as well as chemicals used in drilling, production and refining operations.

These heavy metals have extreme lethal effects on all forms of habitat. Metals like lead, copper, cadmium, nickel, arsenic and zinc are toxic when they exist in high concentrations. Lead is highly toxic to the environment and is regulated as a hazardous waste. The EPA limits set for lead in drinking water standards is 5 ppm. Lead poisoning has been a constant problem. Lead causes plant and animal death as well as anemia, mental deficiency, brain damage, kidney dysfunction and behavioral problems in humans (Mo *et al.*, 1988). Lead poisoning can damage a child's central nervous system and reproductive system and at higher levels, can cause comas, convulsions or even death. An even lower level of Lead ingestion (< 10 ppm) is harmful, and is associated with decrease of intelligence, stature, and growth. Lead can retard red blood-cell formation and may cause low-weight births and permanent brain damage. In developing countries, such as India, water can contain high amounts of lead (>100 ppm, from Ishapore Gun Factory effluent sewer, informal discussion). Wastewater from industries can pollute the nearby

lakes, rivers and sub surface water streams resulting in the contamination of aquatic life. Birds such as kingfishers and eagles that hunt the polluted fish can eventually die from Lead poisoning.

While determining the presence of Lead ions in the sewer, Arsenic was also detected in the subsurface stream. Arsenic as certain allotropes is extremely detrimental for biological habitat and is a naturally occurring carcinogenic element. The EPA has recommended arsenic limit to less than 1 ppm in industrial water. Arsenic (As) and its numerous compounds can be present in wastewaters from the metallurgical industry (e.g. Ishapore Gun Factory), glassware, ceramic production, tannery operation, dyestuff manufacture, pesticide manufacture, some organic and inorganic chemicals manufacture, and petroleum refining industry. Leaching from mine tailings in Australia, Canada and the United Kingdom is also a cause for arsenic pollution.

Arsenic in natural aquifers also causes contamination of water supplies in Bangladesh and India. Sources of arsenic in the natural aquifer (both acidic and basic) are primarily from mining regions where Arsenopyrite rich rock has been exposed. Arsenic (III) and Arsenic (V) are unwanted by-products of the mining and extraction of metals such as copper, gold (Au), lead, nickel (Ni) and uranium (U). Fazal *et al.*, (2001) has reported hyper-pigmentation, skin and liver cancer due to exposure to Arsenic. It has also been reported that common forms of arsenic in groundwater exists as arsenite (H_2AsO_3-), arsenate (H_2AsO_4-) and in organic forms such as methyl arsenic acid ($CH_3AsO(OH)_2$) and dimethyl arsenic acid [$CH_3As(OH)$]. Pontius et al. (1994) observed that trivalent Arsenic, As (III) is ten times more toxic than As (V). The element Arsenic is responsible for gastrointestinal irritation accompanied by difficulty in swallowing, thirst, abnormally low blood pressure and convulsions. Elemental Arsenic can create epidemiological problems and chronic diseases. Due to arsenic's toxicological effects, the allowable arsenic contamination level set by World Health Organization is 10 ppb and Health Canada has assigned a limit of 25 ppb (Toft *et al.*, 1990). At present USEPA is considering lowering their maximum arsenic contamination level in potable water from

50 ppb to 10ppb (American Water Works Association Committee, 1993). Due to hazardous effects of heavy metals, stringent environmental regulations require the treatment of wastewater to remove these metals. Chemical precipitation has often been used as a technique to remove metal ions such as lead from bulk phases, but in most cases this method is insufficient to meet regulatory standards. Adsorption has been proven to be an effective method for removing heavy metals from water (Lee and Davis, 2001). Conventional techniques often lead to secondary problems regarding handling of metal bearing sludge (Volesky, 1999).

There are a number of adsorption technologies available for the removal of heavy metals from wastewater that include ion exchange and membrane techniques (Ahmed 2001). A variety of natural materials such as sand, clay, Bentonite (Jordan, 1994), Spodic (Lindberg et al., 1997) and aquifer materials from mining areas (Carrillo and Drever, 1998) has been studied for metal removal from wastewater. The removal of Arsenic species have been studied using antimony pentoxide and manganese dioxide (Galer et al., 1997), using rare earths (Tokunaga et al., 1997), Iron hydroxides (Raven et al., 1998) and iron-coated catalysts (Huang et al., 1997). Silver ions have been reported to be effectively removed by Aspergillus Niger biomass (Akhtar et al., 1996). Another adsorption technology, the application of Granular Activated Carbon, has been immensely popular for decades (Corapcioglu and Huang, 1987). However carbon is extremely expensive for wastewater treatment in a mass scale. In the last decade, researchers have tried with different cost-effective alternate adsorbents. Bailey *et al.* (1999) defined an adsorbent as 'inexpensive' if it requires little processing, is abundant in nature, or is a by-product or waste material from another industry.

The term 'waste material' can be defined as a material that is of no use and is usually disposed. Thus if this waste material can be used for some purpose, needless to say, it becomes an asset. Fish scale is a biomass and is generally considered to be a waste product. In coastal and harbor areas, where fishing is a major occupation, use of fish scale to remove heavy metals can be a better alternative. The idea of using a waste material

such as fish scale to remove heavy metal was initiated using Shouairi Fish scale (Chaalal and Islam, 2001). Later, some observations and reports encouraged the authors to explore this waste material further. On 3rd July 2001, the BBC reported the presence of mercury (Hg) poison in Sharks. On 4th July 2001, CNN (Cable News Network) reported that the Health Ministry in Thailand advised people to stay away from shark fin soup anticipating that it might contain high level of mercury. Fleming *et al.* (2000) reported the patterns and rates of increases of mercury contamination in different marine food chains. They presented the measured trends in mercury contamination over the past 100 years in seafood webs and displayed a 3-10 fold increase in mercury contamination. They noted that methylation of inorganic mercury deposited from the atmosphere occurs especially in low oxygen environments such as the deep sea. Also their laboratory and field studies fully validated the use of seabird feathers as a reliable monitor of mercury contamination in their food chains. Thus the accumulation of heavy metals like mercury in fish has been known for a while. However, a feasible solution for abatement of the heavy metal ions in waste streams has not been extensively defined in developing countries.

1.2 Objective

The major objective of this research is to introduce a novel bio-mass, fish scale, as an adsorbent to remove metals from both single and multi-component aqueous phases. The chemical nature of the fish scale surface is such that it has an affinity for certain ions when present in the bulk phase that is in contact with the adsorbent. The foremost priorities is to identify the functional groups associated with the adsorbent and propose chemical interactions associated with the ions in the aqueous medium. After identifying the functional groups, batch tests were conducted. Experimental observations of the adsorption capacities of various heavy metal ions with respect to adsorbent dosage, pH of the medium and concentration of the various contaminants were studied with respect to two types of fish scales at equilibrium conditions. This objective assists in determining the batch capacities of the adsorbent at different pH levels.

The purpose of performing column studies is to establish data on a dynamic system that will ultimately determine the effectiveness of adsorption as determined from the batch isotherms. The batch isotherms will be used for initial investigations and their operating parameters will be utilized to study the ability of the adsorbent to be used in column operations. The major parameter to be reviewed in column operations is the breakthrough capacity. The breakthrough capacity of an adsorbent is an indispensable indicator of effectiveness of a material for abatement purposes in a dynamic system. Its significance can be assessed from the fact that a wastewater treatment plant in Western Canada was arbitrarily loading an adsorbent without estimating its breakthrough and saturation capacities (Islam and Chakma, 1990). During this operation, it must have overspent its resources for waste remediation.

However, the set of experimental runs are limited to laboratory scale designs. In order to correctly predict the adsorption behavior of the pollutants in relation to the specific adsorbent at a larger scale, a numerical model is required to study the variance of various physical parameters with respect to the adsorption behavior. The specific parameters that were studied in the column include flow rates of the effluent solutions, effective porosities of the adsorbent and dispersion behavior. Their variations will be correlated to the breakthrough and saturation behavior of a dynamic column. The accomplishment of this task requires a proper selection of a numerical model, which will be tested rigorously at various boundary conditions. This approach will provide a deeper insight for 'scaling up' design procedures.

1.3 Methodology

In order to achieve the objective of this research, following steps were taken:

i. Determine the possible functional groups associated with the fish scale.

ii. Investigate the adsorptive behavior by fish scales from the metal salt solution, considered as an aqueous phase, under static conditions.

iii. Investigate the adsorptive behavior by fish scales from the metal salt solution, in presence of interfering ions, under static conditions.

iv. Investigate the adsorptive behavior by fish scale from a heavy metal salt solution, considered as a aqueous phase, under dynamic conditions.

v. Investigate the adsorptive behavior by fish scale from a heavy metal salt solution, in presence of interfering ions, considered as an aqueous phase, under dynamic conditions.

vi. Determine the effect of the following parameters on removal of contaminants from an aqueous stream:

   a. Type of fish scale
   b. State of fish scale
   c. Type of pretreatment
   d. Type of heavy metal contaminant
   e. Flow rate of the bulk phases
   f. Initial pH of the bulk phases
   g. Grain size and porosity of fish scale
   h. Effect of precipitation in bulk phase

vii. Develop a numerical model for sorption on the internal pores of the substrate and compare the numerical simulations with the experimental results.

viii. Observe the effect of several parameters numerically for scaling up purposes.

1.4 Scope and limitations

The removal of lead, arsenic and chromium was studied using Atlantic Cod scale. Shouairi scale was studied with respect to the removal of cobalt, lead, strontium and zinc. Because of its limited availability in Canada, the sorption behavior of Shouairi scale was studied less intensively than Atlantic Cod scale. Atlantic Cod and Shouairi fish may not be available in all parts of the world. In order to study the discrepancies in adsorption behavior of different species of fish scale, two types of scale were studied. The availability of a particular scale is also limited by location, market demand,

meteorological conditions and fishing practices to name a few factors. Since 1992, with minor occasional variations of regulatory orders in localized areas, the Federal Government of Canada has placed most forms of ground fish harvesting throughout Atlantic Canada, including codfish, under a moratorium that continues to date. This moratorium provides ample reason to study the adsorption behavior with different types of fish scales. It is essential to have an extensive knowledge of sorption characteristics of various species of fish scales because supplies may be affected by regulations with time. The effect of initial pH, grain size and effect of precipitation was studied in both acidic and alkaline aqueous stream environments.

1.5 Contributions of this research

Bio-sorption using fish scale may serve as an alternative for purifying industrial waste effluents that contain toxic metal ions. In comparison to other adsorbents, such as, Granular Activated Carbon, metal oxides and synthetic resins, the advantages of fish scales are the high purity of the treated wastewater and inexpensive raw material. This is in line with the theme that uses conversion of waste materials into value-added products that can be used in place of expensive, and often toxic, chemicals. In proposing this new water purification technique, this research makes the following fundamental contributions.

i. Opens up opportunities for conversion of biological wastes into value-added products that will create a basis for 'zero-waste' remediation techniques. At present, mostly processed chemicals are used to remediate metallic contamination. The waste removed by the adsorbent may be extracted from the substrate for industrial purposes.

ii. Develops a mathematical model for simulating multi-component adsorption. This model is based on pore-diffusion consideration and opens up opportunities to using the pore diffusion concept in a wide range of applications.

iii. Studies microstructures of Atlantic cod scales. This study reveals a number of features that can be correlated with reaction mechanisms, prevalent during water purification.

iv. Provides a basis for scaling up of experiments in chemically active porous media. This is complemented with a field-scale numerical modeling that provides insight into the scaling up process.

Additional research based on the conclusions of this project can be used for further work. This includes:

i. Usage of the 'adsorbed scale' for leaching characteristics. This may be valuable to extract valuable chemicals after the 'clean-up' process.

ii. To determine if fish-scale powder can be used as a remediation medium for oil slicks on ice.

1.6 Organization of this research

The following algorithm defines the possible route for a comprehensive adsorption study of a bio-adsorbent such as Fish Scale (Figure 1.1)

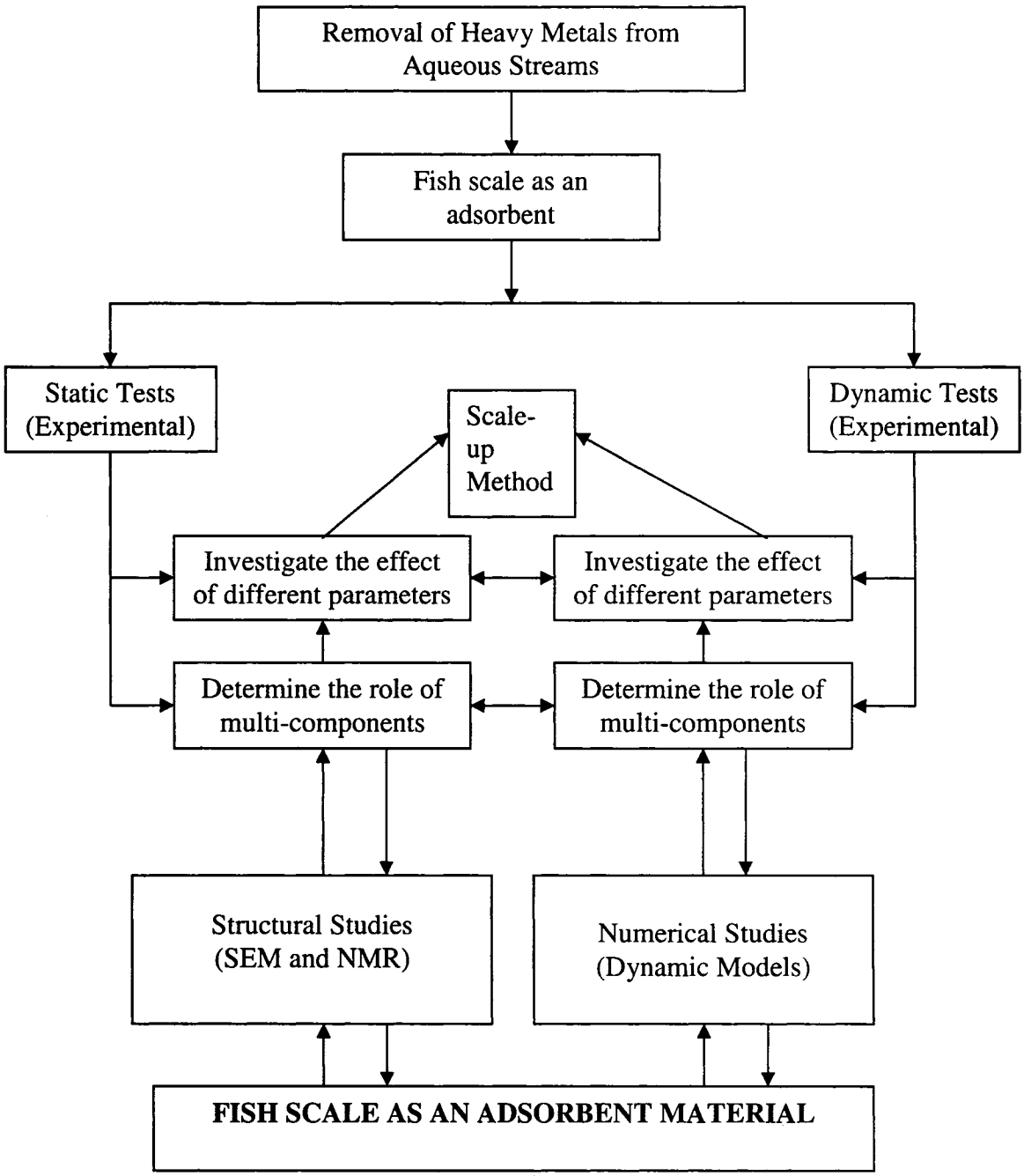

Figure 1.1 Organization of the study

Chapter 2

2 LITERATURE REVIEW

Summary

The conventional methods used for the abatement of metallic ions from aqueous streams are illustrated in this chapter. The adsorbents include both biomass and non-biomass; some are considered as waste materials. This chapter also includes a review concerning the origin, chemistry and heath effects of mainly lead, arsenic and cobalt elements. Some background information is also provided on the fish species of Atlantic Cod and Shouairi fish. The scales of these species are used during experimental stage. An initial effort has been attempted to study the structure of the Atlantic Cod Scale using SEM and NMR techniques.

2.1 Chemical Electronic Properties of Lead, Cobalt and Arsenic

The binding of transitional metals to the adsorbent is strongly dependent on their electronic configurations. In this section, the electronic properties of lead, cobalt and arsenic are presented.

2.1.1 Chemical properties of Lead

The valency shell of the lead atom in ground state is $6s^2$, $6p^2$. In divalent lead compounds, the s-electrons are inert and are more abundant than the quadrivalent compounds in which all the electrons in the valency shell of the lead atom are used for formation of the bond. Lead in divalent conditions form planar complexes as four covalent bonds. Table 2.1 displays the properties of lead.

Table 2.1. Properties of Lead (Durrant, and Durrant, 1964)

Parameter	Value
Atomic number	82
Oxidation number	+2, +4
Electronic configuration	$1s^2 2s^2 2p^6 3s^2 3p^6 3d^{10} 4s^2 4p^6 4d^{10} 4f^{14}$ $5s^2 5p^6 5d^{10} 6s^2 6p^2$

The compounds in which the oxidation state of lead is II are termed as plumbous salts. The adsorption behavior of a lead ion at any adsorbent /water interface is strongly pH dependent and is characterized by a general agreement between the hydrolysis of the plumbous ion and its enhanced adsorption, charge reversal and coagulant properties. Models used to define the adsorption phenomena, include ion exchange and the adsorption of lead ions at specific sites of an adsorbent.

The lead (II) ion in the presence of hydrochloric acid forms Lead Chloride. The lead chloride has a solubility of 0.67 grams in 100 grams of water at 25 C. Lead Chloride ($PbCl_2$) is hydrolyzed by water to a basic salt Pb(OH)Cl. Plumbous chloride dissolves in concentrated hydrochloric acid to form H_2PbCl_4.

$$Pb + 2HCl \rightarrow PbCl_2 + H_2 \quad (2\text{-}1)$$

$$PbCl_2 + H_2O \rightarrow Pb(OH)Cl + HCl \quad (2\text{-}2)$$

$$Pb(OH)Cl + 3HCl \rightarrow H_2PbCl_4 + H_2O \quad (2\text{-}3)$$

Lead in Plumbous condition forms compounds including both non-chelate and chelate complexes and anions. Among the salts containing lead atoms in non chelating anions include potassium formatoplumbite, $K_2[Pb(HCO_2)_4]$. The bisenzoylacetone complex has a structure that includes two chelating oxygen atoms linked to a single lead atom. The

coordination number of the lead atom in the complexes is four for the plumbous ion. But since the electrons at $6s^2$ level are unused, the tetrahedral hybrids are formed by a combination of 6p and 7s orbitals. At an excited state, one electron from $6p_x$ orbital is transferred to another $6p_y$ orbital. Thus there are two incomplete orbitals at p level and and two vacant orbitals at p and s levels. This allows formation of two coordinate bonds and identical number of covalent bonds surrounding the lead atom.

The adsorption behavior of hydrolysable lead ions at solid water interface is strongly pH dependant. An experimental model can be characterized by hydrolysis of an aqueous metal ion with enhanced adsorption. Models used to depict the phenomena, include ion exchange and specific adsorption of certain species. In contrast, a second model can be considered in which all the species of the hydrolysable lead ion are considered to be adsorbates. However, only the less strongly hydrated complexes have favorable free energies for the adsorption mechanism.

For each metal like lead, there is a critical pH range over which the fractional amount of the metal ion adsorbed increases from zero to unity. Different substrates when interacting with lead ions have different critical pH ranges based upon their point of zero charge values. At a pH value above point of zero charge (PZC), the substrate has a negative surface charge and is ideally suitable for adsorption of the Lead ions. This evidence is substantiated by the fact that the original substrate is coated with hydroxides of the adsorbing lead ion (Healy, et. al., 1968).

Lead ions are considered to be intermediates of Pearson's concept of hard and soft acids (Pearson, 1990). According to the Soft and Hard acids and Bases (SHB) theory, lead ions can form complexes with oxygen as a donor atom (hard acids) and simultaneously coordinate with soft bases (bases containing S, P and N as donor atoms). This will help in understanding the sorption mechanism of lead ions with specific sites on the adsorbent.
In effect the insight to the structure of lead ion will largely benefit in understanding the interaction of the ions with the different functional groups on the fish scales.

2.1.2 Chemical properties of Cobalt

There are no compounds in which it can be definitely stated that the simple ion Co^{2+} is present in nature. Cobaltous chloride is known only to dissolve in water to form a pale blue solution existing as $[Co,6H_2O]^{2+}$ ion. Being divalent in nature, the Cobaltous ion is in search of a negatively charged substrate. The removal of the two electrons from its outermost shell results in an almost 40 per cent shrinkage of its radius from atomic to ionic form (Durrant and Durrant, 1994). Table 2.2 displays properties of cobalt

Table 2.2. Properties of Cobalt (Durrant, and Durrant, 1994)

Parameter	**Value**
Atomic number	27
Oxidation number	+2, +3, +4
Electronic configuration	$1s^2 2s^2 2p^6 3s^2 3p^6 3d^7 4s^1 4p^1$

The shrinkage of the radius leads to a compact binding of the cobalt ion. The reduction in ionic radius of the element is significant compared to Lead ions at this perhaps explains the higher adsorptivity trend of the latter.

2.1.3 Chemical properties of Arsenic

Arsenic is a chemical element in the Nitrogen family (Group V-A of the periodic table), existing in both gray and yellow crystalline forms. Although some forms of arsenic are metal-like, it is best classified as metalloid and non-metal. Apart from the elementary arsenic, where the oxidation state by definition is 0, arsenic is stable in its states +5, +3 and -3. Some important properties of arsenic are listed in Table 2.3.

Table 2.3 Properties of arsenic (Encyclopedia Britannica, 1994)

Parameter	**Value**
Atomic number	33
Oxidation number	-3, 0, +3, +5
Electronic configuration	$1s^2 2s^2 2p^6 3s^2 3p^6 3d^{10} 4s^2 4p^3$

2.2 Principal compounds of Arsenic

Rahaman (2003) has outlined in his work the formation of various compounds of arsenic. Arsenic has a range of oxidation states from -3 to +5, and can form a series of different kinds of compounds. The important commercial compounds are the oxides, the principal forms of which are Arsenious oxide (As_2O_3) and Arsenic pentoxide (As_2O_5). Arsenious oxide, commonly known as white oxide, is the material most widely used for the synthesis of arsenic compounds. It is produced as a by-product of the nonferrous metal industry, primarily from the smelting of copper ores. Naturally occurring metal arsenides also convert to the trivalent oxide when roasted in air. The formation of the trioxide accompanied by the roasting of a sulfide ore as displayed in Equation (2-4).

$$2\,FeAsS + 5O_2 \rightarrow Fe_2O_3 + As_2O_3 + 2\,SO_2 \qquad (2\text{-}4)$$

Elemental arsenic undergoes reaction with oxygen to yield the trioxide as follows:

$$4\,As + 3\,O_2 \rightarrow 2\,As_2O_3 \qquad (2\text{-}5)$$

The trioxide is moderately soluble in water, but dissolves easily in aqueous alkali to produce a solution of arsenic, AsO^{2-}. It is slightly soluble in polar organic solvents such as alcohols and ethers and insoluble in benzene. The most useful reagent for the synthesis of pentoxide (As_2O_5) is concentrated nitric acid. The reaction between elemental arsenic

and nitric acid gives H_3AsO_4. The controlled dehydration of this acid Equation (2-6) gives the pent oxide.

Hypochlorous, hydrochloric and perchloric acids also oxidize the metal or As_2O_3 to the pentavalent state. Arsenic pentoxide dissolves readily in water to produce arsenic acid, H_3AsO_4.

$$4\ H_3AsO_4 \rightarrow 6\ H_2O \quad + As_4O_{10} \tag{2-6}$$

Arsine (AsH_3) is the best known of the hydrides of arsenic. It is a colorless poisonous gas composed of arsenic and hydrogen. The gas, also called arsenic hydride, is produced by the hydrolysis of metal arsenides and by the reduction by metals (e.g., zinc) of arsenic compounds in acidic solutions. Arsenic pentoxide, the anhydride of arsenic acid (H_3AsO_4) is very soluble in cold water and dissolves to form a solution of arsenic acid.

Arsenic also forms numerous organic compounds, as for example, tetramethyldiarsine, $(CH_3)_2$ As-As $CH_3)_2$, used in preparing the common desiccant cacodylic acid. Several complex organic compounds of arsenic have been employed in the treatment of certain diseases, such as ameobic dysentery, caused by the microorganism. Some of the most important compounds and species of arsenic are shown in Table 2.4.

The elementary arsenic inherits an oxidation state of 0, arsenic is stable in the oxidation states of +5, +3 and –3 (Table 2.4), but generally found in water only in the trivalent and pentavalent states. The oxides of both As (III) and As (V) are soluble in water. The dissolution implies direct reaction with the water, where the oxides behave as non-metals and exhibit acidic character. As (III) forms arsenious acid also called arsonic acid. The dissociation of arsenious acid is given by:

$$H_3AsO_3 \quad = H^+ + H_2AsO_3^- \quad pKa = 9.22 \tag{2-7}$$

$$H_2AsO_3^- \quad = H^+ + HAsO_3^{2-} \quad pKa = 12.13 \tag{2-8}$$

$$HAsO_3^{2-} = H^+ + AsO_3^{3-} \quad pKa = 13.40 \qquad (2\text{-}9)$$

As (V) forms the arsenic acid. The two acids dissociate to form respectively arsenite and arsenate ions as shown in the following reactions. The disassociation of arsenic acid is given by:

$$H_3AsO_4 = H^+ + H_2AsO_4^- \quad pKa = 2.20 \qquad (2\text{-}10)$$

$$H_2AsO_4^- = H^+ + HAsO_4^{2-} \quad pKa = 6.97 \qquad (2\text{-}11)$$

$$HAsO_4^{2-} = H^+ + AsO_4^{3-} \quad pKa = 11.53 \qquad (2\text{-}12)$$

In order to understand the mechanism of dissolution of arsenic species both (trivalent and penta-valent), it is imperative to study its speciation with respect to the pH of the surrounding aqueous media. In the following section, the speciation with relation to pH is presented in Table 2.4. The table helps in correlating the various ionic mechanisms associated with removal of arsenic at various pH levels.

Table 2.4 Arsenic species and their environmental importance in water (Rahaman, 2003)

Compounds	**Example**	**Environmental significance/ Dominant pH region**
Arsine Oxidation state: -3	As^{3-}	Minor importance [Most toxic As species]
Elemental arsenic Oxidation state: 0	As	Minor importance [Least toxic As species]
Trivalent arsenic Oxidation state: +3	As(III)	Dominant under anaerobic condition [10 times more toxic than As(V)]
Arsenite, Inorganic	H_3AsO_3 $H_2AsO_3^{1-}$ $HAsO_3^{2-}$ AsO_3^{3-}	pH = 0 – 9 pH = 10 – 12 pH = 13 pH = 14 Important
Pentavalent arsenic Oxidation state: +5	As(V)	Dominant under aerobic condition [10 times less toxic than As(III)]
Arsenate, Inorganic	H_3AsO_4 $H_2AsO_4^{1-}$ $HAsO_4^{2-}$ AsO_4^{3-}	pH = 0 – 2 pH = 3 – 6 pH = 7 – 11 pH = 12 – 14

Figure 2.1 displays the predominance diagram of arsenic species as a function of pH. From Figure 2.1 it is seen that arsenic acid is stronger than arsenious acid. Within the range of natural waters (particularly groundwater), where pH is usually between 6 and 9, the trivalent inorganic arsenic is found as non-dissociated arsenious acid (H_3AsO_3); while the pentavalent arsenic (Figure 2.2) is primarily found as the ionized di-hydrogen arsenate ($H_2AsO_4^-$) and mono-hydrogen arsenate ($HAsO_4^{2-}$). The relatively more mobile monomethylated and dimethylated forms are observed in ocean and lake waters, but seldom in groundwater. As most treatment processes are more capable to remove ions, the trivalent arsenic is more difficult to remove from the water than the As (V) (Kartinen and Martin, 1995). Probably this ionization of As(V) is also important for the fate of arsenic in the human body. The reduced toxicity of the As(V) may be, to a large extent, due to its ionization, which enables easier control of its intracellular transportation (Dahi, 1997).

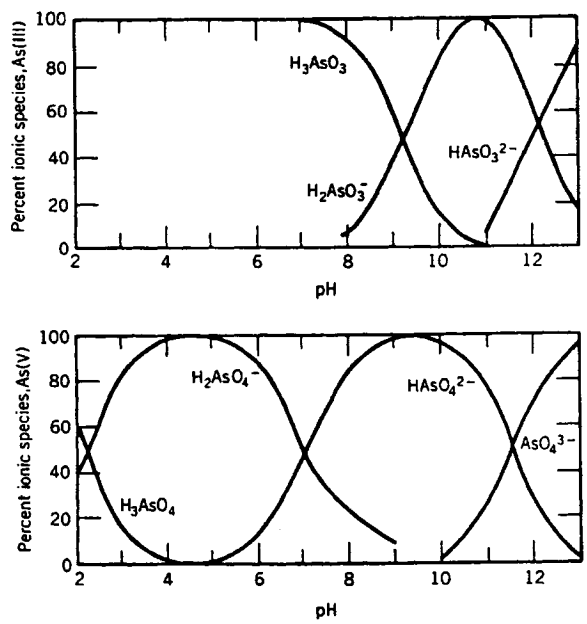

Figure 2.1. and 2.2 Predominance diagram of As(III) and As(V) as a function of pH (Montgomery, 1985).

2.3 Redox chemistry

Arsenic is a redox sensitive element. Arsenate [As(V)] and arsenite [As(III)] are common oxidation states of arsenic in water. The mobility of arsenic is controlled, in large part, by oxidation-reduction (redox) transformations. The valence in which arsenic exists is related to both pH and the oxidation-reduction (or redox) potentials, *Eh*. The hypothetical electron activity at equilibrium, pE, is used interchangeably with *Eh*. These parameters are related by:

$$pE = (F/2.3\ RT)\ Eh \tag{2.13}$$

where T is the absolute temperature, and F and R are the Faraday and Gas constants, respectively.

Thus at 25°C,

$$2.3RT/F = 0.059\ V \tag{2.14}$$

$$pE = Eh/0.059 \tag{2.15}$$

The equations linking arsenic speciation to pH and pE are readily available, but *Eh* versus *p*H diagrams (Figure 2.3), which indicate the predominant soluble species and relevant solids, are the most concise way of presenting this information.

The *Eh*-*p*H diagram for arsenic (total concentration 10^{-5} mol/L) in a system including oxygen, H_2O and sulfur (total concentration 10^{-3} mol/L) is shown in Figure 2.3. The diagram represents equilibrium conditions of arsenic under various redox potentials. Well-aerated surface waters would tend to induce high *Eh* values, therefore, any arsenic present should be in the arsenate [As(V)] form. Mildly reducing conditions, such as can

be found in groundwater, should produce arsenite [As(III)]. By determining the *p*H and *Eh* of water, it is possible to determine which species of arsenic will be prevalent.

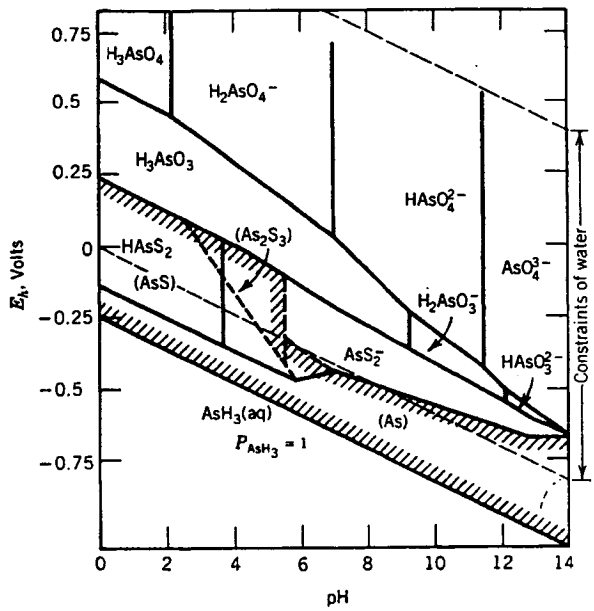

Figure 2.3 The Eh-pH diagram of inorganic arsenic species (Montgomery, 1985)

2.4 Oxidation reactions

As stated earlier, arsenate is dominant in oxygenated water while arsenite is dominant in non-oxygenated water. Although thermodynamics can provide an accurate prediction of possible changes in a given non-equilibrium condition, it gives no insight to the rate at which those changes will occur. While As (III) and As(V) acid-base reactions can be assumed to occur instantaneously, changes between oxidation states require indeterminate time periods in natural waters. For instance, the conversion of As (III) to As (V) in oxygenated water is thermodynamically favored, yet the transformation takes days, weeks or months depending on the specific conditions. The reduction of As (V) to As (III) is similarly kinetically constrained. As (V) can be found in some anoxic waters (Dahi, 1997). The process is however also known to be facilitated through catalysis and require bacterial mediation.

In strongly acidic or alkaline solutions, the presence of copper salts, carbon, certain catalysts and higher temperatures can increase the arsenic oxidation rate (Ferguson and Davis, 1972). Catalytic oxidation of arsenic can be achieved by powered active carbon and dissolved oxygen in stirred reactors. The rate of oxidation can be described by a first-order equation.

The effective removal of arsenic from water requires the complete oxidation of As (III), especially if the drinking water standard is low. There are various means of oxidation available, but in drinking water treatment there are important considerations such as the limited list of safe chemicals, the residuals of oxidants, oxidation by-products and the oxidation of other inorganic and organic compounds. In the oxidation processes with dosing of chemicals, effective oxidants are free chlorine, hypo chlorite, ozone, permanganate, and hydrogen per oxide/Fe^{2+} (Fenton's reagent), but not the chloramines (Frank and Clifford, 1986). These oxidants can directly transform As (III) to As (V) in the absence of oxygen. Chlorine is widely used for oxidation purposes, but may lead to chlorinated by-products, namely trihalomethenes (THMs), from reactions with natural organic matter. Ozone, widely used in surface water treatment for oxidation and disinfection, is quite effective but is not feasible for a specific application with As(III) oxidation. The most feasible oxidants are potassium permanganate and Fenton's reagent (H_2O_2/Fe^{2+}). Permanganate oxidizes As (III), ferrous and manganese ions specifically and quickly. Chlorine and permanganate are able to oxidize As (III) to As (V) within a very short time, e.g., half an hour or even few minutes (Dahi, 1997). Arsenious acid oxidation by most common oxidants is shown in the following reactions (Dahi, 1997):

$$H_3AsO_3 + \tfrac{1}{2}\,O_2 = H_2AsO_4^- + 2H^+ \quad (2\text{-}16)$$

$$H_3AsO_3 + HClO = H_2AsO_4^- + 2H^+ + Cl^- \quad (2\text{-}17)$$

$$H_3AsO_3 + 2/3MnO_4^- = H_2AsO_4^- + 2/3MnO_2 + 1/3H^+ + 1/3H_2O \quad (2\text{-}18)$$

2.5 Conventional methods and types of adsorbents

To remove metal ions such as lead and arsenic from wastewater, a number of technologies are applicable. Precipitation techniques by hydroxide, sulfide and carbonate anions are a few processes. Conventional treatment technologies such as precipitation and coagulation have become less effective and more expensive when there are high volumes of wastewater and low metal concentrations (Salinas *et al.*, 2000). Water treatment with coagulants such as ferric chloride and ferric sulfate are effective in abatement of both arsenic and lead. Another option for abatement of Arsenic pollutant is by a 'lime softening' technology (Jekel, 1994). The precipitated calcium hydroxide behaves as an adsorbing flocculant with respect to arsenic. Efficiency of such removal is within the range of 40 to 70%. Ion exchange and membrane separation technologies are appealing for removal of heavy metal ions, when present in high concentrations (Matheichal and Yu, 1999). The usage of ion exchange resins is in high demand by current industries. The solid phase resin consists of a cross-linked polymer with charged ionic species. The ions embedded in the resin exhibit affinity for all ionic species of opposite charge. An ion exchanger's capacity is highly dependent on pH. Certain species like Arsenic have a very delicate speciation distribution with respect to the pH of the bulk phase. As(III) in its ionic form is not easily removed from an aqueous phase at a pH range of most natural waters. Thus for its removal it is absolutely necessary to oxidize the species to As (V). The latter component is efficiently removable at a neutral pH value.

2.5.1 Adsorbents

The cost factor is a very important parameter for selection of an adsorbent material. The cost information is seldom reported. Some of the reported (Bailey *et al.*, 1999) low cost adsorbents include:

i. Zeolites
ii. Bark
iii. Coconut Husk
iv. Clay

v. Chitosan
vi. Fly-ash
vii. Lignin
viii. Algae
ix. Wool
x. Cotton

Some of the above adsorbents are discussed below.

Zeolites are highly adsorptive in nature and display high adsorptivities in relation to Arsenic ions (Gonzalez et al., 2001). However the drawback of Zeolite is that it is unstable at a higher pH range. Leppert (1990) reported that the adsorption of Lead on zeolite is significant (155.4 mg/g). The study also displayed a removal of Chromium (III), 26 mg/g. Although the amount of lead removal is significant, removal of Chromium is not substantial. Desborough (1995) demonstrated that clinoptilolite-rich rocks (CRRs) could be utilized for removal of lead from wastewater. Moreover, alteration of zeolite sometimes is essential in the removal of cations such as Chromium (VI) to increase sorption (Santiago *et al.* 1992).

Tree barks are a by-product of the lumber industry and is effectively adsorptive because of its high tannin content. The polyhydroxy polyphenol groups of tannin are considered to be the active sites for adsorption process (Bailey et al., 1999). As metal cations displace adjacent phenolic hydroxyl groups, ion exchange takes place and forms a chelating complex (Randall *et al.*, 1974; Vazquez *et al.*, 1994). The major problem with tannin material is the discoloration of water from soluble phenols. Alves *et al.* (1993) and Vazquez *et al.* (1994) pointed out that the application of pre-treatments such as acidified formaldehyde eliminates the bleeding of colored compounds without appreciable reduction in their adsorption capacities. The pre-treatment, again, increases the expenditures. Randall *et al.* (1974) compared bark adsorption to that of peanut skins, walnut expeller meal and coconut husks. A study with peanut skins was found to effectively remove Lead, Mercury, Copper and Cadmium ions (Randall *et al.*, 1978).

Specific properties of clay assist in the sorption of heavy metals. They include a large specific surface area (800 m^2/g) and a highly negatively charged surface. Several researchers monitored various types of clay as adsorbents. Sharma *et al.*, (1990) worked with Wollastonite and Viraraghavan and Kapoor (1994) employed bentonite to remove Pb^{2+} ions from wastewater. Existence of montmorillonite, a major component in bentonite, attracts heavy metals because of its large surface area and high cation exchange capacity. To increase the sorption capacity of clay, Cadena *et al.* (1990) suggested substitution of the natural exchangeable cation in clay with an organophilic cation; tetramethyl ammonium ion (TMA). This complex modification demonstrated an increase in Lead uptake to 58 mg/g. China clay has been reported to adsorb Lead in insignificant amounts (Yadava *et al.*, 1991).

Chitosan, a deacetylated derivative of chitin, was also documented to be an effective adsorbent for metal pollutants. Masri *et al.* (1974) reported extreme adsorptive capacity of chitosan for Lead, almost 800 mg/g. The source, chitin is also an adsorbent and widely available from crabs, anthropods and some fungi (Berkeley, 1979). In fact, the exposure of free amino acids during deacetylation helps in removing heavier metals. Although the chemical production of chitosan is not expensive, Bailey *et al.* (1999) mentioned some factors such as crystallinity, percent deacetylation, and amino group content affect adsorption. Bailey *et al.* (1999) also appreciated the necessity of loose cross-linking with glutaraldehyde as suggested by Kurita *et al.* (1986) to ensure most effective adsorption and stability, but they also did mention of the limitations of chitosan. It is soluble in acidic solutions and is nonporous and that necessitates the technique of acylation to increase porosity (Hsien *et al.* 1995). Moreover, improvement in sorption by coupling functional groups such as amino acid esters, pyridil etc. (Bailey *et al.*, 1999) is associated with great complexity that may further limit the usage of chitosan.

Powder activated Alumina also demonstrates effective adsorption of metal ions (Yallay et al., 1999), (Gupta and Chen, 1978). Industrial solid wastes with high cellulose content are effective in attenuating metal ions from effluents (Namasivayam et al., 1998). It has

also been reported that Coconut Husk Carbon impregnated with Copper is effective in removal of both organic and inorganic contaminants (Manju et al., 1998).

Ghimerie et al. (2002) has observed that iron loaded orange juice residue can effectively remove Arsenic. Wasiuddin et al. (2002) has demonstrated that human hair can effectively remove As (III) at low concentrations. Alam et al. (2001) has reported the effectiveness of potassium phosphate in extracting transitional elements like Cobalt, Chromium and Arsenic from contaminated sites. The attenuation of Arsenic (V) species in a clay medium is attributed to the exposed hydroxyl groups at the edges of clay minerals (Lin and Puls, 2000).

Ayala *et al.* (1998) used Asturian fly ash as an adsorbent for removal of heavy metal ions. The authors used two types of fly ash: Abono (CVA) and Cangas del Narcea (CVN) to treat Copper and Cadmium ions from wastewater. They studied different parameters that include initial metallic concentration, pH, grain size, contact time and ionic strength. The effect of pH of the initial solution, which ranged between 1 and 5 during the adsorption process, was also studied. Experimental results indicate that the adsorption capacity increased as the initial Copper and Cadmium concentration decreased for fly ash. The adsorption capacity of Abono (CVA) fly ash was distinctly better than that of Cangas del Narcea (CVN). The final pH of solutions increased with increased solid/liquid ratio. The highest metal uptake recorded was 8.1 mg Cu/g for CVA with only 40 g/L of the adsorbent. It is also noted that the adsorption equilibrium was attained in 5 minutes. It was also observed that initial pH affected the adsorptive capacity of Copper and Cadmium. The authors also reported that in the pH range 2 to 5, the removal capacity for Copper displayed almost identical values for 200g/L of fly ash of both types. An advantage of using fly ash is that its pozzolanic particles can participate in reactions with lime in the presence of aqueous streams to form a cementitious compound after adsorption. Limitations of using fly ash include extreme variation in properties, significant variation in adsorption capacity with lime content (Kapoor and Viraraghavan, 1996) and a very low surface area, usually 1-6 m^2/g.

Apak *et al.* (1998) used bauxite waste red mud and coal fly ash to remove Copper, Lead and Cadmium from aqueous phase. They highlighted that pure adsorbents such as activated carbon or hydrated oxides are highly expensive. They predicted that the removal mechanism for red mud and fly ash comprises of four steps: sweep flocculation or surface precipitation, where most hydrolysable heavy metals are removed by co precipitation of their insoluble hydroxides; flocculation by adsorption, where multi-nuclear hydrolysis of metals act as more effective flocculants than their parent ions due to their high charge and strong adsorptivities; chemical adsorption based on surface-complex formation and ion exchange. The authors illustrated that hydrous oxide gel containing the heavy metal hydroxide promotes adsorption in a dynamic column. Apak *et al.* (1987) mentioned that although adsorption and precipitation were believed to play the dominant role in removal of heavy metal cations, no distinction was recorded between true adsorption and precipitation (McKay *et al.*, 1985).

Sawdust, as a waste product, has proven to be appealing to researchers. Usage of red fir sawdust has been reported to remove Copper and Chromium (Bryant *et al.* 1992). Sabadell and Krack (1975) studied adsorption of Lead, Cadmium, Copper and Nickel on oak sawdust, cedar sawdust and ash shavings. Kleiv and Sandvik (2000) noted that silicate tailings, a waste material produced as a result of mining operations, could be used to treat heavy metal ions in wastewater. They regarded tailings as a potential resource and mentioned its economic and environmental impact. In the presence of high pH, adsorbents such as tailings are capable of removing heavy metal ions efficiently from waste effluents.

Lignin, an extract from the waste product (black liquor) of the paper industry, displayed very good adsorptive capacity for Lead. Srivastava *et al.* (1994) reported that this capacity might attain a level of 1865 mg/g. Moreover, the authors have also reported removal of Zinc; capacity being 95 mg/gm. Polyhydric phenols and several functional groups on the surface are considered to be responsible for high adsorption on lignin. The

functional groups include ketones, aldehydes, carboxylic acids and alcohols that participate in cation exchange mechanisms.

Roy *et al.* (1993) compared the adsorption capacity of single metal tests with multi-component tests in presence of the green algae. In this regard, they noted that the ratio of the initial metal concentration in the two tests could be very significant. They compared the product of observed adsorption capacity in single test and the ratio with the observed adsorption capacity of the mixture test and found that the predicted and observed values were almost identical. The close agreement between the predicted and observed adsorption capacity suggested that the adsorption process was non-competitive. Heavy metals such as Ra, Pb and Zn demonstrate less than 1% difference between the predicted and observed adsorption capacity values. Aderhold *et al.* (1996) reported the usage of biomass of a marine alga, *Durvillaea potatorum*, for Lead removal. In this process, metal ions replaced carboxyl groups to form alginate from algin, which is a high molecular weight polymer. Adsorption occurs when calcium ions were exchanged with metal cations. However, the applications of the biomass were discovered to be limited due to leaching of alginate into the solution and subsequent entrapment of the columns packed with biomass. Rahmani and Sternbergs (1999) investigated the ability of duckweed *Lemna minor* to remove soluble Lead ions from an aqueous medium. Volesky and Prasetyo (1994) used *Ascophyllum nodosum*, a brown marine algae in a sorption column to remove Cadmium. Wilson and Edyvean (1994) performed experiments with brown seaweeds, *Laminaria digitata* and *Fucus serratus* for removal of Mercury and Cadmium ions. The problem of seaweed is that it may swell and disintegrate and cause hindrance in use of a dynamic column (Bailey *et al.*, 1999). To avoid that, Bailey *et al.* (1999) suggested the treatment of seaweed through cross-linking with formaldehyde or divinyl sulfone.

Recently, Chaalal and Islam (2001) illustrated that after injecting a solution of strontium ions into a biomass (algae) column, a considerable decrease of the effluent concentrations of the cations was achieved. The preliminary design calculations demonstrated that a

scaled-up system of the adsorption column coupled with a fluidized bed and a minimum suspension bed reactor could effectively reduce Strontium ions at low residence time intervals. Cationic species, such as Chromium, Arsenic and Lead are a massive source of contamination problem in drinking water supply of south-Asian countries. Thirunavukkarasu *et al.* (2005) proposed the use of Manganese green sand to eliminate Arsenic in drinking water system.

Crusberg (1999) investigated the thermodynamics of heavy metal biomineralization within mycelia beads of the fungus *Penicillium ochro-chloron.* This work has demonstrated promising results for the removal of Copper ions from aqueous solutions.

Niu *et al.* (1993) reported several species of biomass such as *Penicillium chrysogenum, Bacullus mycoide, S. longwoodensis.* He noted that *Penicillium chrysogenum* removes about 116 mg/g of Lead ion.

Salinas *et al.* (2000) used *Rhodotorula rubra* to adsorb Cadmium and Lead. They examined the influence of solution physicochemical parameters and different physiological states of the cells due to heavy metal adsorption. The physicochemical parameters included pH and temperature of the solution. Their results appeared to be capable of removing heavy metals from dilute aqueous solutions (5-40 mg/l) in batch systems. They concluded that the results could be due to the composition of the cell walls. The wall of *Rhodotorula rubra* is composed of mannan and chitin with traces of glucan. The authors also assumed of the possible contribution of some polymers.

Avery and Tobin (1992) demonstrated that an organic substrate (yeast) named as *Saccharomyces cervisiae* was effective in removing divalent metal cations onto its cell walls from dilute solutions.

Peat moss is mined and processed for fuel and has been considered a relatively inexpensive adsorbent. Peat, a soil material, is composed of lignin and cellulose. Chen *et*

al. (1990) explained adsorption of copper on peat as a result of both ion exchange and complexation. However, the effect of pH and concentration of the solution was neglected. Shiskowski and Viraraghavan (1993) observed high affinity of chromium ions on peat filters. Sharma and Forster (1993) reported that peat moss can be effective for chromium (VI) removal and a maximum adsorptive capacity of 119 mg/g is possible. To increase the adsorptive capacity of peat, several authors have also suggested the treatment of peat. Kertman *et al.* (1993) indicated that modified peat could remove lead in the amount of 90-230 mg/g. Though the type of treatment was not mentioned, the authors noted the coupling of inorganic sulfide groups on peat, as the responsible factor for significant removal.

Treated raw wool and cotton were utilized as adsorbents by several researchers [(Masri and Friedman (1974), Freeland *et al.*, (1974)]. Masri and Friedman (1974) reported that the removal capacity increased for Mercury with the addition of sulfhydryl functional group that bind the heavy metal ions. Freeland *et al.* (1974) indicated excellent adsorption of Mercury (331 mg/g) by treating wool with polyethylenimine. The limitation of using cotton is that without treatment, this cellulose fibrous itself does not adsorb heavy metal cations.

Besides the adsorbents discussed above, several researchers used several other types of materials as adsorbents. Masri *et al.* (1974) experimented with the following materials to remove Chromium and Mercury from a contaminant phase:

i. Orange peel (outer skin and white inner skin)
ii. Dry redwood leaves
iii. Dry pine needles
iv. Activated sewage sludge

The outer epidermis of orange was more effective than the inner part in terms of removing Chromium. The epidermis of the orange removed Chromium at a level of 275

mg/g. Activated sludge was very effective in removing Mercury (460 mg/g). Pine needles removed Mercury in moderate amounts (175 mg/g). Moreover, the following adsorbents have also displayed encouraging results to many researchers:

i. Turkish coffee (Orhan and Buyukgungor, 1993)
ii. Coconut shell based carbon (Sharma and Forster, 1993)
iii. Rice husk and Bambara nut husk (Said *et al.*, 1992)
iv. Jute (Shukla and Sakhardande, 1992)
v. Leaf mould (Sharma and Forster, 1994)
vi. Bone gelatin beads (Petersen *et al.*, 1991)
vii. Dye-coated moss (Low *et al.*, 1993)
viii. Iron oxide coated sand (Bailey *et al.*, 1992)
ix. Xanthate (Tare *et al.*, 1992)

Also, adsorbents such as synthetic resins are very effective and provide some selectivity toward certain metals, but they are very costly. The use of activated carbon is very common but it is time consuming and expensive. Processes that are suitable at high concentrations are often either effective or cost prohibitive when applied to dilute wastes with heavy metals concentrations of less than 100 mg/l (Volesky, 1990). Several researchers investigated the effect of pH on sorption of heavy metals. Salinas *et al.* (2000) reported that the initial pH of the solution could significantly affect the uptake of cadmium and lead. They demonstrated that at low pH, the removal of lead and cadmium decreased while the removal of the metals increased with increasing pH. Kapoor and Viraraghavan (1997) examined the effect of pretreatment of *Aspergillus niger* biomass on sorption of lead, cadmium, copper and nickel. Though they did not mention pH directly but chemical pretreatment displayed the effect of pH. It was also reported that maximum sorption might be observed around a certain range of pH. Say *et al.* (2001) reported that maximum sorption of heavy metal species [Pb(II), Cd(II) and Cu(II)] is observed at around pH 6.0 on fungus *Phanerochaete chrysosporium.* Park *et al.* (1999) found the optimum pH for Cd (II) uptake is 6.0 for immobilized *Zoogloea ramigera* cells. It is to be

understood at this stage, that the sorption behavior of heavy metals with respect to the adsorbents is highly dependant on pH of the bulk medium. The sorption mechanisms are a combination of ion exchange, chemisorption, cross and coordinate linkage of the contaminants with the substrate and each mechanism may dominate at a specific pH of the medium. The chemical structures of the adsorbents in relation to their functional groups bear a strong impact to the nature of the sorption mechanism. Thus an adsorbent may have its source of origin as a natural product like fish-scale or it may be classified as a synthetic product. A detailed study of classification of the products is illustrated in Table 2.5.

Table 2.5 Summary of the products discussed

Products	**Possible mechanism of Adsorption**	**Advantages and disadvantages**
Organic substrates i.e., Chitin, Algae, Cellulose waste.	Presence of hydroxyl, amino groups initiate retardation of metal ions. (Coordinate, Covalent and Chelating Linkages)	Low cost adsorbents. High adsorptivities. Limitation is the availability of the products in specific regions.
Mineral substrates i.e., Powder Activated Alumina, Zeolite, Bentonite	Presence of strong electrostatic fields in cavities results in electrostatic interactions.	High adsorptivities. Limitation is the cost factor and instability of some of these products at extreme pH levels.
Synthetic products i.e., Resins, Coconut Husk impregnated with Copper	Possible combination of organic functional groups and specific electrostatic charged sites.	High adsorptivities associated with large expenses.

Chapter 3

3 EXPERIMENTAL SET UP AND PROCEDURE

Summary

Experimental runs on fish scales, based on single and multi-component adsorption methods, were conducted using two types, namely Atlantic Cod and Shouairi scale. The latter were studied at the University of UAE, as part of collaborative research; some of these experimental runs were replicated at Dalhousie University. Due to the limited availability of Shouairi scales in Halifax, however, most of the tests there were conducted on Atlantic Cod scales. The protocol combined a series of static tests, followed by dynamic tests, alongside physico-chemical tests aimed at elucidating the adsorption process.

3.1 Equipment

The following pieces of equipment were utilized in the Dalhousie experiments:

1. Atomic Absorption spectrometer (Varian Spects/44 model)
2. Image analyzer (Zeiss, 459310 model)
3. X-Ray Diffraction Method (Philips, PW 1140 model)
4. Scanning Electron Microscope (JSM, 35CF model)
5. Nuclear- Magnetic Resonance (Bruker, 500 MHz model)
6. Automatic Sieve Machine

3.1.1 Atomic Absorption

The Atomic Absorption spectrometer (AA), provided by the Minerals Engineering Center, Dalhousie University and used to measure the strength of heavy metals, is a spectra 55B absorption spectrophotometer. Its detection limit is 0.01 ppm, with confidence limit of 95 percent. The mechanism and its arrangement are as follows: inside the device sits a lamp with a hollow cathode made of the element to be determined. This

emits a sharp resonance line of the element to be determined. Also present is a flame system (such as the air-acetylene system) into which the sample solution may be aspirated at a steady rate, at a temperature sufficient to produce an atomic vapor of the required species from the compounds present in solution. Although the overwhelming percentage of metal atoms will remain in a non-emitting, ground state, the idea – utilizing the techniques of emission flame photometry – is that some metal atoms may achieve an energy level sufficiently high to emit the characteristic radiation of the element under study. Meanwhile, the atoms that remain at ground-state are receptive to light radiation at their own specific resonance wavelength (in general, the same wavelength that they would emit if excited).

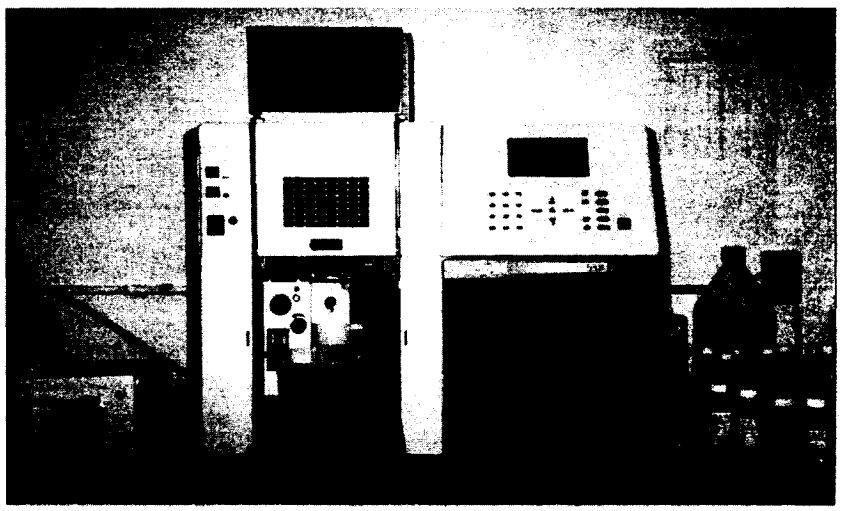

Figure 3.1 Spectra 55B Atomic Absorption spectrometer

When light of this wavelength is passed through a flame containing atoms of the element, part of that light, proportional to the density of the atoms in the flame, is absorbed. In this spectrophotometer, lamp emission is modulated such that its radiation only (i.e., not that emitted from the flame) is recorded as a galvanometer signal. A monochromatic device isolates the resonance line, focusing it on a photo multiplier. This detects the intensity of light energy. The apparatus includes means of amplification and readout. Figure 3.1 depicts an image of the Atomic Absorption spectrometer at Dalhousie University.

3.1.2 Image Analyzer

Major components:

i. Optical Microscope of a magnification of 1000X.

ii. High-speed desktop computer consisting of two softwares, Axio-Vision and KS 3000.

The objective of the Axio-Vision software is to obtain as clear an image as possible from the microscope (Figure 3.2).

Figure 3.2. Image Analyzer(*Courtesy*: Geo-mechanical laboratory, Department of Civil Engineering, Dalhousie University)

3.1.4 X –Ray Diffraction and Diffractometry

The Diffractometer consists of a PW 2233/20 Copper Tube for X-Ray development. The sample is inserted in a PW 1050/37 goniometer. A PW 3011/00 scintillation detector detects the spectrometric signal, and a PW 3710 interphase controller connects an analyzer to the computer screen. This arrangement is operated at 40 Kilo-volts and 40 microamperes, with a scan angular range from 5- 90 degrees, step size = .020 and employing a copper anode. The instrument possesses no detection limit but produces

qualitatively meaningful results. The fish scale subjected to this arrangement displayed amorphous nature (Figure 3.3).

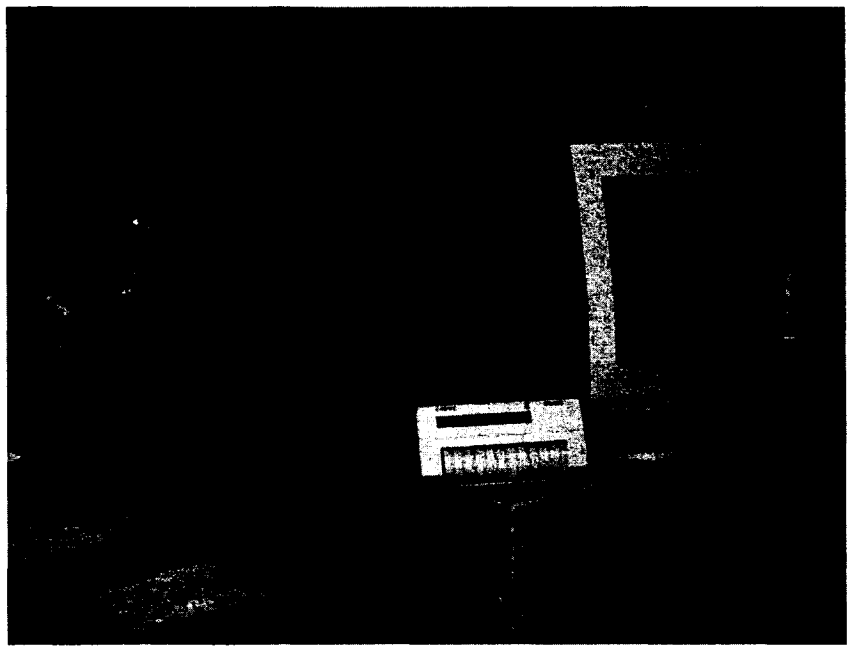

Figure 3.3 X-Ray diffraction and diffractometry (*Courtesy:* Department of Earth Sciences, Dalhousie University)

3.1.5 Scanning Electron Microscope

The JSM-35CF scanning electron microscope (SEM) in the Department of Metallurgy, Dalhousie University includes an energy dispersive spectroscopy detector, N1H image version for imaging of the slides, and a desktop spectrum analyzer for chemical mapping. Its detectable resolution is 1 weight percent, i.e., 1 g may be detected from a 100 g sample. Sample preparation entails placing a double-sided carbon tape around the sample, which is then coated with gold with sputter coating by 30-second exposure to a 16 micro-ampere current. The SEM operating characteristic is 25 Kilovolts voltage with a probe current of 80 micro-amperes.

The upgraded version of the instrument allows quantitative detection of the adsorbed cations and anions on the substrate of the fish scale (Figure 3.4a and Figure3.4b).

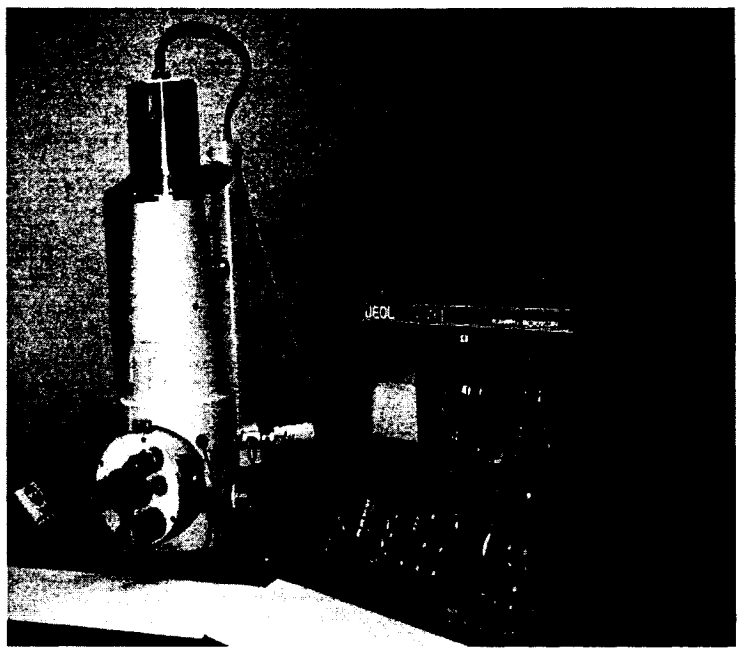

Figure 3.4a Scanning Electron Microscope and associated apparatus used in this work

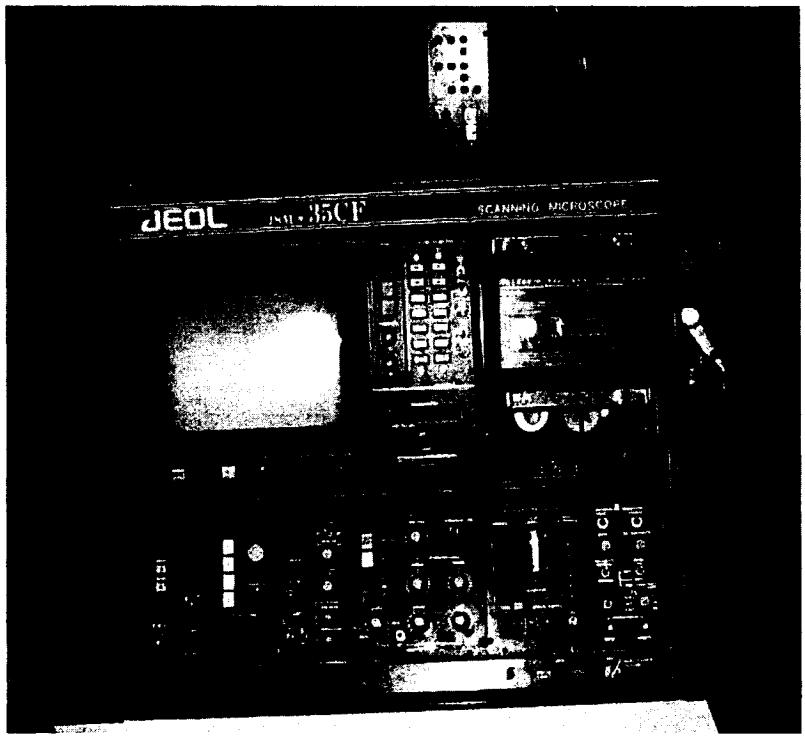

Figure 3.4b Scanning Electron Microscope (front view)

(*Courtesy*: Department of Metallurgy, Dalhousie University)

3.1.6 Nuclear Magnetic Resonance (NMR) Spectroscopy

The NMR spectroscope in the Chemistry Department of Dalhousie University characteristically generates a magnetic field of 9.4 Tesla at 400 MHz. A perturbation of the electron cloud of the substrate by means of an external magnetic field, results in resonance of the structure. This disturbance is transferred into an image processing system. There is no detection limit associated with the instrument; what is detected is a chemical shift (Figure 3.5).

Figure 3.5 Nuclear Magnetic Resonance setup
(*Courtesy*: Department of Chemistry, Dalhousie University)

3.1.7 Automatic Sieve Analyzer

Performed to observe how the size of fish scale affects adsorptivity of ions on its substrates, this experiment proceeded as follows:

- after collecting a sample from the market, cod scale was oven dried for two days at a temperature of 65°C
- using the automatic sieve machine in the soil mechanics laboratory of the Civil Engineering Department at Dalhousie University, a dried 256.1 g sample was sieved to isolate scales of different size. The sieving ran 4 minutes and two arbitrarily-chosen sizes of sample, namely #4-#8 (2.37-4.75 mm) and #8-#16 (1.16-2.37 mm) sieve fractions, were collected from the sieves in the lower part of the machine. (Although there are several methods for particle size measurement including as sieving, microscopy, sedimentation and radiation scattering methods [Allen 1987], each suitable for a specific purpose, sieving was employed in this experiment as the easiest and most widely used method of size analysis for adsorbent particles; weight distribution of the samples collected for different sieve sizes is discussed in Chapter 4.)

3.2 Introduction to dynamic tests

Several dynamic tests were conducted to observe the adsorption behavior and breakthrough characteristics of heavy metals. The dynamic runs can be categorized mainly in three groups:

i. Dynamic tests with original mass scale
ii. Dynamic tests with pulverized mass scale
iii. Dynamic tests with treated mass scale

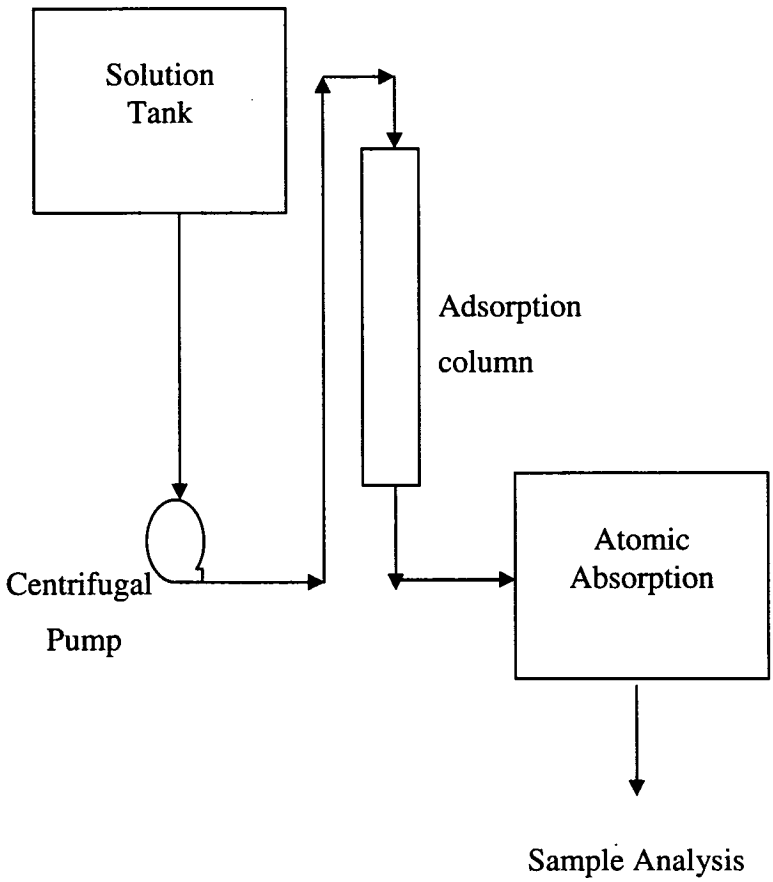

Figure 3.6 Schematic of the Dynamic System (Downward Flow)

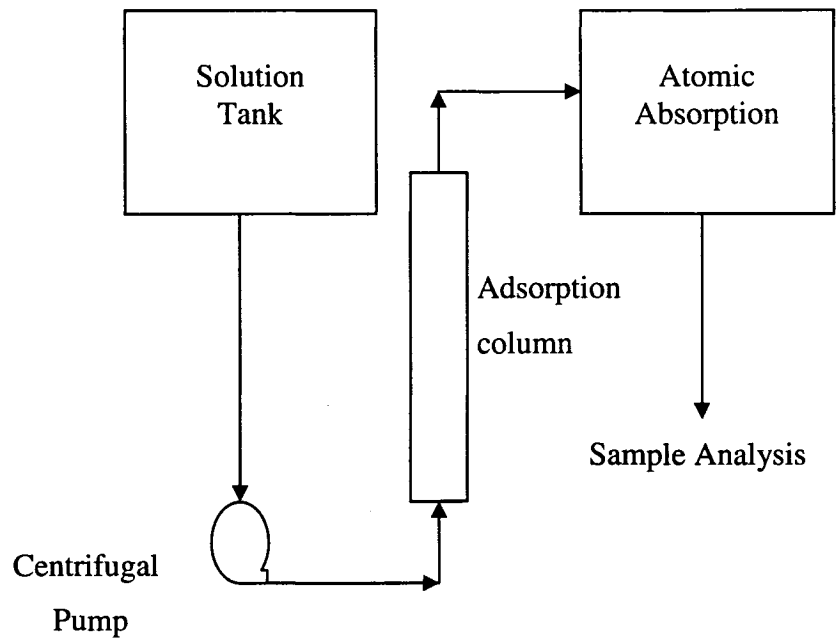

Figure 3.7 Schematic of the Dynamic System (Upward Flow)

Figures 3.6 and 3.7, respectively, represent upward flow and downward flow.

For the dynamic tests (Figure 3.6 and Figure 3.7) at Dalhousie, a PVC column (chemically inert) some 20 cm in height (including two 1.4 cm caps at the top and bottom of the column), with an internal diameter of 3.81 cm and weighing (including caps) 150 g, was used. Similar experiments performed in the laboratory of the Department of Chemical Engineering at UAE University used a PVC (chemically inert) column 30 cm long and 10 mm in diameter containing material to a height of 22 cm. To supply sufficient rigidity for the multi-component continuous flow test, a 30 cm-high, 10 mm-internal diameter column made of glass was used. The pumps used in the dynamic tests are positive displacement pumps of Cole and Palmer Company.

3.3 Sample collection

Atlantic Cod scale was collected from the Fisherman's Market, Bedford Highway, Halifax, Canada for all of the experiments with Atlantic Cod scale. Shouairi scale was collected from the Carfour supermarket, Al-Ain , United Arab Emirates (UAE) for all of the experiments with Shouairi fish. The grain size tests were performed in both acidic and alkaline environment and the size of the grains varied from 4.75 mm to less than 50 microns. The experimental conditions and procedures include three types of fish scales. They are:

3.3.1 Original Scales

Original scales include either Atlantic Cod or Shouairi scales. The scales are rinsed with distilled water to remove the Sodium ions and then dried at a temperature of 65° C (Cole, 2001) for 12 hours. The drying was complete after 12 hours.

3.3.2 Treated Scales (Shouairi)

The following chemicals are used for the treatment of Shouairi scale:

1) 5% Hydrochloric acid (HCl)
2) Acetone
3) Liquid soap
4) 5% Sodium Hydroxide (NaOH)
5) Water

The treatment of the fish scales with each of the reagents (1 through 5) mentioned above included allowing the bio-adsorbent to be in contact with the reagent for 5 hours. The adsorbent was then rinsed with deionised water until a stable pH value of the leachate was observed. The sample was completely dried in a baking oven at a temperature of 65 C (Cole, 2001:to avoid destruction of the substrate instead at 100 C) for 16 hours.

3.3.3 Pulverised Scales

The fish scale collected from the market was oven dried (after washing with deionised water repetitively) for two days at 65^0 C. The dried scales were then grounded in mining laboratory by pulveriser, to produce powdered mass of size in the range of 5-50 μm (Cole, 2001). Four sets of static tests were conducted for both trivalent and penta-valent arsenic ions with pulverized fish scale. The experiments were conducted with initial concentrations of Arsenic species from a range of 325- 1000 μg /L and at the optimal pH condition of the solution. These experiments are conducted to demonstrate the effect of grain size on arsenic removal.

3.4 Chemicals

Lead Nitrate, Chromium Nitrate, Cobalt Chloride, Sodium Arsenate and Sodium Arsenite salts used in the Atlantic Cod scale tests were provided by the Minerals Engineering Centre and the Safety Department, Chemical Exchange Program, UAE respectively.

The Shouairi and Atlantic Cod scale tests used the following chemicals:

- Cobalt Chloride [$CoCl_2$]
- Zinc Nitrate Hexahydrate [Zn $(NO_3)_2.6H_2O$]
- Strontium Nitrate [Sr $(NO_3)_2$]
- Lead Nitrate [Pb $(NO_3)_2$]
- Sodium Arsenate [Na_2 $HAsO_4$.7H2O]
- Sodium Arsenite [$NaAsO_2$]
- Chromium nitrate [Cr $(NO_3)_3$] $9H_2O$

All chemical solutions are prepared by mixing the chemical salts with de-ionized water. The adjustments of pH of the solutions were conducted with hydrochloric acid or caustic soda solutions.

3.5 Experimental Procedures for batch tests

The experiments may be classified in three categories:

a. Cations
b. Anions
c. Multi-component

The general procedural outline of the tests conducted is summarized in Figure 3.8, depicting how different variables were studied for anions and cations, as well as multicomponent phases.

The roles of the following parameters were studied (for various cases):

- pH of the influent
- Flow rate of the effluent in dynamic column
- Initial concentration of the influent
- Porosity of the medium
- Pre-treatment of the adsorbent

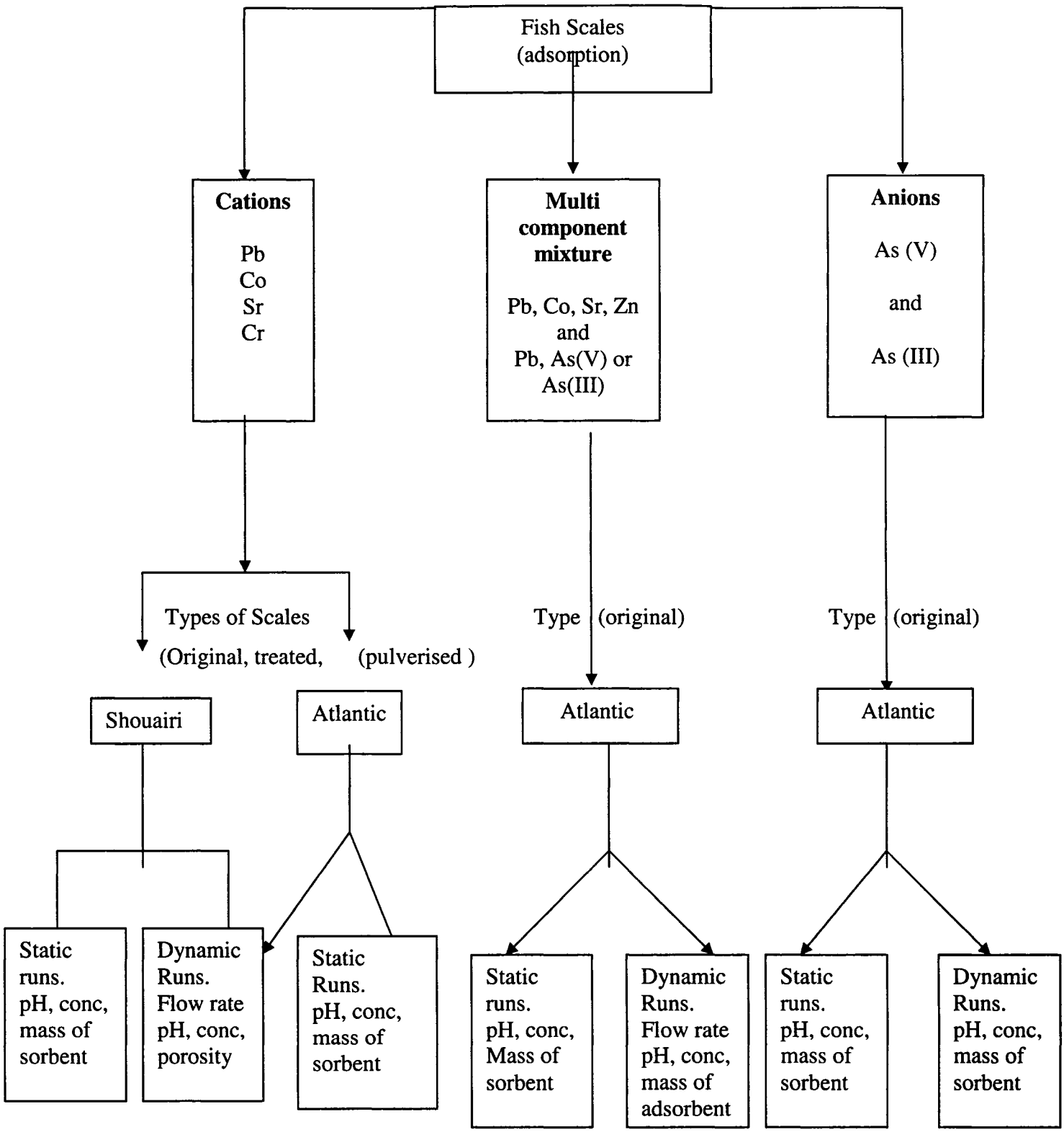

Figure 3.8. Flow chart of the experimental runs (Static and Dynamic)

3.5.1 Static tests with original mass-scale (Atlantic Cod)

Original scale (meaning: fish-scale brought from the market) was rinsed with de-ionized water to remove the Na^+ ions (to abate electrostatic interference in sorption) from the substrates (Schiewer and Wong, 2000). Some samples were treated with caustic soda to enhance the negative charge on the substrate by deprotonation. After addition of lead ions in bulk phase, the sodium ions from the substrate are removed by ion exchange mechanism.

3.5.1.1 Original scale treated with de-ionized water

The Atlantic Cod scale sample was soaked for 24 hours in distilled water and after rinsing four times with distilled water it was air-dried by a laboratory fan for 6 hours.

The first experiment was conducted with 150 ml of 40ppm lead ion solution, prepared by mixing lead nitrate $Pb(NO_3)_2$ salt with de-ionized water in a beaker and then adding 5 g of Cod scale. Before initiating the experiment proper, sodium ions were removed from the original mass of material. Concentrations of heavy metal were determined by applying atomic absorption (AA) technique to samples collected from the beaker at different time periods (2-70 hrs), in test tubes using a pipette rinsed with de-ionized water between collections.

Another experiment was performed for higher concentrations of lead nitrate solutions. Scales were soaked in distilled water for 24 hours and air-dried (with a fan) for 6 hours (for complete moisture removal). Three initial concentrations of 444 ppm, 473 ppm and 452 ppm of Lead ions were added to 1 g, 3 g and 5 g of Cod scales respectively in three beakers. Volume for all solutions was 200 ml. Preliminary tests were conducted to study the effect of sorbate-sorbent ratio.

Dried scale (oven dried at 55-65°C) in the amount of 1 g, 5 g and 10 g respectively were added to 250 ml of 485 ppm solution of Chromium ions. Samples from three beakers were collected after 48 hours.

3.5.1.2 Tests at different initial pH environment

This experiment was performed:

i. Observe the removal efficiency (ratio of amount of ions adsorbed to the original concentration in the effluent) of heavy metal ions at different initial pH conditions;

ii. Determine the change in pH over time in the presence of adsorbent.
In this way, the variations at different pH levels might be observed and studied for any possible correlation with removal efficiencies.

The experiment was conducted (at alkaline phases) for three initial pH conditions 8, 9 and 10. For each initial pH, five different initial concentrations of lead nitrate solution (by weight) were prepared. The initial concentrations of Lead ions were 2.5 ppm, 5.0 ppm, 10.0 ppm, 20.0 ppm and 40.0 ppm (by weight) for each pH set. For each concentration of each pH set, 150 ml of lead nitrate solution was taken. In total, 15 beakers were used. Five grams of fish scale of Atlantic Cod was utilized as an adsorbent for all fifteen static runs. The tests were conducted to analyze the adsorption behavior of lead cations on fish scales in an alkaline bulk phase. The pH of the solutions were adjusted accordingly with addition of caustic soda (0.1N) solution

Samples from the static tests were collected at different time intervals in test tubes from each beaker and tested for the concentration of lead ions. The volume of samples collected for concentration determination was about 1-2 ml. During the experiment, pH was also measured from each sample collected, using a SympHony Low Maintenance 3-in-1 pH electrode (SP21).

3.5.2 Batch tests for As(III) and As(V)

Sodium Arsenate hydrate, $Na_2HAsO_4.7H_2O$ (Baker Analyzed Reagent) and Sodium Arsenite, $NaAsO_2$ (Merck Reagent) were used in the preparation of As(V) and As(III) solution respectively. All chemicals were of analytical reagent grade, which were collected from Mineral and Mining Department, Chemical Exchange Program of Dalhousie University. All solutions were prepared by mixing the above chemicals in de-ionized water. The pH of the solution was adjusted accordingly with hydrochloric acid or caustic soda solution.

3.5.2.1 Arsenate solution

As(V) solutions were prepared using a Baker Analyzed Reagent, sodium arsenate hydrate with a 1000 mg/L concentration. The standard solution was made by dissolving 4.164 g of the arsenic salt into one liter of desired acidic, basic or neutral aqueous phase. From this standard solution two stock solutions were prepared, one 100 mg/L and another 10 mg/L. The 100 mg/L standard, prepared by diluting 100 ml of 1000 mg/L standard into 900 ml of distilled water; and the 10 mg/L standard, prepared by diluting 100 ml of 100 mg/L standard into 900 ml of de-ionized water, were then further diluted for these particular tests.

3.5.2.2 Arsenite solution

An As (III) stock solution, prepared by dissolving 1.73 g of sodium arsenite salt into 1L of de-ionized water (pH adjusted) with 1000 mg/L concentration, was diluted repeatedly to achieve the initial concentrations of 1000 μg/L, 500 μg/L, 300 μg/L and 250 μg/L. Samples were collected in 35-ml glass test tubes for analyzing arsenic concentration. The test tubes were washed with detergent, rinsed with distilled water and oven dried prior to using them in sample collection.

3.5.3 pH measurement

Portable pH probe (SP 21, VWR scientific products) was used to measure the pH and the temperature of the solution to an accuracy of +0.2 units and +0.1 units, respectively. The

pH meter was calibrated using three standard pH solutions (pH 4, pH 7 and pH 10) prior to the every measurement of pH.

3.5.4 Preliminary screening experiments

Initial batch experiments were conducted with fish scales as an adsorbent for both As (III) and As (V). The reaction mixtures consisted of 200 ml of arsenic solutions and 50 gm/L of sorbent. An initial concentration of 1000 µg/L and 350 µg/L of both As(III) and As(V) were used.

In all the above experiments the solutions with adsorbents are kept covered in beakers for several hours and the samples are collected after certain time intervals. The experiments were continued until equilibrium conditions were reached. The samples were then analyzed by using either colorimetric method or an Atomic Adsorption Spectrophotometer (Spectra 55B).

3.5.5 Analysis of Arsenic ions in relation to adsorbent dose, pH and initial concentrations

Three sets of static batch tests were conducted with three different initial concentrations, of 333, 535 and 1100 µg/L. Identical amounts of fish scale (50 g/L) were added for each test, the solution mixtures kept undisturbed until the achievement of equilibrium. Samples extracted after reaching equilibrium, i.e., any point in time after which effluent concentration ceased to vary, were then analyzed for arsenic concentrations. The pH of the solutions was adjusted appropriately, in the 4-11 range, and appropriate adsorption models were developed for both trivalent and penta-valent arsenic ions, using the different equilibrium conditions.

3.5.5.1 Effect of adsorbent dose

Three different sets of static tests are conducted both for As (III) and As(V) with different amounts of adsorbent added. The initial concentrations are 333 and 500 µg/L for As (III)

and As (V) solution, respectively. The amounts of fish scale added were 20 g/L, 30 g/L and 50 g/l

3.5.5.2 Effect of initial concentration

From the stock solution, three working standards, namely 1100, 535 and 333 μg/L, were prepared and then left with a fixed amount (30 g/L) of fish scale for several hours to reach equilibrium. Samples were then collected, at different time intervals. The pH of the aqueous phase was adjusted prior to adding the arsenic salts.

3.5.5.3 Effect of initial pH values

The effect and state of pH in water on As(III) and As(V) adsorption were studied by performing equilibrium sorption tests at different initial pH values in the range of 2-12. The pH values were adjusted either with 0.1 N HCl or 0.1 N NaOH as required. The initial concentrations were maintained in the range of 500-540 μg /L for As (III) and of 275-375 μg /L for As (V). Identical amounts of fish scale (30 g/L) were used for every run. Samples were collected at different time intervals and pH values of the solution mixtures were also monitored at regular intervals. The quantitative effect on adsorption of sodium ions on the substrate was not tested with respect to adsorption of arsenic anions.

.

The initial concentration and the pH of As (III) solution was kept at 500 μg/L and 7, respectively. The initial concentration and the pH for As (V) was identical to that of As (III). The static sorption time intervals with respect to the fish scale was varied at 2 hrs, 6 hrs, 12 hrs, 24 hrs, 48 hrs, 72 hrs and 110 hrs. Other procedures were maintained identical as to the earlier experiments.

3.5.5.4 Static tests with treated Atlantic Cod scale

Fish-scale was soaked in 0.1N Sodium Hydroxide solution for 48 hours (until completely dried). They were washed with de-ionized water until the leachate attained a constant pH (Niu and Volesky, 2001). They were air dried for 24 hours. One gram, three grams and

five grams of scale was put into four beakers each containing 200 ml lead nitrate solution. Then the change in concentration due to adsorption was recorded with time.

3.5.5.5 Static tests with pulverized fish scale

The effect of grain size was studied for Atlantic Cod scales in range of :

-2.37-4.75 mm

-1.16-2.37 mm

-less than 0.05 mm

Four different concentrations (5 ppm, 10 ppm, 20 ppm and 40 ppm) of lead ion solution were prepared. Five grams of Cod scale was added to each flask containing 150 ml of solution for each sieve fraction. It was prepared for each concentration level described earlier. The samples were collected at different time intervals to measure the concentration of Lead ions. The pH of the bulk phase was 7.00 for all the tests. The following tests were conducted to study the initial effects of pH with respect to pulverized samples. Three static tests were also performed with three different concentrations of 25.0 ppm, 12.5 ppm and 6.25 ppm of lead ions respectively. The fish-scales were dried in an oven for 48 hours at approximately 65°C. The dried sample was pulverized to less than 50 microns. 10 g of fish scale was placed in each beaker. Samples were collected in test tubes at regular time intervals. The effect of sodium ions in treatment of substrate (as competitor to Pb ions) is negligible (Schiewer, 1999).

3.5.5.6 Static Tests with original Shouairi fish scale

A 50 ml of cobalt ion solution was used for each of these tests. Shouairi scale was washed with de-ionized water. The initial concentrations were varied from 25 ppm to 200 ppm in increments of 25 ppm. The initial pH of the solutions was 7.00 in all the cases.

3.5.5.7 Static tests with treated Shouairi mass-scale.

Several experiments were conducted to monitor the role of chemical treatment of fish-scales. Cobalt Chloride [$CoCl_2$] solution was prepared from de-ionized water. The following chemicals were used for the treatment of Shouairi scale:

a. 5% Hydrochloric acid (HCl)
b. Acetone
c. Liquid soap
d. NaOH (5%Caustic soda)
e. Water

Each of the five flasks contained 50 ml of 100 ppm cobalt ion solution. An amount of one gm of dried scale was placed in each flask after treating the scale with one of the five reagents mentioned. The flasks were kept under shaking condition for 24 hours. Each treatment was considered as a single run.

3.5.5.8 Treatment of Shouairi scale with Sodium Hydroxide in presence of single component of heavy metals

For this experiment, four metal ions, cobalt (Co), zinc (Zn), strontium (Sr) and lead (Pb) were considered. Each of the metal ions was tested alone. The four metal salt solutions were put into four separate flasks. Each flask contains 50 ml of 100 ppm metal ion solution. 1 gm of Caustic Soda treated scale was put in each flask and was left under shaking conditions for 48 hours.

Another experimental run was conducted with 1 g of scale treated with 5% Sodium Hydroxide. The scale was added to a flask filled with 50 ml of 1000 ppm of Lead salt solution. After 24 hours, a sample was collected and the Lead ion concentration was measured.

3.5.5.9 Treatment of Shouairi scale with Sodium Hydroxide in presence of multi-component of heavy metals.

One gram of fish scale treated with 5% Sodium Hydroxide was placed in a 200 ml solution. The mixture solution consists of Cobalt, Zinc, Strontium and Lead. The mixture contained 50 ml from each salt solution having an initial concentration of 50 ppm of each metal ion. The solution with the adsorbent was left under shaking conditions for 48 hours.

3.6 Experimental Procedure for Dynamic Tests

A series of dynamic tests was conducted using the experimental set-up as depicted in Figure 3.9. The column containing the adsorbent was placed vertically while storing the contaminated water at a higher level, while collecting the effluent at the bottom. Fluid flow took place from the bottom of the column while effluent collected from the top. A hydrostatic head was maintained in order to assure a near-constant rate during the entire dynamic test. The dynamic tests were classified as either treated or original adsorbents. The tests were conducted to study the effect of pH, porosity and flow rate of the contaminants.

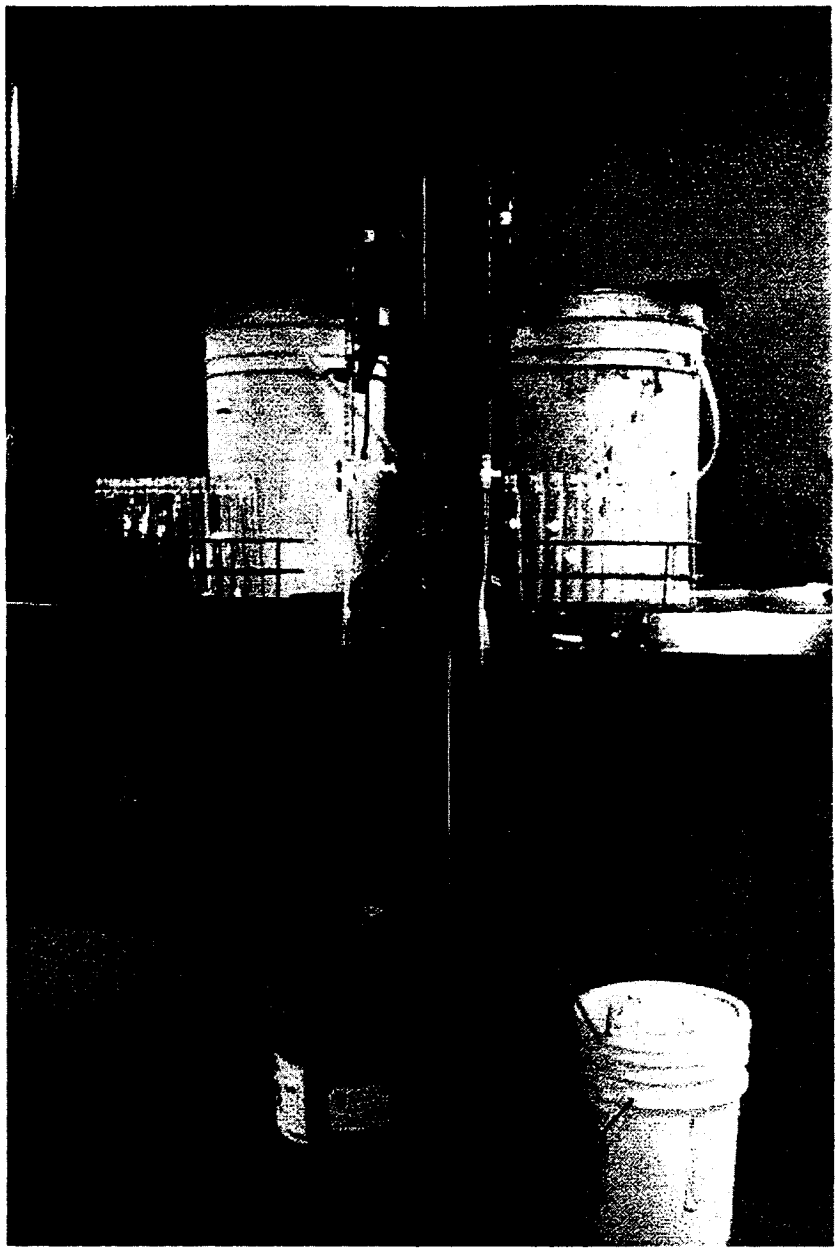

Figure 3.9 Experimental set-up for dynamic column studies (part of dynamic set-up)

Table 3.1 through 3.9 displays the nature of all the static and dynamic experimental runs considered in the thesis.

Table 3.1 Characteristics of experimental static tests conducted with original (cod and shouairi) scales and deionized water (neutral pH conditions)

Type of scale-mass	Type of Conta-minant	Run no.	Initial conc. (ppm)	Mass of scale (g)	Vol. of soln. (ml)
Original (cod)	Lead	1	40	5	150
Original (cod)	Lead	2	444	1	200
		3	473	3	200
		4	452	5	200
Original (cod)	Chro-mium	5	485	1	250
		6	485	5	250
		7	485	10	250
*Original (Shouairi)	Cobalt	8	25	1	50
		9	50	1	50
		10	75	1	50
		11	100	1	50
		12	125	1	50
		13	150	1	50
		14	175	1	50
		15	200	1	50

* Indicates collaboration with Department of Chemical Engineering, UAE

Table 3.2 Characteristics of experimental static tests conducted with treated (cod and Shouairi) scales

Type of Scale	Treat-ment of adsor-bent	Type of cation	Run	Initial conc (ppm)	Mass (g) scale	Volume Solution (ml)
Treated (cod)	-	Lead	16 17 18	25.0 12.5 6.25	10 10 10	500 500 500
Treated (cod)	0.5N Sodium Hydroxi de	Lead	19 20 21	444 473 452	1 3 5	200 200 200 (contd.)
*Treated (Shouairi)	Hydroch loric Acid	Cobalt	22	100	1	50
*Treated (Shouairi)	Acetone	Cobalt	23	100	1	50
*Treated (Shouairi)	Liquid Soap	Cobalt	24	100	1	50
*Treated (Shouairi)	5% NaOH	Cobalt	25	100	1	50
*Treated (Shouairi)	Neutral	Water	26	100	1	50

* indicates collaboration with Department of Chemical Engineering, UAE.

Table 3.3 Characteristics of experimental static tests (neutral and alkaline pH conditions)

State of scale	Initial ph of bulk phase	Treatment Of Adsorbent	Contaminant	Run No.	Initial conc. (ppm)	Mass Of Scale (g)	Volume Solution (ml)
*Treated (Shouairi)	Neutral	5% Sodium Hydroxide	Cobalt Zinc Strontium Lead	27 28 29 30	100 100 100 100	1 1 1 1	50 50 50 50
*Treated (Shouairi)	Neutral	5% Sodium Hydroxide	Co + Zn+Sr + Pb	31	50+50+50 +50 =200	1	50
*Treated (Shouairi)	Neutral	5% Sodium Hydroxide	Lead	32	1000	1	50
Original (Cod)**	8	De-ionized water	Lead	33 34 35 36 37	2.5 5.0 10 20 40	5 5 5 5 5	150 150 150 150 150
Original (Cod)**	9	De-ionized water	Lead	38 39 40 41 42	2.5 5.0 10 20 40	5 5 5 5 5	150 150 150 150 150
Original (Cod)**	10	De-ionized water	Lead	43 44 45 46 47	2.5 5.0 10 20 40	5 5 5 5 5	150 150 150 150 150

**indicates joint experimental runs conducted with (Mustafiz et al., 2002)

Table 3.4 Characteristics of experimental static tests with grinded Cod scales treated with de-ionized water

State of scale-mass	Initial pH of bulk phase	Treat-ment of Adsorbent	Type of Contam-inant	Run no.	Initial concen-tration (ppm)	Amt. of scale (g)	Volume of solution (ml)
Grinded (cod) 2.37-4.75mm	10	Deionized Water	Lead	48 49 50 51	5.0 10 20 40	5 5 5 5	150 150 150 150
Grinded (cod) 1.16-2.37mm	10	Deionized Water	Lead	52 53 54	10 20 40	5 5 5	150 150 150
Grinded (cod) <0.05 mm	10	Deionized Water	Lead	55 56 57	5.0 10 20	5 5 5	150 150 150
Grinded (cod) 300-550 µm	4 7 9 11	Deionized Water	As (III) (ppb)	58 59 60 61	350 (ppb) 350 350 350	10 10 10 10	200 200 200 200
Grinded (cod) 300-550 µm	4 7 9 11	Deionized Water	As (III) (ppb)	62 63 64 65	540 (ppb) 540 540 540	10 10 10 10	200 200 200 200

Table 3.5 Characteristics of experimental static tests with grinded Cod scales treated with de-ionized water

State of scale-mass	Initial pH of bulk phase	Treat-ment of Adsorbent	Type of metal	Run no.	Initial conc (ppm)	Amt. of scale (g)	Volume of solution (ml)
Grinded	4	Deionized	As (III)	66	1070 (ppb)	10	200
(cod)	7	Water	(ppb)	67	1070	10	200
300-550	9			68	1070	10	200
μm	11			69	1070 ppb	10	200
Grinded	4	Deionized	As (V)	70	333 (ppb)	10	200
(cod)	7	Water	(ppb)	71	333	10	200
300-550	9			72	333	10	200
μm	11			73	333	10	200
Grinded	4	Deionized	As (V)	74	535 (ppb)	10	200
(cod)	7	water	(ppb)	75	535	10	200
300-550	9			76	535	10	200
μm	11			77	535	10	200
Grinded	4	Deionized	As (V)	78	1100 (ppb)	10	200
(cod)	7	water	(ppb)	79	1100	10	200
300-550	9			80	1100	10	200
μm	11			81	1100	10	200
Grinded	4	Deionized	As (III)	82	350+2500	1	250
(cod)	7	water	(ppb)	83	350+2500	1	250
300-550	9		+	84	350+2500	1	250
μm	11		Pb (ppb)	85	350+2500 (ppb)	1	250

Table 3.6 Characteristics of experimental static tests with original Cod scales treated with de-ionized water

State of scale-mass	Initial pH of bulk phase	Treat-ment of Adsorbent	Type of Contam-inant	Run no.	Initial concen-tration (ppm)	Amt. of scale (g)	Volume of solution (ml)
Original (cod)	4 7 9 11	Deionized water	As (III) (ppb) + Pb (ppb)	86 87 88 89	350+10000 350+10000 350+10000 350+10000	1 1 1 1	250 250 250 250
Original (cod)	4 7 9 11	Deionized water	As (III) (ppb) + Pb (ppb)	90 91 92 93	350+40000 350+40000 350+40000 350+40000 (ppb)	1 1 1 1	250 250 250 250
Original (cod)	4 7 9 11	Deionized water	As (V) (ppb) + Pb (ppb)	94 95 96 97	350+2500 350+2500 350+2500 350+2500 (ppb)	1 1 1 1	250 250 250 250
Original (cod)	4 7 9 11	Deionized water	As (V) (ppb) + Pb (ppb)	98 99 100 101	350+10000 350+10000 350+10000 350+10000 (ppb)	1 1 1 1	250 250 250 250

Table 3.7.Characteristics of different experimental runs (with lead or cobalt or both) conducted as dynamic tests

State of scale-mass	Mass of Adsorbent (g)	Treatment of Adsorbent	Type of contaminant	Run no.	Flow direction	Flow rate (ml/min)	Initial Concentration (ppm)
Original Cod	80	Deionized water	Lead	1	Upward	8.0	40
Original Cod	80	Deionized Water	Lead	2	Upward	4.5	470
Original Cod	85	Deionized water	Lead	3	Upward	3.0	988
Pulverized Cod		-	Lead	4	Upward	5.5	
Treated Cod	34	0.5N Sodium Hydroxide	Lead	5	Upward	6.0	470
Treated Cod	49	0.5N Sodium Hydroxide	Lead	6	Upward	6.0	1050
Treated Shouairi	3.72	Liquid soap	Cobalt	7	Downward	1.0	50
Treated Shouairi	3.72	5% Sodium Hydroxide	Cobalt	8	Downward	7.0	100
Treated Shouairi	3.72	5% Sodium Hydroxide	Cobalt	9	Downward	55.0	100
Treated Shouairi	4.0	5% Sodium Hydroxide	[Cobalt+ Zinc+ Strontium+ Lead]	10	Upward	2.0	50 ppm each

Table 3.8.Characteristics of different experimental runs (with arsenic) conducted as dynamic tests

State of scale-mass	pH of the solution	Mass of Adsorbent (g)	Arsenic Species	Run no.	Flow direction	Flow rate (ml/min)	Initial concentration (ppm)
Original	7.7	61.54	III	11	Upward	2.0	41.22
Original	7.7	61.54	III	12	Upward	6.5	82.22
Original	9.25	66.87	III	13	Upward	2.75	82.76
Original	9.25	66.87	III	14	Upward	2.75	42.22
Original	2.00	69.44	III	15	Upward	2.0	0.520
Original	11.5	69.44	III	16	Upward	5.62	1.000
Original	7.0	69.44	III	17	Upward	2.0	1.050
Original	7.3	67.13	V	18	Upward	2.2	47.02
Original	8.04	75.90	V	19	Upward	6.5	47.04
Original	7.13	46.76	V	20	Upward	2.0	0.342
Original	11.0	50.31	V	21	Upward	2.0	0.485
Original	3.95	50.31	V	22	Upward	2.0	0.328
Original	3.95	50.31	V	23	Upward	2.0	1.000
Original	2.00	50.31	V	24	Upward	2.0	1.000

Table 3.9 Characteristics of different multi-component runs (lead and arsenic) conducted as dynamic tests

State of scale-mass (cod)	pH of the solution	Mass of Adsorbent (g)	Arsenic Species	Run no.	Lead conc (ppm)	Flow rate (ml/min)	(Arsenic) Initial concentration (ppm)
Original	7.7	61.54	III	25	1000	2.0	41.22
Original	7.7	61.54	III	26	1000	6.5	41.22
Original	9.25	66.87	III	27	1000	2.75	82.76
Original	9.25	66.87	III	28	1000	2.75	42.22
Original	2.00	69.44	III	29	1000	2.0	0.520
Original	11.5	69.44	III	30	1000	5.62	1.000
Original	7.0	69.44	III	31	1000	2.0	1.050
Original	7.3	67.13	V	32	1000	2.2	47.02
Original	8.04	75.90	V	33	1000	6.5	47.04
Original	7.13	46.76	V	34	1000	2.0	0.342
Original	11.0	50.31	V	35	1000	2.0	0.485
Original	3.95	50.31	V	36	1000	2.0	0.328
Original	3.95	50.31	V	37	1000	2.0	1.000
Original	2.00	50.31	V	38	1000	2.0	1.000

3.7 Alkalimetric titrations

The titrations were used to characterize the surface acidity of the fish scale according to the method described (Huang, 1981). To prepare the samples, 100 ml solution of 1 g per liter of fish scales was put into two beakers. The initial pH values were recorded and then titration (both acidic and basic) was performed under continuous mixing. The acid was 0.1N $HClO_4$ (Figure 3.10) and the base was 0.1 N NaOH (Figure 3.11).

The volume of acid/base added and the corresponding equilibrium pH values were recorded. To obtain consistent data, pH readings were taken every half hour after each measured addition of acid and base. The total acid or base added was the sum of the amounts consumed at the sites and the remainder in bulk phase. If all the acid or base added is in the bulk phase it implies that the sites were either saturated with the protons, or removal of protons from the substrate is complete.

Data from the net acid and base titrations were used in the equations 3.61 and 3.62.

$$1/[H+] = (Ns/K_1^{int})\,(1/(S\text{-}H2+)) + 1/K_1^{int} \quad (3.61)$$

$$[H+] = (Ns\,K_2^{int})\,(1/(S-)) - K_2^{int} \quad (3.62)$$

K_1^{int}= intrinsic basic constant

K_2^{int}= intrinsic acidity constant

Ns=number of sites per unit mass of adsorbent

[H+]= protonated sites (moles per g)

Intrinsic acidity and total number of sites per unit mass were constants calculated from slopes and intercepts of the linear equations 3.61 and 3.62. A zero point charge was also calculated from the intrinsic constants. The titrations in the figures 3.10 and 3.11 display the additions when the sites were unsaturated with either acid or base. The titrations after saturation were not recorded on the graph, because it would have interfered with the

regression analysis. The zero point charge was calculated as the average of pk1 and pk2 coefficients. The discrepancy in the result may be attributed to the heterogeneity of the adsorbent. The number of sites (Ns) calculated by acid titration is $2.03*10^{-3}$ moles/g

The pk_1^{int} and pk_2^{int} calculated was 5.9 and 7.68 respectively.

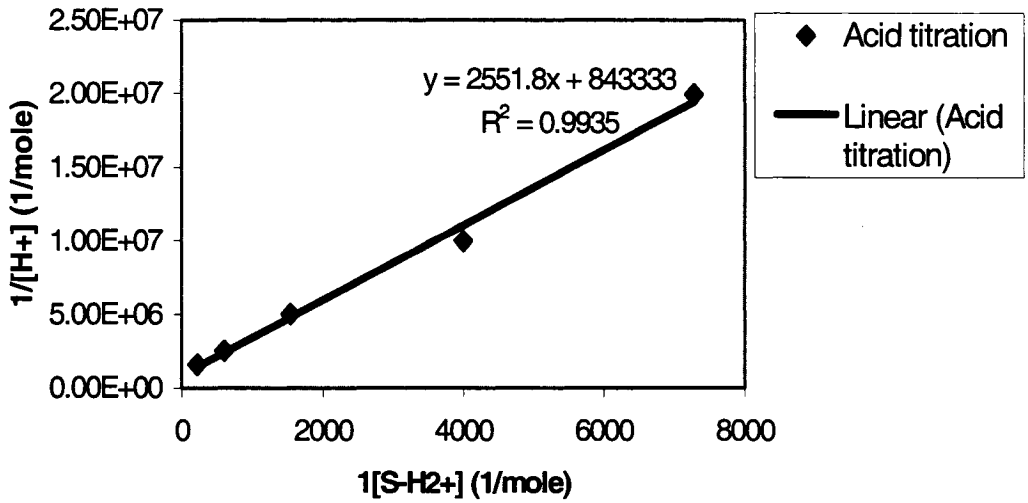

Figure 3.10. Acid titration with $HClO_4$

The total number of sites (Ns) calculated by base titration is $1.50*10^{-3}$ moles/g

The total number of active sites per unit mass of adsorbent is $1.765*10^{-3}$ moles/g

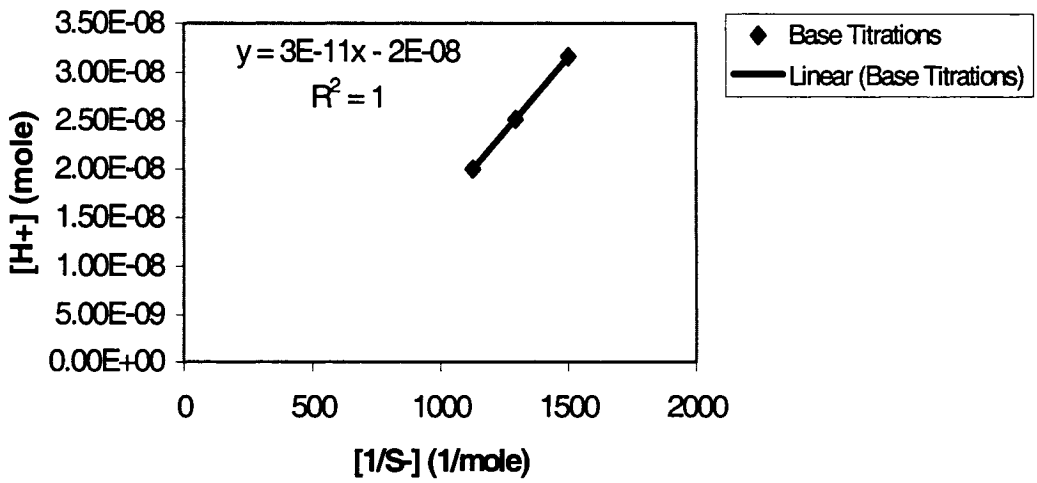

Figure 3.11. Base titration with 0.1N NaOH

Chapter 4

4 RESULTS AND DISCUSSION OF SINGLE COMPONENT SPECIES (CATIONS)

Summary

This chapter deals with both static and dynamic experimental runs with a single cationic component and one run each (both static: run 31 and dynamic: run10) multi-component system. The static test results (quantitative analysis) are presented on the basis of initial concentration of the ion, pH of the solution and mass of the adsorbent. The test runs corresponding to the state (treated, original and pulverized) of fish scales and particle size of the adsorbent are also discussed. In addition, the effect of porosity on adsorption of the contaminants is evaluated.

Finally, the adsorption behavior of different heavy metals in the dynamic system is presented through specific breakthrough curves for various types of adsorbents (Atlantic Cod and Shouairi scales), the initial concentration of the feed solution, pH of the bulk phase, mobility of the cation(s) and its flow rate. The fish scales were always rinsed with deionized water to remove the sodium ions that interfere with adsorption of the contaminants (Schiewer and Wong, 2000). Thus the term 'original scales' refers to the bio-adsorbent that has been rinsed with de-ionized water in order to extract the sodium ions from its substrate.

Following experimental runs, numerical simulations based on the surface excess model and the pore diffusion models are presented. The merits and shortcomings of each model are discussed. The effect of breakthrough behavior on experimentally determined and enforced (by trial and error methods) physical parameters are correlated for future scale up design purposes.

4.1 Results and discussion of static tests with cations

The results of the static tests with cations are primarily discussed in accordance with the state of the fish scale and with the run numbers presented in Tables 3.2 through 3.6 of Chapter 3. In essence, the static tests were conducted to assess the ultimate batch adsorption capacities of the adsorbents with respect to the contaminant ions. The static tests were conducted after measuring the effect of precipitation of lead hydroxides. Tests were conducted with blank samples (without any adsorbent) of 1000 ppm concentrations of lead ions at pH levels of 7, 9 and 11. It is observed that the maximum precipitation occurs at pH 9 with 25 percent removal of lead. At pH levels of 7 and 11, the precipitation of lead ions observed is 14 and 21 percent respectively. The adsorbent is a novel material and the initial batch tests are more associated with qualitative studies of various parameters such as pH, quantity of the adsorbent and two types of scales.

4.1.1 Effect of ratio of initial concentration to mass of adsorbent on adsorption

4.1.1.1 Original scale tests (Atlantic Cod)

Comparing the results of the static runs 1 and 4 that are distinguished by the concentration of the bulk phases, it is observed that after 24 hours, 84% of lead is removed from an initial concentration of lead solution (40 ppm). However, approximately 99% of lead ions are removed from a higher initial concentration (452 ppm) of the contaminant. The total amount of lead ions present in run 1 and run 4 is 6 and 90.4 mg respectively. The total amount of charged sites available in each adsorbent samples (assuming identical in nature) is $5.32*10^{21}$ sites. This is determined by measuring the total number of active sites per unit mass of the adsorbent times Avogadro number. The surface charge available is significantly high. Figure 4.1 illustrates the bulk phase concentration profiles with respect to time intervals for initial concentrations of 40 and 452 ppm. The decrease in effluent concentration is correlated to removal of the cations by adsorption and precipitation.

The total amount (Pb) removed= (initial –final) conc* (volume of solution, per unit mass of adsorbent)

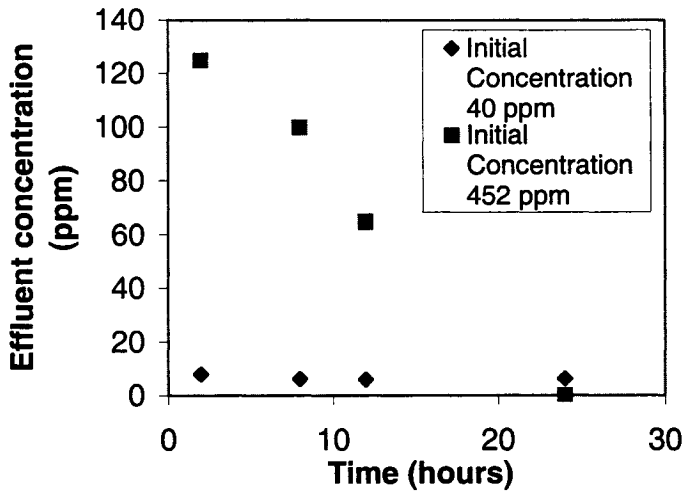

Figure 4.1 A study of adsorption of lead with variance of influent concentration.

If the adsorption system is considered in conjunction to a 'Stern layer concept' where besides the substrate there is a diffused phase and an immobile phase, the 'Debye-Huckel' theory is applicable. The theory explains that with increasing ionic strength, the 'diffuse layer' becomes compressed. The compressed layer allows the charged particles in bulk phase to approach more closely the substrate. It implies that possibility of interaction between the substrate and the adsorbate increases with increasing concentration.

In order to further consolidate the explanation through the 'compressed layer' theory, the results of runs 1 through 4 (tabulated in Table 4.1) is analyzed.

Table 4.1. Sorbent/ Sorbate ratio for Run 1 –4

Run No.	Total Sites	Cation (mg)	Removal efficiency (%)
1	$5.32X10^{21}$	6.0	84.04
2	$1.064X10^{21}$	88.8	90.1
3	$3.192X10^{21}$	94.6	99.53
4	$5.32X10^{21}$	90.4	99.92

The table demonstrates the total amount of cations (lead) in solution, charged sites available for interaction and removal efficiency of each run. The removal efficiency of each run corresponds to percentage decrease in contaminant at equilibrium from initial conditions. Runs 2, 3 and 4 correspond to a significant variance in total number of sites available (Table 4) for interaction with the adsorbate. An increase in mass of the adsorbent corresponds to increase in deprotonation of the number of adsorption sites. The sum of the released protons and total number of cations available is the average ion concentration n_o (total number of species per unit volume).

Considering the Debye –Huckel theory, the following expression may be incorporated into the analysis (Bockris and Reddy, 1970):

$$k^2 = \frac{8\pi e^2 I}{\varepsilon KT} \qquad (4.1)$$

where k^{-1}= Deybe screening length (inverse of length)

e= columbic charge (1.602E-19) (coloumbs)

K= Boltzman constant

T= absolute temperature

I= is the ionic strength of the solution

The ionic strength can be interpreted as $I = \frac{1}{2}\sum Z_i^2 n_i$ (Vera and Vera, 2003),

where Zi represents the valence of the ion, n_i is the number of moles of component i

The 'screening length' is the measure of extent of the cationic adsorption and a decrease of the value corresponds to increase in ionic strength (I) and possible ion interactions to the charged substrate. Comparing runs 1 and 4 (assuming all removal is by adsorption), the 'screening length' is inversely proportional to concentration of the total amount of ions in the bulk phase. It can then be concluded that percentage removal of cations in case of run 1 will be less than run 4. This is because equation 4.1 describes that with increase in ionic strength, the value of 'Deybe screening length' decreases. However, comparing runs 2 through 4, it is observed that in case of run 2 the removal is 90 % and in cases of runs 3 and 4, the removal efficiencies are almost identical. Fewer adsorption sites available in case of run 2 have reduced the possibility of interactions (if compared to runs 3 and 4) between the substrate and the ions in the bulk phase. In case of runs 3 and 4, the increase in deprotonation of the substrate leads to proportionate increase in interaction of the lead ions with the adsorbent.

The presence of appreciable number of sites (directly proportional to the mass of the adsorbent) is one of the most determining factors behind the removal of the cations. However, at lower concentrations and at higher pH values, the hydrolysis of the cations and weaker electrostatic interactions (between adsorbent and adsorbate) may further inhibit the adsorption process.

It is also true that generalization of such sorption phenomena in a wide range of initial concentrations may not always be adequate because their governing conditions strongly depend not only on the nature of the adsorbent but also on the speciation in the bulk phase. Volesky (1990) reported that processes that are suitable at high concentrations are often either ineffective or cost prohibitive when applied to dilute wastes with heavy metal contaminants.

The results of the three static tests (Runs 2 through 4) are displayed in Figure 4.2. For all the three varying masses of adsorbents and their corresponding bulk concentrations, significant amounts of Lead ions are removed. After 24 hours, the removal efficiency using both 3 g of adsorbent and 5 g of adsorbent is over 99%. It was observed that at a 1 g level, the equilibrium concentration is 45.0 ppm. In case of mass of adsorbent corresponding to 3 and 5 g levels, complete removal of the lead species is observed. The tests were repeated (twice). The standard deviation is discussed at the end of the chapter.

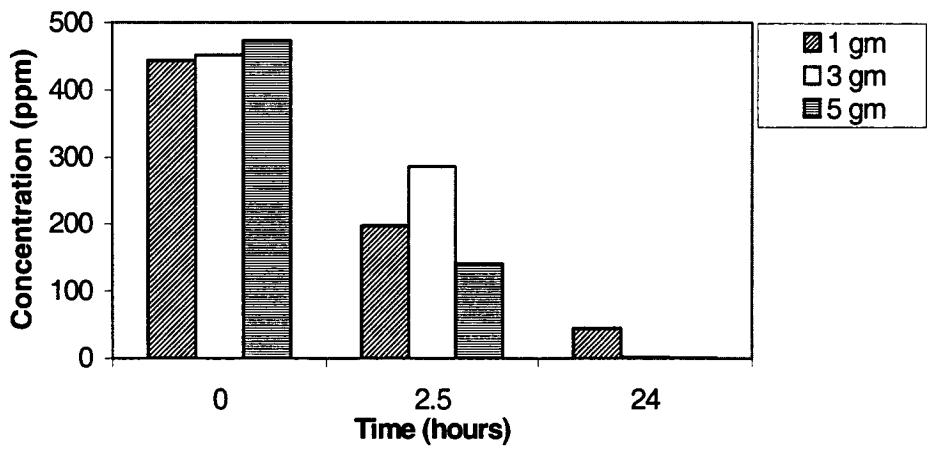

Figure 4.2 Removal of Lead ion with time in presence of varying masses of original Cod scales

4.1.1.2 Effect of Chromium adsorption on Atlantic Cod Scale (Original)

The static test results (Runs 5 through 7) for Chromium (III) are illustrated in Figure 4.3. The removal of Chromium ions increases proportionately to the amounts of adsorbent used for batch tests. The initial concentration of the cations is identical for all three runs.

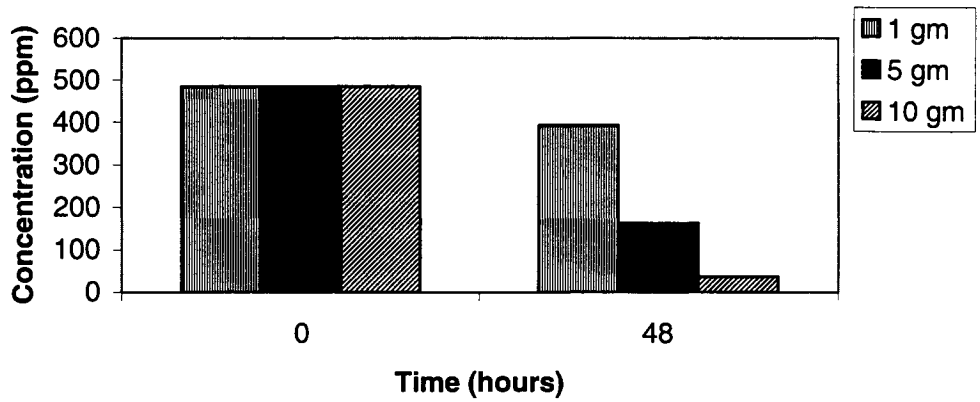

Figure 4.3 Removal of Chromium ion (48 hours) in presence of raw-mass Cod scale

The amounts of Cod scale (1, 5 and 10 grams) are utilised to lower the initial concentrations from 485 ppm to 390, 160 and 37.0 ppm, respectively. Figure 4.3 shows that with increasing number of probable sites, the removal of chromium ions increases. As discussed earlier, based on equation 4.0, the increase in adsorption (with increase in mass of adsorbent) is directly correlated to the overall ionic strength in the diffused phase. The chromium ions are trivalent in nature and the value of z_i is three. Thus the overall ionic strength increases if compared to lead ions (at same concentration levels) that are divalent in nature. In other words, with increase of valence of the cation, the adsorptivity of the contaminant proportionately increases.

4.1.1.3 Original Scales tests (Shouairi)

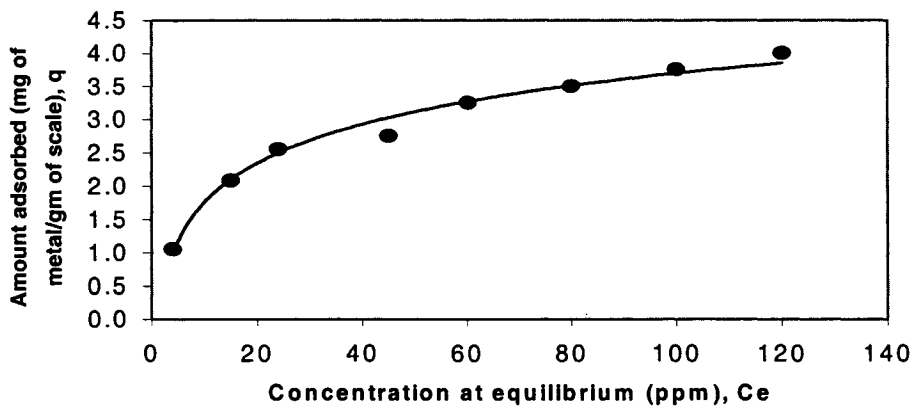

Figure 4.4 Cobalt isotherm on Shouairi fish scale

Runs 8 through 15 were conducted to establish the adsorption behaviour of Cobalt ions on Shouairi Fish scales. The scales were rinsed with de-ionized water before utilized for batch tests. Figure 4.4 demonstrates that with an increase in initial concentration of the bulk phase, the adsorption sites on the substrate are saturated with the cobalt cation. This suggests that the adsorption process follows the path of Langmuir isotherm. The Shouairi scale is perhaps composed of a specific number of interaction sites that allow adsorption of the cations to take place. However, at this present moment it is also important to understand that along with adsorption, precipitation of the cations in the 'diffuse layer' phase cannot be ruled out. Hence, Deybe –Huckel approximation may not be the only theory that is valid for all the mechanisms discussed.

4.1.1.4 Effect of initial concentration of Lead ions on adsorption by pulverized scale (300-550 microns)

The adsorption behaviour of 25 ppm, 12.5 ppm and 6.25 ppm of Lead solutions (with respect to pulverised scales) with time is illustrated in the Figure 4.5. It is observed for the 25 ppm case that the first 70 hours is the most kinetically active (significant decrease of the initial bulk concentration with time) and the adsorption mechanism is irreversible leading to almost complete removal of all the lead ions after 120 hours.

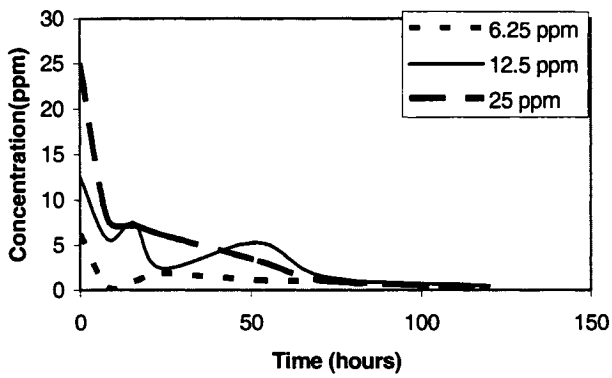

Figure 4.5 Concentration profiles of Lead with time

Perhaps, this is due to a larger surface area available (due to grinding) for interaction of the adsorbate and the adsorbent. The interaction mechanisms of adsorption of lead ions may include ion exchange, electrostatic bonding, precipitation and cross linkage (Sarwar and Islam, 1997), (Krishnamurthy and Harris, 1960). These mechanisms are usually associated with bio-adsorbents such as chitin and sargassum biomass. Each specific group of the adsorbent interacts with the adsorbate in a unique manner. Generally weaker, the electrostatic bonds may be easily developed but such interactions (at higher concentrations) are limited. Higher concentrations of lead ions (due to compression of the screening length) encourage the formation of highly stable bonds that are not easily destroyed. This is primarily due to the fact that a cation at higher concentration has a higher probability to interact with the substrate than at a lower concentration. In case of

lower concentrations of the contaminant, the development of stable covalent linkages is considerably reduced and weaker electrostatic forces play a more dominant.

An important factor that has been ignored is the generation of extra adsorption sites with respect to degree of pulverization. A higher degree of pulverization will generate smaller particles with higher surface areas available for sorption. But extreme pulverizations may cause attrition between the grinder and the sorbent that may result in breakage of some parts of the molecules on the adsorbent, resulting in the inhibition of the sorption mechanism. A detailed study of effect of particle size with respect to adsorption behavior is reported in the end of the chapter.

Table 4.2 demonstrates that nearly all of the pollutant is removed from the solution in the initial concentration range from 6.25 ppm to 25 ppm.

Table 4.2 Removal Efficiency for Lead test in presence of pulverized Cod scale

Amount of lead (initial) (ppm)	**Amount of lead (equilibrium) (ppm)**	**Removal Efficiency (%)**
25.0	0.33	98.7
12.5	0.48	96.1
6.25	0.11	98.2

It reveals that the overall adsorptivity of the cation is insensitive to the initial concentration of the effluent. Since the surface charge of the substrate is high (as calculated earlier plus pulverisation), the overall adsorption mechanism is perhaps not affected by the initial bulk concentration of the adsorbate.

4.1.1.5 Effect of adsorption on mass of treated scale with 0.5N Caustic Soda

Figure 4.6 has been developed based on the results of Runs 19, 20 and 21. Within 24 hours, more than 80 % of Lead is removed from the solution in all test runs. After 24 hours, the removal of lead ions is highest in case of 3 g adsorbent and then in 5 g adsorbent. A unit gram of adsorbent induced lower removal of the contaminant than in case of Runs 20 and 21.

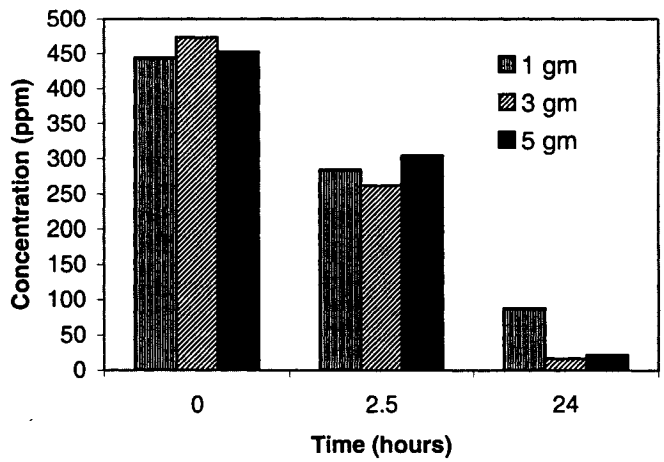

Figure 4.6 Lead ion concentration in presence of Sodium Hydroxide treated Atlantic Cod scale

4.1.2 Effects of different parameters

Based on the different runs conducted, the effects of various parameters on the removal of heavy metals are discussed below:

4.1.2.1 Effect of pretreatment

Comparing the results of Runs 19, 20 and 21 with Runs 2, 3 and 4 (original scales preferable)respectively, the effect of pre-treatment of Cod scale with alkaline treatment can be identified.

Figure 4.7 demonstrates that, for different amounts of adsorbent, original mass of Cod scale performed better in removing Lead cations than it did when the scale was treated with Caustic Soda solution. However the results display that both treated (alkali) and untreated scales display high adsorptive behavior after 24 hours. Thus original scales are a better choice than alkaline treated scales for adsorption purposes.

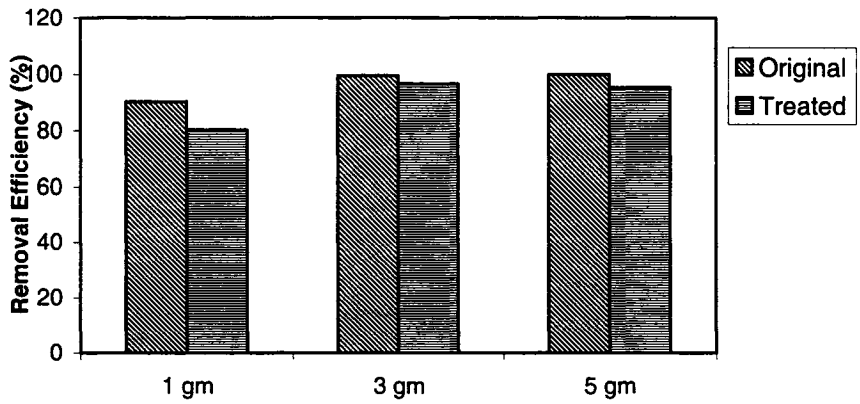

Figure 4.7. Effect of pre-treatment for Atlantic Cod scale in removing Lead cation

The effect of pretreatment of Shouairi scale with different types of reagents is obtained from the results of Runs 22 through 26. The effect of different reagents in removing cobalt cations is shown in Table 4.3. When the scale is treated with hydrochloric acid only 0.3 mg of cobalt is adsorbed from 5 mg of cobalt while 4.93 mg of Cobalt is removed when the scale was treated with Sodium Hydroxide. It is noticeable that in case of water treated scale (Run 26), the bulk phase concentration decreased to 28 ppm from 100 ppm. In relation to Run 25, the equilibrium is attained at a concentration of 5.5 ppm. But treatment of an alkaline solution helps in deprotonisation of the substrate followed by an increase in its negative charge (Xu, et al., 1988). The charge on a solid surface and the metal speciation in solution (determined by pH) are the most important parameters affecting adsorptive behaviour (Xu et al., 1988).

Table 4.3. Result of Cobalt ion concentration in presence of Sodium Hydroxide (treated Shouairi scale)

Run No.	Initial amount of metal in the solution (mg)	Initial Concentration (ppm)	Equilibrium Concentration (ppm)	Amount of metal in the scale (mg)
22 [HCl]	5	100	94.0	0.3
23 [Acetone]	5	100	41.5	3.0
24 [Soap]	5	100	15.5	4.26
25 [NaOH]	5	100	5.5	4.93
26 [Water]	5	100	28.0	3.6

The addition of Hydrochloric acid results in protonisation of the substrate that inhibits adsorption of cations due to mutual electrostatic repulsions. It is built upon the data of Runs 22-26 listed in Table 3.2. When the scale is washed with water, 72 percent of metal is removed. Pre-treatment with Sodium Hydroxide significantly improved the removal efficiency; it is more than 98 percent. Pre-treatment with soap provides 84.5 percent removal efficiency.

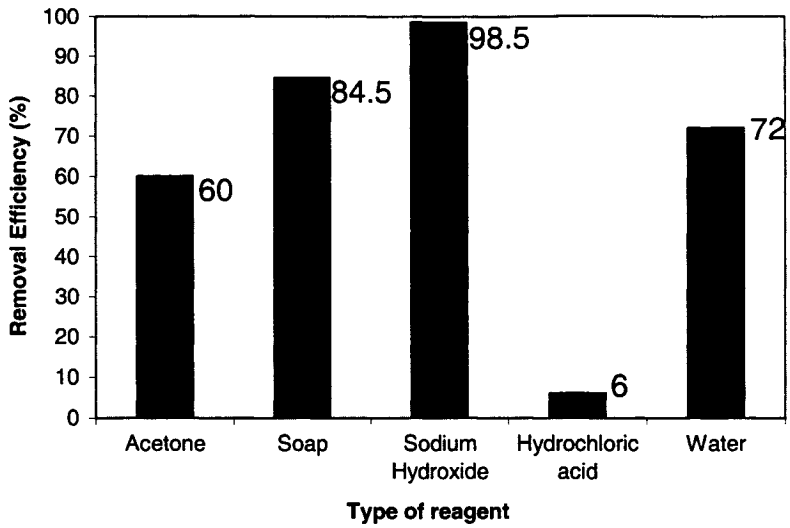

Figure 4.8. Removal efficiency of Shouairi scale pre-treated with different reagents

Figure 4.8 is a bar graph that represents the contribution of pre-treatment with different reagents. It is likely that pre-treatment with soap can contribute significantly, since soap contains Sodium Hydroxide. Acidic treatment of Shouairi scale performed very poorly to remove Cobalt cation, as only 6% metal is removed. A similar observation was noted (Pradas et al., 1994). He studied adsorption of zinc and cadmium on acid-treated bentonite and reported that it decreased the adsorption capacity when compared to the capacity of natural bentonite.

4.1.3 Effect of type of contaminants

Different types of heavy metals represent different types of contaminants. The effect of treated Shouairi scale on the contaminants of cobalt, zinc, strontium and lead has been displayed through the results of Runs 27, 28, 29 and 30.

The adsorption of four different metals in presence of Sodium Hydroxide treated Shouairi scale is illustrated in Figure 4.9. The figure displays that under identical environments. The removal of all the cations is significant with the alkali treated scales.

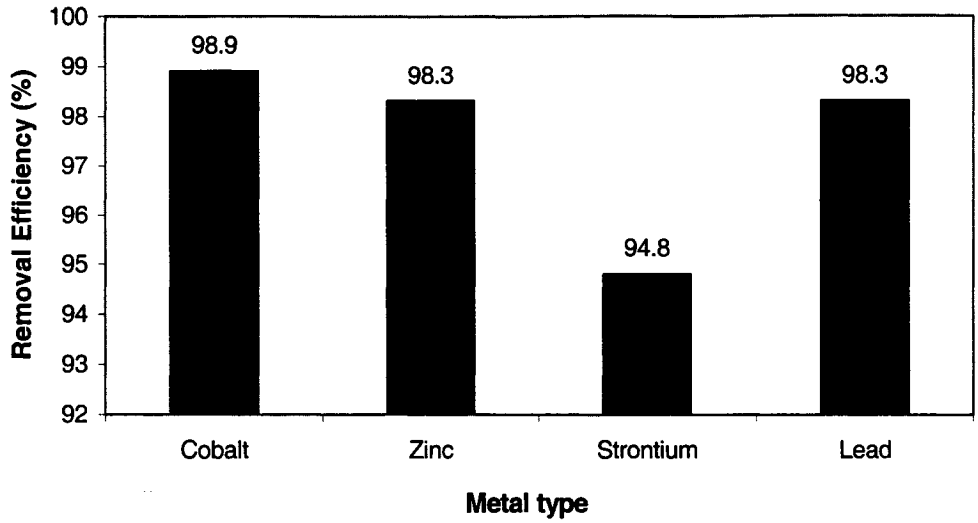

Figure 4.9 Removal Efficiency in single component state of metals in presence of alkali (NaOH) treated Shouairi scales (note: the removal efficiencies of cobalt, lead and zinc are nearly identical, and all are very high)

4.1.4 Effect of multi-components in the influent solution

Run 31 represents the effect of multi-component in the effluent solutions. The results of Run 31 illustrate the removal efficiency of cobalt, zinc, strontium and lead when the metals are mixed in equal ratios. Figure 4.10 shows the effect of competitive adsorption on removal efficiency. It shows that in presence of multi-component systems, the removal of each metal decreases when compared to its removal in a single-component system. It has also been observed that the percent reduction in removal efficiency is the highest for strontium cation followed by zinc, cobalt and finally lead. Thus in effect, at pH 7, the formation of organo-metallic complexation is in descending order with lead, cobalt, zinc and finally strontium.

Figure 4.10 reveals that adsorption of lead ions is less affected by the presence of multi-components. It suggests that in case of competitive adsorption, the lead ions preferentially occupy the sorption sites of the Shouairi scale, followed by cobalt, zinc and strontium ions. The probability of ion exchange mechanisms cannot be ruled out because

lead ions are known to replace calcium ions in bones (Esalah et al., 2000). Ion exchange capacity for Atlantic Salmon scale has been determined as 0.18 moles/(kg of adsorbent) (Chapter 7). Thus it can be concluded that removal of lead ions with respect to Shouairi scales is predominantly ion exchange mechanism.

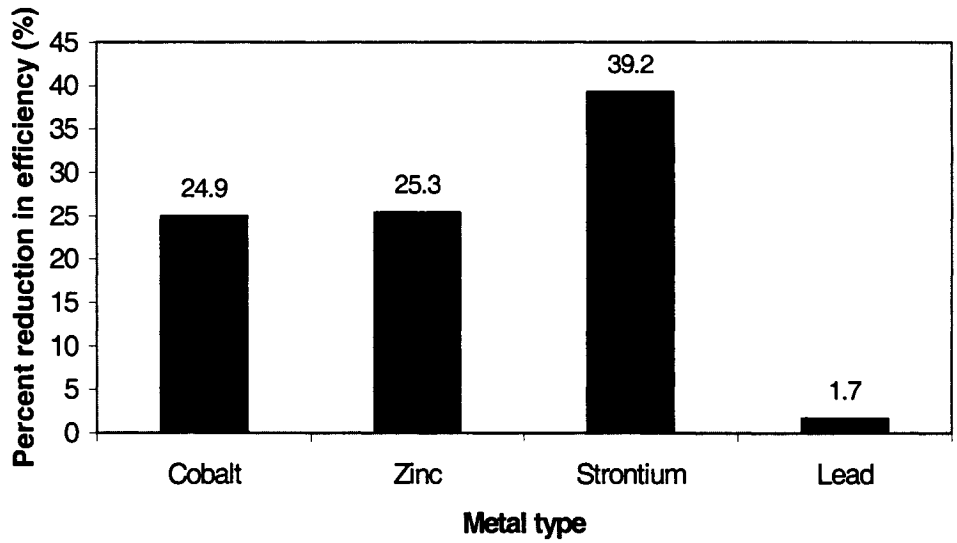

Figure 4.10. Removal Efficiency in quaternary system of metals in presence treated Shouairi scales.

The concept of preferential adsorption of lead ions may be attributed to the size of unhydrated radius of the ion. The larger the unhydrated radius, the stronger it binds to a substrate (Li, 2003). But it must be understood that the speciation of all the cations (including lead) in the bulk phase are associated with the complex formation and thus at a specific pH level, the same trend may not hold valid for other pH values. If the total sorbent site to total adsorbate (equimolar concentrations) ratio is reduced, a further change in efficiency of removal of the various contaminants is possible.

Table 4.4 illustrates a comparison of the adsorption capacity of Shouairi scale for these four metals. Roy *et al.* (1993) suggested this type of presentation to understand the nature of the adsorption process. It is mentioned in Chapter 2 that their experiments demonstrated a non-competitive adsorption phenomenon. On the contrary Table 4.4,

illustrates that, for all metals, there is a significant difference between the observed single component capacity and the observed multi-component capacity.

Table 4.4. Comparison of the adsorption capacity (mg metal/gm biomass) of Shouairi scale for four metals added in the mixture

Metal	Ratio of initial Concentration to Total Concentration	Observed adsorption capacity in single test, mg (adsorbed)/g of adsorbent	Observed adsorption capacity in mixture test, mg(adsorbed)/ g(adsorbent)
Co	0.25	4.95	1.85
Zn	0.25	4.92	1.83
Sr	0.25	4.74	1.39
Pb	0.25	4.92	2.40

This indicates that a notable competitive adsorption process was involved in the static tests.

4.1.5 Effect of initial concentration (treated Shouairi)

Figure 4.11 shows the comparison of Runs 30 and 32. After 48 hours, the Lead ion concentration decreased to 1.7 ppm from an initial concentration of 100 ppm. It also shows that when the initial concentration is 1000 ppm, after 24 hours, it is reduced to 1.2 ppm. It clearly demonstrates the fact that the treated Shouari scale has a removal efficiency of over 99%.

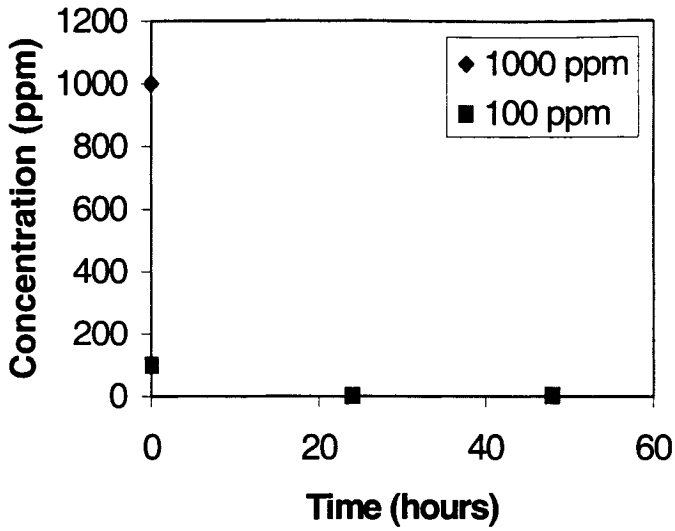

Figure 4.11. Effect of initial concentration (lead) on treated Shouairi scale (note: the concentrations at 24 and 48 hour intervals overlap)

4.1.6 Effect of pH values

The pH is measured for Chromium and Lead tests. Table 4.5 shows that with an increase in the amount of adsorbent the pH increases (in acidic range). This is because the pH of the bulk solution typically ranges between 5.5-7 and, therefore, from the initial pH of 3.14 of the chromium salt solution, it increased to 5.61-5.66 in presence of 10 g of adsorbent. This phenomenon confirms the fact that the hydrogen ions interact with the carbonate anions in the adsorbent. An important factor that needs to be mentioned is that effect of anionic adsorption at low pH levels can be significant.

Table 4.5. pH in presence of fish scale in Chromium salt solution

Amount of adsorbent in the solution (gm)	**pH**
0(blank sample)	3.14
1	3.38
5	3.61
10	5.61

Effect of initial pH will be discussed under different sections according to varying initial concentration of contaminant and at different initial pH levels.

4.1.6.1 Initial concentration of contaminants at varying initial pH levels (Runs 33-47)

Experimental results of various runs are plotted for five initial concentrations of 2.5 ppm, 5.0 ppm, 10.0 ppm, 20.0 ppm and 40.0 ppm at different initial pH values of 8, 9 and 10. Figure 4.12(a) shows concentration versus time profile for an initial concentration of 2.5 ppm. It is observed that the concentration decreased with increasing pH. Christophi and Axe (2000) observed the similar results in their experiments of competitive adsorption of cadmium, copper and lead on goethite. They reported that as pH is increased, the net surface charge of adsorbent becomes more negative. The increase in negative charge results in a proportionate increase in cationic adsorption. Salinas *et al.* (2000) supported this theory. They reported that some fluctuations were due to desorption. However, with increasing pH, the fluctuations diminished considerably.

When hydroxyl ions are added in the bulk phase, the Hydrogen radicals attached to the amide bond and the alkyl groups may dissociate from the fish scale structure. This results in formation of carboxyl (COO-) and amide groups (N-). In the presence of a strong base, there is a π- orbital shift from the carbon atom to the Oxygen atom in the carbonyl bond. The highly electronegative oxygen and nitrogen atom (amide) acts as a nucleophile and readily forms bonds (coordinate) with heavy metal ions such as lead. These coordinate bonds are highly stable in nature. However, the carboxyl groups contain a carbon oxygen double bond and a carbon oxygen single bond. A resonance hybrid across this region leads to delocalisation of the electron clouds that induces an electrostatic behavior (Morrison and Boyd, 1960). These delocalised sites allow some lead ions to be electrostatically attracted to the substrate. However, fluctuations of pH values in the bulk phase can lead to de-sorption of lead ions from such sites. At higher pH values, the charge densities of nucleophilic sites are relatively higher than at lower pH values. This results in both covalent and electrostatic adsorption of the lead ions on the bio-adsorbent.

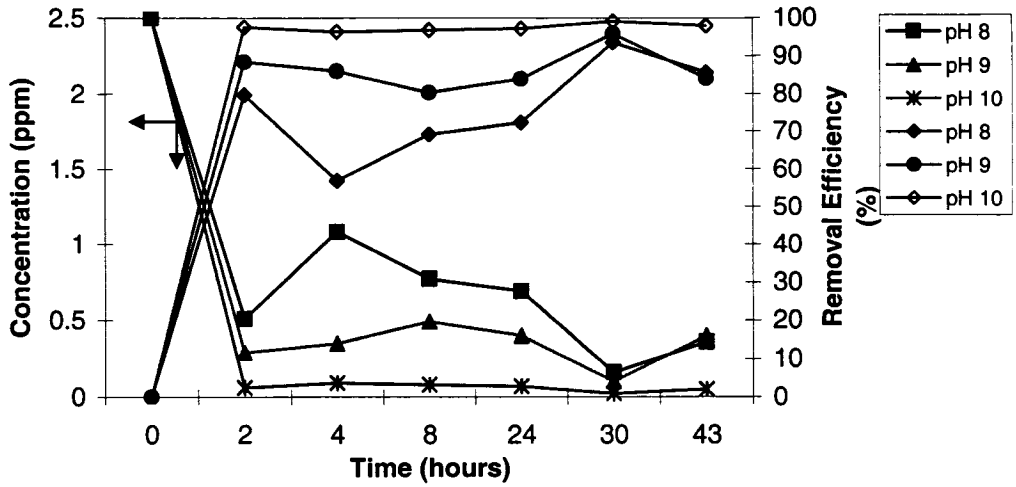

Figure 4.12(a). Lead ion concentration and removal efficiency with time for different initial pH condition (Initial concentration 2.5 ppm) (Mustafiz, 2002)

Figures 4.12(b), 4.12(c), 4.12(d) and 4.12(e) reflect the change in concentration with time when the initial concentrations are 5 ppm, 10 ppm, 20 ppm and 40 ppm, respectively. Initially, it is observed that the rate of chemisorption is significant. A dampening fluctuation has been identified in these figures with an increase in initial concentration. This phenomenon may be attributed to the fact that at lower concentrations, the hydrated lead ions in the bulk phase are widely separated from the adsorbent. This leads to adsorption but to a lesser extent if compared to a higher ionic strength. Larger intermolecular separations result in the formation of weaker bonds that can be easily broken. Cleavage of such electrostatic bonds may be attributed to the desorption of the ions in dilute solutions.

It is also observed that percentage removal capacity of lead exhibited by fish scale depends on the pH of the initial metal solution. The removal capacity is inversely proportional to pH value. This type of behavior has also been reported for the removal of copper and cadmium using fly ash. Moreover, Ayala *et al.* (1998) reported that for relatively high initial concentration, the removal capacity is identical for copper and cadmium in the pH range of 2 to 5.

4.1.6.2 Nature of pH

The nature of pH for experimental Runs 33-37, 38-42 and 43-47 as designated in Table 3.1 are illustrated in Figure 4.13. Figure 4.13 shows that from an initial pH of 8.0, the addition of pulverized cod scale decreases the pH spontaneously. The initial concentration of the Lead ions is varied in the range of 2.5 ppm to 40.0 ppm. In all cases, pH behavior is almost identical. The deprotonisation of the substrate in the presence of a strong base leads to the decrease in pH of the bulk phase. The initial rate of removal of protons is high, but after a certain time interval, equilibrium is attained between the protons and the hydroxyl ions.

Overall, in the Figure 4.13, the effect of change of pH is negligible after 4 hours. It indicates that the rate of change of protons in the bulk phase is in effect in early hours.

Runs 34, 39 and 44

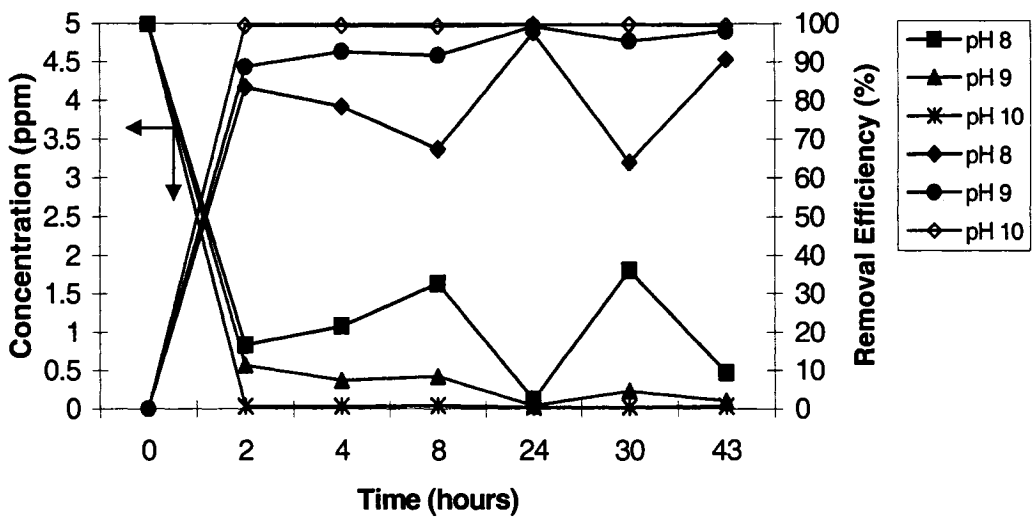

Figure 4.12(b). Lead ion concentration and removal efficiency with time for different initial pH condition (Initial concentration 5 ppm) (Mustafiz, 2002)

Runs 35, 40 and 45

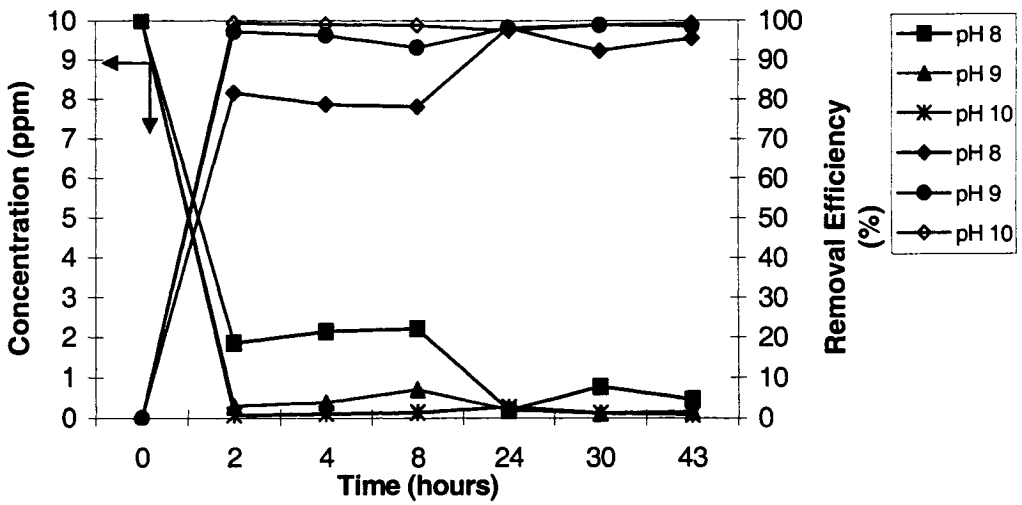

Figure 4.12(c). Lead ion concentration and removal efficiency with time for different initial pH condition (Initial concentration 10 ppm) (Mustafiz, 2002)

Runs 36, 41 and 46

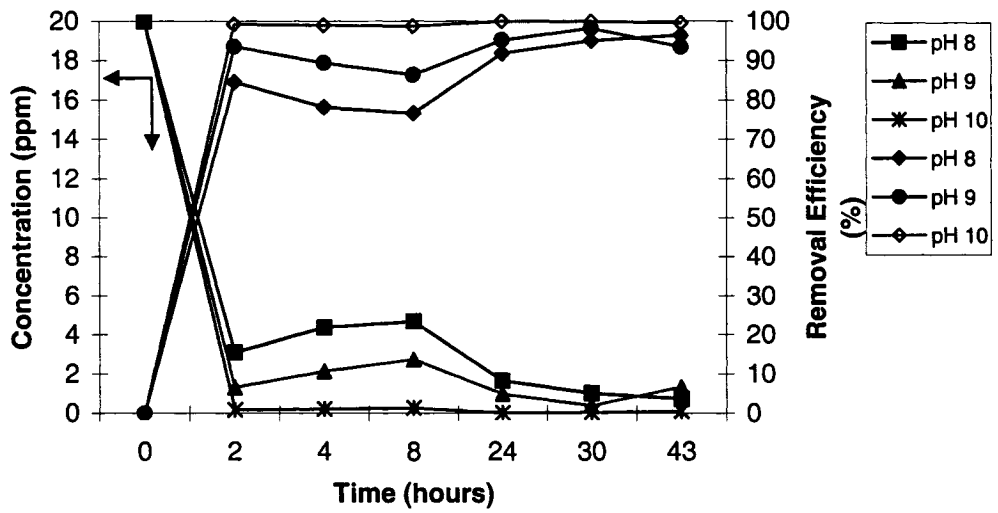

Figure 4.12(d). Lead ion concentration and removal efficiency with time for different initial pH condition (Initial concentration 20 ppm) (Mustafiz, 2002)

Runs 37, 42 and 47

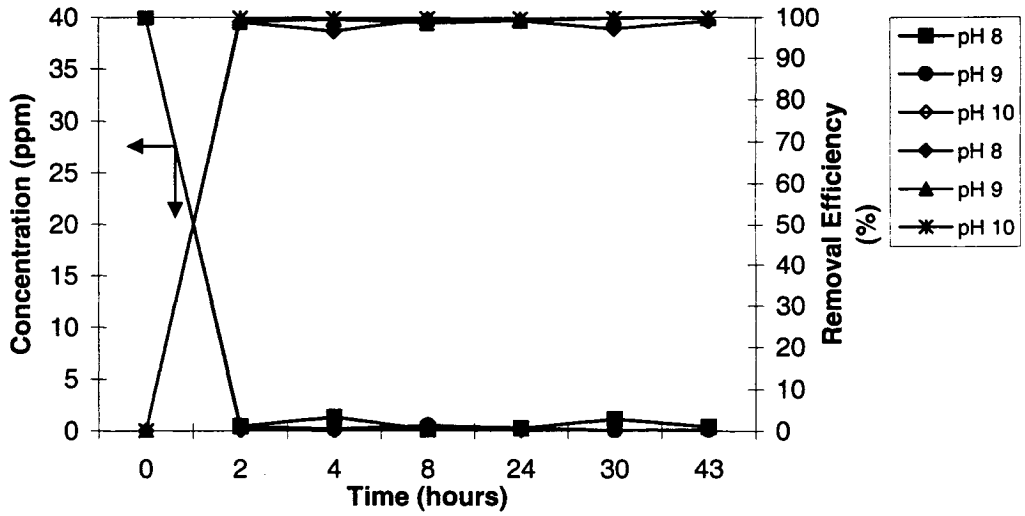

Figure 4.12(e). Lead ion concentration and removal efficiency with time for different initial pH condition (Initial concentration 40 ppm) (Mustafiz, 2002)

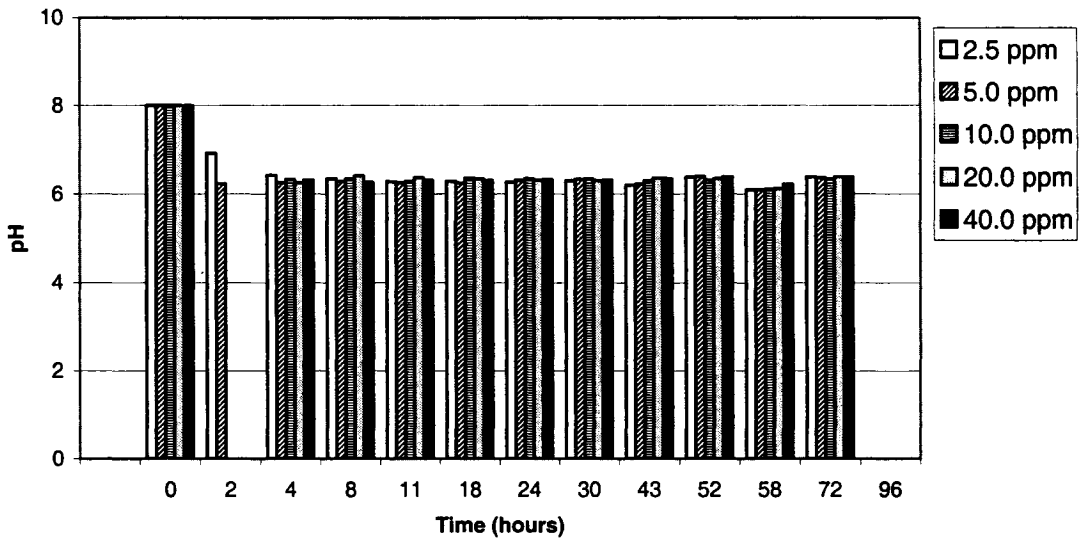

Figure 4.13. Variation of pH with time for different concentrations (initial pH 8.0) (Mustafiz, 2002)

4.1.7 Effect of metal binding

Metal uptake represents the amount (mg of metal) of heavy metal that can be adsorbed per unit mass (gram) of fish scale. The metal binding capacity is defined as the difference in final and initial concentration levels per unit mass of adsorbent in a unit volume of bulk phase. After quantifying the equilibrium concentrations, the metal uptakes are calculated. Figure 4.14 illustrates the metal uptake at initial pH values of 8, 9 and 10 when the initial Lead ion concentrations are varied 2.5 ppm to 40 ppm. It shows that in batch tests, metal uptake is proportional to the initial concentration of metal ion. The results of Runs 33-37 demonstrate that the Lead uptake varies between 18 to 80 mg/gm (Figure 4.3). Also, Runs 19 through 21 demonstrate that the adsorptivity of the cations are between 17 to 71 mg(contaminant) adsorbed/g (mass of adsorbent). The metal uptake also depends on the number of adsorption sites available per unit mass of the adsorbent. The unique feature of Figure 4.14 is that the effect of initial pH of the bulk phase is insignificant with respect to metal uptake by the adsorbent.

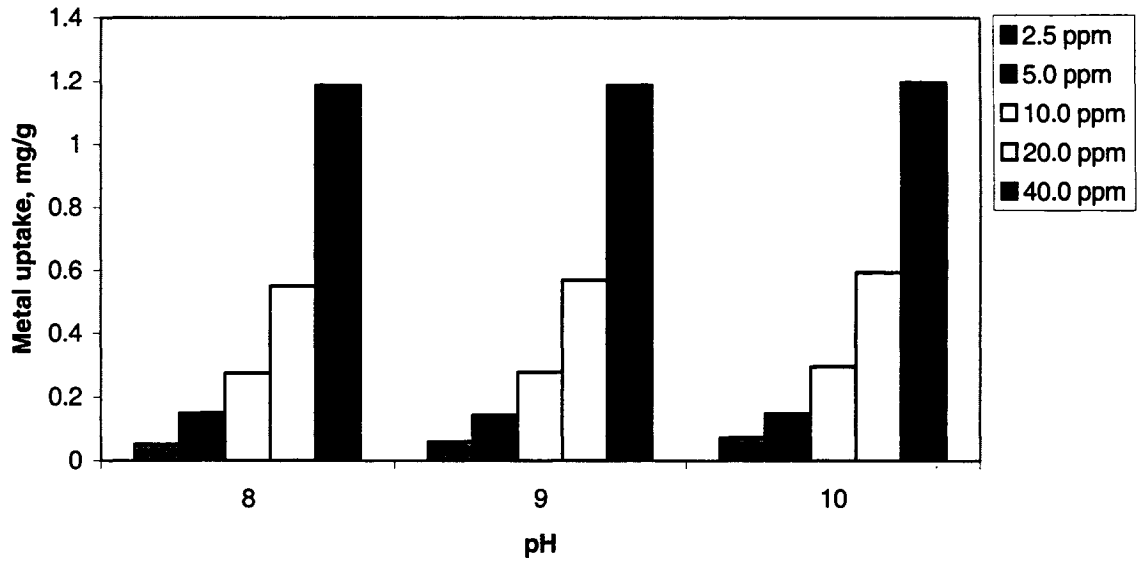

Figure 4.14. Metal uptake vs. pH for various initial concentrations

4.1.8 Effect of grain size

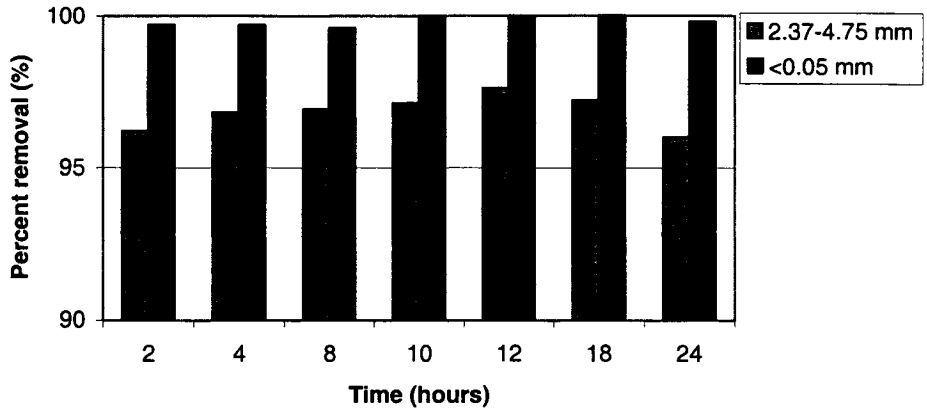

Figure 4.15 (a). Percent removal at different size of scale (initial concentration 5 ppm)

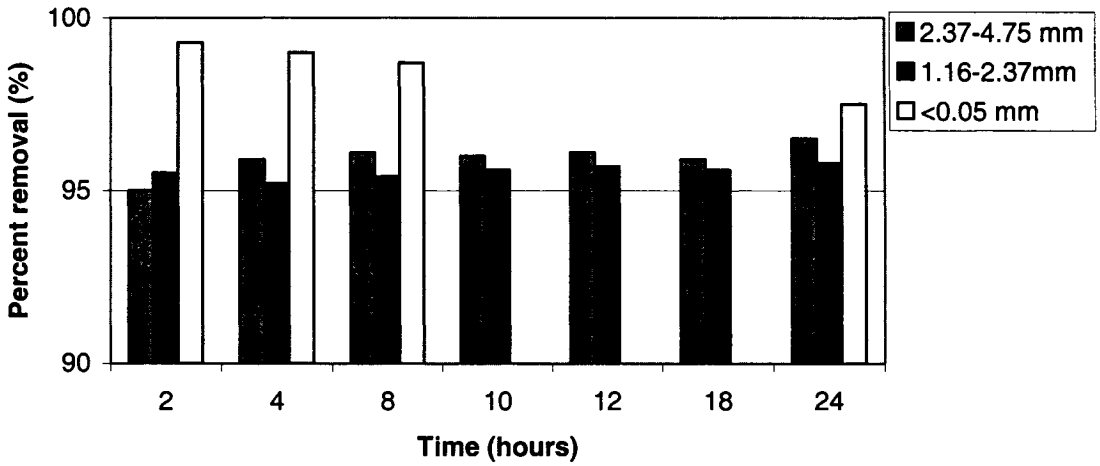

Figures 4.15(b). Percent removal at different size of scale (initial concentration 10 ppm)

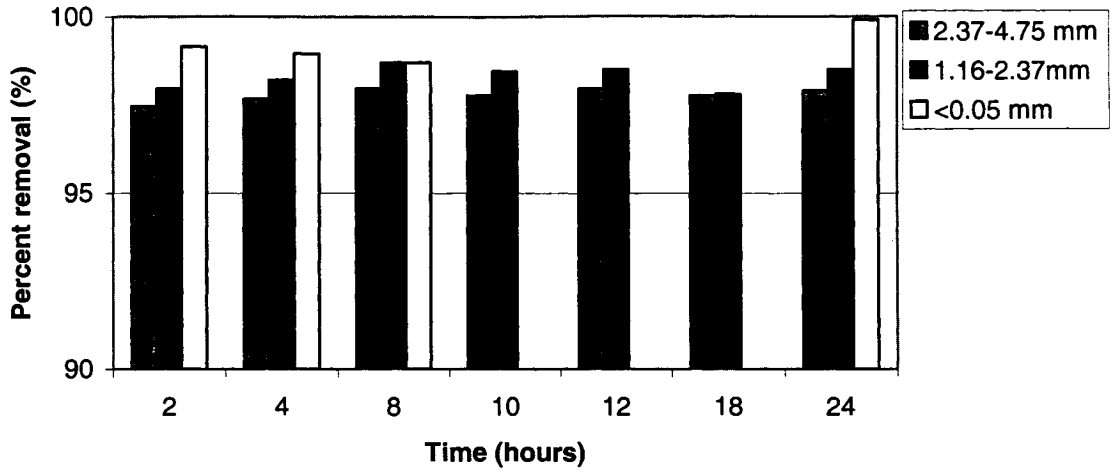

Figures 4.15(c). Percent removal at different size of scale (initial concentration 20 ppm)

Figures 4.15 (a), 4.15 (b), 4.15 (c) and 4.15 (d) display the effect of grain size on removal of Lead cation. The effect of initial concentration is observed in the range of 5 ppm to 40 ppm. For this range, the experimental results demonstrate that the removal efficiency is high. The important feature is that for a wide range of grain sizes and for a variation

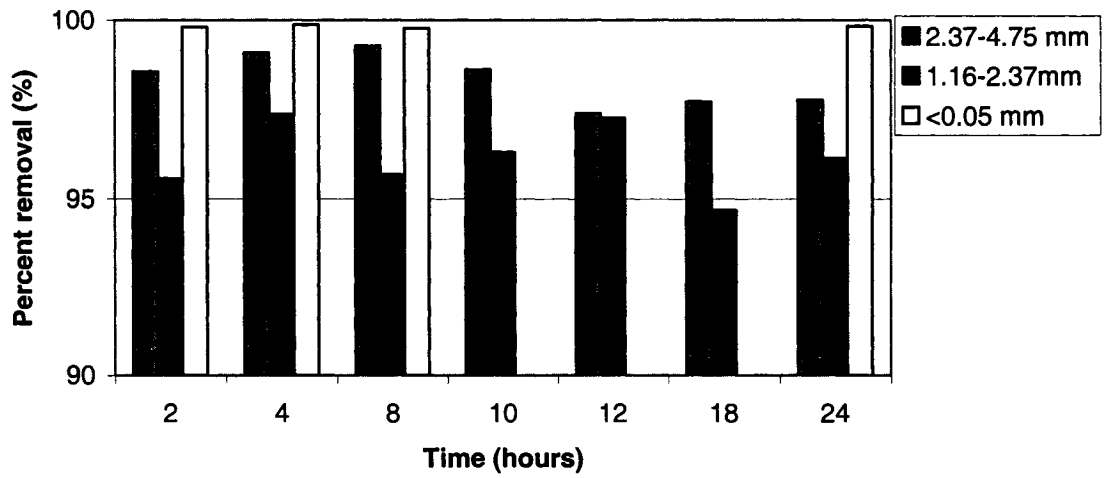

Figures 4.15(d). Percent removal at different size of scale (initial concentration 40 ppm)

between less than 0.05 mm to a maximum of 4.75 mm, the removal efficiency is over 95% in almost all cases. The percentage removal is within percentage error limit and the results signify that adsorptivity of the contaminant is independent of particle size of the adsorbent. Say *et al.* (2001) and Park *et al.* (1999) reported the maximum sorption could be observed at an alkaline pH level and that is observed in this experiment as well as was observed for pulverized samples. The time factor demonstrates that over 95% removal of the cations is achieved in first two hours. It can be generalized to some extent that the effect of particle diameter on solid phase diffusion coefficient and mass transfer coefficient is minimal. In this case, the adsorption appeared to be almost identical for different sieve sizes. Much of the adsorption in fish scales is related to the pore sizes of the adsorbent. While developing the numerical model, the internal porosity and the external voidage will be taken to consideration for adsorption of the cations. The charge density of the Atlantic Cod scales is estimated (using a 3mm dia particle) to be .082 coulombs per cm^2. The structure of the Atlantic Cod scale (discussed in detail in Chapter 7) illustrates that it is a composite of long chain polymers. After extreme pulverization, most of the original sites remain intact with some possible attrition of the end functional groups. Thus, the effects of grain size of the biomass on adsorption of lead ions are nominal. Bio-adsorbents such as Sargassum chips also displayed that particle size did not affect the rate of adsorption (Yang and Volesky, 1999).

4.2 Results and discussion of dynamic tests with cations

The results of all of the dynamic runs performed are discussed in this section. The contaminant for all Atlantic Cod tests is Lead and the contaminant for all single component Shouairi runs is Cobalt. While discussing the results, the associated parameters that can affect the breakthrough behavior will also be highlighted. Results are expressed in dimensionless time, pore volume, PV. (PV = cumulative water injection by pore volume available).

4.2.1 Effect of physical parameters (initial concentration and flow rates) on breakthrough values (Cod original mass scale)

Runs 1, 2 and 3 represent the original mass Cod scale dynamic tests. These runs are the first dynamic runs being reported with respect to Atlantic Cod Scales.

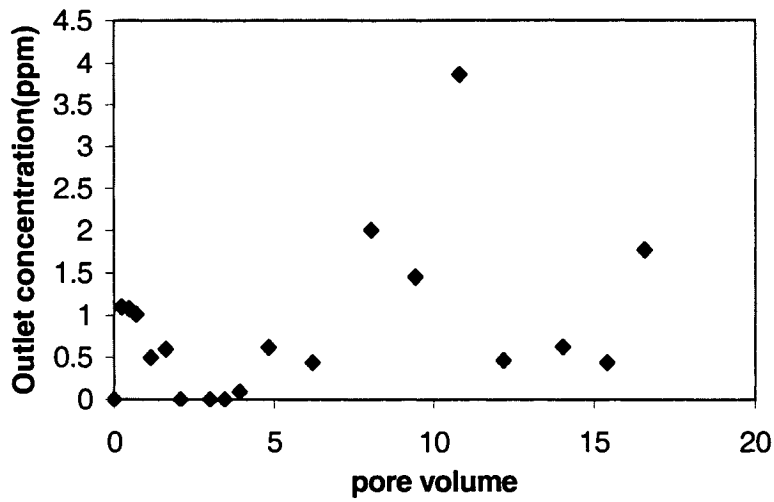

Figure 4.16. Breakthrough curve for Lead (initial concentration = 40 ppm, flow rate = 8 ml/min)

The selections of the values of the parameters (flow rate and initial concentration, in all the runs) were invoked to observe the combined effect on breakthrough intervals.

Figure 4.16 illustrates the rate of decrease of outlet concentration with dimensionless time (pore volume). In order to determine if removal of lead ions from the bulk phase does take place, the first three runs are conducted by considering the effect of variation in feed rate, initial concentration of the adsorbate and porosity of the medium on the breakthrough behavior of the dynamic tests. The initial concentration of lead is 40 ppm. At a pH level of 7, the adsorption phenomenon is dominant even after injection of 4 pore volumes. Since the charge density is perhaps considerably high, most of the ions are adsorbed. In fact, at a flow rate of 8 ml/min, after 15 pore volumes, over 98 % of the pollutant is removed.

Increasing the initial concentration of lead to 470 ppm and maintaining a flow rate of 4.5 ml/min, an early breakthrough behavior is observed (3.13 pore volume). (Figure 4.17).

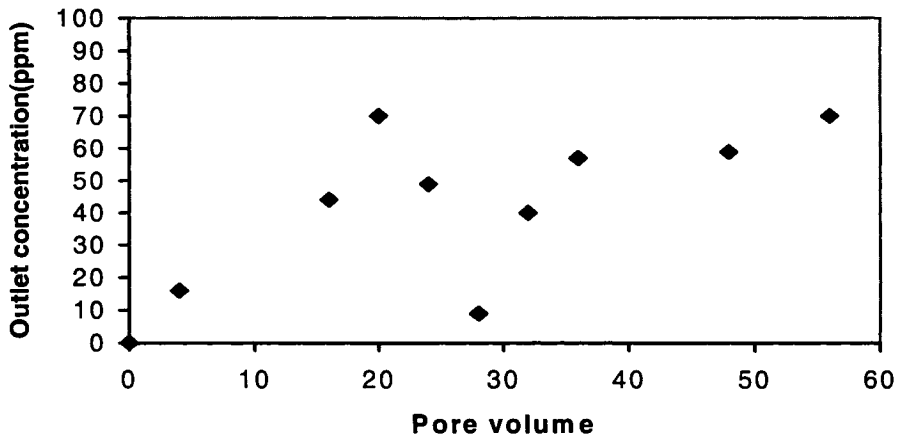

Figure 4.17 Breakthrough curve for Lead (initial concentration = 470 ppm, flow rate = 4.5 ml/min)

In fact, this implies that increase in initial concentration from 40 ppm to 470 ppm may have adversely affected the sorption behavior (Figure 4.17). The decrease in flow rate may have initiated an earlier breakthrough interval. Also the possibility of sufficient number of adsorption sites available for the removal of cations cannot be neglected.

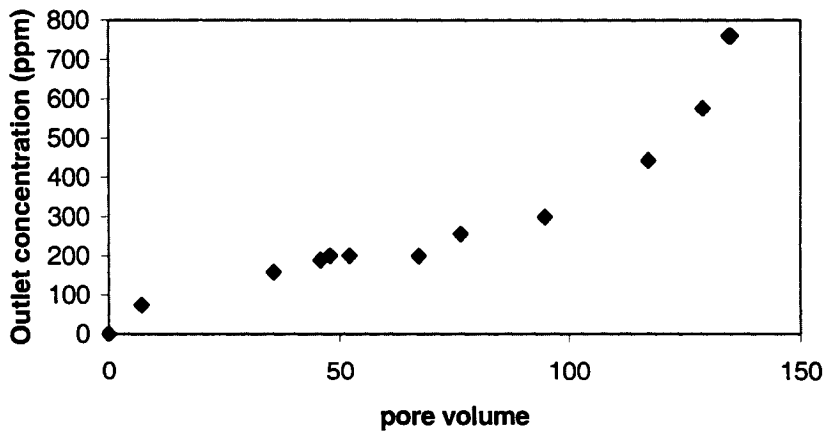

Figure 4.18 Breakthrough curve for Lead (initial concentration = 988 ppm, flow rate = 3 ml/min)

However, increasing the initial concentration to 988 ppm of Lead solution (Figure 4.18) resulted in a breakthrough after injection of approximately 4 pore volumes. Comparing to Figure 4.16, an increase in initial concentration did not initiate an early breakthrough but it is possible that a decrease in flow rate in case of run 3 might have annulled the effect of concentration.

4.2.2 Effect of physical parameters on breakthrough values on pulverized mass scale (Atlantic Cod)

Initial testing of pulverized scale was conducted in Run 4. This dynamic run with pulverized scale could not be continued to for various reasons. Initially, there was no problem in the run and the scale powder was gradually being saturated. But after a short period of time, the highly granulated adsorbent was adsorbed with water. The filter paper placed in the mouth of the entry point of the column was clogged. The pumping rate was maintained constant but no progression of stream flow occurred within the column, thereby increasing the pressure in the tube. Finally, the tube was disconnected from the system. The water molecules are adsorbed on the substrate that results in swelling of the porous medium. Hydrogen bonding is the dominant mechanism that resulted in binding of the water molecules to the substrate of the fish scale.

4.2.3 Effect of physical parameters on breakthrough values on treated mass scale (Atlantic Cod)

Figures 4.19 and 4.20 illustrate the breakthrough curves for treated Cod scale in runs 5 and 6. The breakthrough time interval in case of Run 5 is observed after 12 pore volumes and the system attains saturation after injection of 40 pore volumes. Comparing this run with run 2, the breakthrough interval is larger in this run. This is in sharp contrast to Run 2, for which significant breakthrough of the contaminant was observed after approximately 3.13 pore volumes. The amount of adsorbent in case of the Run 5 is less

than half used in case of Run 2. For the first 12 pore volumes, the adsorption in case of run 5 is higher than in Run 2.

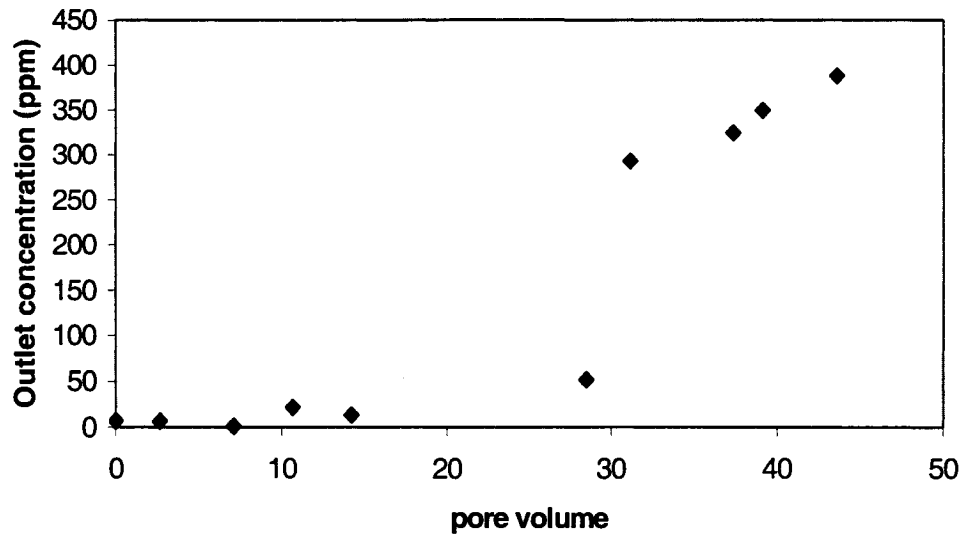

Figure 4.19 Breakthrough curve for Lead (initial concentration = 470 ppm, flow rate = 6 ml/min) (pH of influent is 7.00)

This is likely because of the negatively charged sites that are available through treatment of Caustic Soda solution (Mustafiz, 2002). However, after injection of 12 pore volumes, the amount of adsorbent available and flow rate of the influent outweighs the effect of the caustic treatment of the adsorbent and the trend seems to be reversed. The pH of the effluent is observed to be 7.1 after injection of 40 pore volumes.

It can be observed from Figure 4.20 that for 470 ppm, an appreciable breakthrough takes place after 14 pore volumes. For an initial concentration of 1050 ppm as illustrated in Figure 4.20, the breakthrough is initiated after approximately 12 pore volumes. An interesting feature is that there is no significant discrepancy in breakthrough behavior between Run 5 and Run 6. In other words, the effect of original concentration of the contaminant did not significantly affect the breakthrough behavior. The mass of the adsorbent is 16 grams more in Run 6 than in Run 5. This indicates an extra number of

sorption sites in the case of Run 6. However, the mobility of the cation is perhaps a very significant parameter resulting in an insignificant change in breakthrough behavior at identical flow rates.

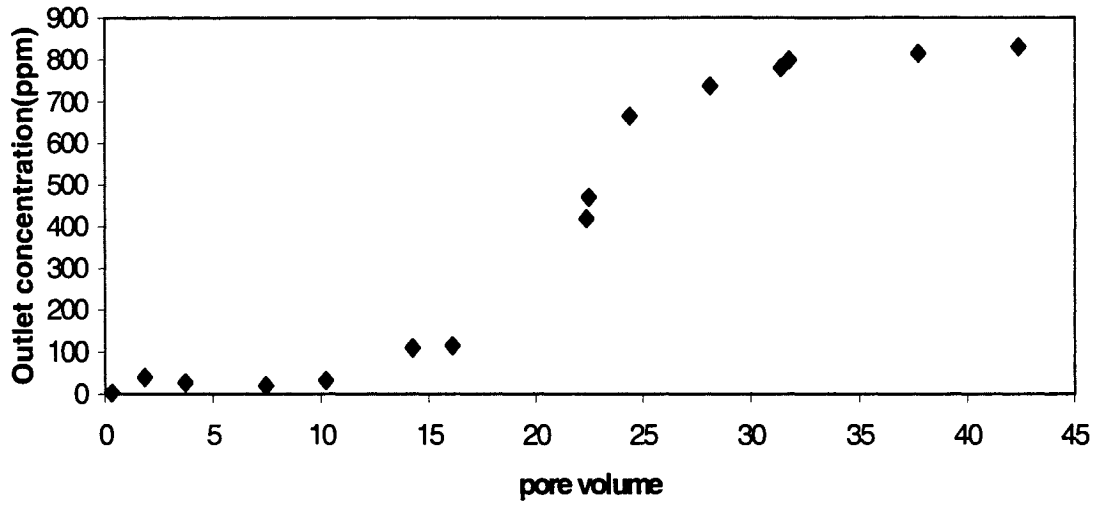

Figure 4.20 Breakthrough curve for Lead (initial concentration = 1050 ppm, flow rate = 6 ml/min) (Run 6)

4.2.4 Effect of physical parameters on breakthrough values on treated mass scale (Shouairi)

Some characteristic breakthrough curves have also been determined for Shouairi fish scale.

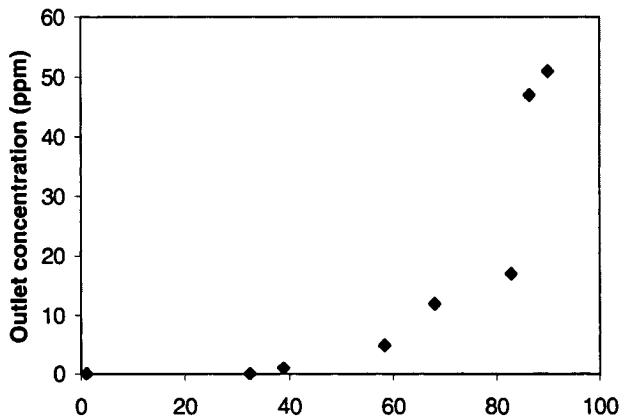

Figure 4.21 Breakthrough curve for Cobalt (initial concentration = 50 ppm, flow rate = 1 ml/min) (Run 7)

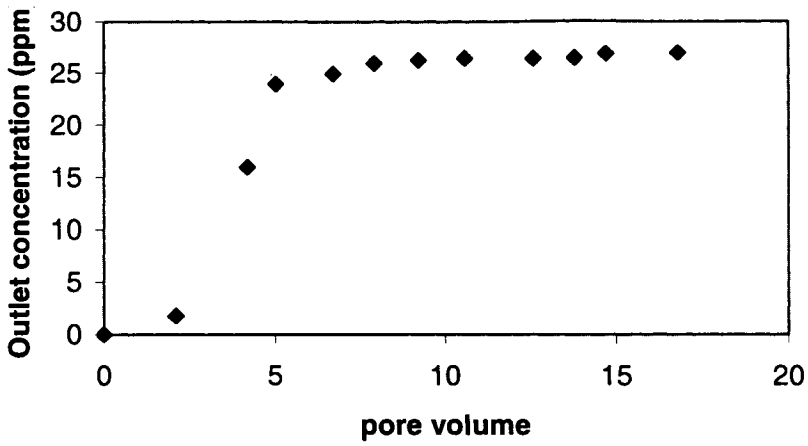

Figure 4.22 Breakthrough curve for Cobalt (initial concentration = 100 ppm, flow rate = 7 ml/min) (Run 8)

Figures 4.21, 4.22 and 4.23 (Runs 7-9) display the breakthrough curves for Cobalt cation on treated Shouairi scale. Comparing the breakthrough curves of Figure 4.22 and 4.23, it can be observed that with an increase in flow rate from 7ml/min to 55 ml/min, the breakthrough is achieved after injection of 1 pore volume. In contrast, in case of Run 8, the desired effect is achieved after injection of 2.5 pore volumes.

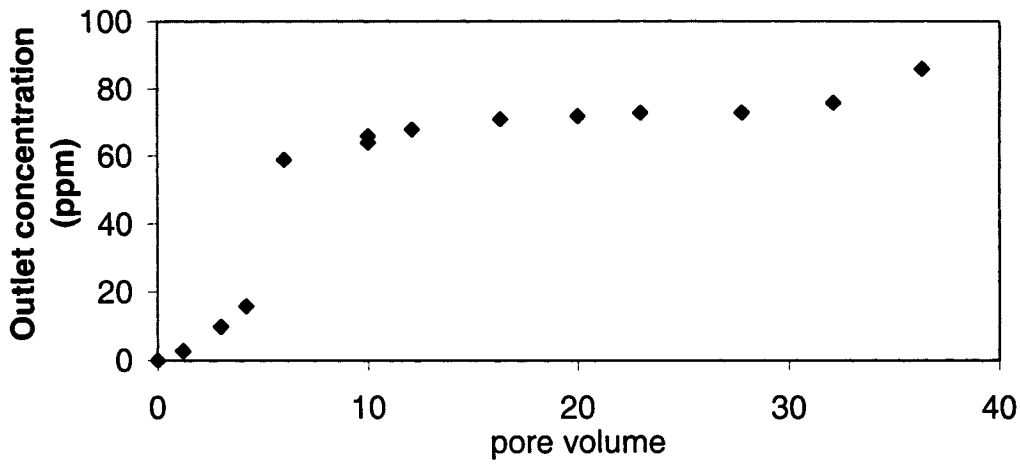

Figure 4.23 Breakthrough curve for Cobalt (initial concentration = 100 ppm, flow rate = 55 ml/min) (Run 9)

The breakthrough interval in case of run 8 is considerably higher than Run 9. At both lower flow rates and initial concentrations, the breakthrough behavior is considerably enhanced compared to higher values.

Run 10

Run 10 consist of a multi-component case. Figures 4.24 through 4.28 represent the outlet concentration as the function of time interval for each species. The contaminant phase is a mixture of strontium, cobalt, zinc and lead. Unlike in single component solutions, a constant flow rate may not allow a uniform mobility of all the cations in the contaminant phase. The mobility of each contaminant is dependant on its inheriting retardation factor and is independent of the values of its co-ions at a specific flow rate of the medium.

From Figure 4.24, it is observed that in case of strontium ions in the mixture, breakthrough did take place after the first 12 minutes as the scale adsorbed the influent.

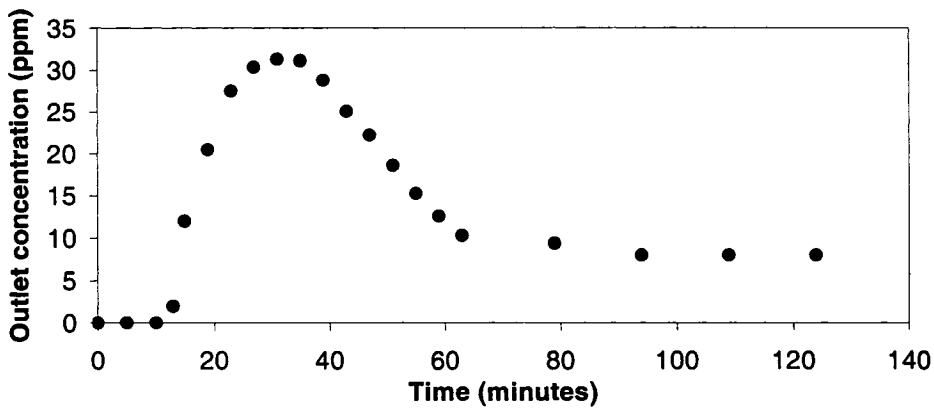

Figure 4.24 Strontium breakthrough in the mixture (Run 10)

This might be due to the fact that strontium is competing with lead and zinc ions and both display tremendous affinity for the adsorbent. As a result, a concentration gradient develops between the adsorbent and bulk phase already present. The strontium ions with the least electron affinity among the four species may diffuse back into the bulk phase

(Lide, 1991). Eventually this may result in a cation exchange mechanism with adsorption of lead and zinc ions. However, significant presence of adsorption sites (discussed in Chapter 7) resulted in proportionate increase in adsorption of lead, zinc and strontium ions. Further, note that all the zinc and lead ions are being adsorbed during that time interval (Figures 4.26 and 4.27). This is due to the combined effect of coordinate linkage, electrostatic attraction and ion exchange (Sarwar and Islam, 1997).

It can be seen from Figure 4.25 that in case of cobalt ions, the equilibrium time interval is attained after 200 minutes. Cobalt appeared in the exit solution after 25 minutes. However, Lide (1991) reported that cobalt ions exhibit higher electron affinity than strontium ions. This behavior is illustrated by the fact that after 50 minutes, the vacant adsorption sites were still being preferentially filled first by the cobalt ions.

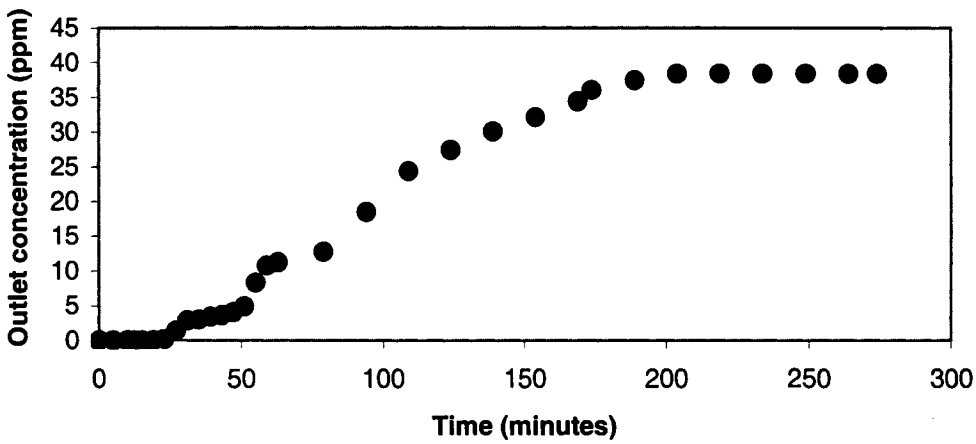

Figure 4.25 Cobalt breakthrough in the mixture

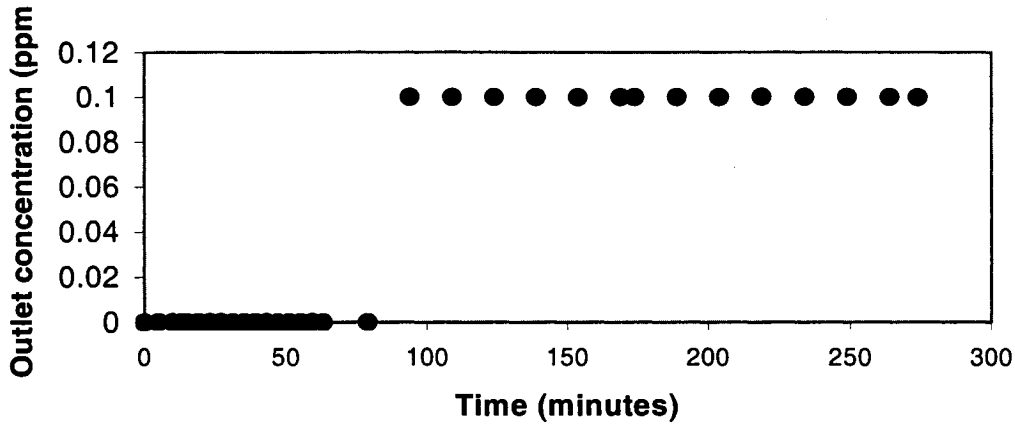

Figure 4.26 Lead breakthrough in the mixture

Figure 4.26 displays the breakthrough curve of Lead ions in the mixture. The larger size of the lead ion is a criterion for lesser mobility. Hence, the residence contact time of the Lead ion with the adsorbent will be higher. Even though Figure 4.26 shows a breakthrough after 75 minutes, this is within a very short range, from 0 ppm to 0.1 ppm. So, breakthrough really did not occur until even after 274 minutes.

For the zinc solution, the electron affinity is unstable. Since the ionic radii of zinc ions are smaller than those of lead ions, it is concluded that the affinity will be lower in comparison to the lead ions. Secondly, due to lower atomic weight, the mobility of zinc ions is greater than that of lead ions. All these factors mentioned above should lead to higher adsorptivity of lead ions in comparison to zinc ions.

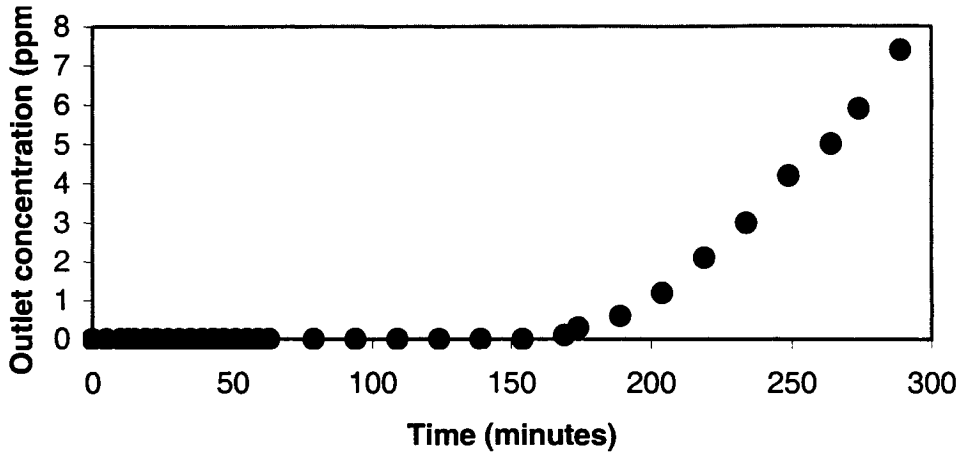

Figure 4.27. Zinc breakthrough in the mixture

The breakthrough curve of the zinc component in the mixture is shown in Figure 4.27. Although the zinc ions break through after 150 minutes, the total amount of Lead ions adsorbed is higher than Zinc ions after 5 hours. However, specific complexation mechanisms may allow zinc to inherit a higher selectivity with respect to a ligand.

4.2.5 Effect of different parameters in dynamic tests

The effect of type of adsorbent, feed rate, state of adsorbent and concentration of solute in the feed will be discussed in this section.

4.2.5.1 Effect of flow rate

Runs 2 and 3 are compared to analyze the effect of flow rates with respect to breakthrough behavior. Contrary to common perception that an increase in flow rate is correlated to decrease in breakthrough behavior, the trend is reversed in this case. The plug flow behavior of the bulk phases for both runs is in a laminar range. At laminar flow, the breakthrough recovery is directly proportional to the feed rate. Later at a transition range, the breakthrough behavior is constant with respect to increase in flow rate. At turbulent flow rates, the breakthrough behavior decreases with increase in flow rates. It has been reported that with increasing flow rates in a fixed-bed adsorption column, the film thickness encapsulating the biomass decreases (Worstell, 2004). A

decrease in film thickness is directly correlated to increase in mass transfer coefficient. However at higher flow rates (turbulent), viscous forces outweigh the effect of dispersive forces resulting in decrease of breakthrough intervals.

4.2.5.2 Effect of initial concentration of cations at identical flow rates (Runs 5 &6)

For Cod Runs 5 and 6, the breakthrough interval slightly decreases with an increase in initial concentration from 470 ppm to 1070 ppm. The adsorbate-to-adsorbent ratio is higher in run 6 than run 5 and a long-delayed breakthrough was expected in case of the latter. The amount of adsorbent for run 5 is 16 grams less than in Run 6. It can be stated that the adsorption phenomenon is non-linear in nature. The sensitivity of breakthrough behavior to certain parameters is unique for different ranges of parametric values. The effect of precipitation of lead ions with respect to treated adsorbents cannot be ignored.

4.2.5.3 Effect of state of adsorbent (runs 2 and 5)

The variables considered for comparison of breakthrough intervals in runs 2 and 5 include:

i. Nature of adsorbent (treated or non-treated)
ii. Flow rates of the influent solutions
iii. Mass of the adsorbent used for each column

The state of the adsorbent often dominates the adsorption behavior in a dynamic system. Figure 4.28 shows that breakthrough arrival occurred earlier using treated Cod scales than for original scales. The test with treated sample is associated with a higher flow rate (6 ml/min for treated and 4.5 ml/min for original). After injection of 37.5 pore volumes (Figure 4.18), 59 ppm of the contaminant is observed at the outlet for original Cod scale. After injection of 37.5 pore volumes, the outlet concentration is 388 ppm for treated Cod scale runs (Figure 4.19). It demonstrates that the original sample of Cod scale has higher adsorptive capacity relative to the treated sample. A bar graph displays that the original

Cod sample had better adsorption characteristics than the treated sample (Figure 4.28). This perhaps explains that besides treatment of the adsorbent, the mass of the substrate makes a significant contribution to the adsorption behaviour.

The equilibrium pH of both the effluents determined was in range of 6.5-7.0

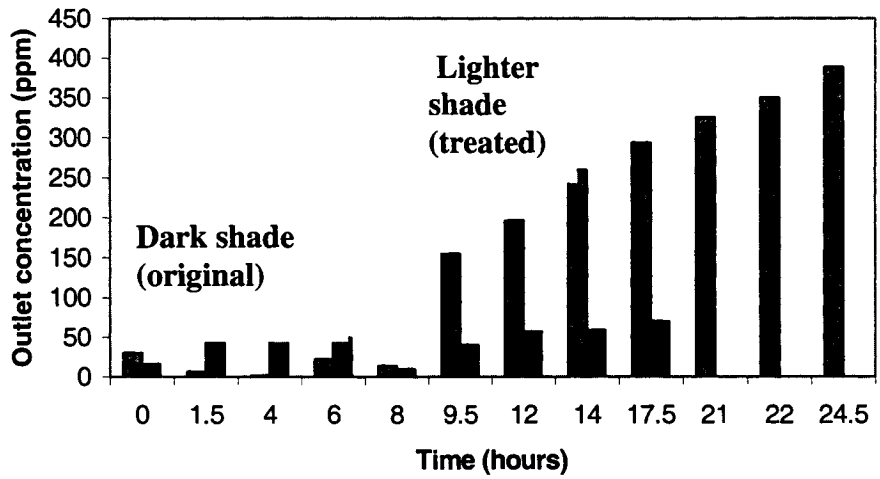

Figure 4.28. Effect of state of scale in dynamic test

4.3 Numerical Modeling of Heavy Metal Cations (lead and cobalt)

In the present study, the concept of surface excess is used to model adsorption of the lead cations on fish scales. Modeling the adsorption process in a solid/liquid interface using surface excess is not new. Mannhardt and Novosad (1988) evaluated the adsorption of three types of foam-forming surfactants (diphenylether sulfonate, betaine and sulfo-betaine) at different conditions of temperature and salinity. These surfactants are anionic components. The mechanism(s) underlying their adsorption is (are) electrostatic in nature. Manhardt and Novosad attempted to develop a surface excess model for the description of surfactant adsorption of widely varying chemical structures and found that the monolayer assumption and simple first order kinetics to be adequate for modeling the system. It was also concluded that the surface excess model could be more flexible in

matching various types of breakthrough curves than a model based on the Langmuir isotherm. This model is particularly suitable for water purification problems that have a non-symmetric adsorption-desorption profile. Conventional models fail to capture this phenomenon (Song and Islam, 1994a). The surface excess concept was also extended to a multi-component system (Islam and Chakma, 1991; Song and Islam, 1994b).

4.3.1 Theory

For a single component solution such as a Lead or Cobalt, the surface excess equation has been given as (Song and Islam, 1994b):

$$n_1^e = n'(x_i' - x_i) \tag{4.2}$$

where i =1 (lead cation) or 2 (distilled water).

The above equation assumes that the bulk phase is the only phase in contact with the adsorbed phase. The model is valid for water wet porous media. Using the monolayer adsorption model, surface excess can be defined as:

$$\frac{1}{n'} = \frac{x_1'}{m_1} + \frac{x_2'}{m_2} \tag{4.3}$$

where m_1 and m_2 represent the amount of monolayer coverage for the contaminant and solvent, respectively.

The relative distribution of the contaminant in the aqueous and the adsorbed phases can be expressed by the selectivity term, S, which is expressed as:

$$S = \left(\frac{x_1'}{x_2'}\right)\left(\frac{x_2}{x_1}\right) \tag{4.4}$$

With the selectivity term expressed as in Equation (4.4), the surface excess model can be written as:

$$n_1^e = m_1 x_1 x_2 (S-1)\left(Sx_1 + \left(\frac{m_1}{m_2}\right)x_2\right)^{-1} \tag{4.5}$$

The actual surface excess of contaminant is given by:

$$n_1^{ea} = (m_1 x_1 S)\left(Sx_1 + \left(\frac{m_1}{m_2}\right)x_2\right)^{-1} \tag{4.6}$$

The one-dimensional mass transfer equation that includes adsorption and mechanical entrapment is given by (Ali and Islam, 1998):

$$\left(\frac{\lambda q \rho_1}{A\phi}\right)\left(\frac{\partial^2 x_1}{\partial x^2}\right) - \left(\frac{q\rho_1}{A\phi}\right)\left(\frac{\partial x_1}{\partial x}\right) = \left(\frac{1-\phi}{\phi}\right)\rho_r\left(n_0\left(\frac{\partial x_1}{\partial t}\right) + \frac{\partial n_1^{ea}}{\partial t} + \frac{\partial V}{\partial t}\right) \tag{4.7}$$

The dispersion parameter, λ, can be correlated to the apparent diffusivity, D_a, as

$$D_a = \frac{\lambda q}{\phi A} \tag{4.8}$$

The value of D_a can be expressed as a function of pore diffusivity, D_p, and retardation coefficient, R_d, (Bear et al., 1993)

$$D_a = \left(\frac{D_p}{R_d}\right) \tag{4.9}$$

The retardation coefficient depends on the sorption coefficient, K, but also to a large extent on the matrix porosity, ϕ, which for small values may make the retardation coefficient significant (Bear et al., 1993).

$$R_d = 1 + K\frac{(1-\phi)}{\phi} \tag{4.10}$$

Substituting R_d as a function of D_a in Equation 4.10, one obtains-

$$\left(\frac{D_p\phi^2}{\phi + K(1-\phi)}\right)\frac{1}{v} = \lambda \tag{4.11}$$

where v is the velocity of the solution injected into the column expressed as a ratio of flow rate (q) to area (A). Substituting Equation (4.10) into Equation (4.6) leads to

$$\left(\frac{D_p\phi^2}{\phi + K(1-\phi)}\right)\frac{1}{v}\left(\frac{q\rho_1}{A\phi}\right)\left(\frac{\partial^2 x_1}{\partial x^2}\right) - \left(\frac{q\rho_1}{A\phi}\right)\left(\frac{\partial x_1}{\partial x}\right) = \left(\frac{1-\phi}{\phi}\right)\rho_r\left(n_0\left(\frac{\partial x_1}{\partial t}\right) + \frac{\partial n_1^{ea}}{\partial t} + \frac{\partial V}{\partial t}\right) \tag{4.12}$$

From Equation (4.12), it can be concluded that the effect of porosity and sorption coefficient, K, is very sensitive to the dispersion parameter, λ.

The first and second terms on the left hand side represent dispersion and advection, respectively. The first and second terms on the right hand side of the equation represent accumulation and cation loss due to adsorption. The third term on the right hand side represents entrapment of the contaminant.

The central concept behind the theory of the mechanical entrapment term is the representation of both particle and pore size distributions by partitioning the porous medium at any cross-section into pluggable and non-pluggable pathways (Ali and Islam, 1998). This hypothetical division involves the representation of the two branches formed in such a way that one is of smaller pores that can eventually be plugged completely. On the other hand, the non-pluggable pathways cannot be completely plugged because as the pore throat diameter is reduced due to solid deposition, the local speed becomes high enough to entrain deposits out of the pore spaces. Two different laws are applicable for two different pathways. For pluggable pathways, a snowball effect equation 4.15 can be achieved by Equation (4.19) that allows the pores to be completely plugged:

$$\frac{\partial V_p}{\partial t} = \left(\delta + \rho V_p\right) u_p x_1 \tag{4.13}$$

Local speed in a pluggable pathway is related to pluggable permeability and is defined as:

$$u_p = \left(\frac{k_{pi}}{k_p}\right) u \tag{4.14}$$

Absolute pluggable permeability is expressed by:

$$k_p = k_{pi} e^{\alpha v_p} \tag{4.15}$$

For non-pluggable pathways, Equation (4.16) applies:

$$\frac{\partial V_{np}}{\partial t} = -\alpha\left(u_{np} - u_c\right) V_{np} + \beta x_1 \tag{4.16}$$

The total deposition is related to the depositions in pluggable and non-pluggable pores and is defined as:

$$\varphi_i V = f V_p + (1 - f) V_{np} \tag{4.17}$$

However, in porous media of relatively high porosities as in fish scales, the entrapment due to pluggable pores is negligible. Thus, the value of f in Equation (4.17) is reduced to zero.

The kinetic term is calculated as:

$$\frac{\partial n_1^{ea}}{\partial t} = k_i\left(n_1^{e} - n_1^{ea}\right) \tag{4.18}$$

for adsorption $k_i = k_1$, for desorption $k_i = k_2$.

Thus from Equation (4.17)

$$\varphi_i V = V_{np} \tag{4.19}$$

if f is considered to negligible.

Equation (4.20a) can be expressed and modified as:

$$V_{np}^{n+1} = V_{np}^{n}\left(1 - \alpha\left(u_{np} - u_c\right)\Delta t\right) + \beta C_0 \Delta t \tag{4.20a}$$

The significance of the above equation is that the contaminant will not be mobilized until the local speed, u_{np}, becomes greater than the flooding velocity, u_c. If u_{np} is less than u_c, then they are equal in magnitude. Thus the above equation may be simplified resulting in:

$$V_{np}^{n+1} = V_{np}^{n} + \beta C_0 \Delta t \tag{4.20b}$$

Table 4.6 displays the effect of entrapment due to Cobalt and Lead ions in Shouairi and Atlantic Cod scales, respectively. At bulk phase concentrations of 1000ppm of either Lead or Cobalt ions, the flow rates of the influents are varied from 10 ml/hr to 3 ml/hr. The results display that after (4-8) hours, no change in flow rates (due to insignificant change in porosity of each medium) is observed. The value of u_c is determined as the

fluidization velocity in the adsorption column. The parameters α and β are assumed to be invariant with time. For all practical purposes it is postulated that the effect of entrapment is solely due to precipitation of the species in the bulk phase. However, at a pH range from 7-7.5, the effect of precipitation on entrapment is negligible. As an assumption, no charge balance is considered in the surface excess model.

Table 4.6 Precipitation effects

Adsorbent	Cation (ppm) in original bulk solution	Time interval for determining flow rates (hrs)	Flow rates (ml/hr)
Atlantic Cod Scale	1000 (Pb)	0	10
Atlantic Cod Scale	1000 (Pb)	2	10
Atlantic Cod Scale	1000 (Pb)	4	10
Atlantic Cod Scale	1000 (Pb)	8	10
Atlantic Cod Scale	1000 (Pb)	0	6
Atlantic Cod Scale	1000 (Pb)	4	6
Shouairi Scale	1000 (Co)	0	5
Shouairi Scale	1000 (Co)	4	5
Shouairi Scale	1000 (Co)	6	5
Shouairi Scale	1000 (Co)	0	3
Shouairi Scale	1000 (Co)	2	3
Shouairi Scale	1000 (Co)	4	3

Based on the theory of surface excess, the simulator was developed by Mustafiz and co-workers. The results interpreted in the model by the author were compared with the pore diffusion model. The theory behind the Pore diffusion model is discussed in detail in Chapter 6.

4.3.2 Adsorption isotherms

Batch adsorption studies with different concentrations are performed in order to determine the Langmuir isotherms for the removal of cations using fish scales. Isotherms are the representations of the amount of a metal ion adsorbed per unit mass of the adsorbent as a function of the equilibrium concentration in bulk solution, at constant temperature (Faust *et al.*, 1999). It is imperative to construct isotherms to assess the ability of fish scales to remove pollutants. An adsorption isotherm is useful in depicting the variation of adsorption with concentration of adsorbate in the bulk solution at a constant temperature. There are several isotherm models such as Langmuir, Freundlich and the Brunaur, Emmett, Teller (BET) models. In these studies only the Langmuir isotherm is examined. The reason for selecting Langmuir model is because it has been demonstrated that the bio-adsorption mechanism is dependant on thetotal number of adsorption sites available on the substrate. The numerical model is based on pore diffusion theory, which requires the usage of parameters that are derived as Langmuir constants.

The Langmuir model is based on the following assumptions:

i. Molecules are adsorbed at a fixed number of defined sites.

ii. Each site can hold one adsorbate molecule and the binding strength is proportional to equilibrium constant of the molecule or ion with respect to the fish scale.

iii. All sites are energetically equivalent or in other words it is a homogeneous substrate. (This is a limited drawback, because barring pure chemicals, very few substrates are purely homogeneous). However, application of Langmuir

model seemed to be more appropriate than Freundlich model, in case of using sugar –beet pulp as a heterogeneous adsorbent (Reddad et al., 2003).

iv. There is no chemical interaction between molecules or ions adsorbed on neighboring sights, and adsorption is reversible and a equilibrium is attained.

The Langmuir isotherm curve is developed from the following equation (Mustafiz, 2002),

$$q = \frac{q_0 C_e}{K + C_e} \quad (4.21)$$

where

q = Amount of metal adsorbed per unit mass of fish scale (mg/g),

q_0= Capacity of fish scale (mg/g),

C_e= Concentration of the metal in the solution at equilibrium (mg/L),

K= Langmuir adsorption factor (mg/L).

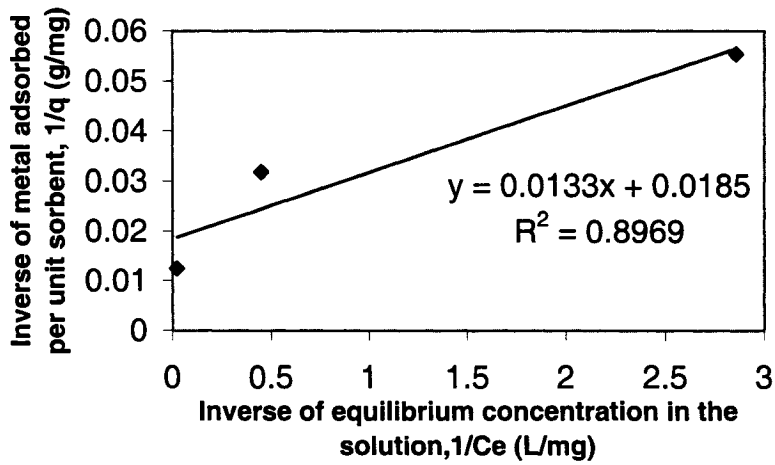

Figure 4.29. Lead isotherm on Atlantic Cod scale (Mustafiz, 2002)

Langmuir isotherm equation (4.21) can be re-expressed in linear form as by plotting 1/q vs. 1/Ce.

$$\frac{1}{q} = \frac{1}{q_0} + \frac{K}{q_0 C_e} \tag{4.22}$$

The experimental results of Runs [2-4] (static) are fitted to the linearized Langmuir model as illustrated in Figure 4.29 and the following values are obtained:

q_0=54 mg/gm

K=0.72 mg/L

where the correlation coefficient of the linear regression (R^2) was found to be 0.896.

Therefore, the model for adsorption on Cod scale is:

$$q = 54\frac{C_e}{0.72 + C_e} \tag{4.23}$$

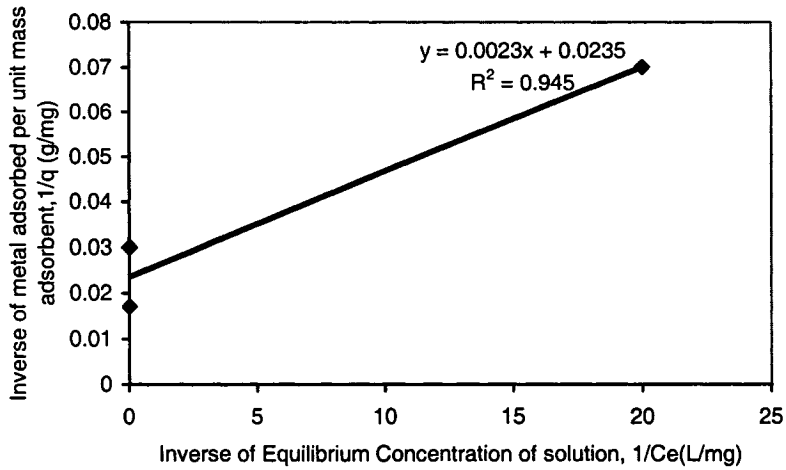

Figure 4.30. Lead isotherm on Atlantic Cod scale (repeated)

This is a non-linear isotherm and to confirm its validity, the run is repeated. It is observed to behave differently from the original run. The limitation of this linearized

model is that it could provide a capacity of 54 mg/g where the experiment result displayed a capacity of 80 mg/g (Mustafiz, 2002).

The experimental results of Runs [2-4] are again fitted to linearized Langmuir isotherm equation are illustrated in Figure 4.30 and the following values are obtained:

q_o= 42.55 mg/g
K = 0.09 mg/l

Comparing these results with that of deduced from Figure 4.29, the percentage errors determined for q_0 and K are 21 and 87 respectively. The results signify that in order to quantify the adsorption behavior scaled experimental models and study of the mechanisms of adsorption is essential.
Hall *et al.* (1966) defined a dimensionless parameter, R_L, as

$$R_L = \frac{K}{K + C_0} \quad (4.24)$$

where

C_o= initial cobalt ion concentration (mg/L)

C_0 can be considered as a separation factor that determines the type of isotherm.
The values of R_L for adsorption of Lead on Cod scale were between 0 and 1, which indicates favorable adsorption of Lead on Cod scale.

Formulation of adsorption on Shouairi scale

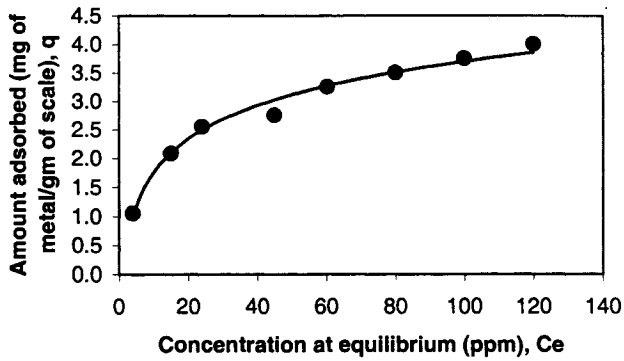

Figure 4.31. Cobalt isotherm on Shouairi fish scale

Figure 4.31 shows the isotherm curve of Cobalt on Shouairi scale. It is based on the eight experimental Runs [8-15]. A best fitting curve displays that the isotherm tends to linearity for higher equilibrium concentrations. A Langmuir isotherm may be applicable for this case.

Fitting the experimental results of Runs [8-15] with the linearized Langmuir isotherm Equation (4.22), the following values are calculated:

q_0=3.812 mg/gm

K=10.69 mg/L

Therefore, the model for adsorption on Shouairi scale can be described by the following equation:

$$q = \frac{3.812 C_e}{(10.69 + C_e)} \quad (4.25)$$

or

$$\frac{1}{q} = \frac{1}{3.812} + \frac{2.80}{C_e} \quad (4.26)$$

The dimensionless parameter (R_L) as described in Equation (4.24) is determined and the values of R_L were between 0 and 1, which indicates decent adsorption of Cobalt cationon original Shouairi scale.

The values of the model adsorptive capacity (q_0) and the adsorption factor (K), the model curve are drawn in Figure 4.33. The estimated ponts fit well with the experimental points. The limitation of the model is that it does not exactly represent the maximum adsorptive capacity of Shouairi scale. In the experimental range, the saturation is not attained as demonstrated by Figure 4.32. However, Figure 4.33 illustrates that with the increase in C_e/C_i, q_{expt} increases, but the slope of q_{model} tends to approach zero.

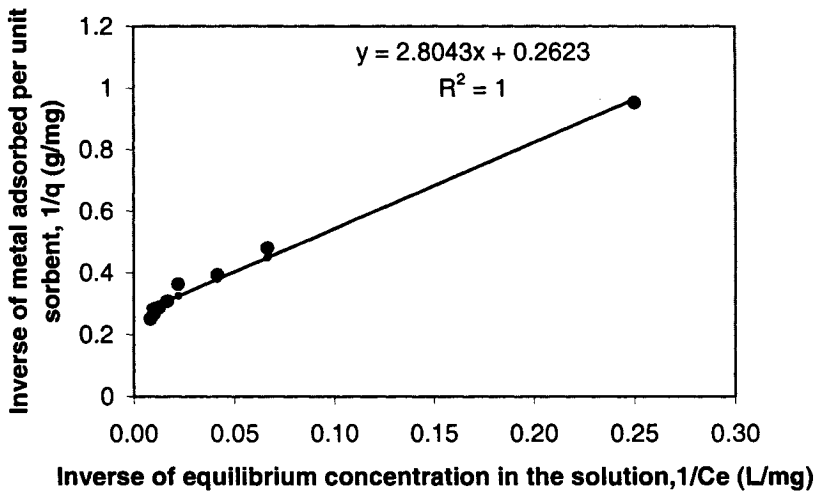

Figure 4.32 Linearly rearranged Langmuir isotherm curve for Cobalt cation on Shouairi scale

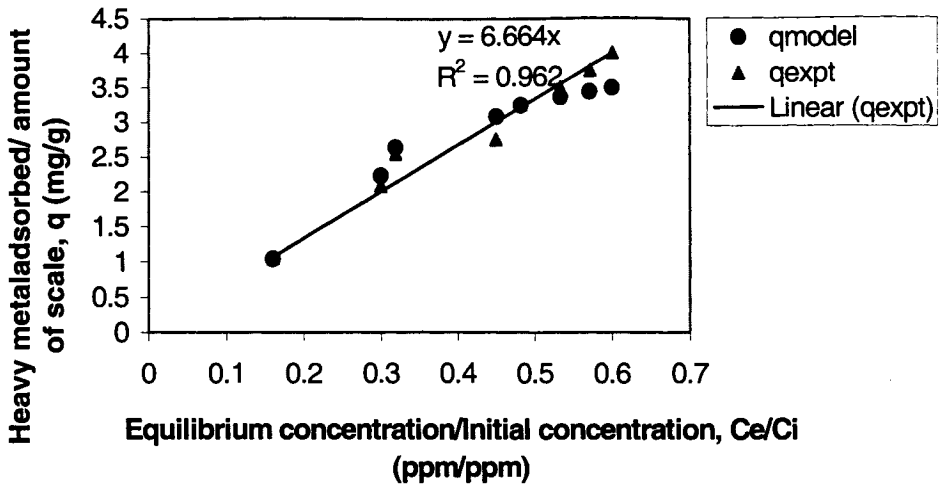

Figure 4.33 Metal adsorbed per unit mass of Shouairi fish scale as a function of Relative concentration

It clearly implies that saturation of the adsorbed phase is possible but experimental runs did not validate it.. In a broader sense, the experimental and simulation results will vary unless the surface of the adsorbent is characterized. Due to limited access of the Shouairi fish scales, the SEM and NMR techniques could not be performed. However, at this stage, it may be assumed that Shouairi fish scale is a composite like the Atlantic Cod scale. Its substrate is accommodated by nucleophilic functional groups that propagate both covalent and electrostatic bonding between the adsorbent and the metal pollutant.

4.3.3 Surface Excess Model Simulations

Six experimental runs were conducted with Lead and Cobalt ions to investigate the effect of flow rate and chemical concentration on the bulk solution . Runs 1 through 3 are in relation to Lead cations and Atlantic Cod scale. Runs 4 through 6 are conducted through a porous medium consisting of Shouairi fish scales (treated with either soap or caustic soda solution). The corresponding solutions for the dynamic runs consisted of Cobalt ions.

Table 4.7: Parametric Values used for numerical simulations
(Note: parameters of runs 1-3 (Mustafiz and coworkers, 2002)

Run	Selectivity, S	Adsorption Cons.t, k (hr^{-1})	Dispersion Parameter, λ (cm)	Water Sorbed/ Sorbent, n^0 (mg/gm)	Flow rate, Q (ml/hr)	ϕ	Density, ρ_a (gm/cm^3)
1	100	1.5	2.0	310	180	0.74	1.67
2	100	1.5	3.0	220	360	0.89	1.67
3	100	1.5	0.5	100	360	0.85	1.67
4	10	0.6	2.0	190	60	0.91	1.75
5	10	0.6	35.0	190	420	0.91	1.75
6	10	0.6	6.0	700	3300	0.91	1.75

The physical and experimental model parameters for Atlantic Cod scale and Shouairi scale runs are given in Table 4.7. The adsorption constant, k, is varied from 0.6 hr^{-1} to 1.5 hr^{-1}. However, it is observed that the adsorption constant, k, and Selectivity, S, are not highly sensitive variables for the range of parameters determined experimentally.

The distinctive feature of the model is that it depends exclusively on the total number of excess sites available for interaction with the contaminant. The dispersion parameter (λ), is a lumped coefficient and it depends on the following parameters

i. The pore diffusivity of the contaminant from bulk phase
ii. The equilibrium adsorption coefficient
iii. The retardation factor of the element
iv. The porosity of the substrate

The above factors do contribute to the overall sensitivity of the dispersion value.

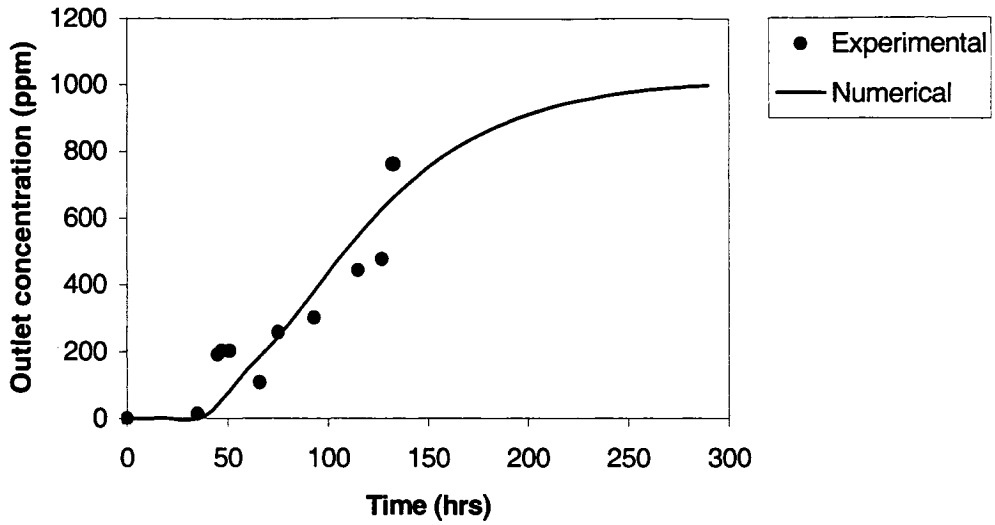

Figure 4.34. Comparison of experimental and numerical results of Lead transport in Atlantic Cod scales (Run 1: flow rate 3 ml/min and concentration 1000 ppm).

The parameters that are sensitive to small perturbations include dispersion, λ, and mass of water adsorbed per unit mass of adsorbent, n^0. A comparison of the numerical and experimental results is shown in Figures 4.34 through 4.39. Figures 4.34 – 4.36 compare the numerical and experimental results for the Atlantic Cod fish-scale. Figure 4.34 illustrates that the breakthrough time interval for Run 1 is determined after 40 hours with a flow rate of 180 ml/hr. The concentration of the influent solution is 1000 ppm for this run. However, in the case of Run 2 (Figure 4.35), breakthrough is observed after 5 hours with a flow rate of 360 ml/hr. The influent concentration for the run is 470 ppm. By increasing the influent concentration to 1000 ppm and maintaining a flow rate of 360 ml/hr (Figure 4.36), there is no significant change in breakthrough time interval. From this set of observations, it can be concluded that the effect of variance in the concentration of the contaminant at identical flow rates did not bear any significant impact on the breakthrough time intervals. Conventionally, an increase in concentration of the influent should have initiated an earlier breakthrough, but the overall effect of porosity may have annulled the effect. The porosity in case of Run 3 was only slightly less than the porosity in case of Run 2. However, since the adsorbent is highly adsorptive by nature (54mg of Lead ions adsorbed per unit mass of the adsorbent at pH 7), a small

decrease in porosity has a profound effect on the adsorption behavior of the cation (Mustafiz et al., 2002). This may have led to the delay of the breakthrough time interval when compared to the originally anticipated break through time in case of Run 3. The porosity for Run 1 was determined to be 0.74. It is comparatively less than those of Runs 2 and 3 (Table 4.7). From Equation 4.15, a decrease of the porosity value can be correlated to an increase in the retardation factor of the influent solution. At higher concentration levels, lower values for porosity confirm an increasingly tortuous path of the cation and, as a corollary, higher probability of being adsorbed to the media. This has resulted in proportionately larger breakthrough time intervals for higher concentration influents (Run 1). However from Figure 4.36 it can be seen that the numerical results do not match well with the experimental run at later time intervals. Non-uniform packing of the adsorbent in the column may have enforced the transport of the contaminants in a largely complex manner.

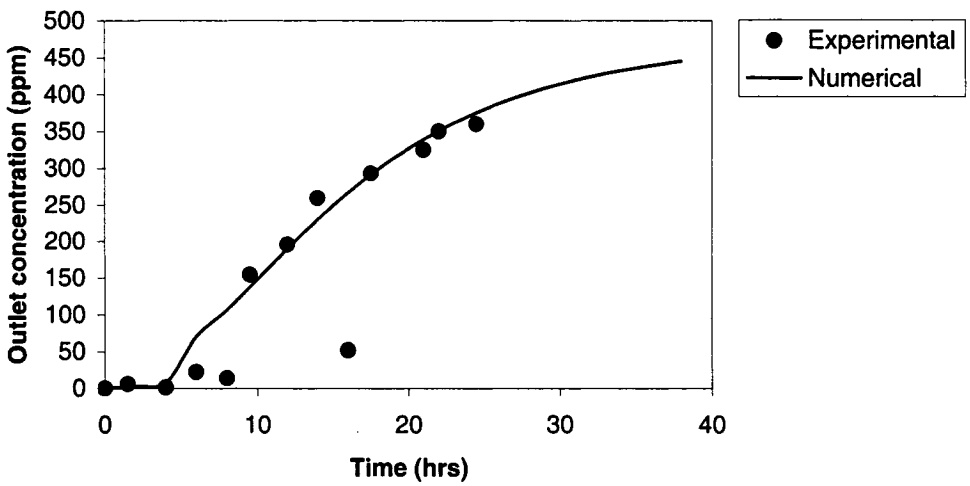

Figure 4.35. Comparison of experimental and numerical results of Lead transport in Atlantic Cod scales (Run 2: flow rate 6 ml/min and concentration 470 ppm)

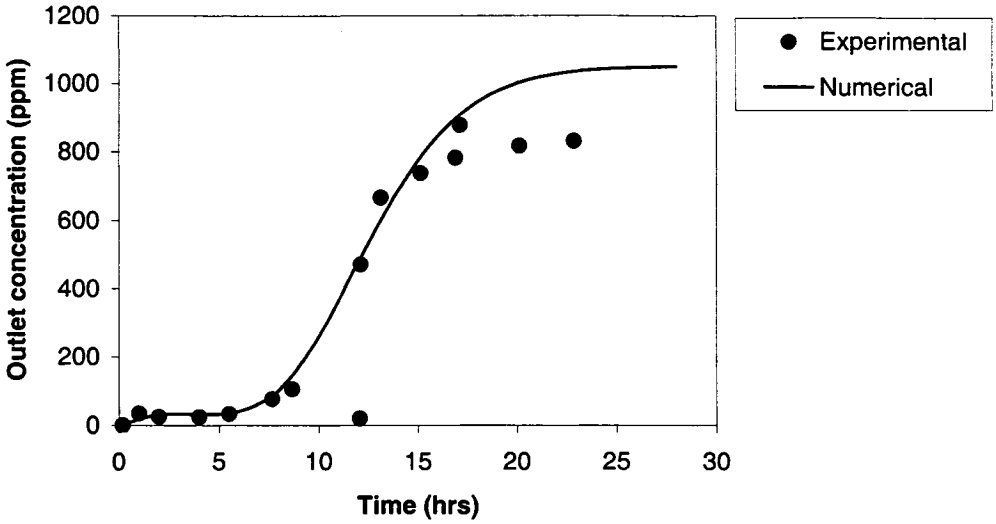

Figure 4.36: Comparison of experimental and numerical results of Lead transport in Atlantic Cod scales (Run 3: flow rate 6 ml/min and concentration 1000 ppm)

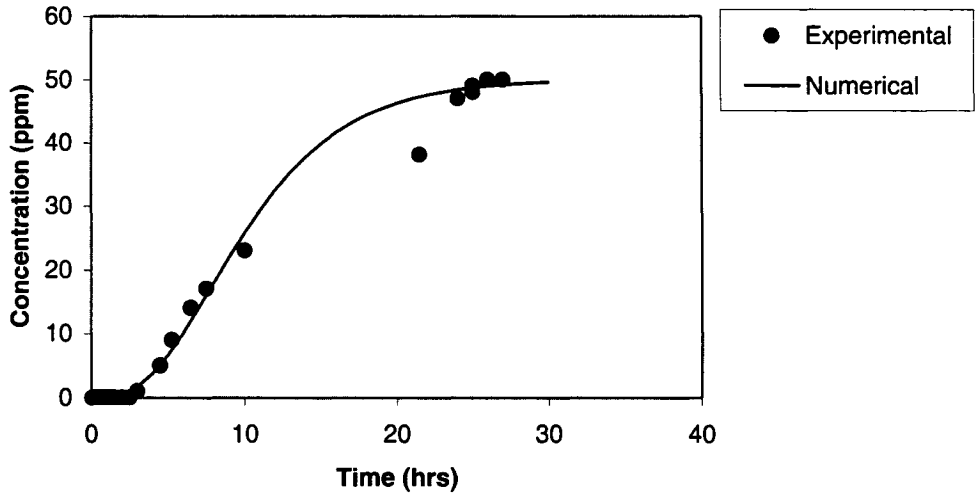

Figure 4.37. Comparison of experimental and numerical results of Cobalt transport in Shouairi scales (Run 4: flow rate 1 ml/min and concentration 50 ppm)

It is also possible that the non-homogenous adsorptive behavior of the medium might have generated higher adsorption after 15 hours. Figures 4.37 shows the experimental and numerical results for Cobalt transport in Shouairi scales with a flow rate 1 ml/min and concentration 50 ppm.

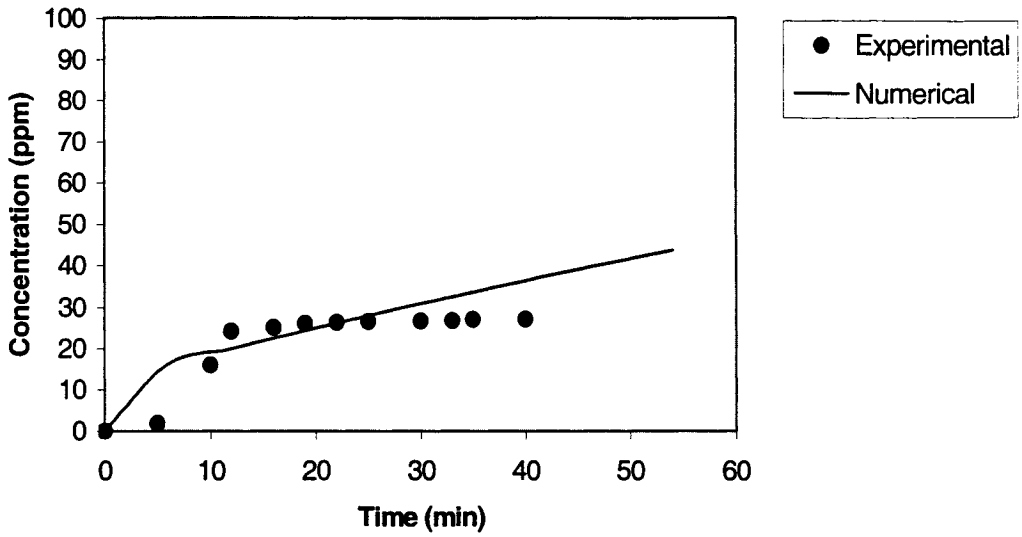

Figure 4.38. Comparison of experimental and numerical results of Cobalt transport in Shouairi scales (Run 5: flow rate 7 ml/min and concentration 100 ppm, NaOH treated)

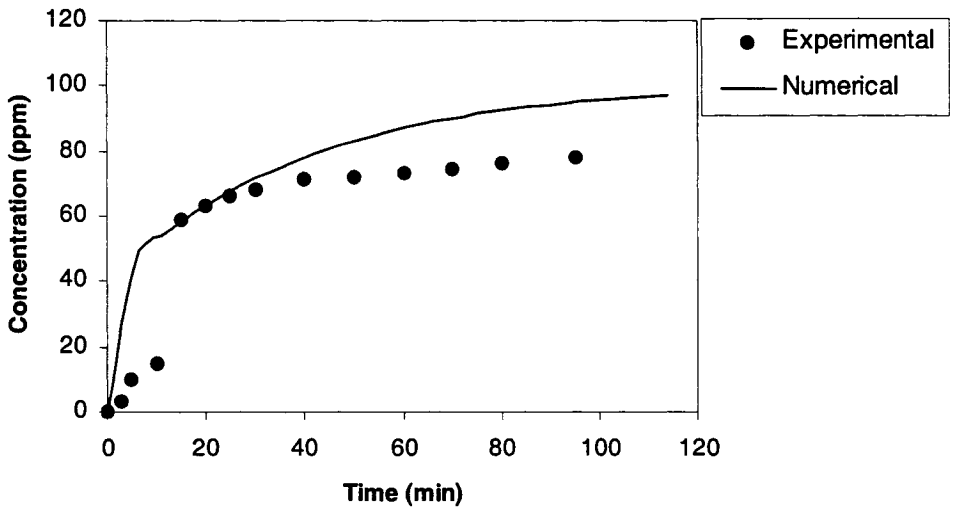

Figure 4.39: Comparison of experimental and numerical results of Cobalt transport in Shouairi scales (Run 6: flow rate 55 ml/min and concentration 100 ppm, NaOH treated)

The numerical results closely matched the experimental values. Figures 4.38 and 4.39 display the experimental and numerical results for concentration of 100 ppm Cobalt

solution with flow rates of 7 ml/min and 55 ml/min, respectively. Both runs with respect to Cobalt ions show a reasonable agreement between experimental and numerical observations. It is noted that, with an increase of flow rate from 7ml/min to 55 ml/min, a significant drop in the value of dispersion parameter, λ, from 35 to 6 is observed. It is found that in relation to both the cations, if flow rate increases, λ decreases provided that the other simulation parameters are constant. On the other hand, if the concentration increases, λ should increase (Sarwar and Islam, 1997). However, from Table 4.7, it is observed that in case of Runs 2 and 3, an increase in concentration of the influent at a constant flow rate did not result in an increase of the dispersion value. The decrease in porosity resulted in an equivalent increase in adsorption, resulting in a proportionate decrease in concentration of the effluent and dispersion value. Thus, it can be concluded that the effect of concentration on breakthrough interval and dispersion value is offset by the effect of porosity of the medium. Using the SEM (Scanning Electron Microscope), it was discovered that the surface of the fish scale is not homogenous in nature. The surface contains specific sites where adsorptions of the metal cations take place. It is highly possible that the adsorbent used for run 6 might have had a higher proportion of such sites leading to increase in adsorption behavior (Figure 4.40).

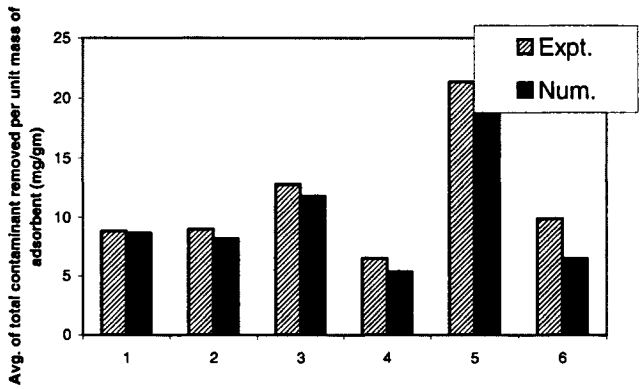

Figure 4.40 A comparison of adsorptivities between experimental and numerical results for all the runs 1-6.

Adsorption values as determined by experimental and numerical procedures are compared in Figure 4.40. This figure shows that the average adsorptivities determined by the numerical runs are slightly less than the adsorptivities measured from the dynamic experimental runs. A number of factors that include non-uniform packing and fluctuation in flow rates in the adsorbent medium may have actually increased the retardation factor than was originally anticipated. It is also probable that the value of entrapment (though negligible) may have contributed to the adsorption-precipitation phenomena resulting in delay in transport of the contaminants. However, since the effect is minimal, the difference in values between experimental and numerical runs is insignificant.

4.3.4 Pore Diffusion Model Simulations

Table 4.8 displays the experimental and enforced parametrs in pore diffusion model.

Table 4.8. Simulation model parameters using pore diffusion model

No.	Flow rate (ml/ hr)	Porosity (Φ)	Initial Conc (ppm)	Amount Adsorbent (gm)	Dp (cm*cm /hr)	Ds (cm*cm/hr)	$C_{t\,(O)}$ Moles/g	$C_{c\,(N)}$ moles/g
1	480	0.78	40	80.00	8	2	$1.2*10^{-3}$	$.52*10^{-3}$
2	270	0.78	470	80.00	8	2	$1.2*10^{-3}$	$.52*10^{-3}$
3	180	0.77	988	85.00	8	2	$1.2*10^{-3}$	$.52*10^{-3}$
4								
5	360	0.91	470	34.00	8	2	$1.2*10^{-3}$	$.52*10^{-3}$
6	360	0.86	1050	49.00	8000	2000	$1.2*10^{-3}$	$.52*10^{-3}$

Note: K1 and K2 (equilibrium constants) for all runs are 1000L per millimole.

Notes:

i. The numerical runs could not be performed on Shouairi scales because no alkametric titration was performed to calculate the variables C_t and C_c. It is also assumed that no carboxyl group is attached to the side chain of the substrate. After considering Langmuir isotherm, it is also assumed that the number of sites involved in adsorption is independent of pH of the bulk phase (Scheiwer et al., 1999).

ii. The important assumption considered in the model is that the adsorption of the cations is exclusively dependent on the ion exchange mechanism. The extent of the influence of both electrostatic forces and precipitation has been ignored.

iii. The value of Q_m is insensitive to the numerical model.

iv. Q_m is 54mg/g and d (langmuir coefficient) is 0.00346 L per mmol

v. The value of overall porosity, Φ, is a combination of external and internal voidages of the medium. The ratio of external and internal porosity is equal to the ratio of surface to pore diffusivities.

The theory behind the pore diffusion model is discussed in detail in Chapter 6. However, at this juncture it can be justified that advantages of pore diffusion model include:

i. The pH of the bulk phase in surface excess model is a lumped coefficient with kinetic adsorption parameter. The effect of pH is significantly coupled with the numerical simulations using pore diffusion model.

ii. The pore diffusion model provides a broader insight to the adsorption mechanisms between the contaminant and adsorbent. Simple match fitting

of numerical simulations with respect to experimental runs may not clearly define a bio-adsorption process (Volesky, 2003).

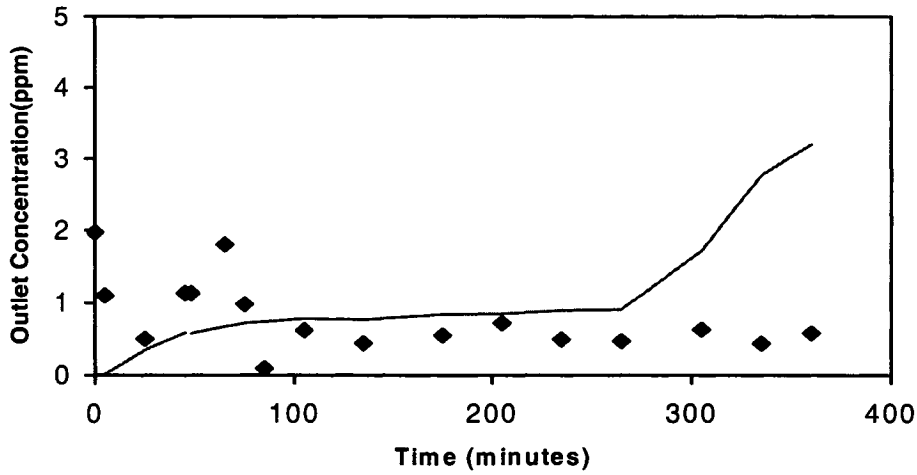

Figure 4.41. Comparison of experimental and numerical results of Lead transport in Cod scales (Run 1: flow rate 8 ml/min and concentration 40 ppm)

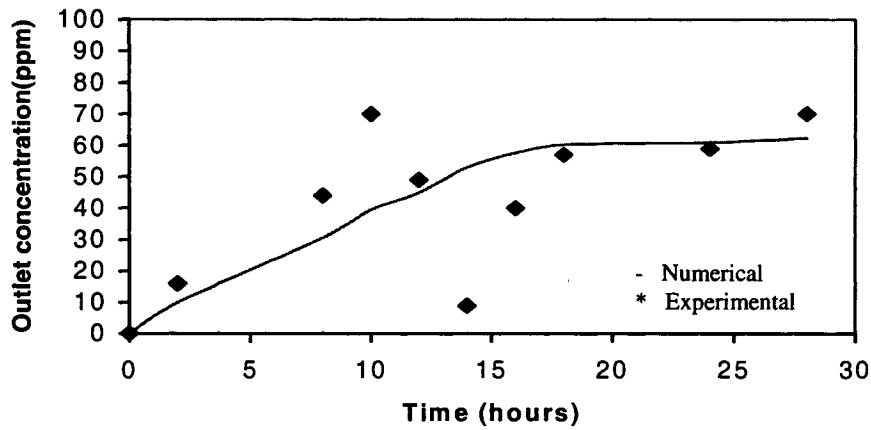

Figure 4.42. Comparison of experimental and numerical results of Lead transport in Cod scales (Run 2: flow rate 4.5 ml/min and concentration 470 ppm)

Figure 4.43 in contrast to earlier runs display significant discrepancy between numerical and experimental run. A significant feature of the Figure 4.42 is the relatively higher

effluent concentration of the contaminant than in cases of Run 1 and Run 2 (Figures 4.41 and 4.42). It is important to understand the nature of the exact mechanism(s) in relation to the bulk and adsorbed phases. It is highly probable that abatement of metal contaminants is a combination of ion exchange, electrostatic forces and precipitation. The significance of precipitation in relation to the ease of attainment of the value of the solubility product at a higher concentration cannot be ruled out.

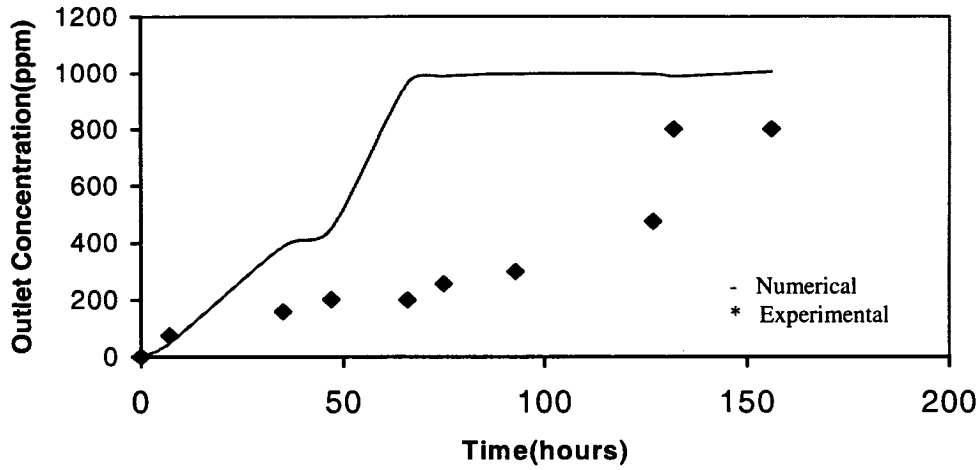

Figure 4.43: Comparison of experimental and numerical results of Lead transport in Cod scales (Run 3: Flow rate 3 ml/min and concentration 1000 ppm)

Figures 4.44 and 4.45 illustrate that near curve fitting of numerical runs with experimental results at higher concentrations of the effluent is possible. This is in clear contrast to run 3. However, the curve fitting in this case is achieved by increasing the values of both pore and surface diffusivities by a factor of 1000. If the adsorption phenomena at higher concentrations display a non – Fickian approach (where diffusivity values are functions of inlet concentrations), then the parameter estimation may hold valid.

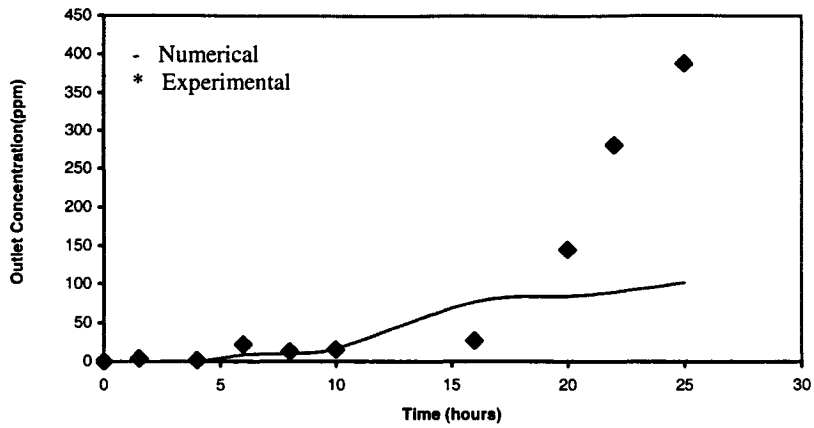

Figure 4.44: Comparison of experimental and numerical results of Lead transport in Cod scales (Run 5: Flow rate 6 ml/min and concentration 470 ppm)

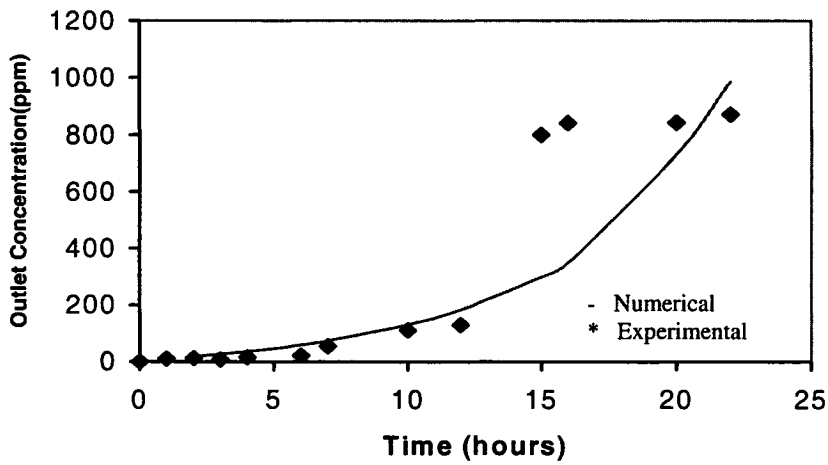

Figure 4.45. Comparison of experimental and numerical results of Lead transport in Cod scales (Run 6: Flow rate 6 ml/min and concentration 1050 ppm)

By coupling the simulation model parameters into the numerical model, the simulations were generated. At this stage, the effectiveness of validating numerical runs to experimental results is debatable. Thus as mentioned earlier, a thorough understanding of

mechanisms underlying adsorption would seem to be a prerequisite for effectiveness of the numerical model.

4.3.5 Reproducibility of the results

The static Runs 2, 3 and 4 and the dynamic runs 4 and 5 were repeated twice to observe the variance of the results in Figures 4.46, 4.47 and 4.48.

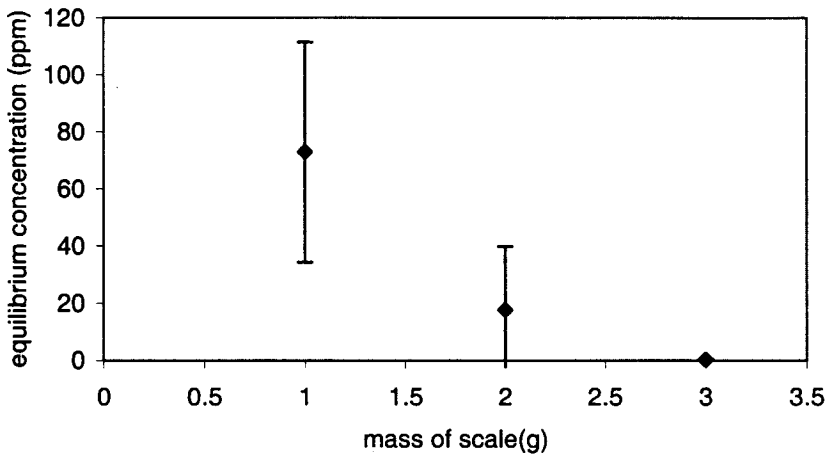

Figure 4.46. A study of Runs 2, 3 and 4 (static) n=2

Figure 4.46 displays that with increase in mass of the adsorbent, the standard deviation is considerably reduced. This implies that with increase in adsorption sites, the variance in equilibrium concentrations of the cation is reduced. In case of Figures 4.47 and 4.48, the standard deviation is significant in mid intervals signifying that fluctuations in pore velocities have a significant impact on effluent concentrations. However, un-scaled dynamic runs (e.g. in petroleum industry) are never repeated. There are no changes in the analyses if an error bar is added. Un-scaled dynamic runs are conducted to illustrate the comparison of the phenomenon with respect to various physical parameters.

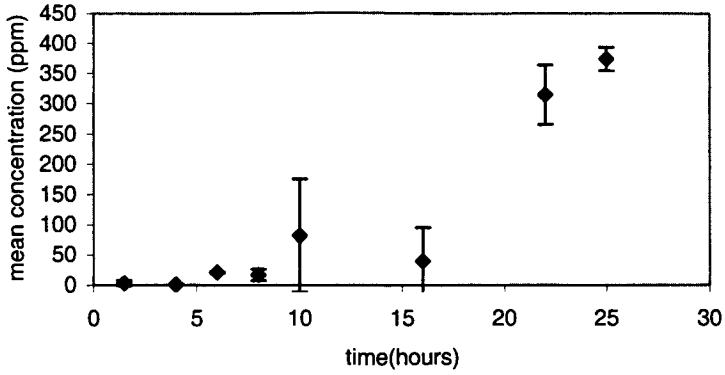

Figure 4.47. A study of Run 4 (dynamic) n=2

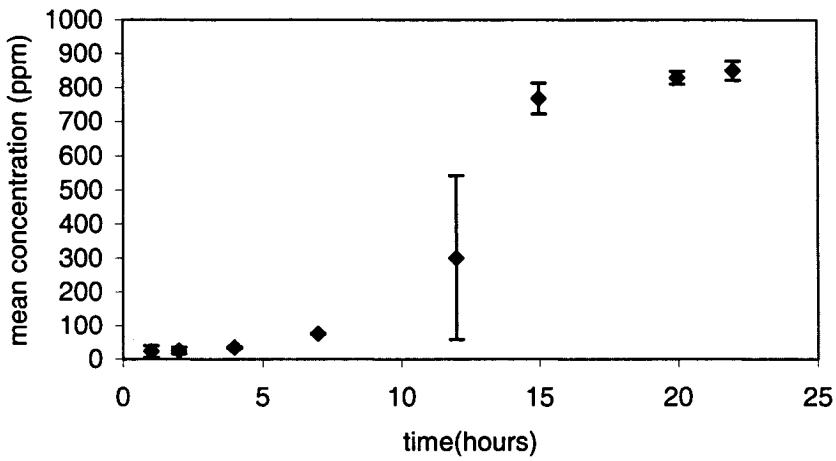

Figure 4.48. A study of Run 5 (dynamic) n=2

It has been reported that limitations in reproducibility continue to be a major problem that stems from unknown variables (Miles et al., 1995). Such problems in relation to adsorption may be attributed to a host of parameters that include the nature of the substrate (Haferl et al., 2001).

The parameters that may contribute to limitations in reproducibility in adsorption may include:

i. The total number of adsorption sites per unit mass of the adsorbent.

ii. The discrepancy in wetting behavior of the substrate due to irregular outer surface area.

iii. The orientation and nature of the functional groups associated with a composite like Atlantic Cod scale. The nature of the Atlantic Cod scale is discussed in detail in Chapter 7.

Chapter 5

5 EXPERIMENTAL AND NUMERICAL MODELING OF ARSENIC SPECIES

In this section, the results for runs of As (III) and As (V) as uni-component species in the presence of Atlantic Cod scale will be discussed. These results correspond to Runs 58-81 in Table 3.1. The effect of pH and ionic strength of the arsenic species are studied with respect to pulverised cod scale (300-550 microns). The detection limit of arsenic ions is 7ppb. The extent of calcium ions released from the substrate has not been quantitatively analysed. The pH at equilibrium for batch tests is determined in range of 6.5-7.0.

5.1 Batch Adsorption characteristics of Arsenic species on Atlantic Cod scale

Batch tests of arsenate and arsenite species conducted as follows:

5.1.1 Effect of Concentration of As (V) and As (III) anions on Reaction Kinetics

As (III) species

The removal of Arsenic from water by fish scales is investigated in this work. To better understand the reaction mechanism of arsenic removal by fish scales, a series of static and dynamic tests were conducted. The results are analyzed based on adsorbent properties (pore size and charge) and arsenic speciation. The effect of pH is studied to analyze the adsorption behavior of the contaminants on the substrate. Figure 5.1 displays the rate of As (III) removal using fish scale with different initial concentrations. The uptake rate is higher with larger initial concentrations. However, in terms of percentage of total contaminant removal, better results are obtained with lower initial concentrations. It has been reported that released manganese ions from its oxides are adsorbed on the oxide surfaces that provide a net increase in positive charge of the substrate (Bajpai and Chaudhari, 1999). Similarly, in case of fish scales, the calcium ions (present as oxides on substrate) released into the bulk phase may also get adsorbed on the adsorbent. The further reduction in negative charge on the adsorbent may be a major factor that leads to adsorption of arsenate and arsenite ions at lower pH levels. The kinetics is dominant during the first 50 hours for a concentration of 1ppm of the arsenite contaminant (Figure

5.2). The As (III) species for pH range of 4 through 9, exists predominantly as H_3AsO_3 molecules. Figures 5.3 and 5.4 indicate that the effect of increasing the pH of the bulk phase on the adsorption of As (III) species is significant. At a pH value of 11, it is identified that the adsorptivity of the As (III) on fish scale is almost insignificant for all ranges of concentrations (400-1100 ppb) when compared to pH value of 7. However, when compared to pH value of 11, the protonated substrate at pH 4 displays better adsorption behavior. This follows the general trend where higher adsorption behavior is expected at acidic ranges for arsenic species.

It is also reported (Seidel et al., 2001) that adsorption of As (III) increases with an increase in arsenic concentration.

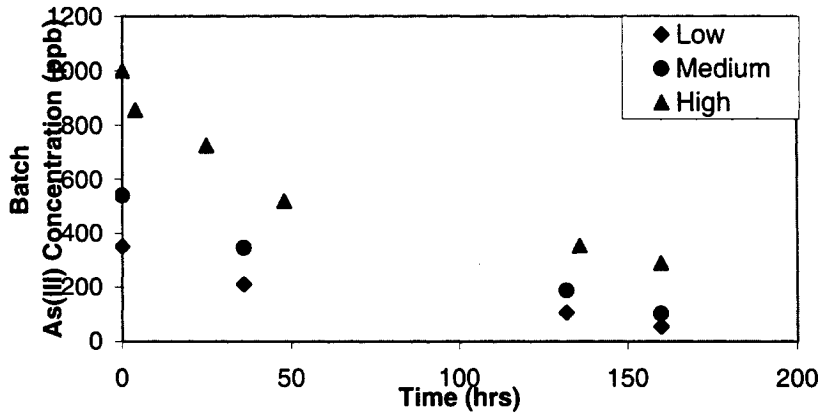

Figure 5.1 Kinetics of As (III) removal using Atlantic Cod fish scales at pH 4 (Rahaman, 2003)

Increasing the bulk phase concentration of the contaminant at pH level of 4 results in significant dispersion of the As (III) species. The net result is an additional increase in interaction between the contaminant and sorbent due to the higher ionic strength of the anions. Since the species are undisassociated at pH 4, the effect of mutual repulsion between the contaminant and substrate is considerably reduced. At pH 4, the nature of adsorption is predominantly electrostatic(lone pair on arsenic atom and protonated substrate) in nature. In order to validate this phenomenon quantitatively, Speigler and

Kedem (1966) developed a membrane transport model to evaluate the solute flux into the adsorbent as a function of bulk phase concentration.

$$J_s=P\Delta x(dc/dy)+(1-\sigma)J_v c_{mean} \quad (5\text{-}1)$$

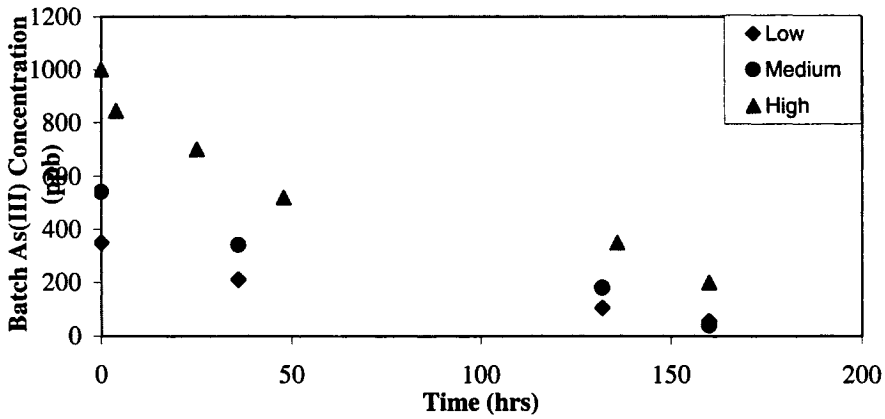

Figure 5.2 Kinetics of As (III) removal using Atlantic Cod fish scales at pH 7

The high degree of solute flux (Js) is attributed to a proportional increase in concentration gradient (dc/dy) and permeability (P) between the bulk and adsorbed phases. The net result is that with passage of time as the concentration gradient between the bulk and adsorbed phases decreases, the rate of adsorption is considerably reduced. Δx represents membrane thickness, σ and c_{mean} represents reflection coefficient and logarithmic mean of the membrane solute concentration respectively.

The equilibrium concentrations obtained for some experimental batch runs are lower than the regulatory standards set by Environment Canada (25 μg/L for Arsenic). The species remain undissassociated in the range of pH values (4-9) (Reference, Table 2.4). However, the presence of a lone pair of electrons on the arsenic atom may induce a coordinate linkage to a protonated substrate. The existence of a lone pair of electrons on the arsenic atom in the H_3AsO_3 molecule is possible (Durrant and Durrant, 1964). The dominant As (III) species in pH range of 9-11 is $H_2AsO_3^-$ anions. The existence of the repulsive forces between the negatively charged adsorbent and $H_2AsO_3^-$ anions should imply lower

adsorptivity of As (III) species with increase in pH of the medium. However, a comparative study of Figures 5.3 and 5.4 indicate the opposite. It is likely that at higher pH levels, the shift in the π electron cloud in carbonyl bond may induce a partial carbonium ion (Morrison and Boyd, 1960). Such sites are electrophilic in nature and may initiate electrostatic attraction with the nucleophilic contaminant. The probability of electrostatic interactions has been accepted as a feasible mechanism when metal ions interact with a bio-adsorbent (Krishnamurthy and Harris, 1960). The results presented in Figures 5.5-5.8 suggest that adsorption of arsenic (V) ions on fish scales is to a large extent irreversible and dependent on initial concentration.

At a pH level of 4.0, arsenic adsorbs to fish scales and its complete removal is feasible (Fig 5.5).

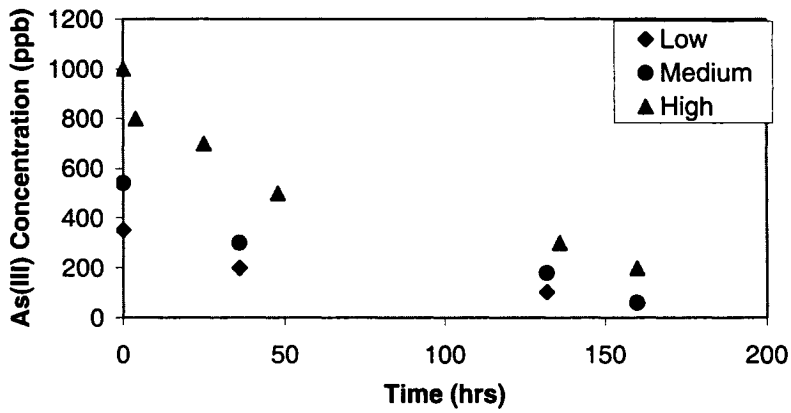

Figure 5.3 Kinetics of As (III) removal using Atlantic Cod fish scales at pH 9

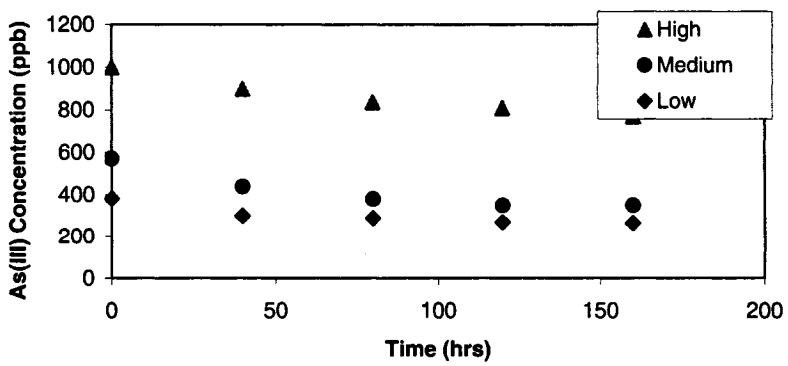

Figure 5.4 Kinetics of As (III) removal using Atlantic Cod fish scales at pH 11

The mechanisms include electrostatic attractions and specific adsorption (surface complexation). When the pH is below P_{ZPC}, (6.8 in case of Atlantic Cod, illustrated in Table 7.2 (page 246), as average of pk1 and pk2) the substrate is positive and the adsorption of the As (V) anions ($H_2AsO_4^-$ and $HAsO_4^{2-}$) is enhanced by electrostatic attraction (Anderson et al., 1976).

At pH less than 9:

$$\equiv Ca\text{-}OH + H_3AsO_3 + H^+ \rightarrow \equiv Ca\text{-}H_3AsO_3 + H_2O \quad [5\text{-}2]$$

At pH more than 9:

$$\equiv Ca\text{-}OH + H_2AsO_3^- \rightarrow \equiv Ca\text{-}HAsO_3 + H_2O \quad [5\text{-}3]$$

As (V) species

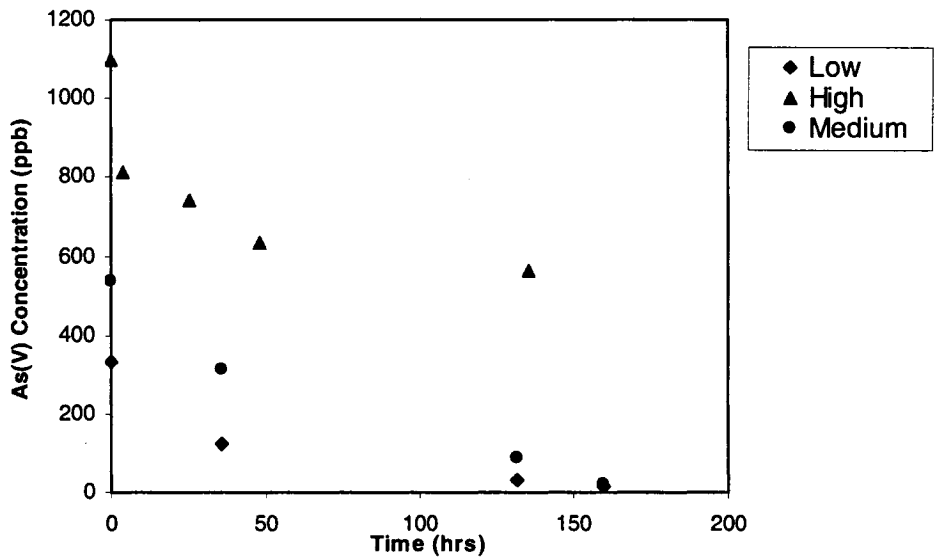

Figure 5.5 Kinetics of As (V) removal using Atlantic Cod fish scales at pH 4 (Rahaman, 2003)

Runs 70 through 81 characterize the adsorption behavior of pentavalent arsenic species. Figures 5.5 and 5.6 display the removal kinetics of As (V) species on Atlantic Cod Scales at pH of 4 and 7, respectively. The adsorption of the anions on fish scales is reduced with increase in pH from 4 to 7. This is attributed to the degree of protonisation, which is inversely correlated to the change of pH of the medium. The effect inhibits the adsorptive behavior and reveals that adsorption in the pH range of 4 through 7 is partly an electrostatic mechanism.

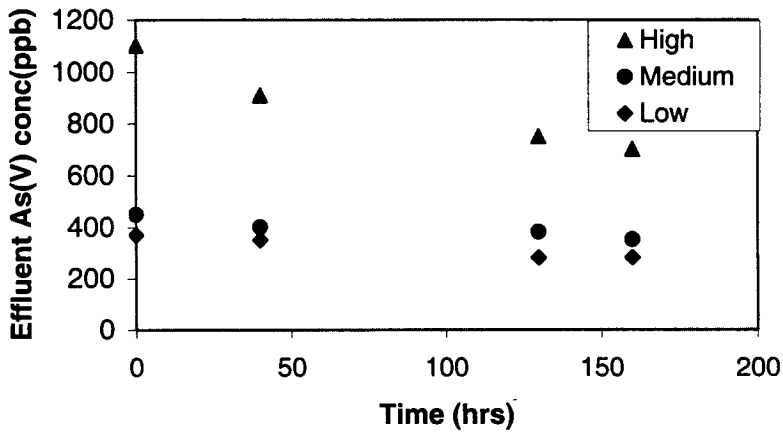

Figure 5.6 Kinetics of As (V) removal using Atlantic Cod fish scales at pH 7

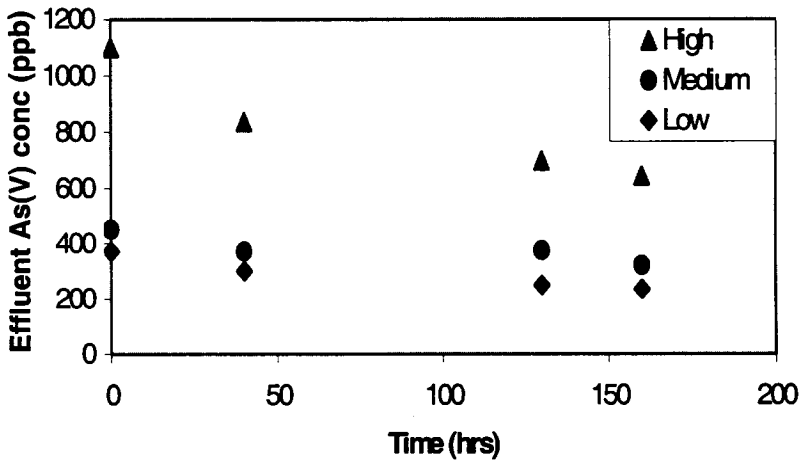

Figure 5.7 Kinetics of As (V) removal using Atlantic Cod fish scales at pH 9

The extent of the effect of calcium ions on adsorption mechanism cannot be concluded at this stage. The calcium ions may either precipitate with the anions and/or undergo ion exchange with the protons on the substrate. The extent of either of the mechanisms may have a profound effect on the removal of the anions.

It can be seen from Figures 5.6 and 5.7 that as pH is increased from 7 to 9, the degree of adsorption remains significantly unchanged. However, surface complexation may occur when a proton from an un-dissociated arsenate ion forms a molecule of water with the hydroxyl group. At a pH value of 11 (Figure 5.8), the degree of deprotonation of the Arsenate ions is significant compared at lower pH values. Thus the removal of arsenic at high pH is primarily due to anion exchange at calcium oxide sites. Since the substrate consists of considerable amounts of oxides of calcium, specific bonding of arsenate to the oxide surface takes place (Diamadopoulos et al., 1993).

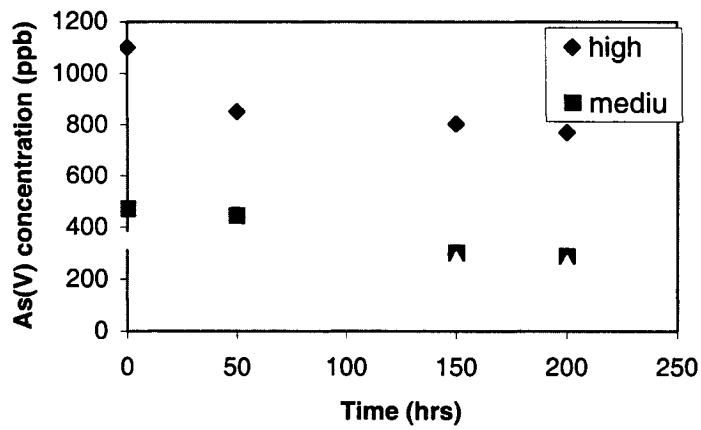

Figure 5.8 Kinetics of As (V) removal using Atlantic Cod fish scales at pH 11

At 4<pH<7,

$$\equiv Ca\text{-}OH + H_2AsO_4^- \rightarrow \equiv Ca\text{-}HAsO_4 + H_2O \quad (5\text{-}4)$$

At pH>7,

$$\equiv Ca\text{-}OH + HAsO_4^{2-} \rightarrow \equiv Ca\text{-}HAsO_4 + OH^- \quad (5\text{-}5)$$

By increasing the degree of deprotonation of the species, the mutual attraction between the adsorbate and the adsorbent is lowered, resulting in further reduction in removal of the As (V) ions. Thus anion exchange, electrostatic attraction and precipitation are the dominant mechanisms of arsenic removal. The concept seems to be valid at pH values below zero point charge. In case of an alkaline medium, anion exchange with the adsorbate is the key to abatement of the contaminant. The fundamental properties of cation exchange capacity and anion exchange capacity with respect to fish scales is discussed in detail in Chapter 7.

5.1.2 Effect of initial pH behavior on adsorptivity of As (III) and As (V) species

The results of As (III) and As (V) adsorption at specific initial concentrations on Cod fish scales as a function of initial pH values are shown in Figures 5.9 through 5.17. The adsorbent demonstrates that an increase in metal uptake is correlated to increasing As (III) species. An adsorptivity of 71 μg/g is determined with an initial concentration of 1070 μg/L at initial pH level of 4.0 (Figure 5.1). For initial concentration of 540 μg/L in the pH range of 4 through 9, it is observed that the variations of As (III) adsorption on trend implies that repulsive forces reduce the removal of the anions.

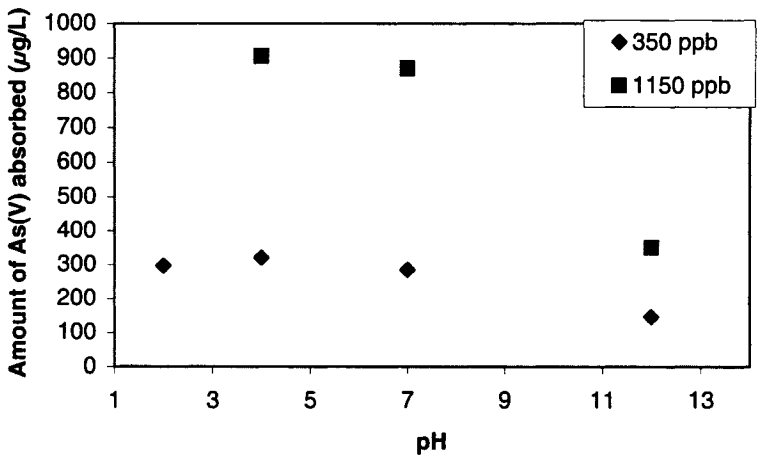

Figure 5.9 Effect of pH for adsorption of As (V) on Atlantic Cod fish scale adsorbent (Rahaman, 2003)

This is attributed to the dominant species H_3AsO_3, which are uncharged. The lone pair effect of arsenic atom (as discussed earlier) is likely to be constant by nature and is insensitive to the change of pH. However, the removal of both the species decreases sharply above pH 9 as represented in figures 5.9 and 5.10. Figure 5.9 demonstrates the effect of pH on As (V) adsorption by fish scale with different initial concentrations. The metal uptake is proportional to the amount of initial concentration as in the case of As (V) (Figures 5.9-5.12). However, if the results at pH 4 are compared between the two species at higher concentrations (1100 ppb), the rate of removal of arsenate anions is less than in the case of the arsenite species (Figure 5.10). The higher rejection of arsenate can be correlated to higher repulsion among the co-ions and chloride ions (Niu and Volesky, 2001). At lower concentrations, the repulsive effects between substrate and anions are not dominant and this results in increase in adsorption of arsenate anions (Figures 5.1 and 5.5).

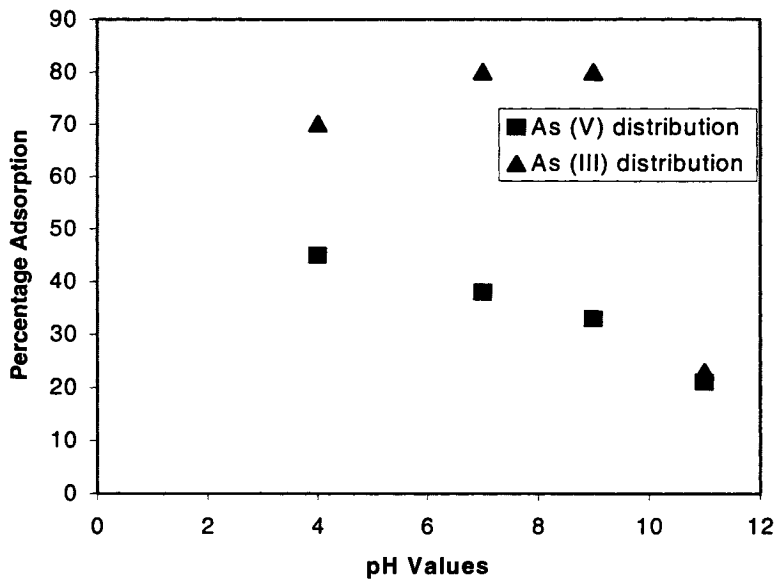

Figure 5.10. Variation of adsorption to initial pH of bulk phase at 1100 ppb

With increasing pH values, the fish scale surface is negatively charged by adsorbing hydroxyl ions on the surface or by the ionisation of very weak acidic functional groups on the surface, or both. This confirms the observation by Faust *et al.* (1999). The repulsion is attributed to the decreased metal uptake at higher alkanity values. The same path exists for As (V) batch solutions having higher initial concentrations where a sharp decrease in the uptake rate in the pH range of 4-11 is observed. This can be related to the repulsion among the anions themselves in this range of pH. Thus, it can be concluded from Figures 5.7-5.11, that initial concentration of As (V) at levels of 1ppm, is not adsorbed beyond a certain range. However, at lower concentrations, the removal process is near complete. This phenomenon of mutual repulsion is practically non-existent in the case of adsorption of As (III) ions. At a pH range from 4-9, the Arsenic (III) species remain in an undisssociated form. Lack of uncharged species inhibits mutual repulsion behaviour that enhances adsorptivity of the As (III) species in the pH range of 4-9.

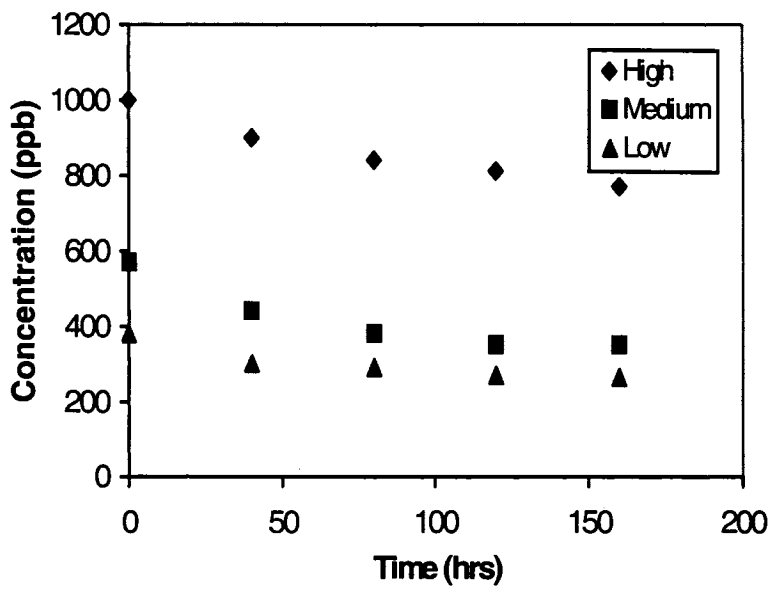

Figure 5.11. Concentration profiles of As (V) at different time levels (pH 11)

Overall, at every pH value, the percentage of adsorption of both Arsenic (III) and Arsenic (V) ions are dependent on the nature of electric charge on the adsorbent (neutral in nature) and the speciation in the bulk phase. The overall adsorption phenomenon is a

competition between the extent of mutual repulsion between the adsorbates and electrostatic attraction between the adsorbate and adsorbent. It can be observed from Figure 5.11 that at higher concentration levels of As (V), mutual repulsion is significant when compared to lower concentration levels at 570 ppb and 350 ppb. At lower pH values, the adsorptivity values of both the species increase with decrease in concentration levels (Figures 5.10, 5.11 and 5.12). In case of As (III) where the speciation remains unaffected at a pH range from 4-9, the adsorption behavior remains significant in the pH range of 4-9. At a pH level of 11, the adsorption capacity of trivalent species depreciates considerably if compared at pH 4.

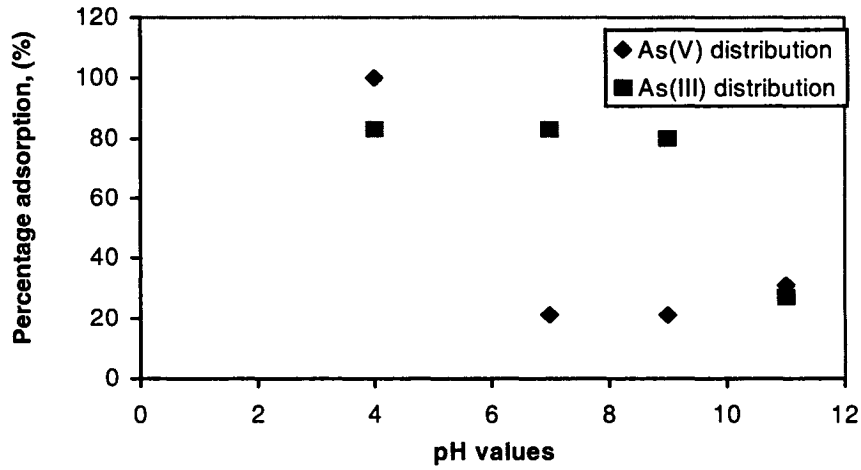

Figure 5.12 Variation of adsorption to initial pH of bulk phase at 570 ppb

In relation to As (V) anions, at lower concentration levels and lower pH values, the adsorption is significant. At lower pH values, the positive charge enhances the mutual attraction between the substrate and the ionic species. At lower concentrations the species in the bulk phases are not severely subjected to mutual repulsions because of larger mean free path distances between them.

It is reported from the elemental analysis that Atlantic codfish scale has calcium as its element, which is dissociated in the bulk solution. These calcium ions combine with hydroxyl radicals in the alkaline condition resulting in a decrease of the pH value in the

reaction solution. In acidic medium, a large number of H^+ ions are present in bulk phase. These H^+ ions react with fish scales at high electron density sites, such as C=O, COO^- and N^- groups resulting in protonation of the adsorbent and proportionate increase of pH values of the acidic solution. The calcium ions may either undergo ion exchange mechanism with the protonated sites on the substrate or (and) precipitate as calcium chloride salts.

5.2 Dynamic runs with As (III) and As (V) [single component] fish scale

In the following dynamic runs, As(III) or As(V) solutions are passed through a column packed with Atlantic codfish scale.

5.2.1 Effect of initial concentration on breakthrough behavior of As (III) species at pH 7.7

Figure 5.13 represents a comparative study of breakthrough curves for Runs 11 and 12. In relation to Run 11, the breakthrough interval is observed after two pore volumes. At a pH level of 7.7, the dominant species exist in form of H_3AsO_3. Under such pH conditions, the amide and carbonyl sites on the substrate are extremely nucleophilic in nature. The molecular diffusion and convection of uncharged As (III) species result in significant interaction of the species with the specific nucleophilic sites on the adsorbent. The structure of the H_3AsO_3 molecule generates a lone pair of electrons that are seeking nucleophilic sites on the substrate. Such sites are few at a pH

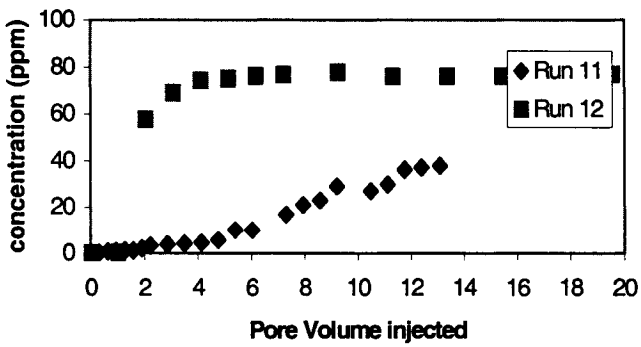

Figure 5.13 A Comparative breakthrough study of runs 11 and 12(Effect of initial concentration on breakthrough behavior of As(III) species at pH 7.7)

level of 7.7 The only feasible mechanism for removal of arsenic anions is the anion exchange mechanism described in Equation 5.2. In comparison, the pH of the bulk phase in Run 12 is identical as in Run 11. However, the influent concentration is adjusted to 83.4 ppm. The concentration profile for Run 12 displays an early breakthrough behavior of the effluent as compared to Run 11.

The increase in initial concentration of the influent is the major factor for an early breakthrough behavior. The higher adsorbent to adsorbate ratio encourages favorable response to removal of the anions. This is attributed to the number of sites available for adsorption of the contaminant and at higher adsorbent to adsorbate ratios, the abatement of the species is significantly enhanced.

5.2.2 Effect of pH on breakthrough behavior of As (III) species at identical concentrations

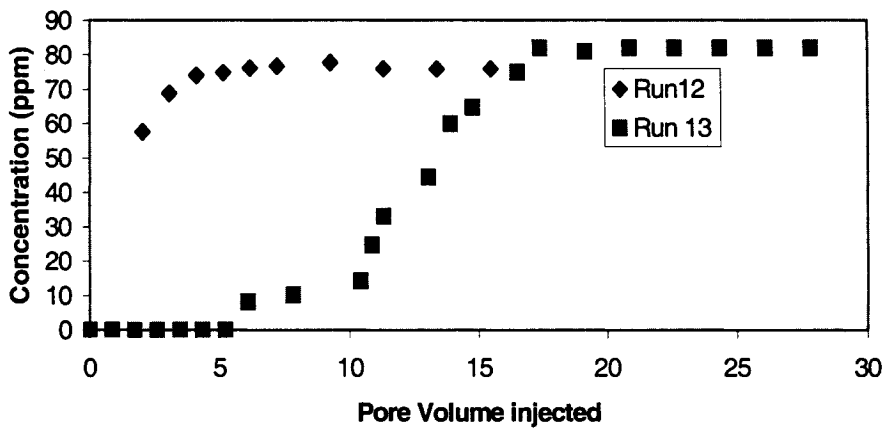

Figure 5.14. A comparative breakthrough study of runs 12 and 13
(Variance in initial pH of the influents)

Figure 5.14 shows the comparative breakthrough curves for Runs 12 and 13. The runs operate at identical initial concentrations with the exception of the flow rate parameter. However, the pH of Run 13 is slightly higher than Run 12. The sensitivity of pH parameter is then directly correlated to the speciation of trivalent Arsenic at various pH levels. At pH values above 9, the trivalent arsenic species exists predominantly as mono-

valent anions. This is in sharp contrast to behavior of the species at pH levels below 9. At such conditions, the species display molecular patterns without any significant ionization. Anionic species are affected by electrostatic repulsions that should induce an earlier breakthrough interval in case of Run 13 as compared to Run 12. Figure 5.14 illustrates an opposite trend. In other words, the effect of electrostatic forces at operating conditions for Run 13 is negligible. Perhaps the anion exchange mechanism is the dominant mechanism for interpretation of breakthrough characteristics. It has been observed that specific bonding of arsenite to the oxide surface of calcium is possible, and that these effects are stronger than the repulsive coloumbic forces between the substrate and the pollutant (Xu et al., 1988). It is further noted that the flow rate of Run 12 is higher than Run 13 resulting in earlier breakthrough of Run 12.

5.2.3 Effect of initial concentration on breakthrough behavior of As (III) species

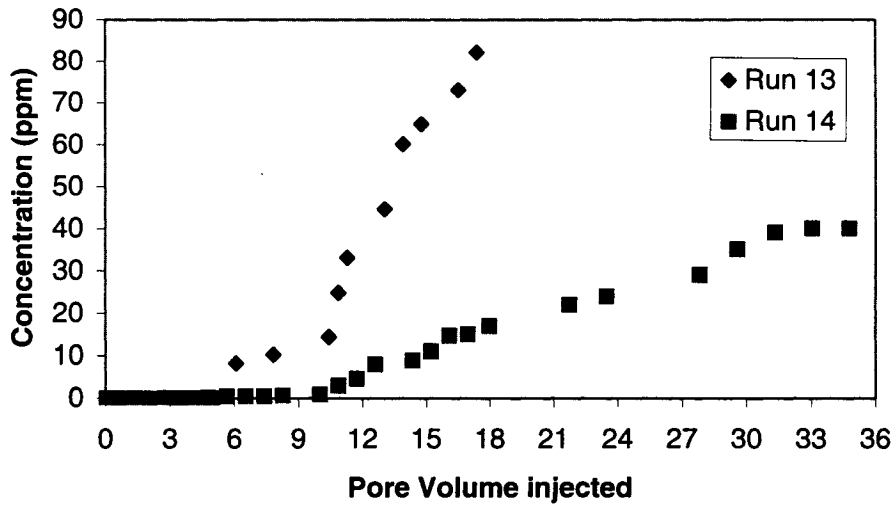

Figure 5.15. A comparative breakthrough study of Runs 13 and 14 at constant flow rate (2.75 ml/hr) and initial pH 9.25(variance in concentrations of the influents)

Figure 5.15 compares at pH levels of 9.25, the mono-valent anions may behave similarly as the un-dissociated molecules with respect to breakthrough intervals. At higher concentrations (Run 13), the breakthrough is attained earlier than at Run 14.

5.2.4 Effect of acidic, basic and neutral conditions on breakthrough behavior of As (III) species

Figure 5.16 compares the breakthrough characteristics of Runs 15 through 17 on the effect of pH of the bulk phases. In case of Run 15, the influent concentration is highly acidic in nature. The H_3AsO_3 molecules are undissociated at pH 2, but strong dipole moments may induce electrostatic attractions between the electron cloud surrounding the molecule and the highly positively charged substrate. This is substantiated by the fact that the substrate is strongly protonated and the contaminant bears an arsenic atom which posses a lone pair of electrons. The interaction energy of the substrate dipole interaction will depend inversely on the dielectric constant of the medium (80 for solutions) and the distance of the dipole from the substrate (r). The induced dipole in a neutral molecule will interact with the charged substrate and the overall interaction energy will be inversely proportional to r^4. At lower concentrations, the dipole interaction will be weak due to longer distances from the substrate and molecule. The breakthrough point is observed after approximately 23 pore volumes of the injected effluent. The mechanisms of removal of the contaminant may include anion exchange, electrostatic attractions between the species and adsorbent and precipitation of the anions in the bulk phase. However, at highly acidic conditions, the disassociation of the arsenic species is negligible. Thus it can be concluded that the removal mechanism in case of run 15 is predominantly electrostatic in behavior. The calcium ions released from the adsorbent, may also form a mono-layer of positive charge engulfing the substrate. The highly diffusive chloride ions (co-ions) are perhaps neutralized by the calcium ions that result in enhanced removal of arsenic species by electrostatic behavior.

In case of Run 16, the breakthrough is noted after two pore volumes. This demonstrates that at highly basic conditions, the dominant species ($H_2AsO_3^-$ species) are subjected to electrostatic repulsions with the negatively charged substrate. The only mechanism that allows the removal of the contaminant from the bulk phase is the anionic exchange between the calcium sites and the anions. The summations of these factors influence an early breakthrough behavior if compared to the earlier run.

In case of Run 17, the zero point charge of the substrate is slightly lower than pH of the medium (zpc is 6.8 for cod scales). The attractive columbic forces between the substrate and adsorbate are negligible if compared to Run 15. However, the extent of repulsion between the arsenic species and the adsorbent is significantly less if compared to the

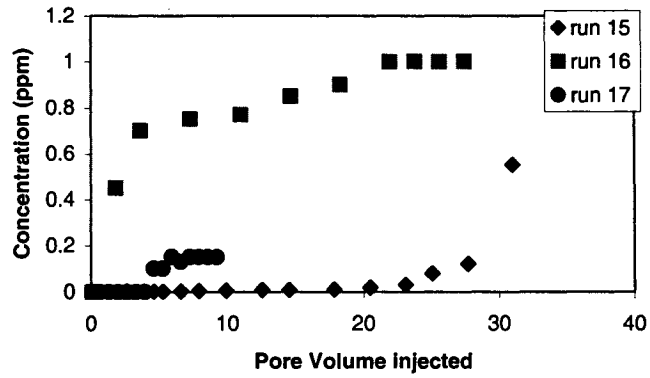

Figure 5.16. A comparative study of breakthrough behavior of runs 15, 16 and 17

columbic forces associated with Run 16. The removal of the species is highly (Variance in pH, flow rate and initial concentration of the influents) dependent on the anion exchange mechanism with the calcium sites on the substrate. Thus the effect of columbic forces coupled with ion exchange phenomena, influence the overall removal behavior of the contaminant. It is also possible that at lower flow rates the sorption mechanism in relation to columbic forces is a dominant mechanism and this perhaps delays the contaminant breakthrough (Run 17).

As in case of As (III) anions, the breakthrough behavior of As (V) species will also be discussed in this section. In the following runs, As (V) solutions of different concentrations and pH values are allowed to diffuse through a column packed with Atlantic Cod fish scale. The outlet concentrations are measured at different pore volumes and the results are plotted to develop the breakthrough curves.

5 .2.5 Effect of initial concentration on breakthrough behavior of As (V) species

Figure 5.17 shows the breakthrough curves for columns packed with fish scale supplied with initial concentrations of 47.00 and .340 mg/L of As (V) solutions. The pH of both the bulk phases is in a neutral range. The speciation of the pentavalent arsenic

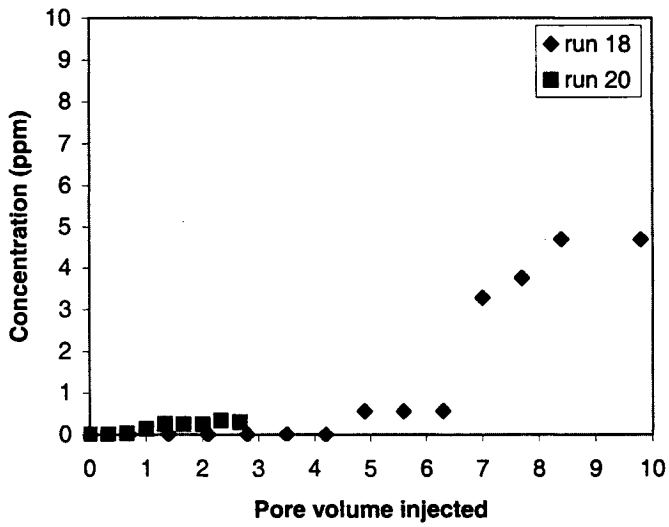

Figure 5.17. A comparative breakthrough study of runs 18 and 20 (variance in initial concentration of pentavalent arsenic species)

contaminant is in the form of a mono-valent anion. The unique feature of Figure 5.17 is that the breakthrough behavior of the species is not directly related to the adsorbent-to - adsorbate ratio. The trend is in sharp contrast to the earlier breakthrough curves in relation to the arsenite species. It has been documented that the removal of the

contaminants becomes increasingly difficult at lower concentrations of the influent. This may be the factor would explain reversal of the patterns observed in earlier runs.

5.2.6 The effect of pH on breakthrough behavior of As (V) species

The breakthrough curve for Run 21 is illustrated in Figure 5.18. The breakthrough interval is observed after injection of eight pore volumes. It is observed in the static test results, that at pH 11, the electrostatic behavior is the major factor behind sorption of As (V) species. At this range of pH, the dominant species existing in the bulk phase is $HAsO_4^{2-}$ ions. These divalent anions are strongly repelled by the negatively charged substrates. Strong repulsive forces are the main criteria behind rejection of adsorption of the anions. Detection limit of arsenic is 7 ppb.

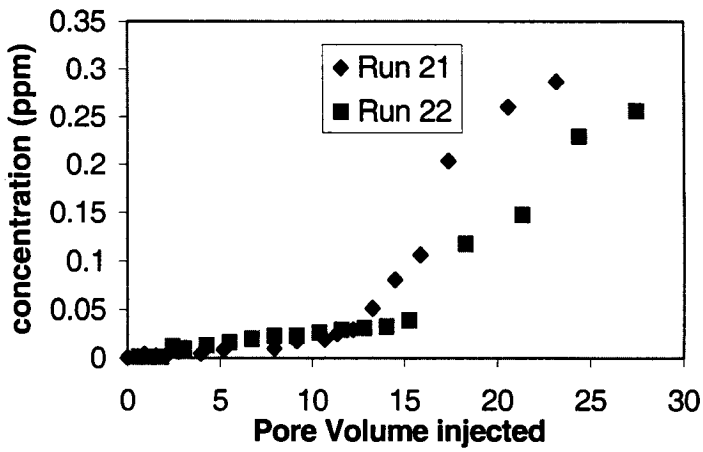

Figure 5.18. Comparative breakthrough study of runs 21 and 22 (Effect of pH on breakthrough behavior of As (V) species)(pH 3.95 and 11)

Comparing Run 22 to Run 21, the Atlantic Cod Fish scale reveals higher adsorptivity in removing As (V) from the aqueous streams. Although the breakpoint is observed earlier than in case of Run 21 (two pore volumes), the overall adsorption capacity of Run 22 is higher than Run 21. The amount of Calcium ions released under acidic conditions is higher than under basic conditions. The released calcium ions may precipitate with the

mono-valent anions resulting in significant reduction of the arsenic species. In contrast, the lack of precipitation of calcium salts at higher pH ranges coupled with significant repulsions between the adsorbate and adsorbent may deter the reduction of the divalent anions.

The effect of pH in an acidic medium is studied in relation to the pentavalent species. The levels of pH chosen for Runs 23 and 24 are 3.95 and 2.00, respectively. Run 23 is continued after injection of 23 pore volumes of the influent. Figure 5.19 displays that As (V) removal through a fixed bed of the bio-adsorbent is significant compared in Run 23 than compared to Run 24. Negative charged anions are electrostatically attracted to the protonated substrate. This enhances the sorption behavior of As (V) at pH level of 4.95. However, in relation to Run 24, it is noted that the removal of the arsenic species is considerably lower than in case of the earlier run. At pH level of 2.0, the penta-valent arsenic species exist predominantly in molecular form. Thus the effect of anion exchange, electrostatic attractions and precipitation is negligible when compared to Run 23.

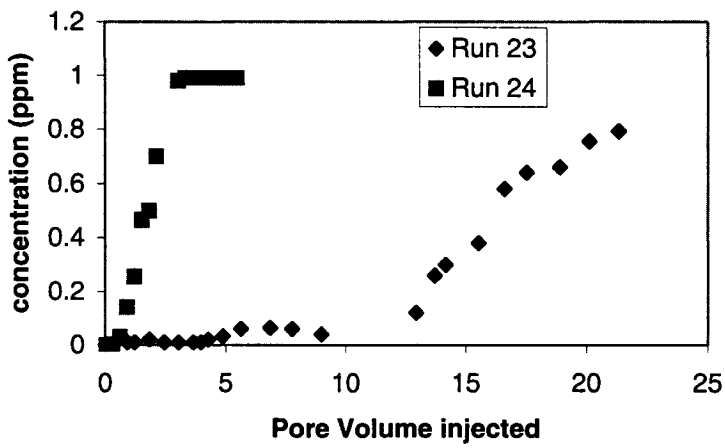

Figure 5.19. Comparative breakthrough study of runs 23 and 24 (Effect of pH on breakthrough behavior of As (V) species) (pH 2.00 and 3.95)

Overall, it may be concluded that the removal of the anions is highly dependant on the speciation of the contaminant that in turn is affected by the pH of the medium.

However, further work is needed to study the combined effect of precipitation, anion exchange and columbic behavior of the pollutant.

5.3 Adsorption isotherms

Batch adsorption studies with different concentrations are performed in order to determine the Langmuir isotherm for both As (III) and As(V) removal using fish scales. Isotherm is the presentation of the amount of arsenic adsorbed per unit of adsorbent as a function of the equilibrium concentration in bulk solution, at constant temperature (Faust *et al.*, 1999).

As described in Chapter 4, the Langmuir model is based on the following assumptions:

i. anions are adsorbed at a fixed number of well defined localized sites.
ii. each site can hold an arsenic radical through anion exchange.
iii. all sites are energetically equivalent
iv. there is no interaction between molecules adsorbed on neighboring sights; and
v. adsorption is reversible and an equilibrium is achieved

The following assumptions are based on applying Langmuir model (Schiewer and Volesky, 1996).

The validity of the Langmuir model for As (III) and As (V) species with varying to pH has serious disadvantages. They include:

i. Each site may holds one adsorbate molecule. A specific site may interact as a combination of both ion exchange and electrostatic mechanisms.
ii. Thus it is likely that the total removal of the contaminants is a combination of both adsorption and precipitation.
iii. The total number of adsorption sites determined on an unit mass of fish scale will vary with changes in pH .

iv. For numerical purposes, the maximum adsorption capacity factor will be a forcing function instead of an experimentally determined factor at various pH values.

Overall, the limitation of numerical modeling with respect to biosorption of anions is being addressed.

5.4 Numerical Approach to dynamic runs of As (III) and As (V) (single anionic)

The numerical approach of the dynamic runs is based on pore diffusion model that utilizes the concept of ion exchange to predict the outlet concentrations for all the 14 cases. However, the extent of ion exchange and precipitation with respect to speciation, pH and initial concentration of the contaminant has not been experimentally studied. It is only after a proper characterization of the adsorbent with respect to the Arsenic species that an appropriate mechanism(s) may be determined.

In order to validate the experimental runs with a numerical model, the effect of speciation with respect to pH has to be analyzed. Arsenic species can exist in multiple forms at various pH levels (Table 2.4). The dominant species at each pH range may be considered for numerical purposes.

Besides elementary arsenic with oxidation state of 0, the element is stable in the oxidation states of +5, +3 and –3 (Table 2.4). In aqueous media, it exists in form of trivalent and pentavalent states. The oxides of both As (III) and As (V) are soluble in water. The dissolution implies direct reaction with the water, hydration, where the oxides behave like non-metals and exhibit acidic character. As (III) forms arsenious acid also called arsonic acid.

Dissociation of arsenious acid: (Rahaman, 2003)

$$H_3AsO_3 = H^+ + H_2AsO_3^- \quad pKa = 9.22 \qquad (5\text{-}6)$$

$H_2AsO_3^-$ = H^+ + $HAsO_3^{2-}$ pKa = 12.13 (5-7)

$HAsO_3^{2-}$ = H^+ + AsO_3^{3-} pKa = 13.40 (5-8)

Dissociation of arsenic acid: (Rahaman, 2003)

H_3AsO_4 = H^+ + $H_2AsO_4^-$ pKa = 2.20 (5-9)

$H_2AsO_4^-$ = H^+ + $HAsO_4^{2-}$ pKa = 6.97 (5-10)

$HAsO_4^{2-}$ = H^+ + AsO_4^{3-} pKa = 11.53 (5-11)

The physical model parameters in Table 5.1 were either experimentally determined or forced into the numerical model to 'match' the experimental runs. Needless to say, the use of isotherm models is not much more than 'curve fitting.' The problem with biosorption is that not much specific information is available on sorption mechanisms involved (Volesky, 2003). Here it is assumed that the mechanism behind arsenic removal is exclusively anion exchange by nature. The influence of electrostatic attractions and precipitations has been ignored because their mechanism has not been quantified.

Note: The total sites available for adsorption is 0.5millimoles per gram, (calculated from molar ratio of elements for Calcium sites). The major assumption considered for all the runs (11-24) are that the total number of calcium sites (available for adsorption in carbonate and phosphate forms) remain unchanged with respect to pH. This is a limitation in numerical modeling of bioadsorbents (Schiewer, 1999). Besides, carbonate sites (0.4 millimoles) and 0.1 millimoles of phosphate sites per unit mass, are present. This is a severe drawback in interpretation of the adsorption mechanism with respect to numerical simulations.

Table 5.1 Physical model parameters for numerical simulations

Run	Flow rate (ml/hr)	Poro -sity (Φ)	pH of bulk solution	Initial conc. (ppm)	Amount (scale) (g)	K1 (L/m mol)	K2 (L/m mol)	Dp cm^2 per hr	Ds cm^2 per hr
11	120.0	0.83	7.7	41.22	61.54	1.00	1.00	100	80
12	390.0	0.83	7.7	82.22	61.54	1E-07	1E-07	100	100
13	165.0	0.82	9.25	82.76	66.87	5.0	5.0	100	100
14	165.0	0.82	9.25	42.22	66.87	10.0	10.0	20000	500
15	120.0	0.81	2.0	0.5	69.44	50.0	50.0	70.0	500
16	337.2	0.81	11.5	1.000	69.44	8E-07	8E-07	60000	500
17	120.0	0.81	7.0	1.050	69.44	6E-04	6E-04	45	45
18	132.0	0.82	7.3	47.02	67.13	2E-06	2E-06	250	500
19	390.0	0.80	8.04	47.02	75.01	2E-07	2E-07	500	500
20	120.0	0.87	7.13	0.342	46.76	2E-07	2E-07	100	500
21	120.0	0.86	11.0	0.485	50.31	2E-04	2E-04	500	500
22	120.0	0.86	3.95	0.328	50.31	90.0	90.0	300	300
23	120.0	0.86	3.95	1.000	50.31	90.0	90.0	300	300
24	120.0	0.86	2.00	1.000	50.31	1E-06	1E-06	300	300

Note:

The Langmuir coefficients of As (V) and As(III) are .0088 and .0052 L per mmole (Rahaman, 2003).

The maximum adsorption capacity Q_m , is 26.67mg/g and 24.75 mg/g for pentavalent and trivalent anions respectively (Rahaman,2003).

Numerical runs with As (III) and As (V) (single component) fish scale

In the following dynamic runs, As (III) or As(V) solutions are passed through a column packed with Atlantic codfish scale.

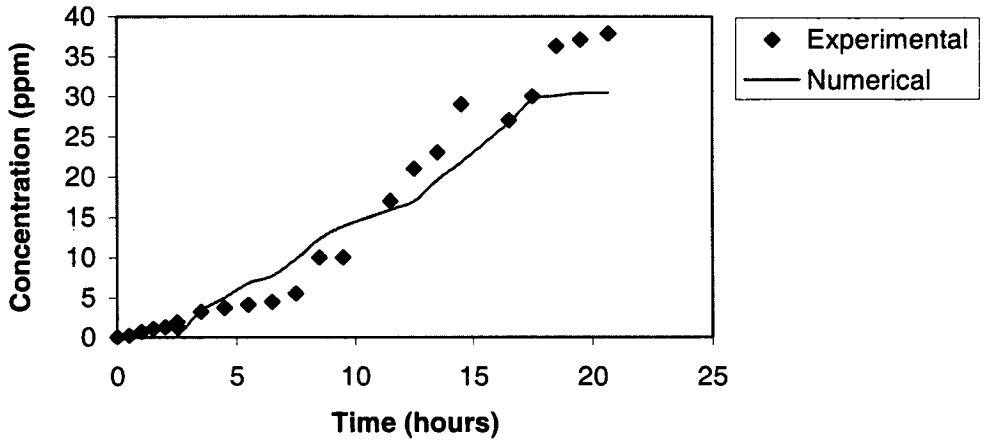

Figure 5.20. A comparative numerical and experimental analysis for As (III) (Run 11)

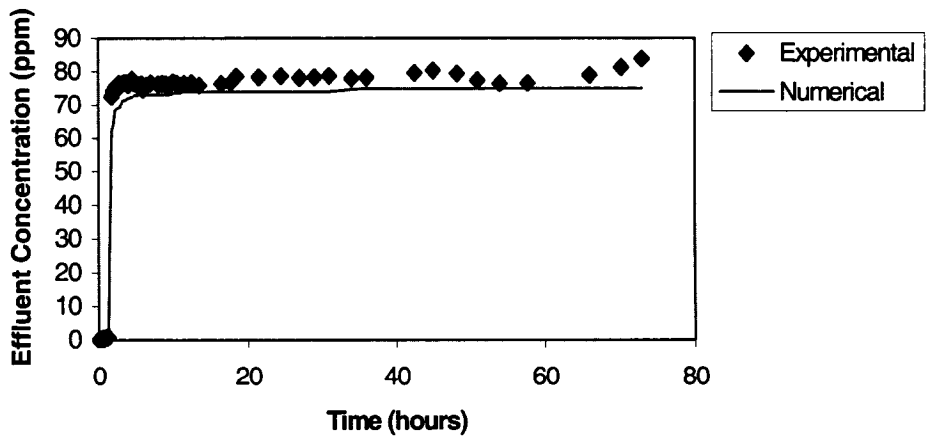

Figure 5.21. A comparative numerical and experimental analysis for As (III) (Run 12)

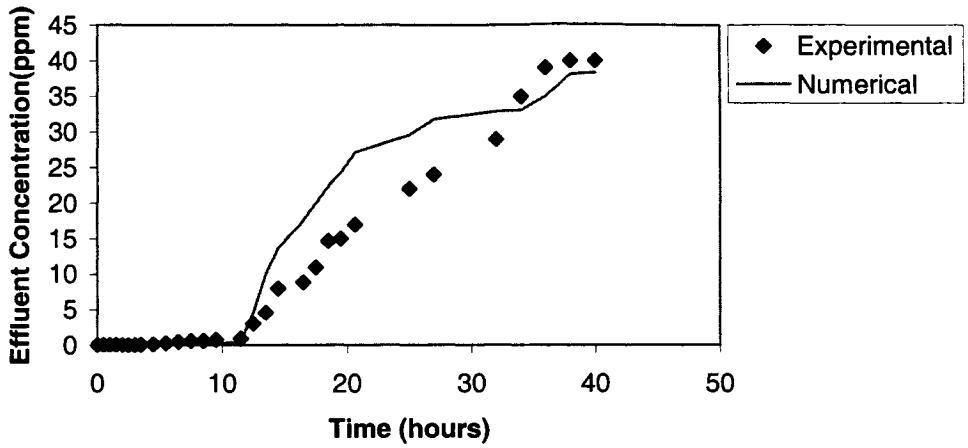

Figure 5.22. A comparative numerical and experimental analysis for As (III) (Run 13)

Runs 11 through 18 (Figures 5.20-5.27) show that effluent concentrations (with exception of Run 12) determined numerically are either higher or lower than the experimentally determined values after breakthrough intervals. The major drawback of the simulations is that the total number of sites involved in adsorption is an assumed value (Schiewer et. al., 1999). At a specific pH value, the number of sites varies with an increase or decrease of the variable. It is also feasible that precipitation and chemisorption mechanisms do interfere in the tests.

In case of Runs 19 through 24 (Figures 5.28-5.32), the numerical simulations did match reasonably better than the previous experimental runs. However, this does not explain that the experimental runs are displaying the same adsorption mechanisms as dictated by the numerical runs. 'Match fitting' by chance, the numerical results need not comply with the chemical behavior of the contaminants. Hence it is extremely essential that future tasks related to bio- sorption of Atlantic Cod scales is correlated to a detailed study of the possible reaction mechanisms of both cations and anions.

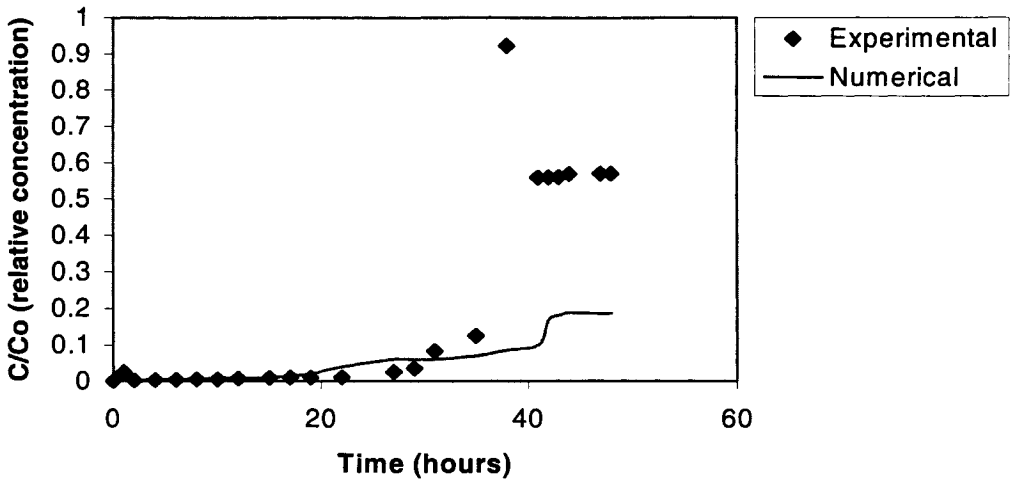

Figure 5.23 A comparative numerical and experimental analysis As (III) (Run 14)

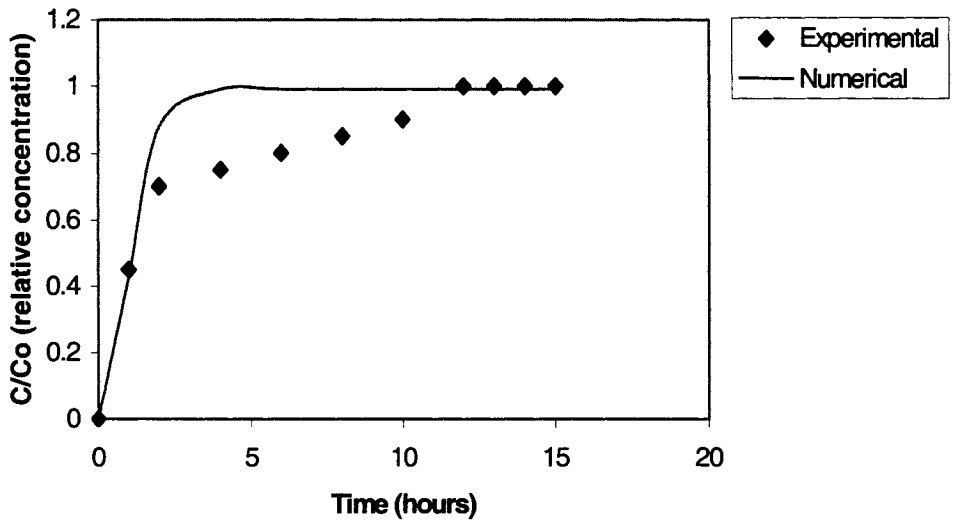

Figure 5.24. A comparative numerical and experimental analysis for As (III) (Run 15)

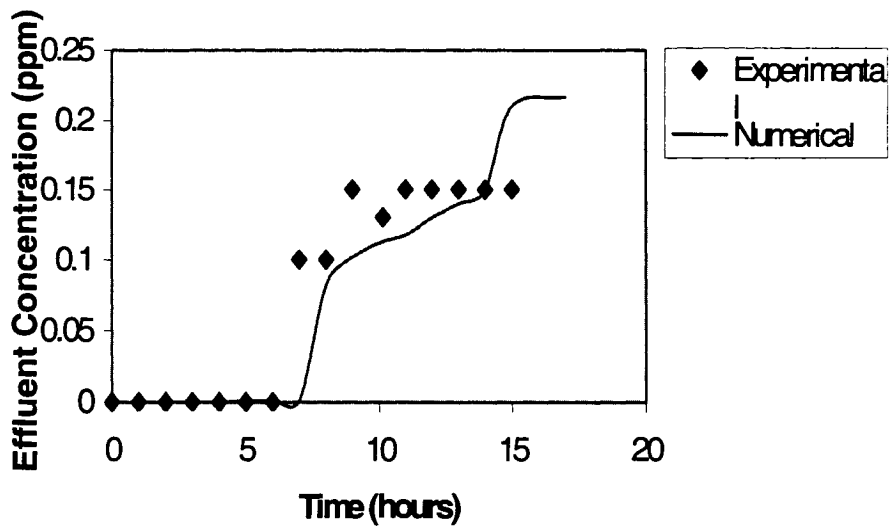

Figure 5.25 A comparative numerical and experimental analysis for As (III) (Run 16)

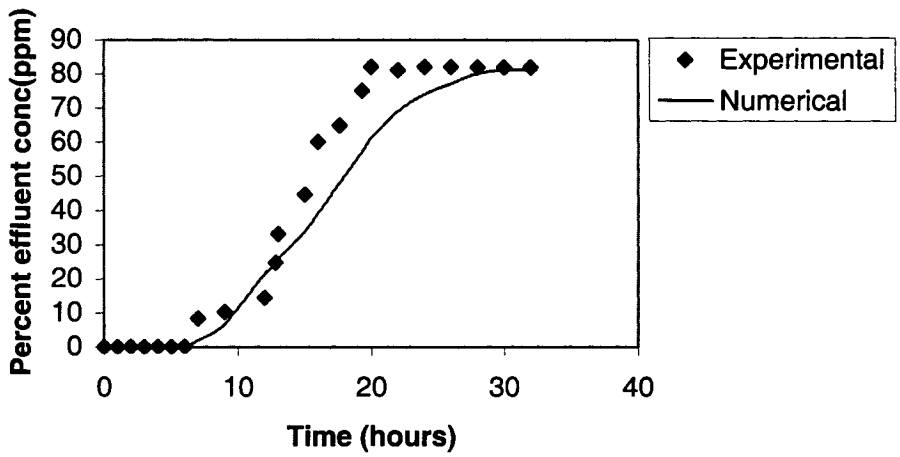

Figure 5.26 A comparative numerical and experimental analysis for As (III) (Run 17)

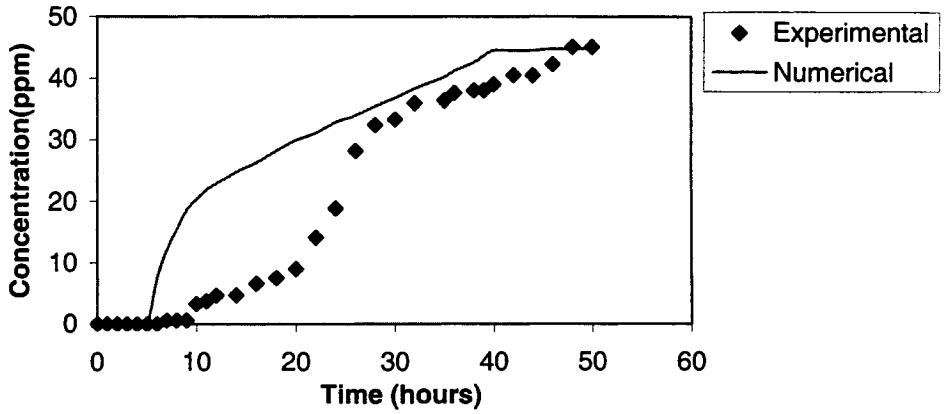

Figure 5.27 A comparative numerical and experimental analysis As (V) (Run 18)

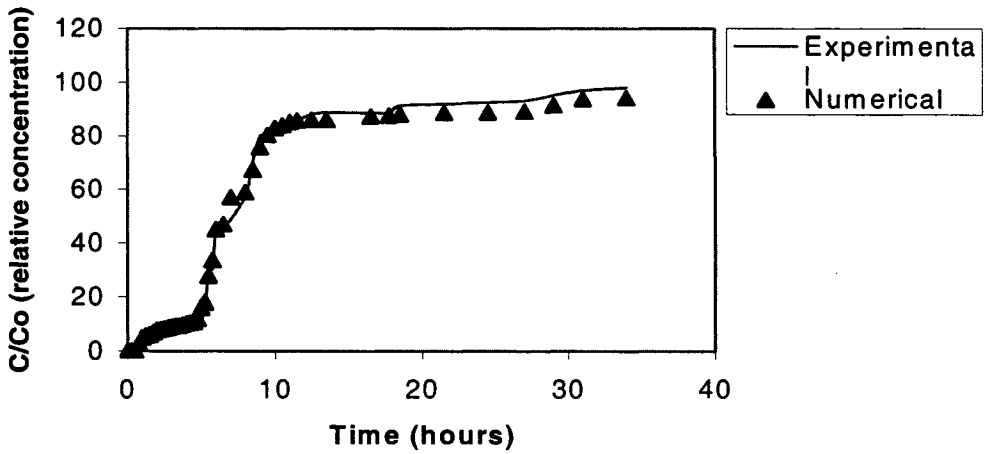

Figure 5.28 A comparative numerical and experimental analysis As (V) (Run 19)

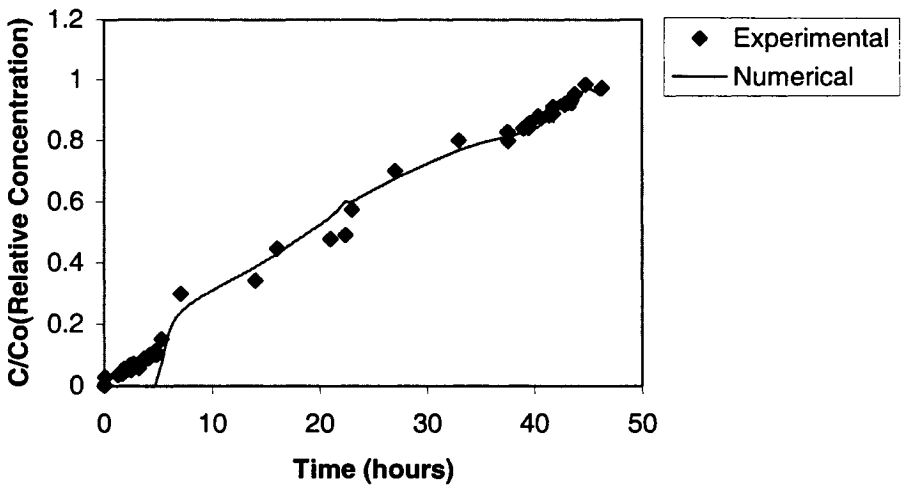

Figure 5.29 A comparative numerical and experimental analysis for As (V) (Run 20)

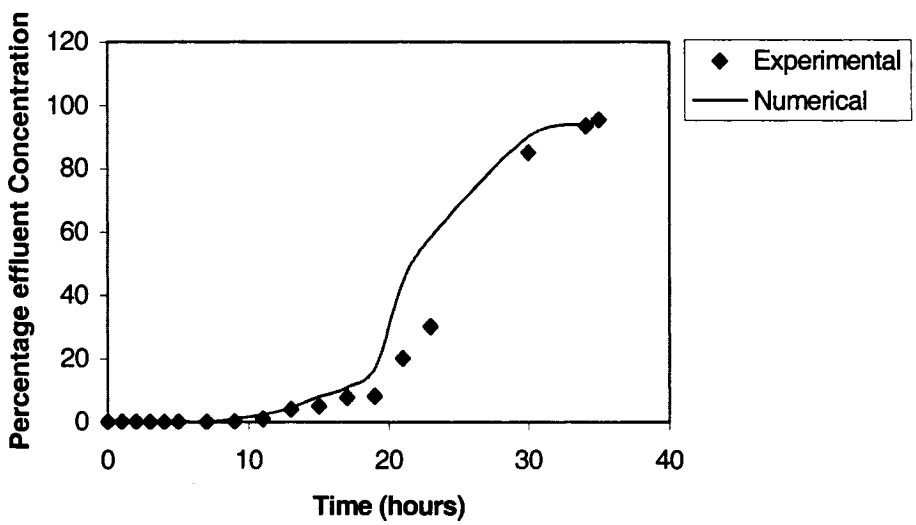

Figure 5.30 A comparative numerical and experimental analysis As (V) (Run 21)

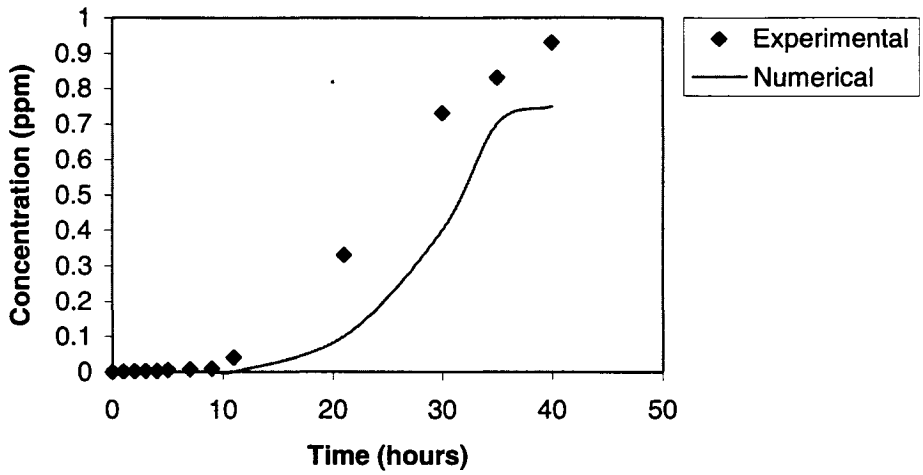

Figure 5.31 A comparative numerical and experimental analysis for As (V) (Run 22)

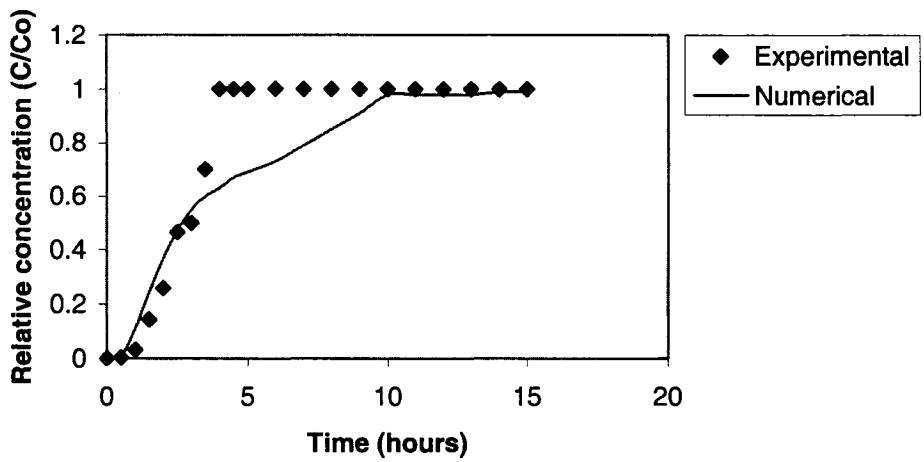

Figure 5.32 A comparative numerical and experimental analysis for As (V) (Run 24)

Chapter 6

6 RESULTS AND DISCUSSIONS OF MULTI-COMPONENT (LEAD AND INTERFERRING ARSENIC) SPECIES

Summary

In this dissertation, "multi-component phase" is mainly a combination of lead and arsenic ions. In this connection, the main focus of study was the adsorptivity of a specific ion (in presence of an interfering ion) with respect to a unit mass of the adsorbent under identical pH and initial influent concentrations.

Often the prediction of adsorption equilibrium is complicated by the presence of several adsorbed ions, requiring the use of multi-component isotherm equations (Chong et al., 1995). This is especially relevant when the sorption of one ion affects the binding mechanism of the second ion, as is the case when different ions compete for the same binding site. Another factor that is observed is the effect of pH on metal binding. Lead ions adsorb better at higher pH values while As (III) and As (V) anions exhibit better adsorption results in acidic ranges (Schiewer and Volesky, 1996). At higher pH values, lower competition by protons for the same binding sites stimulates the adsorption of additional lead ions onto the bio-adsorbent. However, at higher pH values, the negatively charged adsorbent will repel the As (V) and partly the As (III) anions. Overall, the decrease in adsorption of both the As species on fish scales with increasing pH values has been observed and correlated by using Aluminum Hydroxide and other geological materials as adsorbents (Woolson and Kearny, 1977; Frost and Griffin, 1977; Pierce and Moore, 1982). Lack of ionization of As (III) species at a pH range of 4-9 retards the adsorption phenomenon. This chapter is aimed at investigating the impact of As (III) or As (V) anions on the uptake of lead ions by the fish scales. In addition, investigation was

made on the adsorption behavior of As (III) and As (V) anions on fish scales in the presence of lead ions are investigated.

6.1 Batch Adsorption tests

A series of multi-component batch tests were performed to study the sorption behavior of a number of species at various pH and concentration levels. As input parameters to characterize the adsorbent, the total concentration of all species and the equilibrium constants were specified. The equilibrium constants are considered to be a function of pH values. This is connected to the fact that the speciation and nature of the adsorbent is highly dependent on pH. Acidic waters are associated with paper and pulp treatment plants and alkaline effluents are often originating from metal processing industries.

At a specific pH, (as discussed in Chapter 4), the adsorption behavior of arsenic species in presence of lead nitrate (background electrolyte) can be correlated to the 'Stern layer' complexation theory. This theory postulates that adsorption of ions occur at specific sites of a bio adsorbent. The surface charge is correlated to the ionization of specific site groups that interact with the ions in the bulk phase. These interactions lead to formation of an'electric double layer ' which is composed of (a) site surface, (b) Inner plane, where the center of ions are positioned. These ions bond with the functional groups on the substrate. (c) Outer plane or the interface of the diffuse layer (Hayes and Leckie, 1987).

There are two analogs of triple layer model:

(i) Outer sphere analog.

(ii) Inner sphere analog (Niu et al., 1999).

In the outer sphere analog, the background electrolyte (lead nitrate) with increasing ionic strength will exert a significant reduction in uptake of arsenic species. In relation to inner sphere analog, the adsorption of anions bears no influence to variation of ionic strength of the background electrolyte. The application of outer sphere analog was observed to be

appropriate with Sodium-Gold cyanide system (Niu et.al.,1999). Also the presence of nitrate (counter ion) ions significantly reduced the uptake of the arsenic species. The cations such as lead (unlike anions) are adsorbed in both the immobile phases and with functional groups of the adsorbent. Therefore their uptakes in any pH range are comparatively higher than anions (Hayes and Leckie, 1987). The anions may be adsorbed to the biomass by ion pair adsorption or anion exchange mechanism. The feasibility of the either two mechanisms is primarily related to the pH of the bulk phase. At an acidic range, ion pair effect may be dominant and at a basic medium, the anion exchange mechanism will prevail. The objective of the static tests is to observe the effect of ionic strength of the lead ions and the pH on the adsorption behavior of both types of the arsenic species.

6.1.1 Effect of Initial concentration at different initial pH levels (Runs 82-105)

The effective static tests were conducted by combining various Lead concentrations with either As (III) or As (V) species at a pH range of 4-11 (Runs 82-105). The objective was to establish the ionic strengths of both species and the pH values of the bulk phases for interpretation of the possible reaction mechanisms. The equilibrium coefficients were assumed to be function of pH and the overall adsorption of a species are a combined effect of both equilibrium coefficient and its concentration in the bulk phase.

6.1.1.1 Lead Concentration (2.5ppm) and As (III) or As(V) at 350 ppb

Figure 6.1, illustrates the adsorption phenomenon at pH 4 for an initial concentration of 2.5 ppm lead and 350 ppb As (III). The abatement of As (III) species was insignificant. Increasing the pH to 7 (Figure 6.2), the equilibrium concentration of lead was determined to 0.2 ppm. The percentage uptake of lead ions at pH 4 (Figure 6.1) was determined to be 80 percent.

This is in sharp contrast to Figure 6.5. The equilibrium concentration of the bulk phase was determined to be .01 ppm. When compared to Figure 6.1, the decline of lead concentration (Figure 6.5) was about 95 percent of its original concentration at equilibrium. This is attributed to the existence of As (III) as uncharged H_3AsO_3 molecules in a pH range of 4-9.

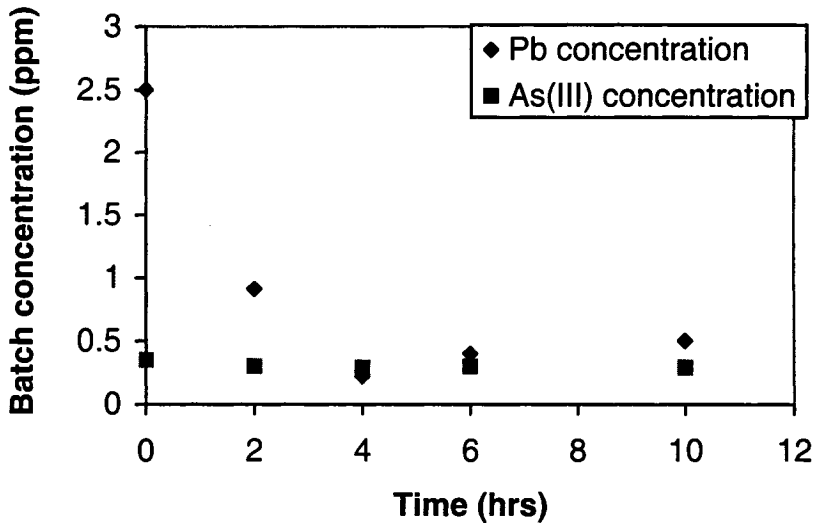

Figure 6.1 Batch tests at pH4 (initial concentration: 2500 ppb (Pb) and 350ppb As(III))

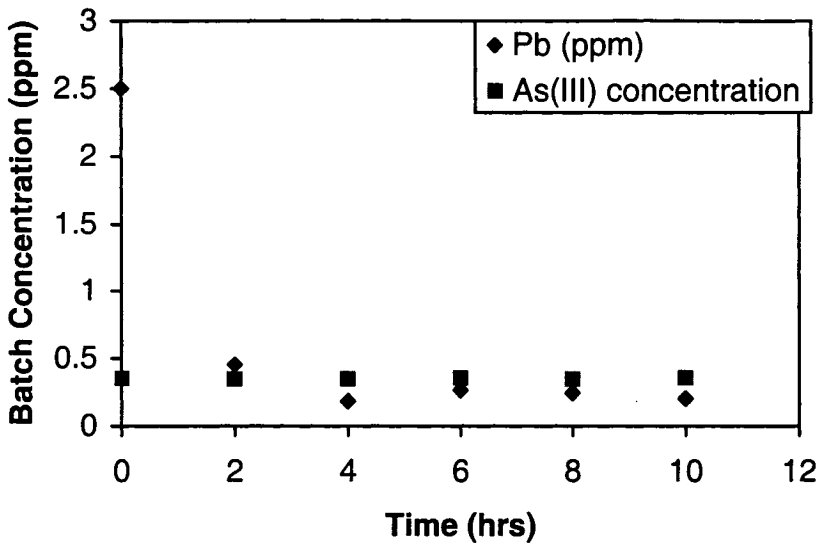

Figure 6.2 Batch tests at pH 7(initial concentration: 2500 ppb (Pb) and 350ppb As(III))

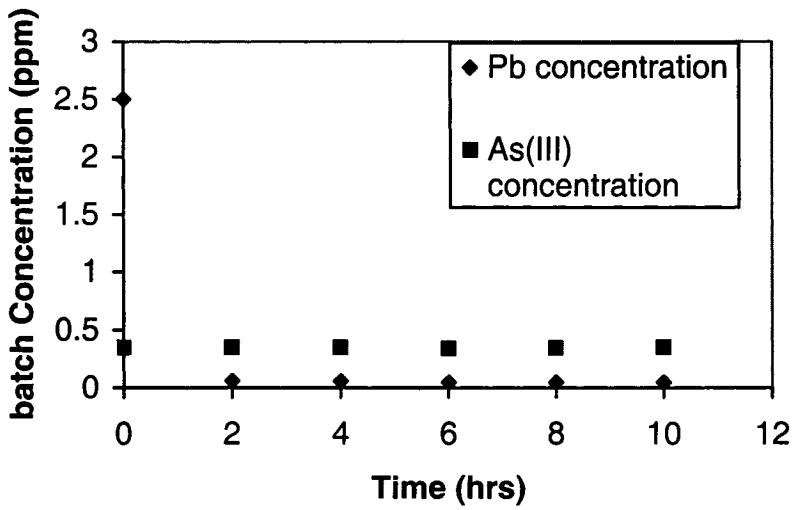

Figure 6.3 Batch tests at pH 9(initial concentration: 2500 ppb (Pb) and 350ppb As(III))

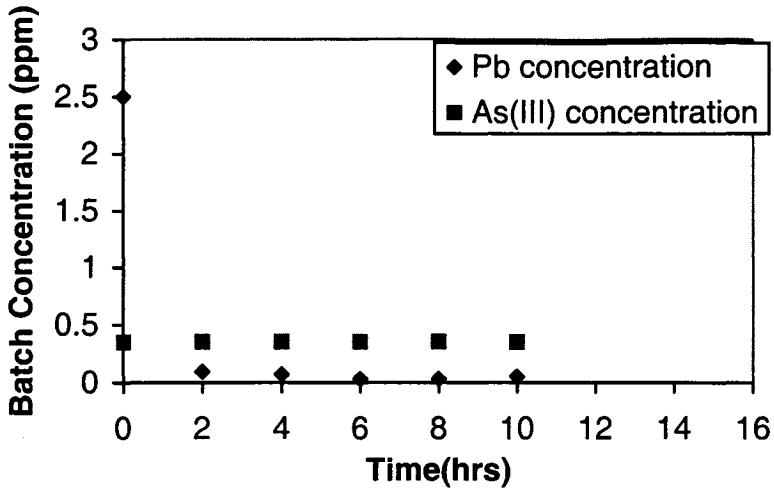

Figure 6.4 Batch tests at pH 11(initial concentration: 2500 ppb (Pb) and 350ppb As(III))

The uncharged species did precipitate with the lead ions. This resulted in an additional 15 per cent reduction of lead species in association to penta- valent radicals. In case of the As (V) solution, the arsenic existed as $H_2AsO_4^-$ species at a pH range of 4-7. At pH 4, the protonated substrate was susceptible to columbic attraction of arsenate anions. The columbic attraction of the arsenate species coupled with complex formations (precipitation of lead arsenates) resulted in comparatively higher reduction of both the contaminants in the case of lead and penta-valent arsenic phase. In Figure 6.5, the decrease of lead ions is about 95 per cent of its original concentration. It may be concluded from Figure 6.6 that at pH 7, the degree of chemisorption of Lead ions was enhanced by the deprotonisation of the substrate. However, the very reduction of positive charge on the adsorbent results in net increase of competition in adsorption between the arsenic and hydroxyl anions. Thus a decrease in removal (from Figure 6.6) of the penta-valent arsenic species was observed. At equilibrium conditions, the degree of reduction of lead (in presence of As (III)) was approximately 90 per cent (Figure 6.2). This small difference in removal behavior may be attributed to precipitation of lead salts. At pH 7, As (III) exists in a molecular form. In short, the removal of lead ions with respect to penta-valent arsenic appears to be a combination of both adsorption and precipitation.

At present it is difficult to predict at existing conditions, which mechanism(s) may prevail over the other? However, decrease in adsorption of arsenic (V) in relation to its repulsive forces can be correlated to the studies conducted by Seidel and co-workers (Seidel et al., 2001). The authors concluded that with increase in pH of the bulk solution, the exclusion of arsenic from the bulk phase in interaction to a nano-membrane was diminished. The observed increase in negativity of the membrane appeared to lead to an increase in repulsive forces that lower the diffusion of arsenic ions into the membrane.

Increasing the pH of the bulk phase to 9 resulted in an increase of adsorption of lead ions as shown in Figure 6.3. In the case of lead and As (V) (at identical conditions), a decrease in the removal of lead ions (74 per cent of original concentration) in a bi-component system with arsenate species (Figure 6.7) was observed with respect to an increase in pH. When Figure 6.3 is compared to Figure 6.7, (to study the effect of speciation of interfering arsenic with respect to adsorption of both contaminants) the degree of rejection of adsorption of the arsenate ions at equilibrium appears to have been considerably enhanced with an increase in pH from 4 to 9. In relation to As (III) ions, the effect of change of exclusion of the ions from the bulk phase with respect to change of pH was negligible (Figure 6.3 and Figure 6.2). The reason behind such an insignificant change in adsorption of arsenite anions at a pH range from 4-9 appears due to the lack of disassociation of H_3AsO_3 molecules. At pH 11, the lead ions in arsenite–lead bulk phase were almost completely removed. Besides chemisorption, complexation of lead and arsenic appears to be another feasible mechanism (Figure 6.4). This may be attributed to the low solubility product of lead arsenate complex. In relation to arsenate-lead solution, chemisorption coupled with complex formation of $PbHAsO_4$ seems likely to be the major cause of reduction of both the species from the bulk phase (Figure 6.8). However, at pH 11, OH^- ions were in abundance in contrast to $HAsO_4^{2-}$ and $H_2AsO_3^-$ ions. Hodgson (1970) explains that in multiple solute solutions, the rejection of an ion is increased by the presence of a more permeable ion of like charge. Since the hydroxyl and nitrate ions

are more permeable (smaller size and higher mobility) than the arsenic ions in the adsorbent, this phenomenon will deter the adsorption of lesser mobile anion.

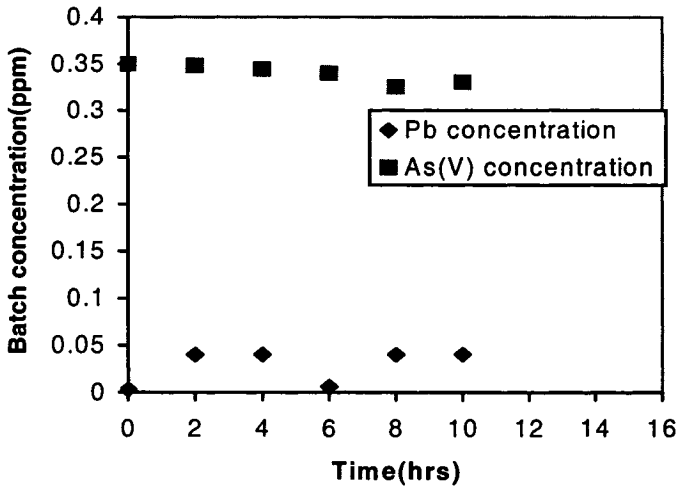

Figure 6.5 Batch tests at pH 4(initial concentration: 2500 ppb (Pb) and 350ppb As(V))

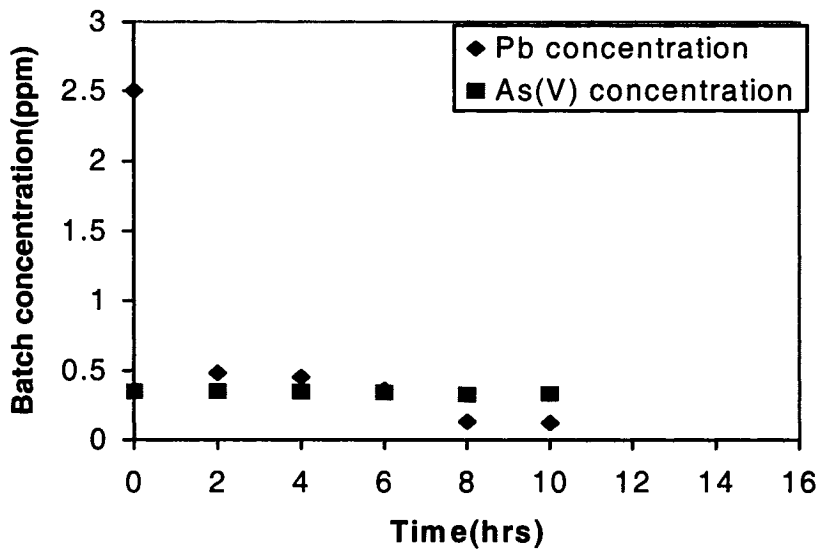

Figure 6.6 Batch tests at pH 7(initial concentration:2500 ppb (Pb) and 350ppb As(V))

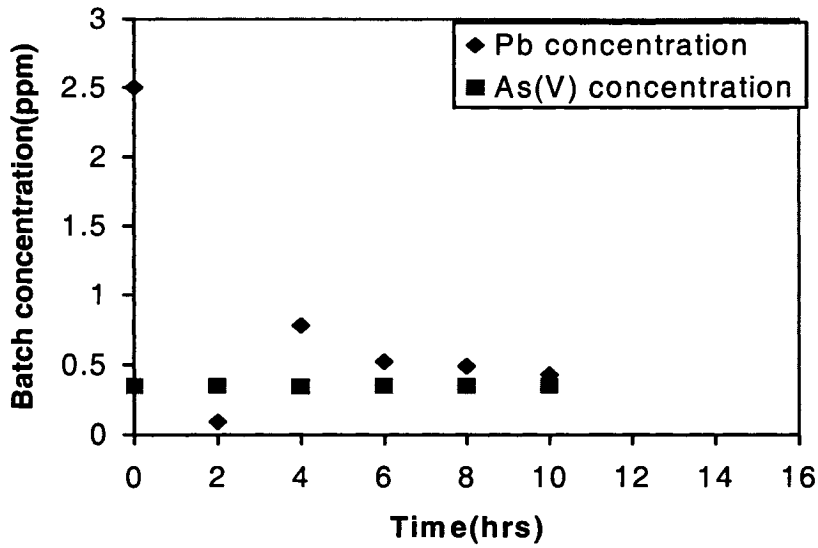

Figure 6.7 Batch tests at pH 9(initial concentration:2500 ppb (Pb) and 350ppb As(V))

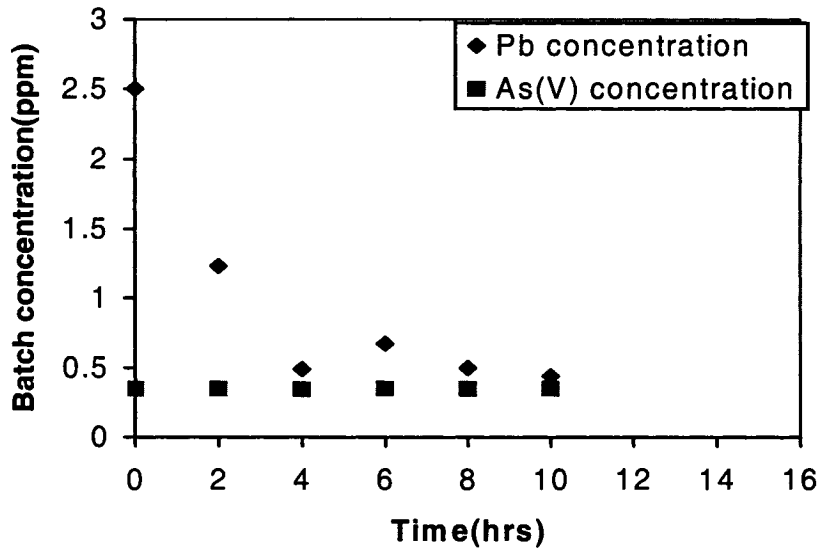

Figure 6.8 Batch tests at pH 11(initial concentration:2500 ppb (Pb) and 350ppb As(V))

It can be concluded that while adsorption of lead ions in both the cases (Figures 6.4 and 6.8) is significant, the removal of As (III) and As (V) species remain insignificant.

6.1.1.2 Lead Concentration (10 ppm) and As (III) or As (V) at 350 ppb

At an initial 10 ppm concentration at pH 4, approximately 70 per cent (calculated by measuring the initial and equilibrium concentrations) of the lead ions were removed from the Pb-As (V) solution (Figure 6.9). In comparison to lead in arsenite phase, reduction of lead was approximately 50 percent (Figure 6.10). As discussed earlier, the removal of lead has been observed to be comparatively higher in presence of pentavalent arsenic ions than in case of trivalent radicals. This is particularly significant at pH ranges from 4-9, because the trivalent arsenic ions remain undissasociated. From Figure 6.11 at pH 7, reduction of lead ions from a lead-rsenite solution was over 90 per cent of its original concentration. At identical pH, 90 per cent of lead ions were excluded from the lead-arsenate solution (Figure 6.12). The effect of pH coupled with increasing concentration of the cation appears largely responsible for significant adsorption of lead. The abatement of protonated sites on the substrate appears to have deterred the removal of both the As (III) and As (V) species. Further increase of pH of the bulk phase to 9 resulted in over 90 per cent reduction of original lead ion concentration in both the solutions with respect to As (III) and As (V) (Figure 6.13 and 6.14). The effect of pH was insignificant in removal of As (III) and As (V) anions. At pH 11, an almost complete removal of lead ions from both the bulk phases was observed (Figure 6.15 and 6.16). At existing pH level, Arsenic (III) and Arsenic (V) species existed as $H_2AsO_3^-$ and $HAsO_4^{2-}$ ions respectively. An insignificant adsorption of As (III) species was noted and practically no removal observed in the case of As (V) anions. As discussed earlier, higher valence charge of As (V) species have resulted in stronger electrostatic repulsions between the anions and adsorbent. At concentration levels of 350 ppb, the effect of repulsive forces of both the As (III) and As (V) (in presence of hydroxyl and nitrate ions) ions on the substrate could

not be gauged; however, the repulsive effect was expected to have a stronger impact at concentrations of 1000 ppb Arsenic.

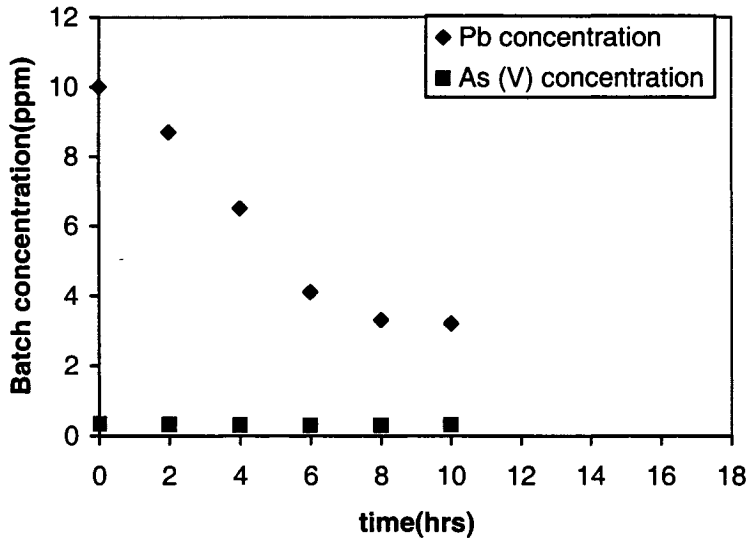

Figure 6.9 Batch tests at pH 4(initial concentration:10 ppm (Pb) and 350ppb As(V))

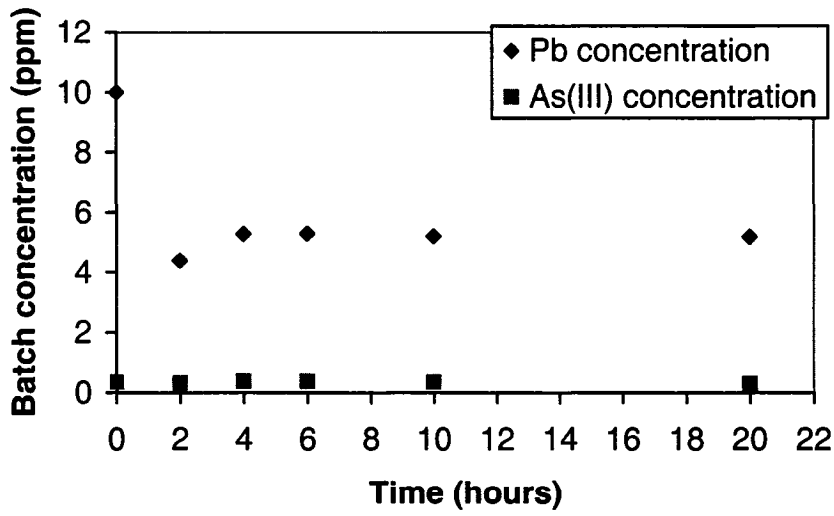

Figure 6.10 Batch tests at pH 4(initial concentration:10 ppm (Pb) and 350ppb As(III))

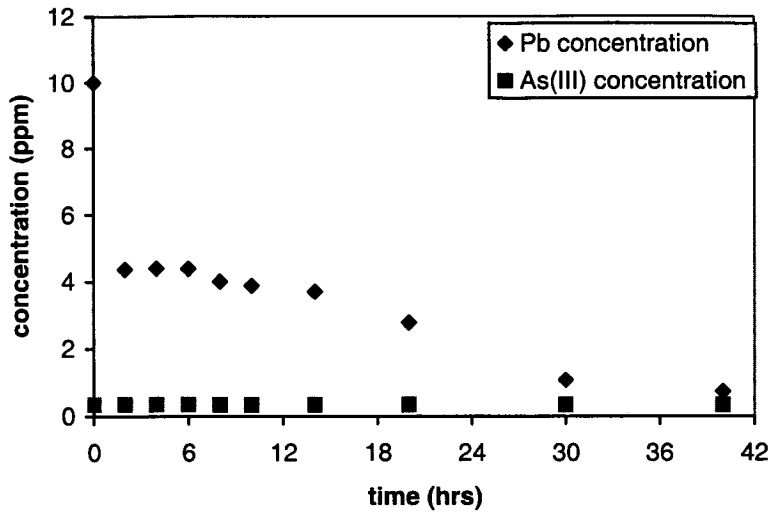

Figure 6.11 Batch tests at pH 7(initial concentration:10 ppm (Pb) and 350ppb As(III))

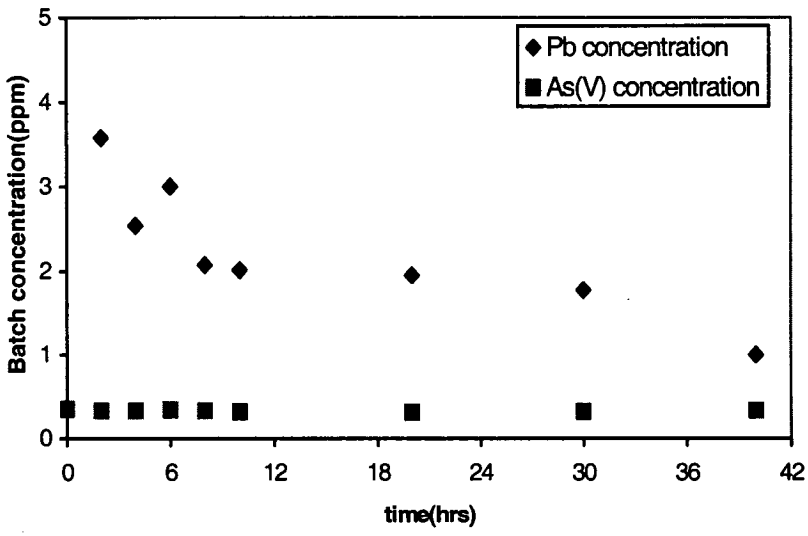

Figure 6.12. Batch tests at pH 7(initial concentration:10 ppm (Pb) and 350ppb As(V))

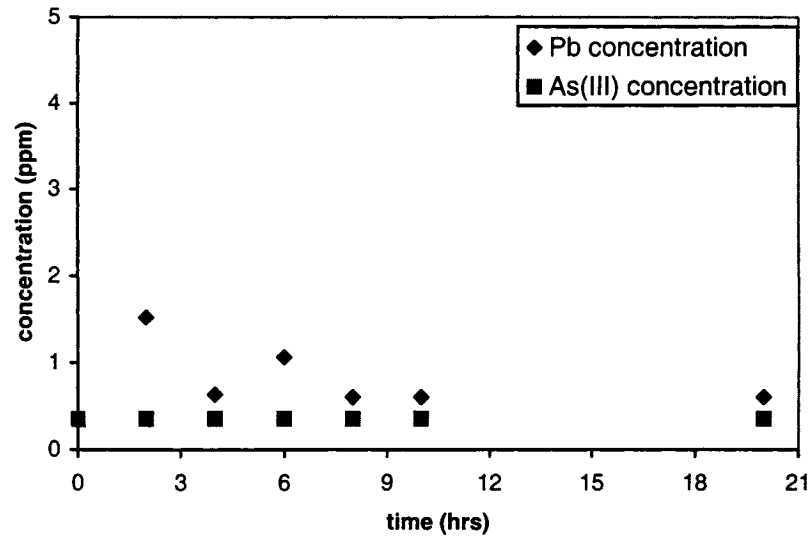

Figure 6.13. Batch tests at pH 9(initial concentration:10 ppm (Pb) and 350ppb As(III))

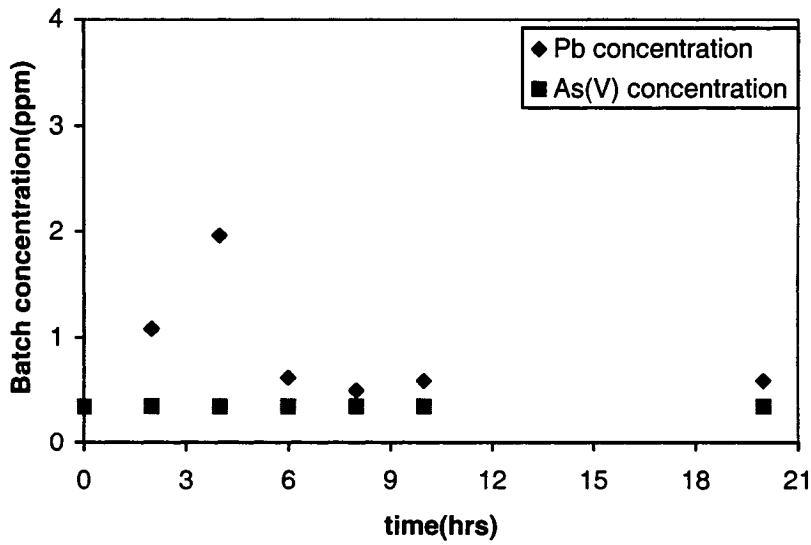

Figure 6.14 Batch tests at pH 9(initial concentration:10 ppm (Pb) and 350ppb As(V))

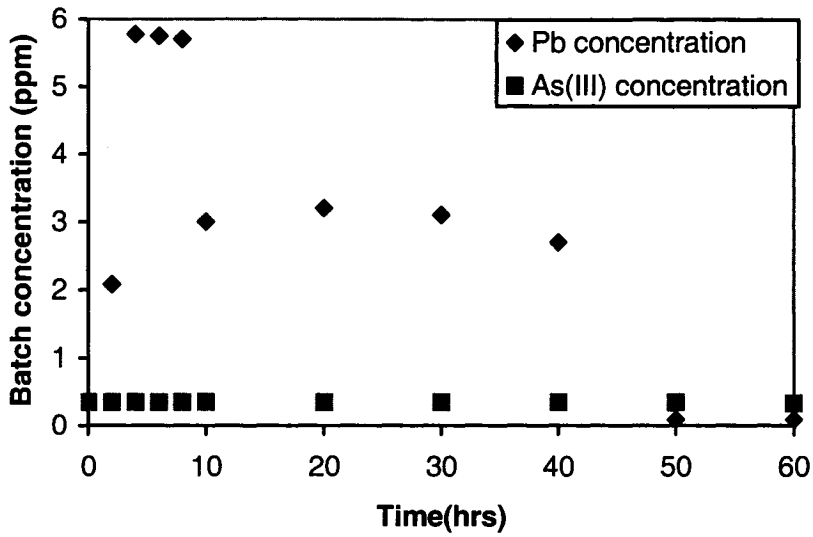

Figure 6.15 Batch tests at pH 11(initial concentration:10 ppm (Pb) and 350ppb As(III))

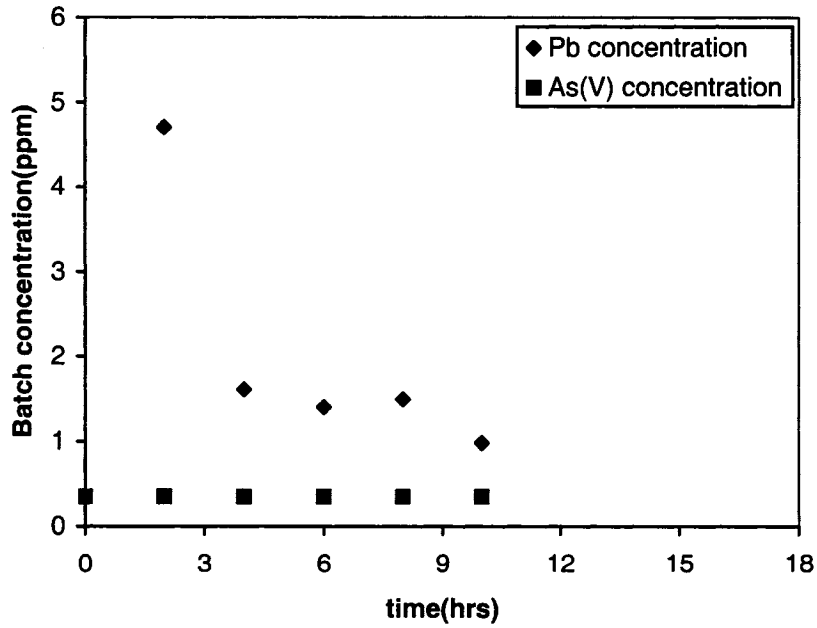

Figure 6.16. Batch tests at pH 11(initial concentration:10 ppm (Pb) and 350ppb As(V))

6.1.1.3 Lead Concentration (40ppm) and As(III) or As(V) at 350ppb

The effect of pH and influent concentration of lead ions in relation to the adsorption of both species is further displayed in Figures 6.17 and 6.18. Increasing the ionic strength of lead ions (40 ppm) allows significant interaction of the contaminant with the substrate. At pH 4, the total adsorption of Lead ions from the bulk phase in the presence of either As (III) or As (V) anions was approximately half of its initial concentration. The amount of arsenic (III) adsorption was insignificant, but As (V) (due to $H_2AsO_4^-$ species) underwent columbic attraction with the protonated substrate. The attraction between reverse charges appears to have enhanced of adsorption of the penta-valent arsenic species.

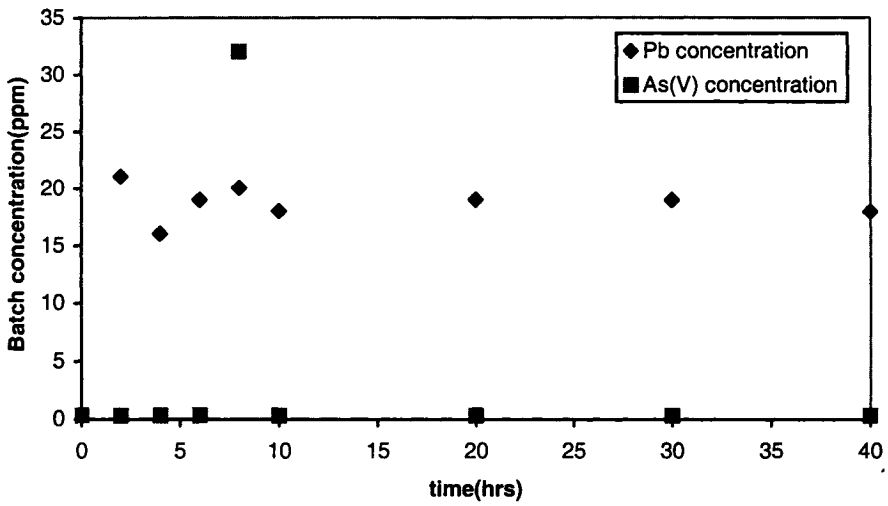

Figure 6.17 Batch tests at pH 4(initial concentration:40 ppm (Pb) and 350ppb As(V))

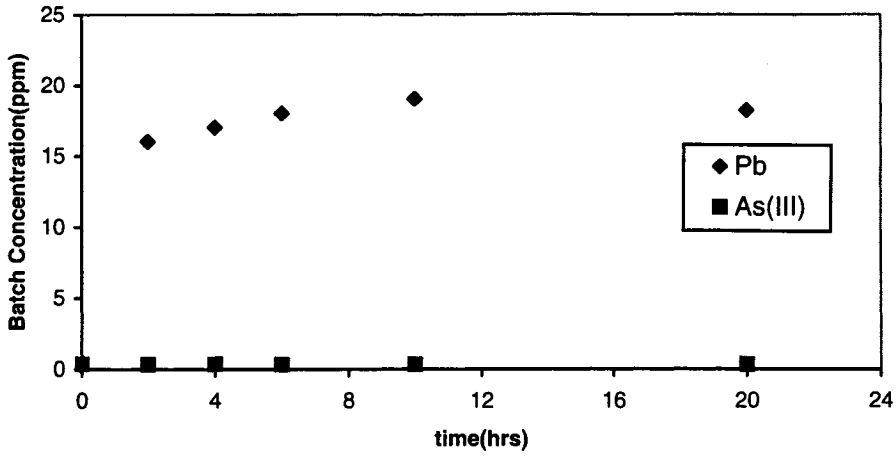

Figure 6.18 Batch tests at pH 4(initial concentration:40 ppm (Pb) and 350ppb As(III))

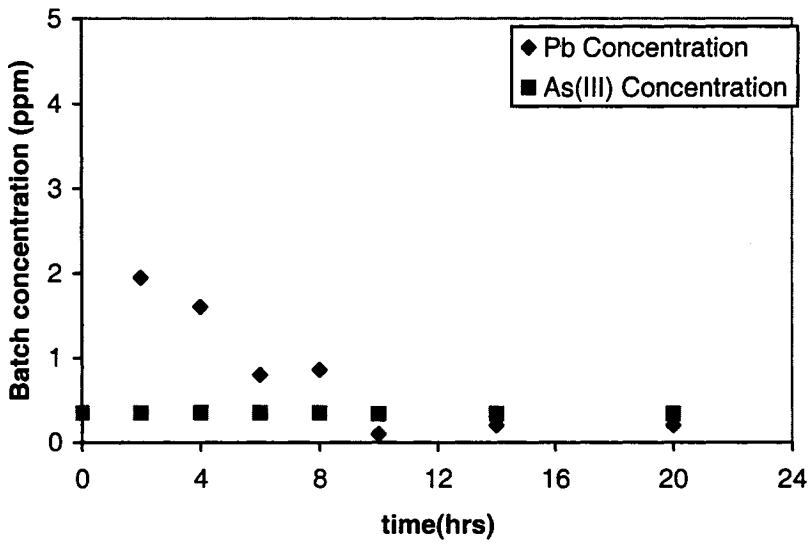

Figure 6.19 Batch tests at pH 7(initial concentration:40 ppm (Pb) and 350ppb As(III))

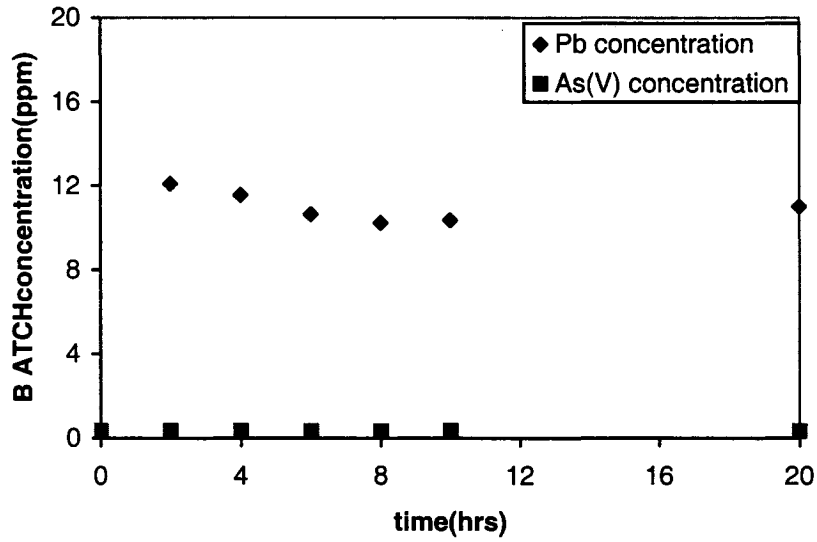

Figure 6.20 Batch tests at pH 7(initial concentration:40 ppm (Pb) and 350ppb As(V))

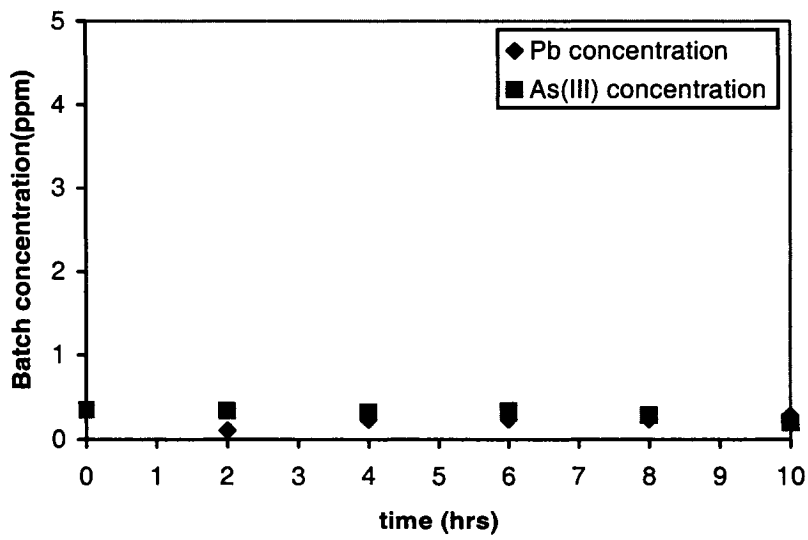

Figure 6.21 Batch tests at pH 9(initial concentration:40 ppm (Pb) and 350ppb As(III))

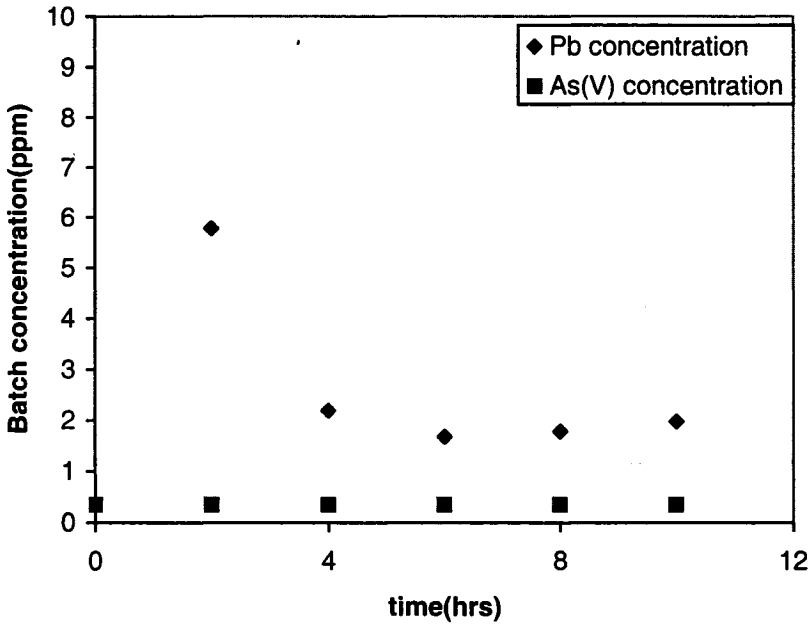

Figure 6.22 Batch tests at pH 9(initial concentration:40 ppm (Pb) and 350ppb As(V))

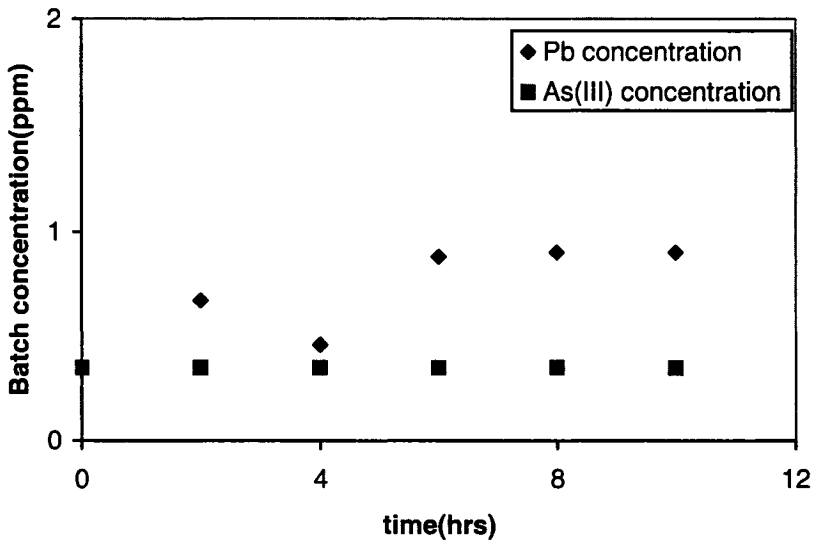

Figure 6.23 Batch tests at pH 11(initial concentration:40 ppm (Pb) and 350ppb As(III))

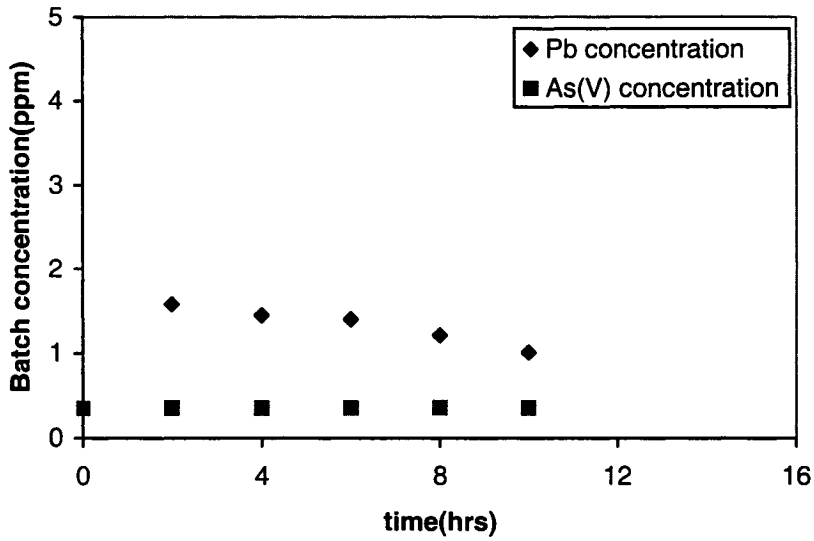

Figure 6.24 Batch tests at pH 11(initial concentration:40 ppm (Pb) and 350ppb As(V))

A reduction of positive charge on the adsorbent was observed with further increase of pH. This accounts for the apparent increase of adsorption activities of lead cations in both the multi-component phases (Figure 6.19 and Figure 6.20). However, the lack of disassociation of H_3AsO_3 species deterred the reduction of trivalent arsenic. In addition, the existence of $HAsO_4^{2-}$ ions at pH 7 validated the inference that mutual repulsion between the As (V) species and the substrate was active. By comparison, at pH 9, the negatively charged substrate was highly nucleophilic in nature. The nucleophilic sites on the adsorbent were ideal for chemisorption of the lead cations at initial concentrations of 40 ppm. Thus, from Figures 6.21 and 6.22, it may be concluded that the increase in negative charges of the arsenic results in an increase in removal of lead ions and decrease in adsorption of As (V) species. The effect of pH on adsorption of the trivalent arsenic cations was nominal. The As (III) species remained un-disassociated at pH 9.

The increased adsorption of lead (with increasing ionic strength from 10 ppm to 40 ppm) with respect to pH of the bulk phase was validated by the results at pH 11. Lead ion concentration in both the multi-component bulk phases was reduced to nearly 2 per cent of its original bulk concentration. However, increase in mutual repulsion between the pollutant and the adsorbent inhibited the adsorption behavior of both the arsenic species (Figures 6.23 and 6.24).

6.1.1.4 Lead Concentration of 2.5 ppm and As concentration of 1000ppb

In comparison to multi-component solutions with As (III) or As (V) concentrations of 350 ppb, over 10 per cent and 20 per cent of As (III) species and As (V) species were removed respectively (Figure 6.25 and 6.26). However, the effect of adsorption of lead ion at pH 4 was highly dependent on the nature of the arsenic species. At the existing pH level, the lack of As (III) anions hindered the removal of the species. As (V) anions, undergo electrostatic attraction with the protonated substrate, may have been form complexes with both the lead and calcium cations in the bulk phase. Thus, in relation to arsenite species, 60 per cent of lead ions were excluded from its original phase. In association with arsenate species, a near complete uptake of lead was observed. With increase in pH to 7, lead ions in the arsenite phase decreased to 40 per cent of its original concentration. In contrast, 95 per cent of the lead species were removed from the multi-component arsenate phase (Figure 6.26 and Figure 6.27a). A comparison of Figure 6.25 to Figure 6.27b discloses no appreciable change in adsorption of lead at pH 7. The decrease in variation of adsorption of Lead ions with increase in pH may be attributed to the presence of significant proportions of H_3AsO_3 species. Because As (III) ions diffuse at a faster rate than the larger sized lead ions (Waypa et al., 1997), a tendency to form a mono layer over the adsorption sites and to retard the removal of lead species from the bulk phase would be anticipated. The As (V) anions undergo electrostatic attractions to the protonated surfaces. Besides complex formations with the lead ions did account for the appreciable reduction (95 per cent) of the cations (Figures 6.26 and 6.27a).

The concentration ratio of lead to arsenic ions was 2.5, the lowest ratio considered for the batch tests with respect to lead ions. Compared to other ratios of lead to arsenic, the penta-valent arsenic species were slightly outnumbered by the lead species, tending to reduce competition of sorption of arsenic species to the adsorbent.

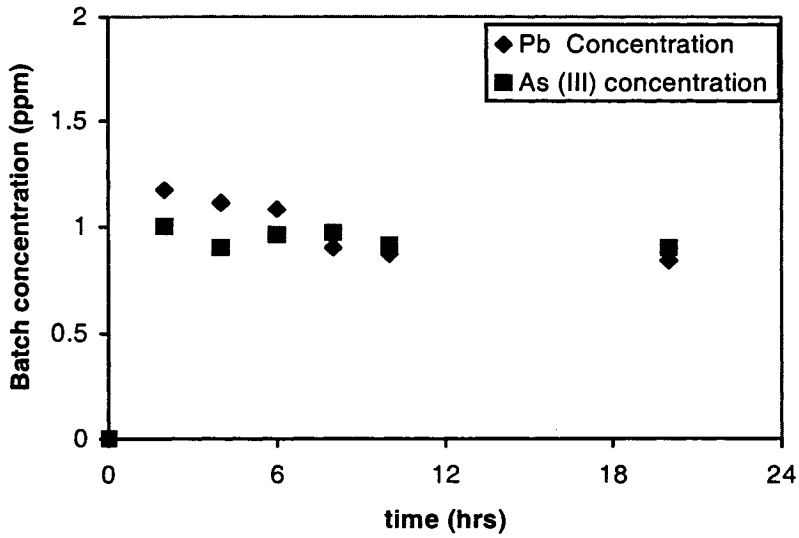

Figure 6.25 Batch tests at pH 4(initial concentration:2.5 ppm (Pb) and 1000ppb As(III))

The presence of As (III) species at pH 9 was noted to have further inhibited the removal of lead ions (Figure 6.29). The increase in pH should have increased the removal efficiency of lead ions. As discussed earlier, the presence of significant amounts of H_3AsO_3 species with Lead ions deters the adsorption mechanism between the latter and the negative surface. In case of lead ions in association with arsenate species, significant ion-pair attraction between the arsenate species (because of higher concentrations, 1000ppb) and lead ions in the bulk phase may have hampered the removal of the cation (Figure 6.28). Comparing Figure 6.28 to Figure 6.7, 80 per cent of the lead cations were removed with respect to 1000 ppb of As (V); 98 per cent was removed with respect to an arsenate concentration of 350 ppb. Further, as discussed by Hodgson (1970), the presence of significant amount of sodium ions (more permeable than lead ions) may have also competed with lead species in the adsorption process.

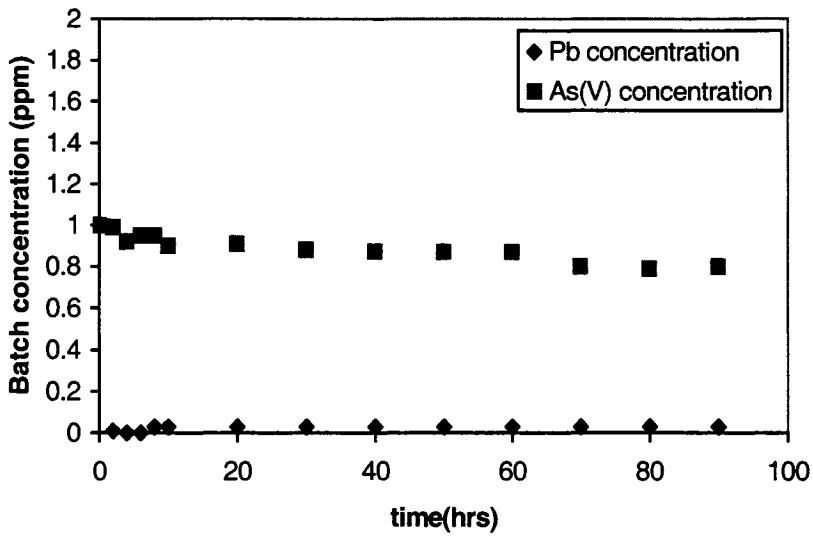

Figure 6.26 Batch tests at pH 4 (initial concentration:2.5 ppm (Pb) and 1000ppb As(V))

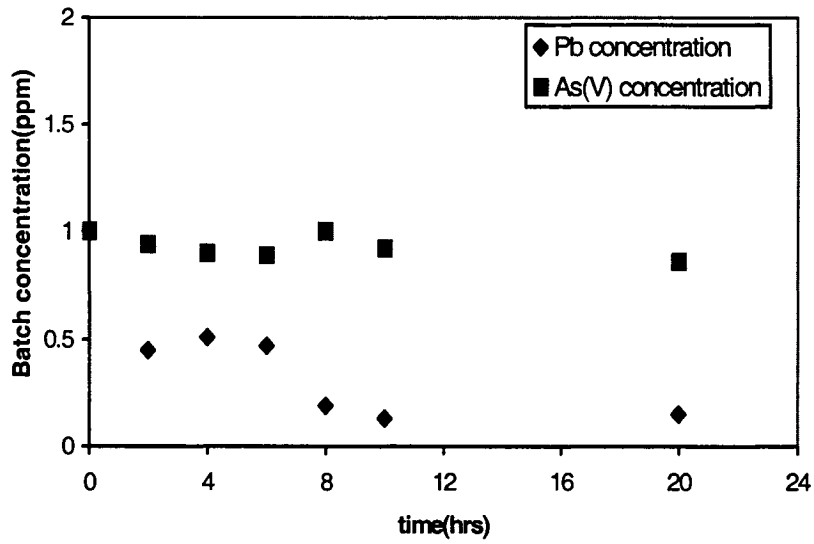

Figure 6.27a Batch tests at pH 7(initial concentration:2.5 ppm (Pb) and 1000ppb As(V))

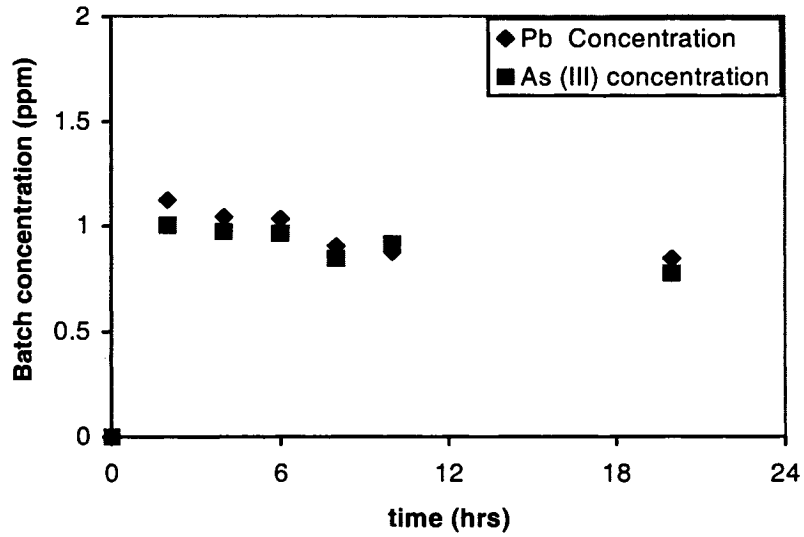

Figure6.27b Batch tests at pH7(initial concentration:2.5 ppm (Pb) and 1000ppb As(III))

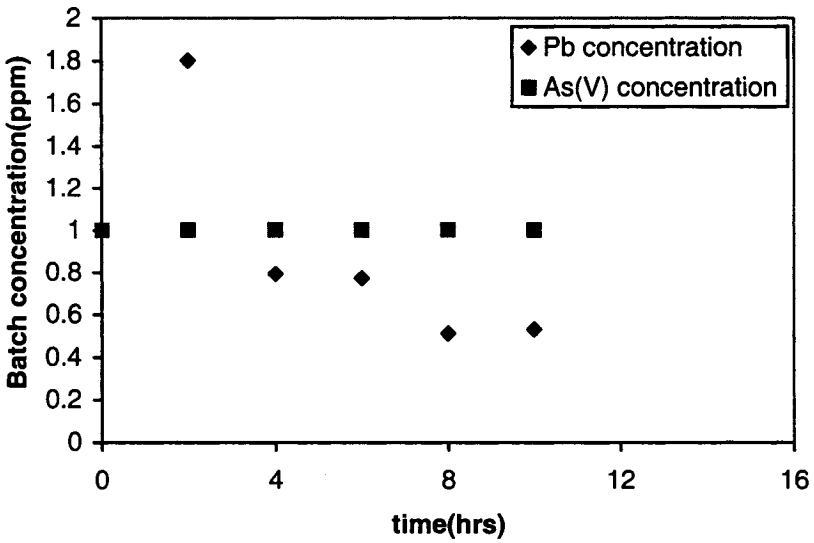

Figure 6.28 Batch tests at pH 9(initial concentration:2.5 ppm (Pb) and 1000ppb As(V))

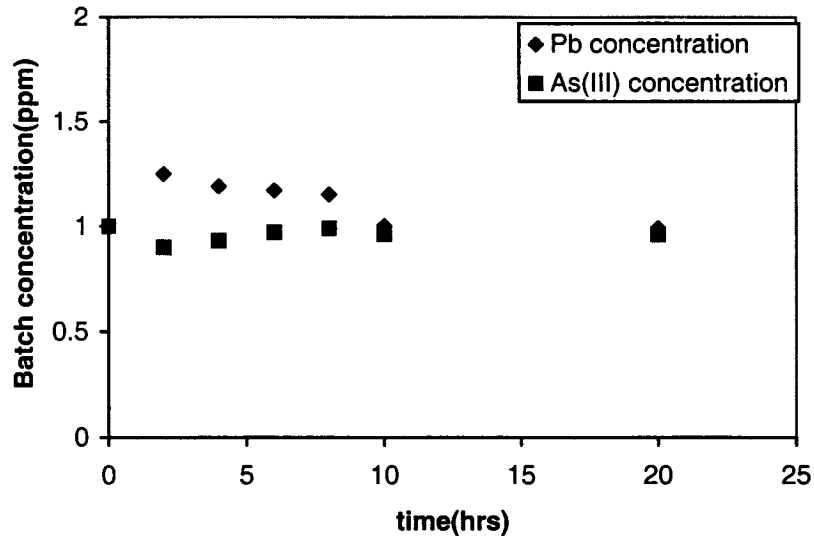

Figure 6.29 Batch tests at pH 9(initial concentration:2.5 ppm (Pb) and 1000ppb As(III))

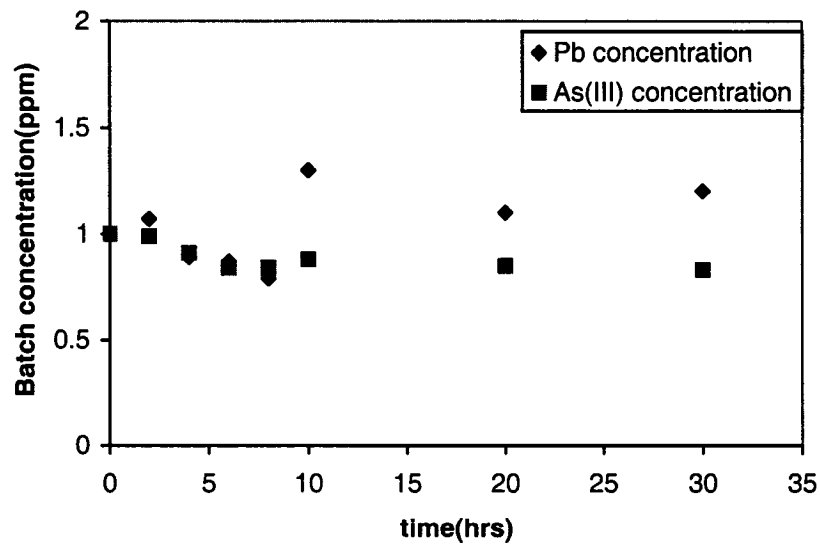

Figure 6.30 Batch tests at pH 11(initial concentration:2.5 ppm (Pb) and 1000ppb As(III))

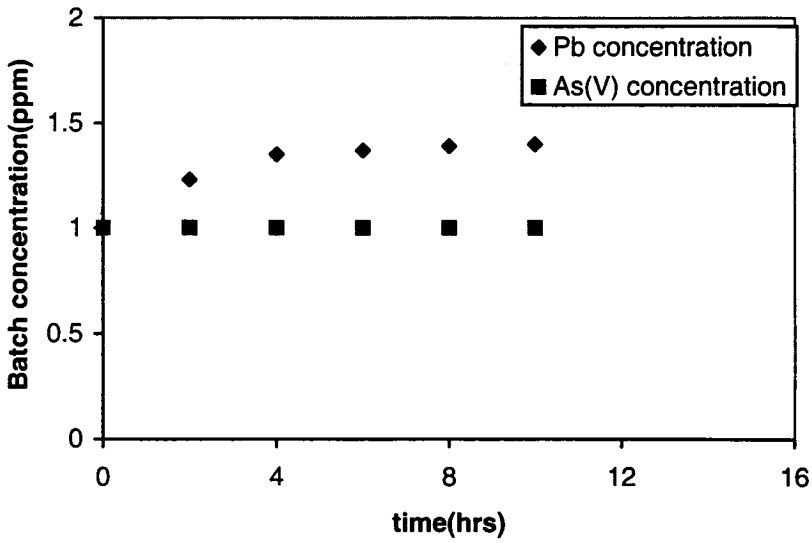

Figure 6.31 Batch tests at pH 11(initial concentration:2.5 ppm (Pb) and 1000ppb As(V))

At equilibrium, the presence of a higher number of negative charged sites induced stronger repulsions than at pH 9, resulting in further decrease of adsorption of lead ions (Figure 6.31). This decreased adsorption was observed with respect to both As (III) and As(V) species (see Figure 6.30). At pH 11, the existence of such As (III) species as $H_2AsO_3^-$, allowed 52 per cent removal of the cation. Compared to Figure 6.31, the removal of lead was weaker (45 percent) in the presence of As (V) anions. The pentavalent Arsenic ions at pH11 existed as $HAsO_4^{2-}$ ions. Being divalent in nature, the effect of repulsive forces between the substrate and adsorbate (Arsenic only) may haved had a stronger impact than the interaction of the adsorbent to the As (III) radicals. In contrast to what is observed in Figure 6.30, the presence of a larger concentration of As (V) species induced stronger repulsive forces that reduced the proficiency of adsorption of the lead ions in dilute solution (Figure 6.31). As discussed earlier (Seidel et al., 2001), an increase in pH results in a reduction of the exclusion of anions from the bulk phase. However, the significance of a discrepancy of 7 percent, due to the valency of the counter

ions, appears to be within the standard error. In Chapter 4, it was mentioned that the charge density of the adsorbent was extremely high. This would allow the lead ions to permeate into the adsorbed phase in an identical manner irrespective of the valence of the counter ions. The effect of variance in charges of the arsenic species may then be negligible. However, the extent of mutual attraction between lead and arsenic species in bulk phase may have retarded the adsorption. At higher lead-to-arsenic concentration ratios, such attractive behavior is abated.

6.1.1.5 Lead Concentration at 10 ppm and Arsenic 1000ppb

After increasing the initial concentration of lead ions to 10 ppm in the lead-arsenite multi-component phase, the effective percentage of its removal at equilibrium condition was approximately 45 per cent of its original concentration (Figure 6.32). However, in the lead–As (V) phase, the negative charged anions readily formed complexes with the lead ions. This validates the inference that removal of the lead ions increased in comparison to As (V) species (Figure 6.33). The As (V) ions also minimized the degree of protonation on the substrate, thereby assisting increased adsorption of lead ions.

Increasing pH from 4 to 7, enhanced the adsorption of lead ions with respect to both As (III) and As (V) species (Figure 6.34 and 6.35). However, a further increase in pH to 9, was supplemented by a decrease in adsorption of lead ions (Figure 6.36 and Figure 6.37). The sharp decrease in adsorption of lead ions with respect to Arsenate phase was perhaps due to the repulsive forces generated by the $HAsO_4^{2-}$ ions with the negatively charged substrate. However, the lack of ionization of the arsenite species minimized the repulsive forces, considerably reducing its effects on adsorption.

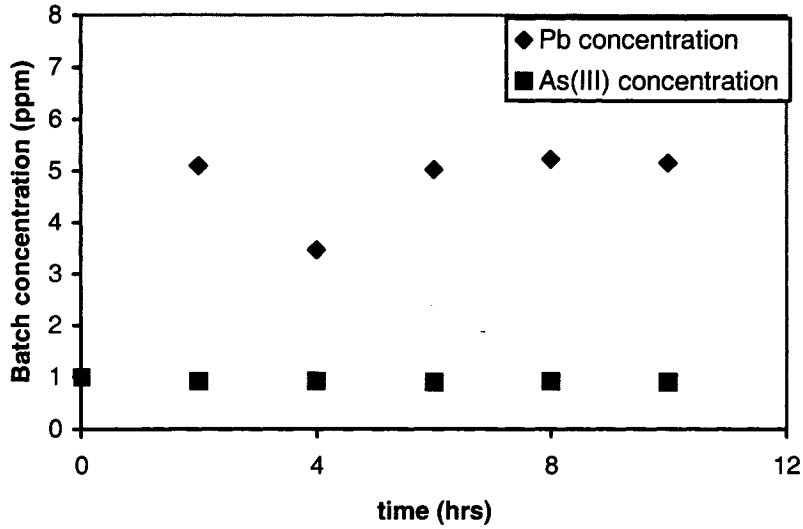

Figure 6.32 Batch tests at pH 4(initial concentration:10 ppm (Pb) and 1000ppb As(III))

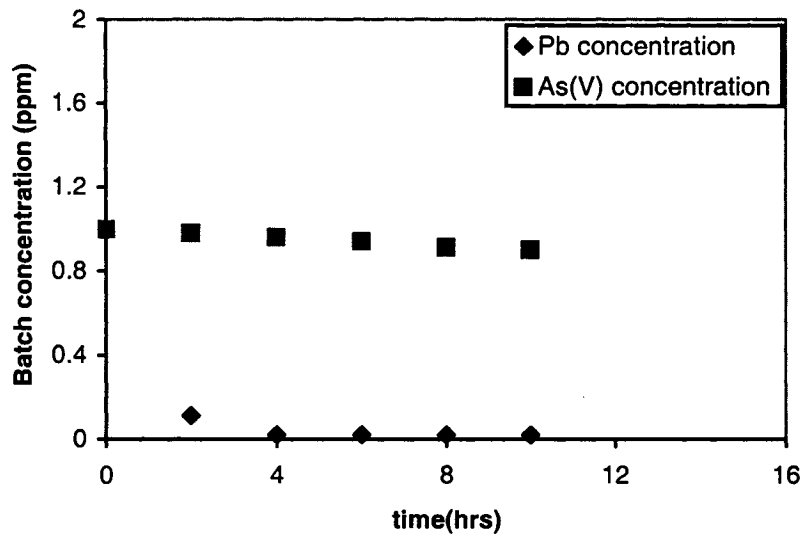

Figure 6.33 Batch tests at pH 4(initial concentration:10 ppm (Pb) and 1000ppb As(V))

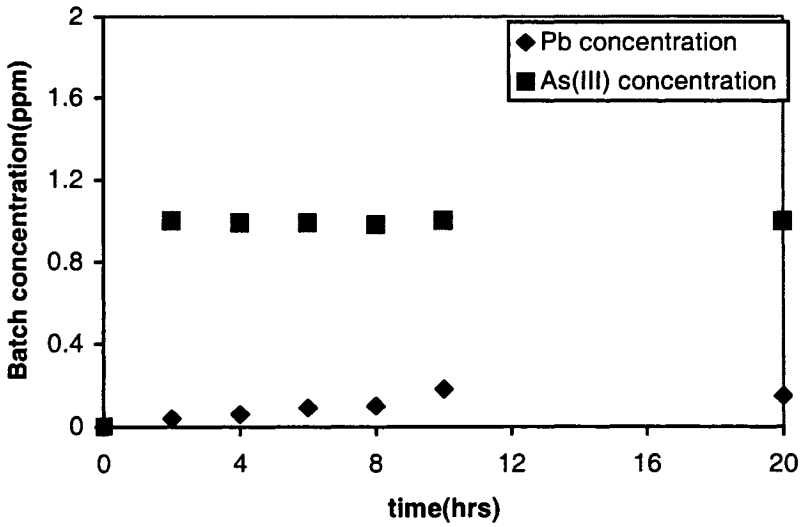

Figure 6.34 Batch tests at pH 7(initial concentration:10 ppm (Pb) and 1000ppb As(III))

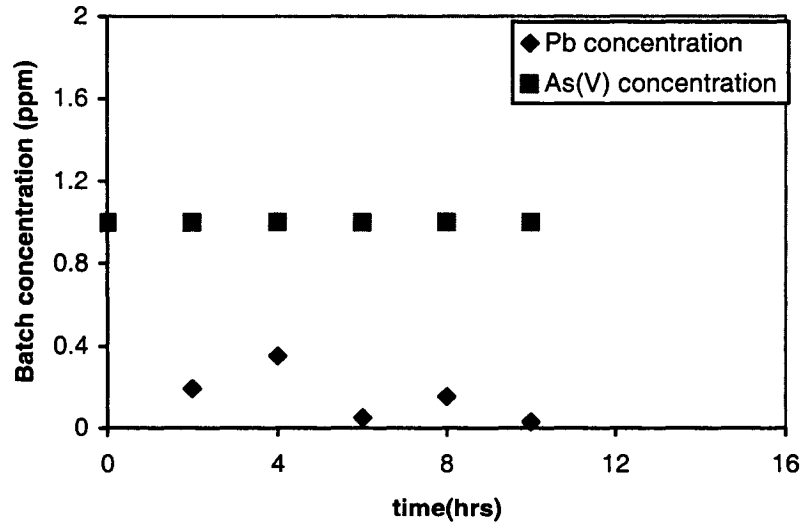

Figure 6.35 Batch tests at pH 7(initial concentration:10 ppm (Pb) and 1000ppb As(V))

At pH 11, increasing deprotonation of the substrate increased adsorption of lead ions in As (III) phase. Even though As (III) species ionized to form $H_2AsO_3^-$ ions, the effect of mutual repulsion was minimal (Figure 6.38). The exclusion of lead ions in arsenate phase was about 80 per cent of its original concentration (Figure 6.39). The divalent nature of the pentavalent arsenic ions contributed to stronger repulsions than the monovalent As (III) species in the bulk phase. However, compared to Figure 6.31, it was confirmed that the increase in concentration of the lead ions in the bulk phase diminished the effect of mutual repulsion of the arsenic species and the adsorbent. The application of Langmuir isotherm (with increasing initial concentration of contaminant) is valid for the process.

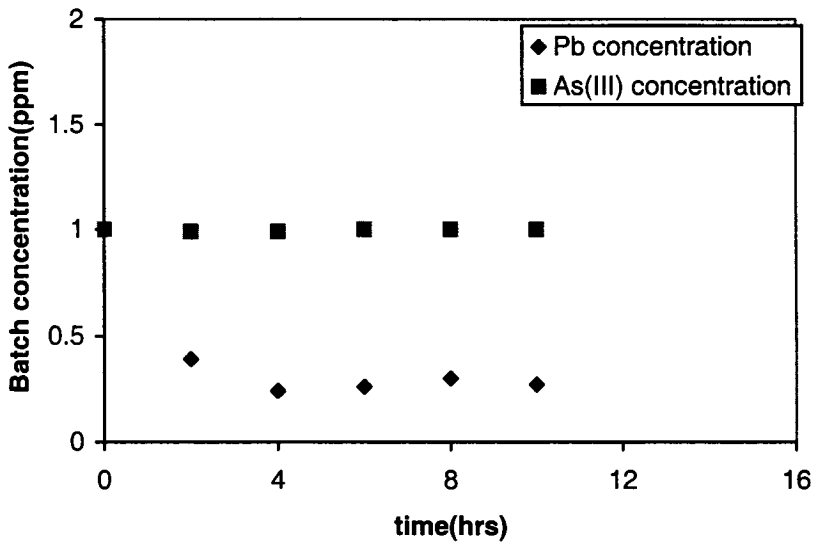

Figure 6.36 Batch tests at pH 9(initial concentration:10 ppm (Pb) and 1000ppb As(III))

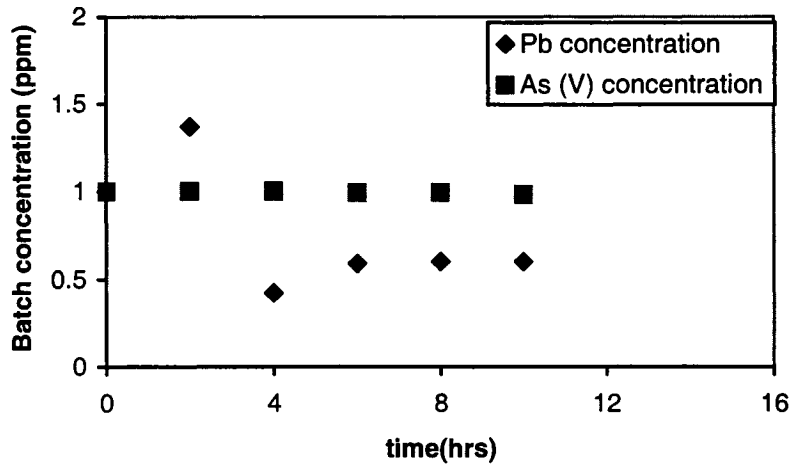

Figure 6.37 Batch tests at pH 9(initial concentration:10 ppm (Pb) and 1000ppb As(V))

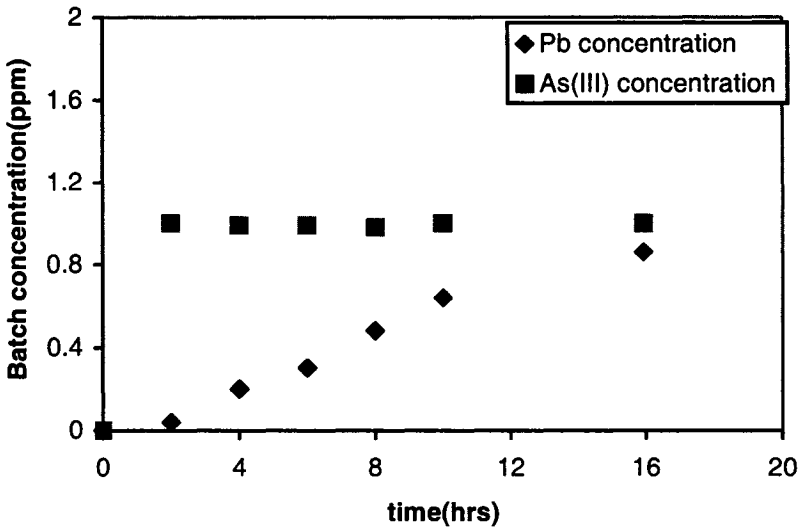

Figure 6.38 Batch tests at pH 11(initial concentration:10 ppm (Pb) and 1000ppb As(III))

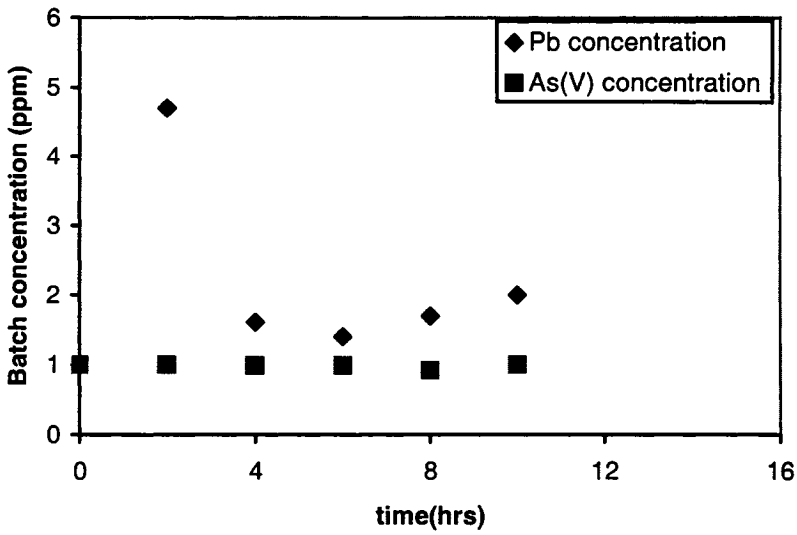

Figure 6.39 Batch tests at pH 11(initial concentration:10 ppm (Pb) and 1000ppb As(V))

In Figures 6.38 and 6.39, improper sampling techniques may have contributed to apparent increase in concentration with respect to time interval. However, the significance of these experimental runs lay in the determining (for each case) the equilibrium concentration with respect to pH of the bulk phase, initial concentration of the adsorbate and mass of the adsorbent.

6.1.1.6 Lead concentration of 40 ppm and As 1000 ppb

The experimental results incident upon increasing the concentration of Lead cations from 10 ppm to 40 ppm serve further to illustrate the dominance of the pH factor in the removal mechanisms operating on both the species. At pH 4, 50 per cent of the arsenic species was removed by the adsorbent (Figure 6.40). In the case of lead ions associated with arsenate species, 60 per cent of the lead species were removed from the bulk phase. This net increase of 10 percentage points appears attributable to the complexation of the arsenate ions to both substrate and the bulk phase.

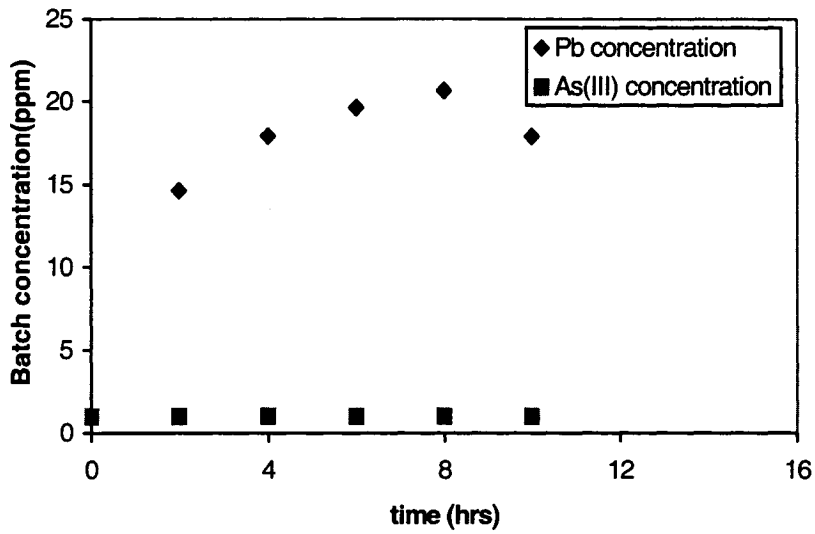

Figure 6.40 Batch tests at pH 4(initial concentration:40 ppm (Pb) and 1000ppb As(III))

The arsenite adsorption remained insignificant at pH 4. The heterogeneous nature of substrate may have led to pH fluctuations, in turn affecting the concentration profile in Figure 6.40.

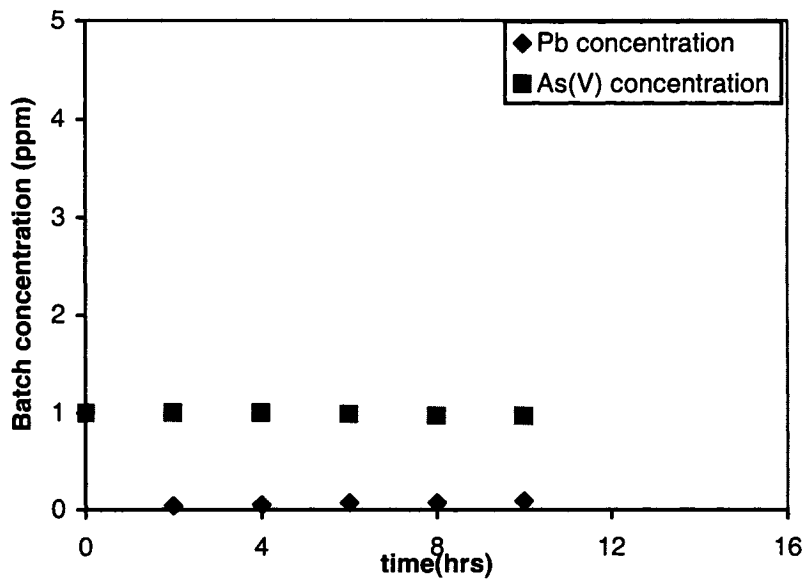

Figure 6.41 Batch tests at pH 4(initial concentration:40 ppm (Pb) and 1000ppb As(V))

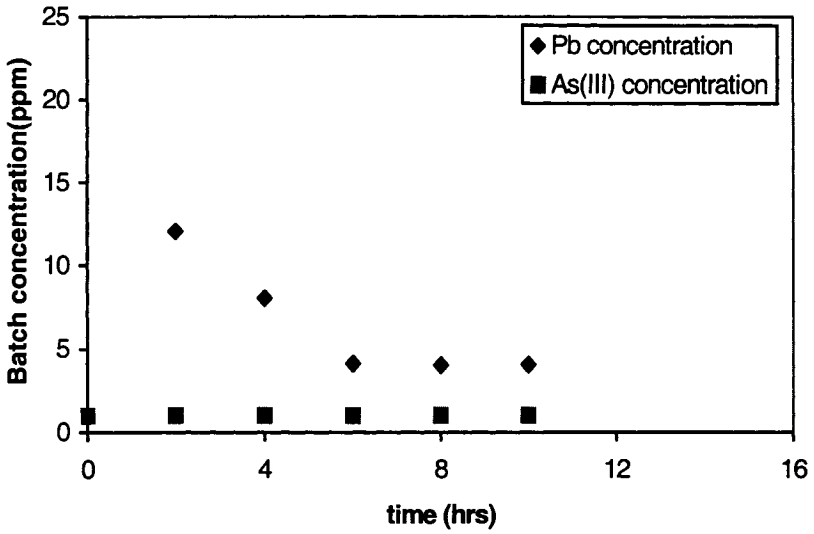

Figure 6.42 Batch tests at pH 7(initial concentration:40 ppm (Pb) and 1000ppb As(III))

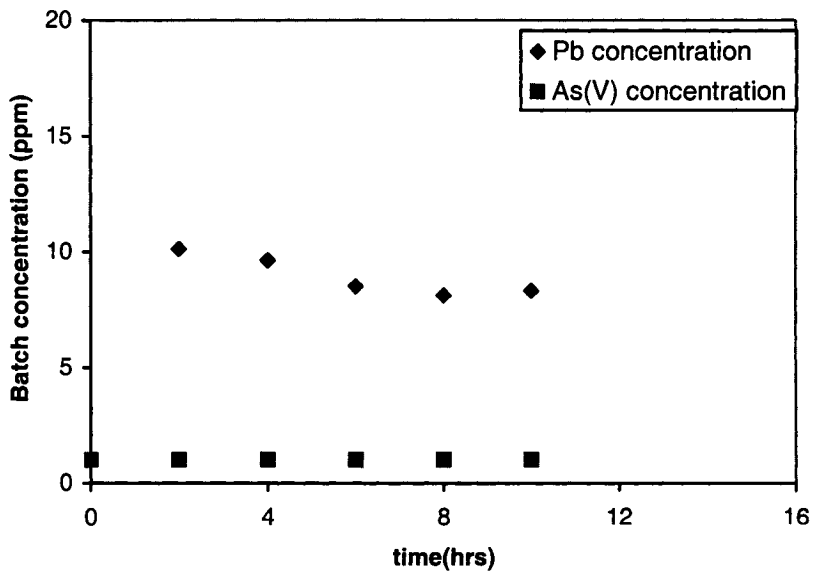

Figure 6.43 Batch tests at pH 7(initial concentration:40 ppm (Pb) and 1000ppb As(V))

At pH 7, approximately 90 per cent of the lead ions from original concentration in the influent was removed (Figure 6.42). Analogously, the increment in pH resulted in increased removal of the lead ions in the arsenite phase. With respect to arsenate ions, an equilibrium concentration of 8 ppm of Lead ions was observed (Figure 6.43). This disparity in removal rates under otherwise identical conditions (the sole exception being a difference in arsenic speciation) appears to have been minimal.

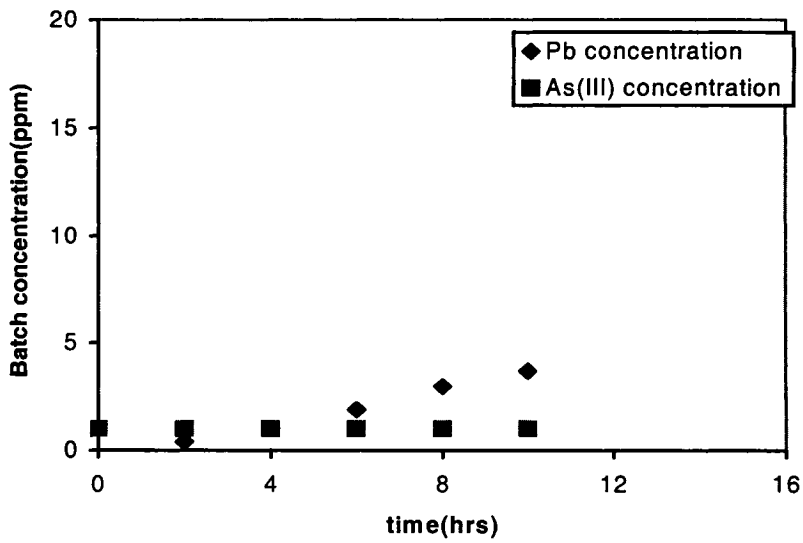

Figure 6.44 Batch tests at pH 9(initial concentration:40 ppm (Pb) and 1000ppb As(III))

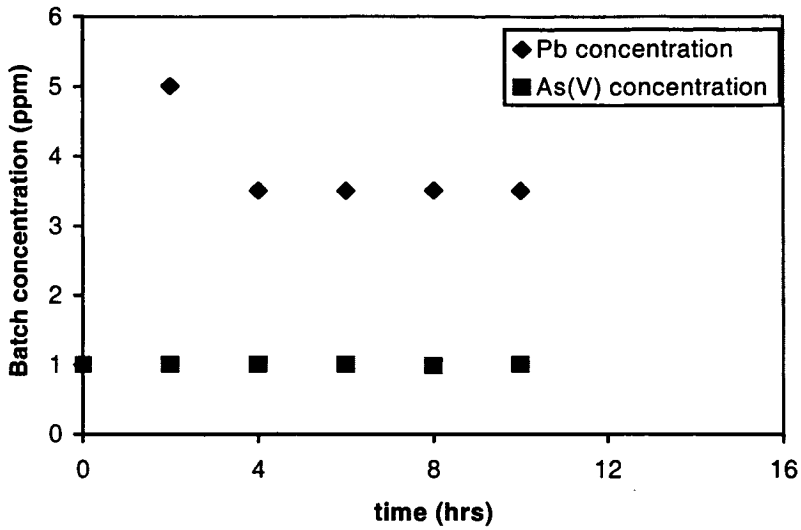

Figure 6.45 Batch tests at pH 9(initial concentration:40 ppm (Pb) and 1000ppb As(V))

With an increase in pH to 9, there appeared a 90 per cent reduction of lead ions in the As (III) phase. In relation to the lead ions in the arsenate phase, a complete removal was observed (Figure 6.45). Reconfirming the ineffectiveness in its removal at a pH range of 4-9, the removal of As (III) species was practically insignificant. However, in relation to the Arsenate species, a reduction of 15 per cent of As (V) anions was observed.

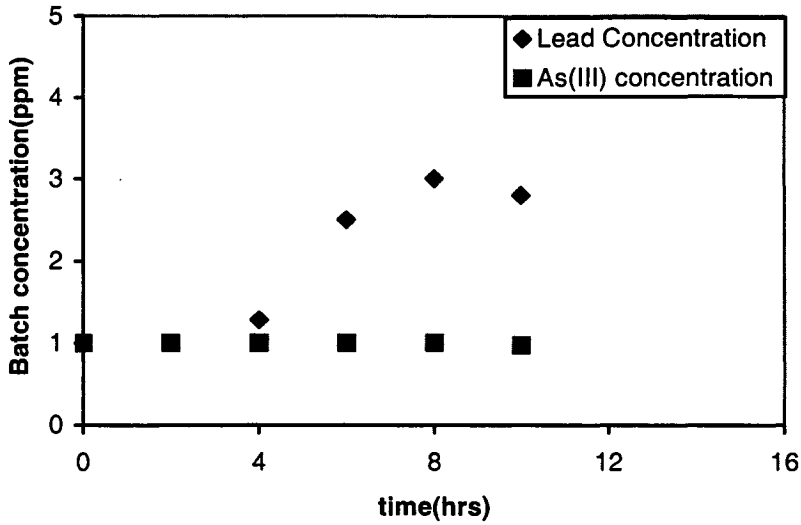

Figure 6.46 Batch tests at pH 11(initial concentration:40 ppm (Pb) and 1000ppb As(III))

At a pH 11, the removal of lead ions was over 90 per cent in relation to As (III) ions and to near completion in relation to As (V) ions (Figures 6.46 and 6.47). At higher pH levels, the degree of negative charge on the substrate was substantial. The increase in negatively charged sites on the substrate favored removal of lead ions by chemisorption, while repulsion among like charges between the adsorbent and arsenic (and nitrate) ions deterred reduction of both types of Arsenic species.

The concentration profiles in Figures 6.1-6.46 demonstrate the observed rates of removal of cations and anions from the bulk phase. After a specified time interval, no change in concentration of the effluent with respect to time interval was observed. The objective in conducting these batch tests was to determine the equilibrium concentrations of each batch. It was proven that the removal of arsenic species in the presence of lead cations was negligible. However, the removal of lead ions was unaffected by presence of arsenic ions. The concept of outer sphere analog (discussed above at page 163) was validated again by the results of the multi-component batch tests.

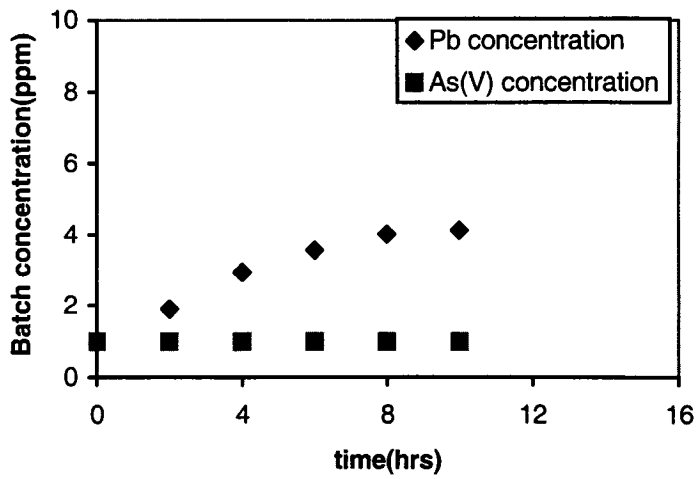

Figure 6.47 Batch tests at pH 11(initial concentration:40 ppm (Pb) and 1000ppb As(V))

6.2 Effect of Multi-component Adsorption Isotherms for Lead and Arsenic Species

Batch adsorption studies with different concentrations of Lead and Arsenic species were conducted at various pH levels from 4-11 (Figure 6.48-6.63). The objective was to determine the Langmuir isotherms for removal of the multi-components using Atlantic Cod scale. Single-component solutions of both lead and arsenic species displayed significant proportion of adsorption at various conditions. For scale-up design studies, it is imperative to analyze the ultimate adsorption capacities of the contaminants existing in multi-component phases.

The Langmuir adsorption isotherm is expressed as (Yun et al., 2003)

$$W_1 = \frac{Q_{m1} d_1 C_{e1}}{1 + d_1 C_{e1}} \tag{6.1}$$

$$W_2 = \frac{Q_{m2} d_2 C_{e2}}{1 + d_2 C_{e2}} \tag{6.2}$$

The above expressions can be further linearized and the value of d estimated for each set of isotherms. However, considering the set of multi-component batch experiments performed, the effect of arsenic species on adsorption of lead was observed to be negligible. Also, insignificant amounts of arsenic species were adsorbed in presence of lead ions. Thus, it is reasonable to modify the extended isotherm to a single-component isotherm with respect to the lead species.

Using indices 1 and 2 to refer to lead and arsenic species respectively, Equation 6.1 is modified to

$$\frac{1}{W_1} = \frac{1}{Q_{m1}} + \frac{1}{Q_{m1} d_1 C_{e1}} \tag{6.3}$$

Expressing W_2 as a function of initial and equilibrium concentrations, then

$$W_2 = \frac{(C_o - C_{e2})}{w} \tag{6.4}$$

d is the Langmuir coefficient of a species(L per mmol)

w is amount of adsorbent per liter of solution (g/L)

W is amount of contaminant adsorbed per unit mass of adsorbent (mg/g)

Ce is equilibrium concentration of a contaminant in bulk phase (mmol/L)

Qm is maximum adsorption capacity of a species (mg/g)

Solving Equations 6.2 and 6.4 simultaneously,

$$d_2 = \frac{(C_o - C_{e2})(1 + d_1 C_{e1})}{(Q_{m2} w + C_{e2} - C_o) C_{e2}} \tag{6.5}$$

The following figures describe the lead isotherms with respect to pH and initial concentrations of arsenic species. Note that the major assumption considered in the studies is that the removal of both the species is associated with adsorption (the extent of

precipitation with respect to speciation and pH of the bulk phases is a subject for further future study).

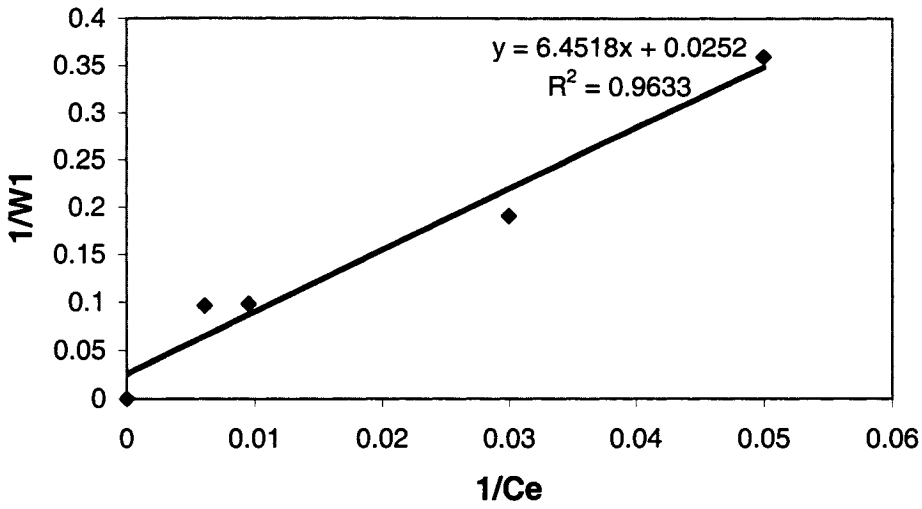

Figure 6.48 Isotherm of Lead with As(III) 350ppb at pH 4

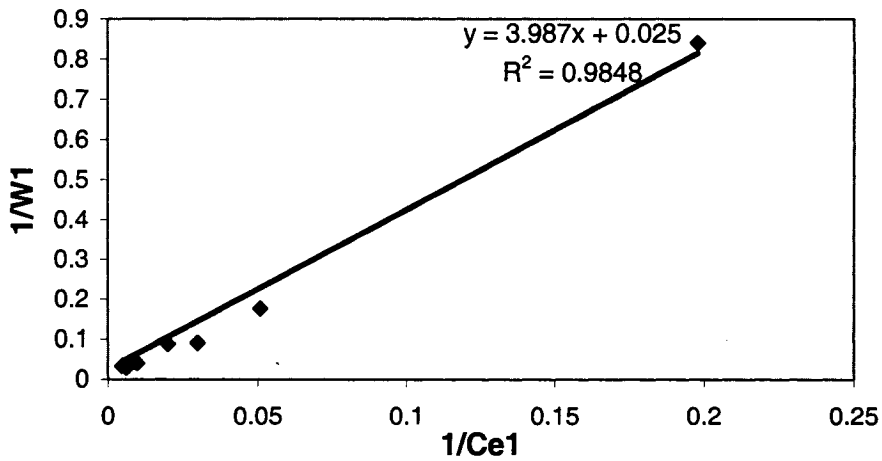

Figure 6.49 Isotherm of Lead with As (III) 350ppb at pH 7

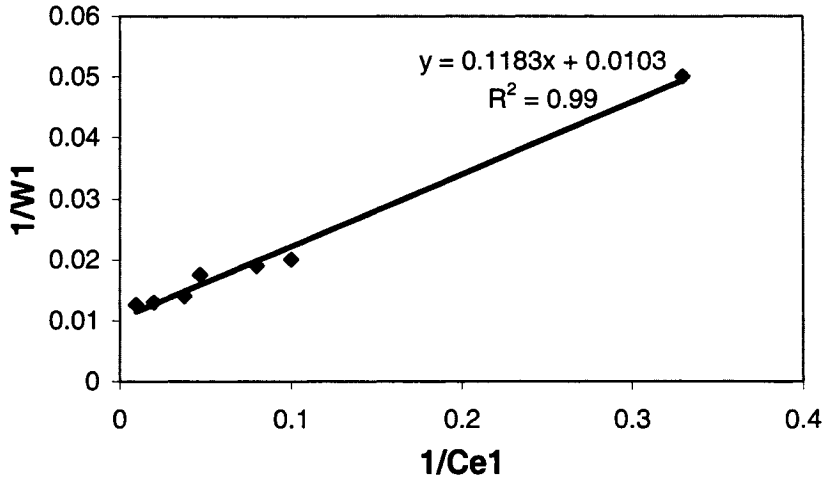

Figure 6.50 Isotherm of Lead with As (III) 350ppb at pH 9

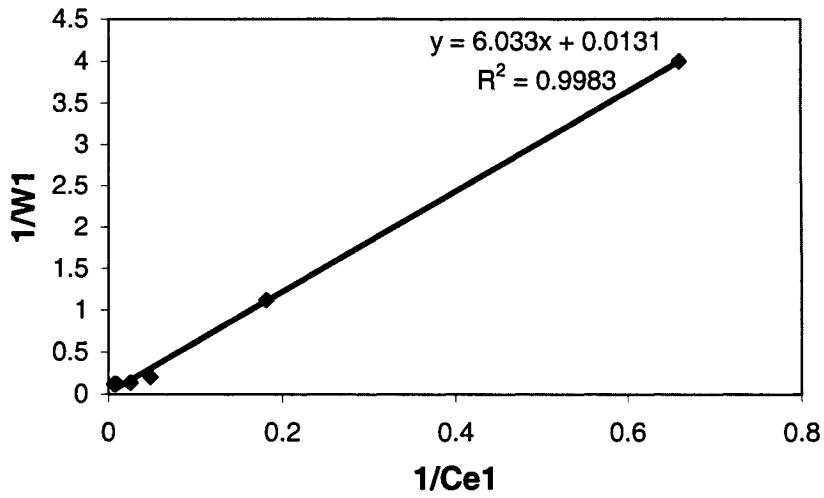

Figure 6.51 Isotherm of Lead with As (III) 1000ppb at pH 4

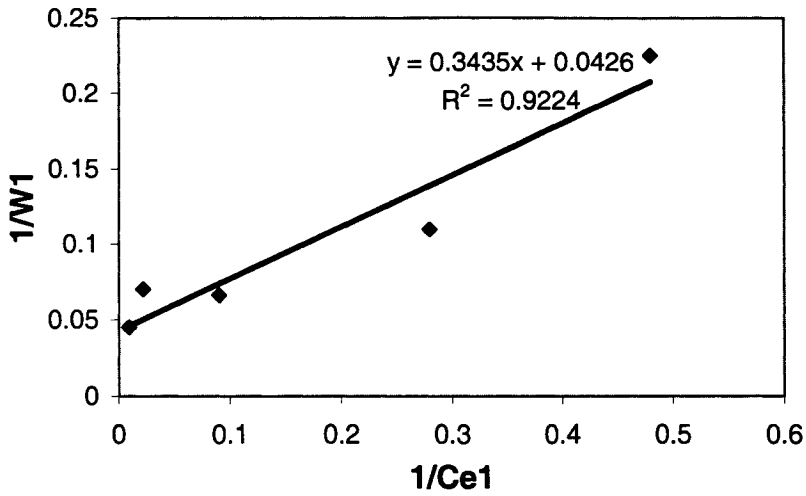

Figure 6.52 Isotherm of Lead with As (III) 1000ppb at pH 7

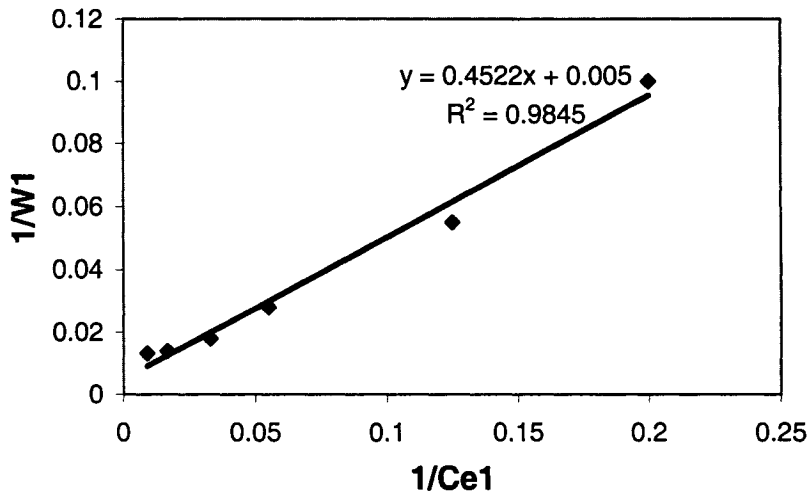

Figure 6.53 Isotherm of Lead with As (III) 1000ppb at pH 9

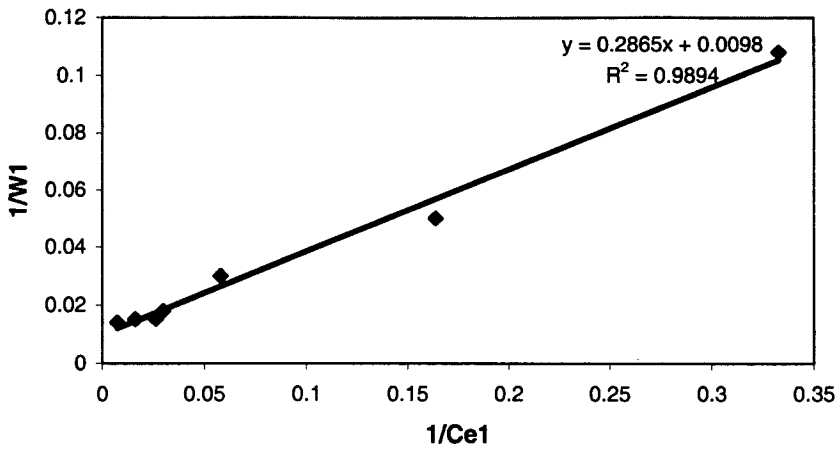

Figure 6.54 Isotherm of Lead with As (III) 1000ppb at pH 11

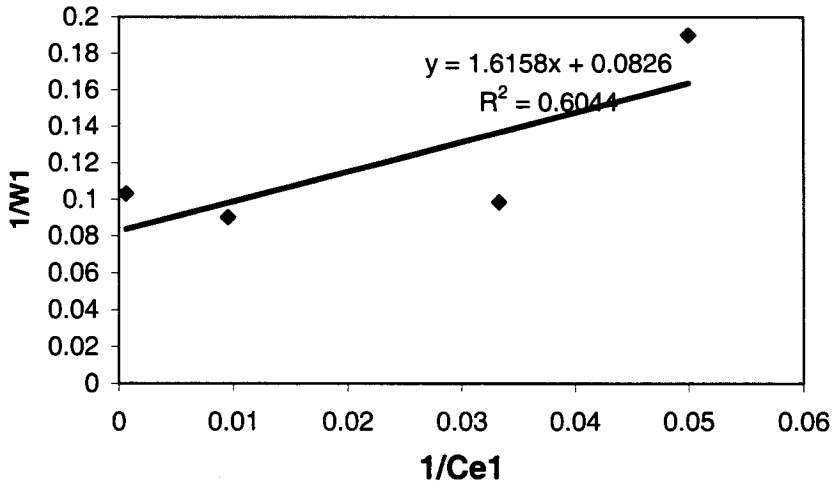

Figure 6.55 Isotherm of Lead with As (V) 350 ppb at pH 4

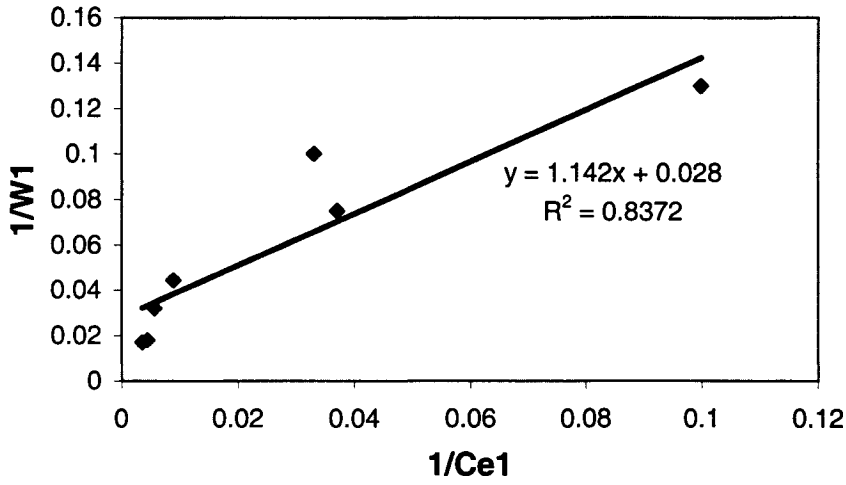

Figure 6.56 Isotherm of Lead with As (V) 350 ppb at pH 7

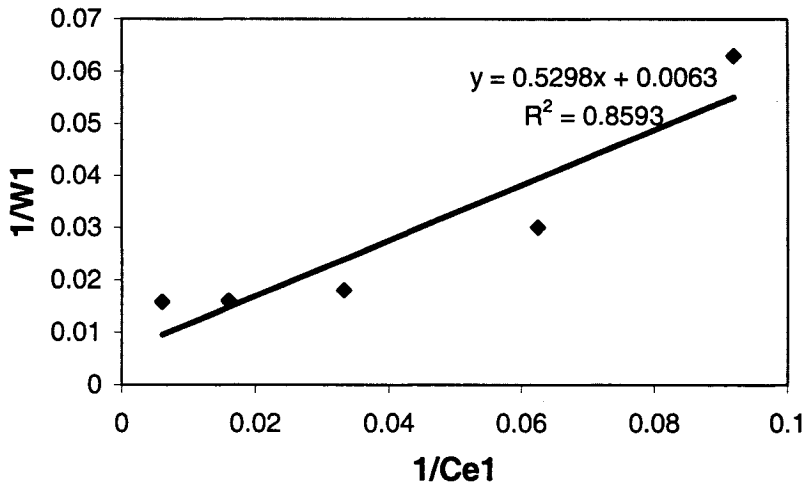

Figure 6.57 Isotherm of Lead with As (V) 350 ppb at pH 9

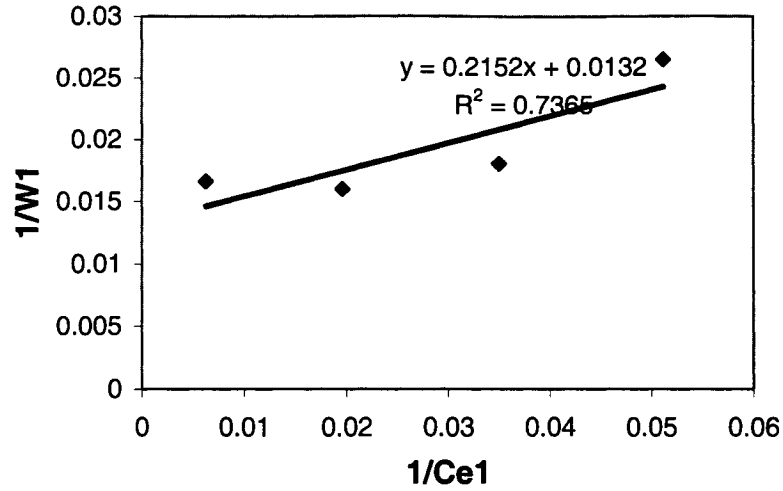

Figure 6.58 Isotherm of Lead with As (V) 350 ppb at pH 11

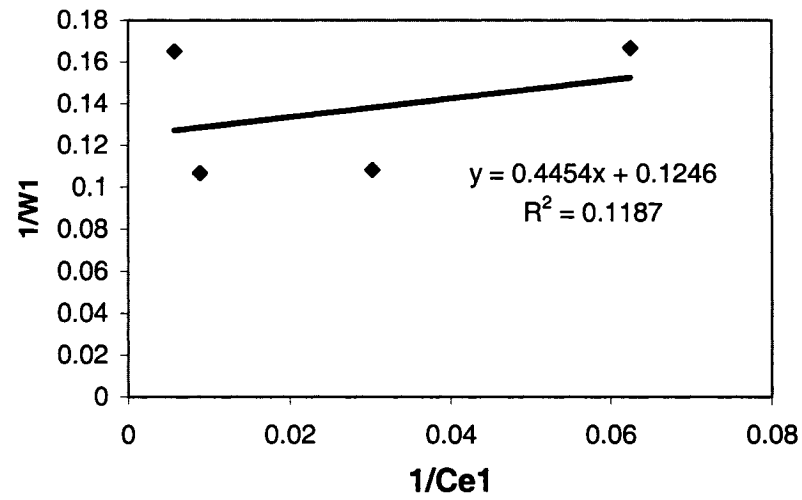

Figure 6.59 Isotherm of Lead with As (V) 1000 ppb at pH 4

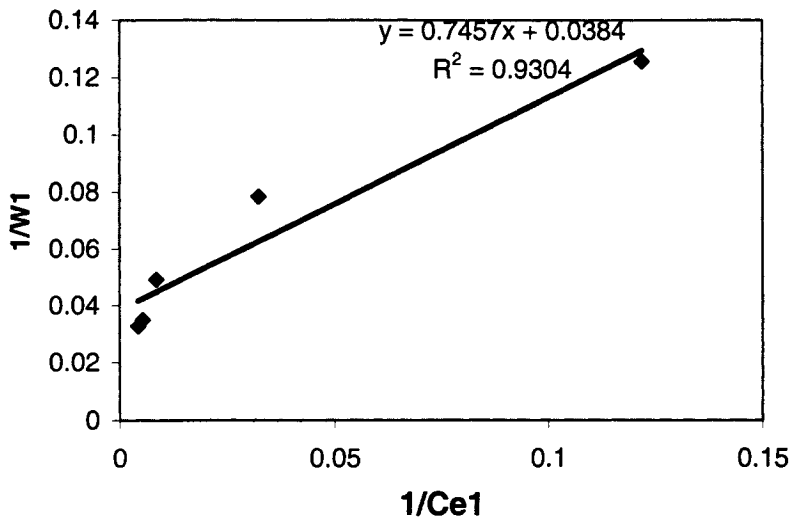

Figure 6.60 Isotherm of Lead with As (V) 1000 ppb at pH 7

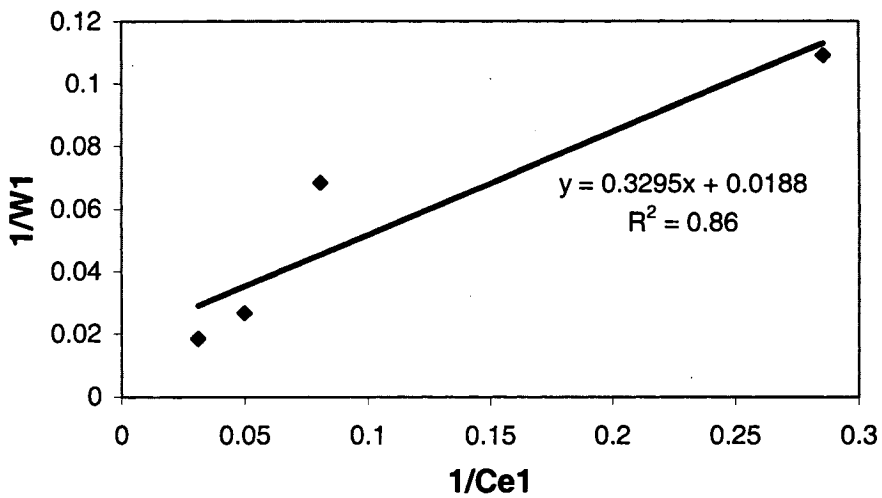

Figure 6.61 Isotherm of Lead with As (V) 1000 ppb at pH 9

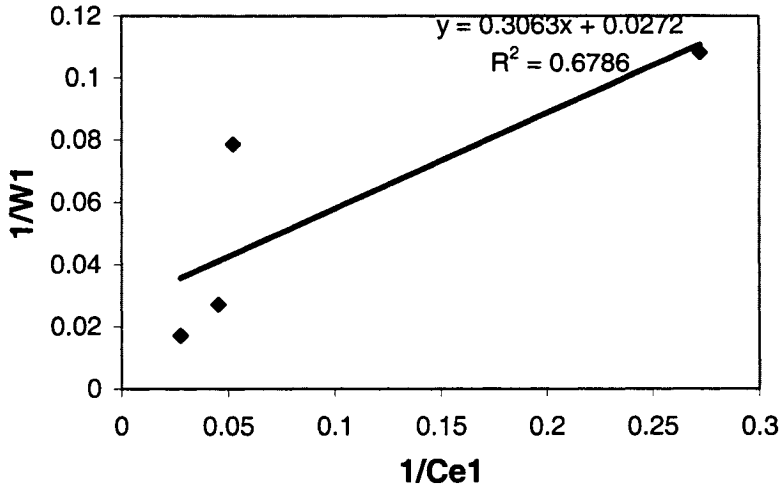

Figure 6.62 Isotherm of Lead with As (V) 1000 ppb at pH 11

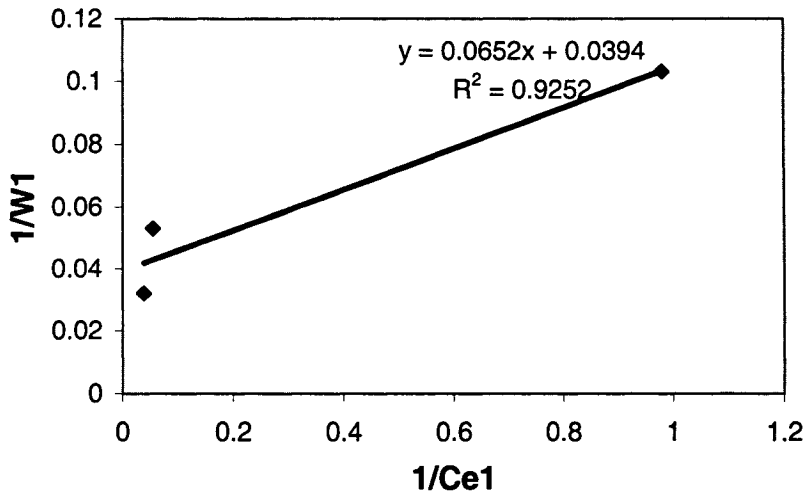

Figure 6.63 Isotherm of Lead with As (III) 350ppb at pH 11

The Langmuir coefficients and the ultimate adsorption capacities of the lead ions at various pH levels are calculated from the Figures 6.48-6.63 and tabulated in Table 6.1. The figures 6.48-6.63 represent equilibrium concentration of contaminants against amount adsorbed per unit mass of adsorbent. The adsorption isotherms of arsenic species are highly dependent on the presence of lead ions. The amount of arsenic removed in presence of lead ions is negligible for all values of pH. Table 6.2 illustrates the maximum

adsorption capacities for specific initial concentrations of the arsenic species and their corresponding pH values in presence of lead ions. Comparing the maximum adsorption capacities of the Arsenic species with the corresponding values of lead species, the values of the arsenic species are negligible. A significant proportion of the abatement of the arsenic anions from the bulk phase may be attributed to the complex formations with the calcium and lead ions. The adsorption of the multi component ions (lead and arsenic) is overwhelmingly competitive in favor of lead ions.

In order to estimate the values of Q_{m1} and Q_{m2}, the ultimate adsorption capacity of a certain species is determined by keeping the mass of the other contaminant constant. The mass of adsorbent for each batch test is 1 gram. The volume of the bulk phase for each run is 200 ml. In relation to values of Q_{m2}, the tests are repeated for both sets of arsenic species at specific pH conditions.

Table 6.1. Maximum adsorption capacities of lead species in presence of arsenic (Q_{m1})

pH/As contamination(ppm)	**4**	**7**	**9**	**11**
As (III) 0.35	39.6mg/g	40mg/g	97.08mg/g	106.3 mg/g
As (III) 1.00	76.3 mg/g	23.4 mg/g	200 mg/g	102.00 mg/g
As (V) 0.35	12.1 mg/g	35.7 mg/g	161.2 mg/g	75.7 mg/g
As (V) 1.00	8.06 mg/g	32.8 mg/g	53.19 mg/g	36.76 mg/g

Table 6.1 illustrates that in all the cases, the removal of lead ions is highest at pH value of 9. The significance of this observation is that the system follows a Langmuir isotherm. However, the effect of precipitation (in bulk phase) cannot be neglected. At pH 9, the precipitation of lead hydroxide is significant and this perhaps correlated to the extent of removal of the cations at this pH level.

Table 6.2. Maximum adsorption capacities of arsenic species in presence of 1000 ppm of lead ions (Q_{m2})

PH /initial conc	4	7	9	11
As (III)	.017 mg/g	.007 mg/g	.015 mg/g	.008 mg/g
As (III)	.022 mg/g	.003 mg/g	.010 mg/g	.048 mg/g
As (V)	.010 mg/g	.007 mg/g	.00 mg/g	0.00 mg/g
As (V)	.050 mg/g	0.00 mg/g	.00 mg/g	0.00 mg/g

Repeated testing points to the conclusion that the heterogeneity of the adsorbent has a significant effect on the maximum adsorption capacity of arsenic ions with respect to the biomass. In the numerical model, an average value of the two sets for each species is introduced. The parameter 'd_2' for arsenic species is calculated from Equation 6.5. Estimation of d_1 parameter is displayed in Table 6.3.

Table 6.3. Estimation of 'd_1' parameter of lead species (liter per mmol) calculated from Equation 6.3

PH	4	7	9	11
As (III) 350ppb	.00423	.00628	.090	0.1176
As (III) 1000ppb	0.413	0.125	.0111	0.034
As (V) 350 ppb	.0802	0.0253	0.0117	0.061
As (V) 1000ppb	0.28	0.0409	0.056	0.089

Estimation of d_2 parameter is displayed in Table 6.4.

Table 6.4. Estimation of d_2 parameters

PH/Arsenic species	4	7	9	11
As (III)	0.13	0.59	0.77	0.56
As (V)	1.07	0.98	0.00	0.00

6.3 Dynamic runs with As (III) and As (V) (multi-component) fish scale

In the following dynamic runs, As (III) or As V) solutions together with 1000 ppm of Pb ions were passed through a column packed with Atlantic codfish scale. The pH and flow rates were varied to study their effects on breakthrough time intervals. The pollutants come in contact with the fixed bed adsorption sites where specific species were retained based on the nature, concentration and flow rate of the species. The adsorbent material was packed in the column and saturated with de-ionized water before the effluent was treated. The effects of pH of the medium coupled with porosity of the adsorbent are also significant parameters that influence adsorption mechanisms. The mass balance of the contaminants was considered without considering the change in density of the effluent. The pressure differences and temperature fluctuations in the column were negligible. The flow in the column was under steady state conditions (mass balances of the contaminants in relation to adsorbed and bulk phases are discussed in the numerical section).

From Figure 6.64, the breakthrough point of the lead ions was observed after 22 pore volumes. The removal of the As (III) ions was insignificant. In an alkaline environment, the lead ions are removed by adsorption on the 'sites' of the fish scale. However, the removal of the As (III) anions in the mobile phase is complicated by several factors that may include the nature of the contaminant and its relative concentration with respect to the major pollutant. The As (III) species at a pH level of 7.7 exists primarily in un-

disassociated form, something that would account for the failure to attain breakthrough with respect to the Arsenic contaminant.

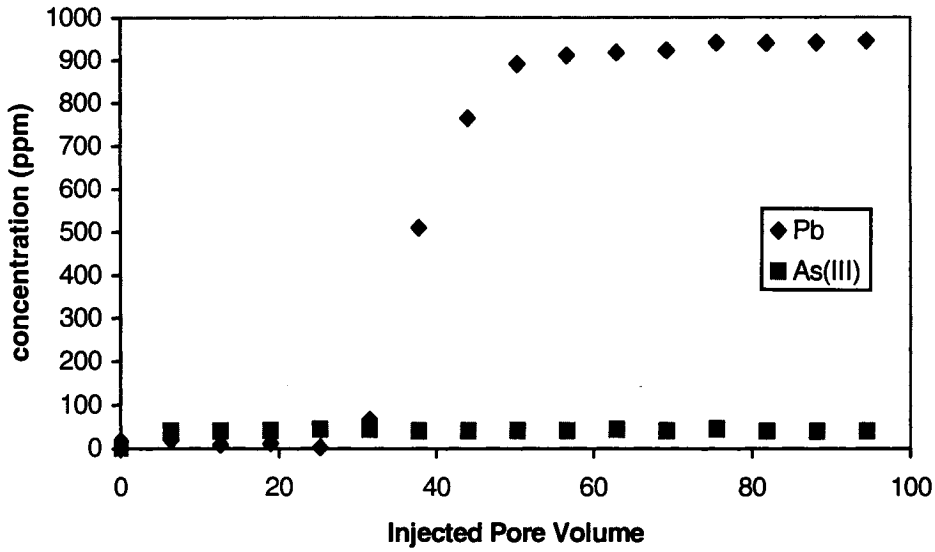

Figure 6.64 Breakthrough behavior of Run 25 (flow rate 390ml/hr, As(III) 82.22 ppm , Pb (1000ppm), pH 7.7

For Run 25, the breakthroughs of contaminants occurred after 25 pore volumes. For Run 26 (flow rate of 6.5 ml per minute and concentration of the Arsenic species at 81.22 ppm), the breakthrough pore volume was estimated to be 45. This run demonstrated that, by increasing the flow rate of the pollutant phase, the breakthrough interval with respect to the lead ions increased almost 15 pore volumes compared to Run 25. The adsorption of the As (III) species was unaffected by the un-disassociated behavior of the contaminant.

In the case of Run 26, the breakthrough behavior of the heavier contaminant was observed after injection of about 45 pore volumes of the effluent, contrasting sharply with the breakthrough behavior of the species observed at both higher pH and flow rate values. The adsorptive breakthrough behavior of the lead ions was observed after 35 pore

volumes. The significance of flow rate of the medium outweighed the effect of pH of the bulk phase.

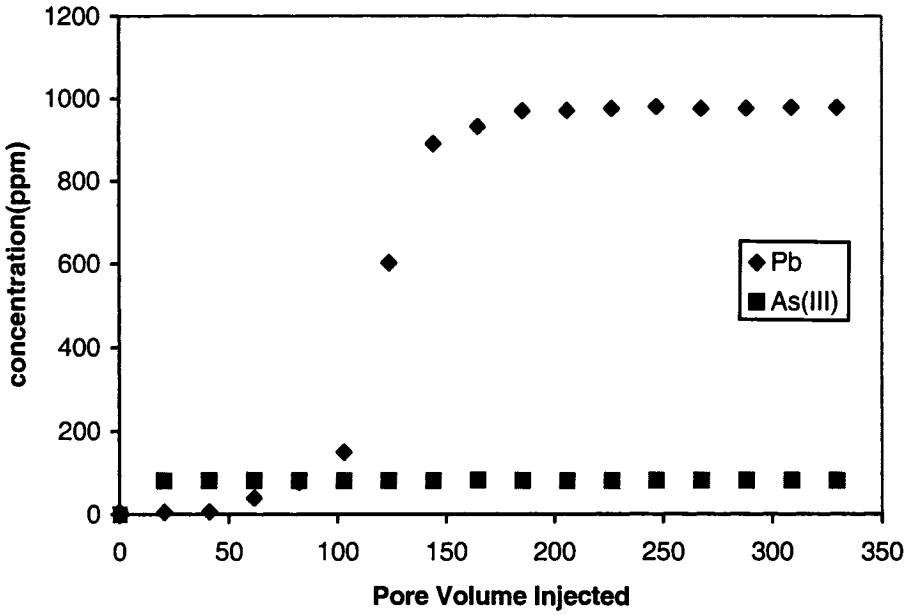

Figure 6.65. Breakthrough behavior of Run 26(flow rate 390ml/hr, As(III) 82.22 ppm , Pb (1000ppm), pH 7.7

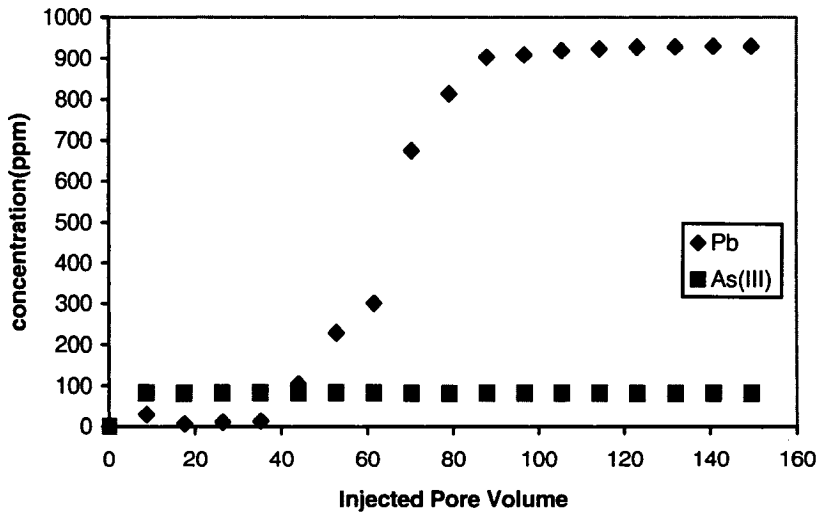

Figure 6.66. Breakthrough behavior of Run 27(flow rate 165ml/hr, As(III) 82.76 ppm , Pb (1000ppm), pH 9.25

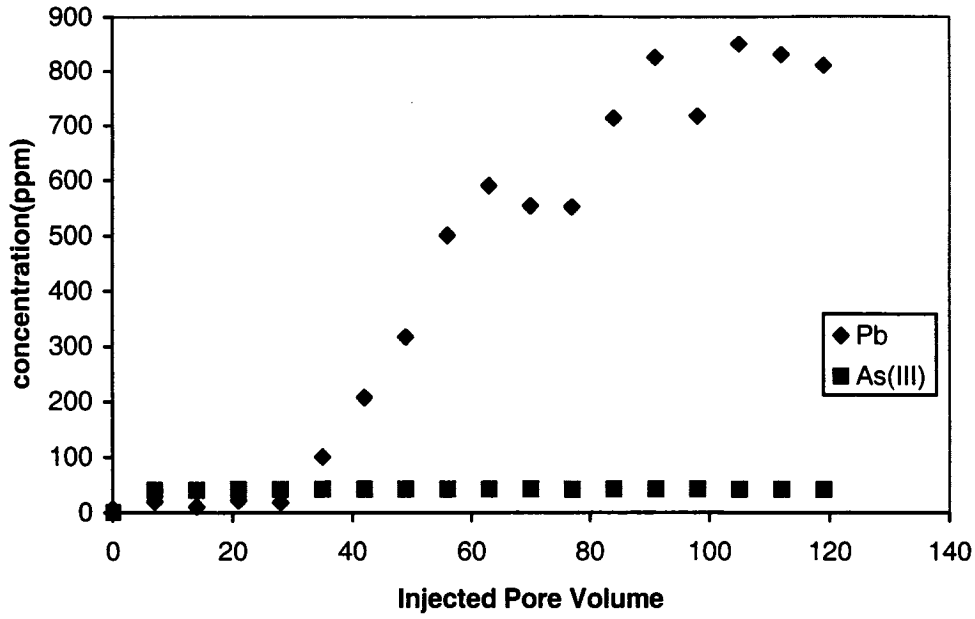

Figure 6.67 Breakthrough behavior of Run 28(flow rate 165ml/hr, As(III) 42.22 ppm , Pb (1000ppm), pH 9.25

Figure 6.67 displays the effects of effluent concentration observed for various lead species with decrease of As (III) species at existing pH levels of Run 28, the objective being to correlate the study of adsorption behavior of the lead species by varying the concentration of the interfering anion As (III) and flow rate of the bulk phase. For this run, the breakthrough took place at 28 pore volumes. It was observed that, contrary to the results expected at ideal conditions, an increase in flow rate increased the breakthrough time. The degree of heterogeneity of the substrate, coupled with a varying internal porosity distribution, may have contributed to this behavior. In a miscible displacement scenario, others have observed such behavior (increasing flow rate leading to increasing breakthrough time) only at very small flow velocities (Coskuner and Bentsen, 1987). However, in the literature existing up to the time of these experiments, no one had reported the breakthrough recovery for a multi-component system.

Figure 6.68 illustrates the adsorption behavior of both the lead and As (III) species in a mobile phase at pH 2.0. The decrease in pH resulted in significant decrease in breakthrough interval of the Lead ions. The undissociated As (III) species were not adsorbed efficiently by the substrate.

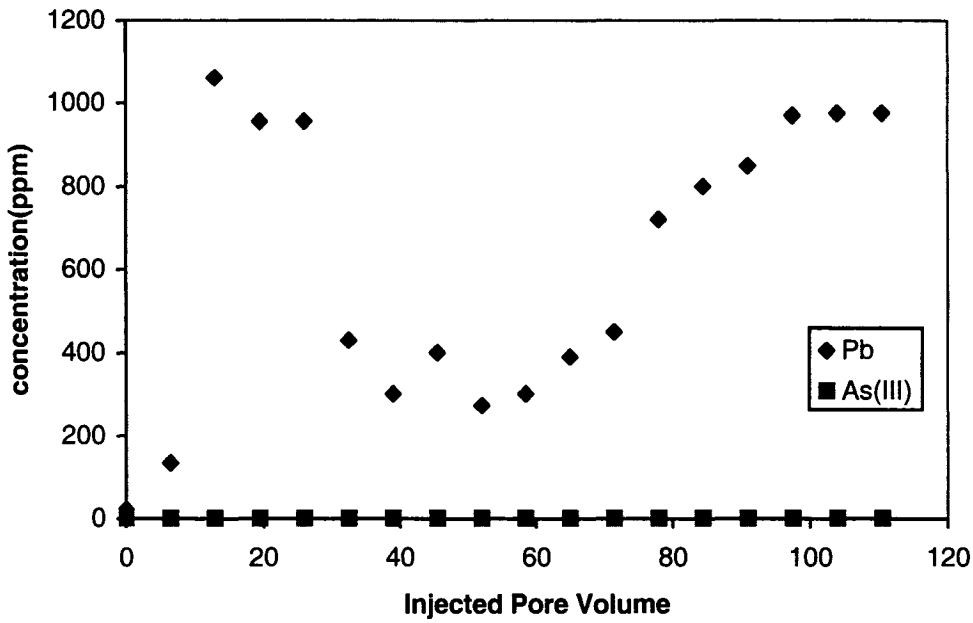

Figure 6.68 Breakthrough behavior Run 29 (flow rate 120ml/hr, As(III) 0.5 ppm , Pb (1000ppm), pH 2.0

The adsorption mechanism of the lead ions with respect to time displays wide-ranging fluctuation. Non-uniform packing coupled with flow rate fluctuations resulted in wide variations of the effluent concentration of lead ions. Note that, since fish scales are naturally heterogeneous, their behavior cannot be compared with conventional packed beds that have more or less uniform packing. The presence of significant amount of protonated sites on the adsorbent likely inhibited the adsorption of the heavy metal ion. The effect of low pH on removal of Lead ions was precisely illustrated in this run.

In Run 30, the pH of the bulk phase was adjusted to 11.5 and the Arsenic species introduced in the 1000 ppm the lead solution was divalent in nature. The breakthrough

behavior of lead was observed after injecting about 150 pore volumes of the influent. The removal of lead ions was perhaps a combination of adsorption and precipitation. At pH11.5, negative charged substrate may have been repelling the divalent anions, decreasing the rate at which the adsorbate (As (III) was being reduced by an adsorption mechanism. However, complexation of lead and arsenic anions was also possible, responsible for perhaps as much as 50 percent of the decrease of the arsenic anions in bulk phase.

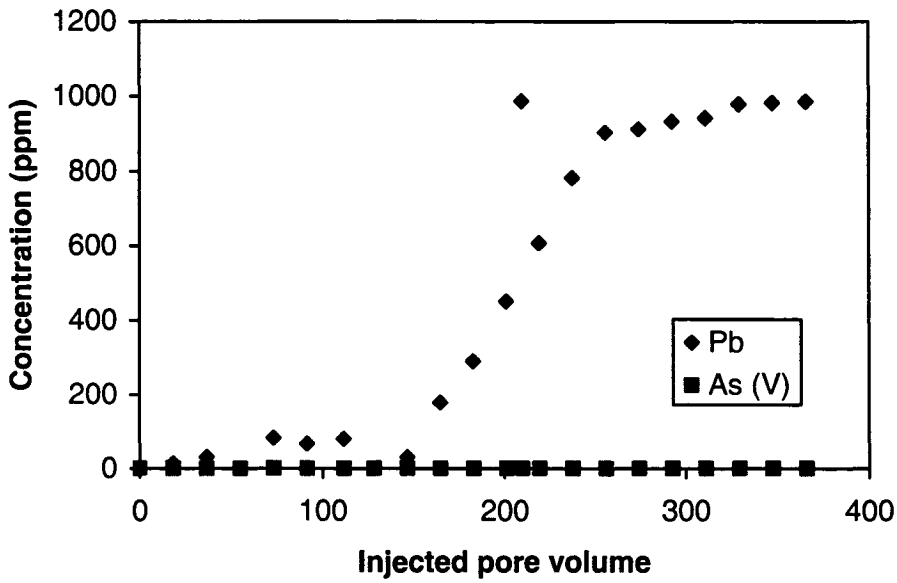

Figure 6.69. Breakthrough behavior of Run 30 (flow rate 337.2ml/hr, As(V) 1.00 ppm , Pb (1000ppm), pH 11.5

Figure 6.70 illustrates the breakthrough behavior observed in a mixture contaminated with 1000 ppm of Pb ions and 1.05 ppm of Arsenate anions. The pore breakthrough interval of the heavier ions was identified after injecting approximately 50 pore volumes of the influent. The adsorption phenomenon of lead ions clearly reflects the profound effect of decreasing pH on pore volume breakthrough, strongly suggesting the possibility that undissociated species are more susceptible to abatement. The existing sites may provide limited columbic interaction of the anion resulting in diminished efficiency of

removal. Secondly, the existence of appreciable quantities of lead ions in the bulk phase may have been shielding the columbic effect of arsenic species.

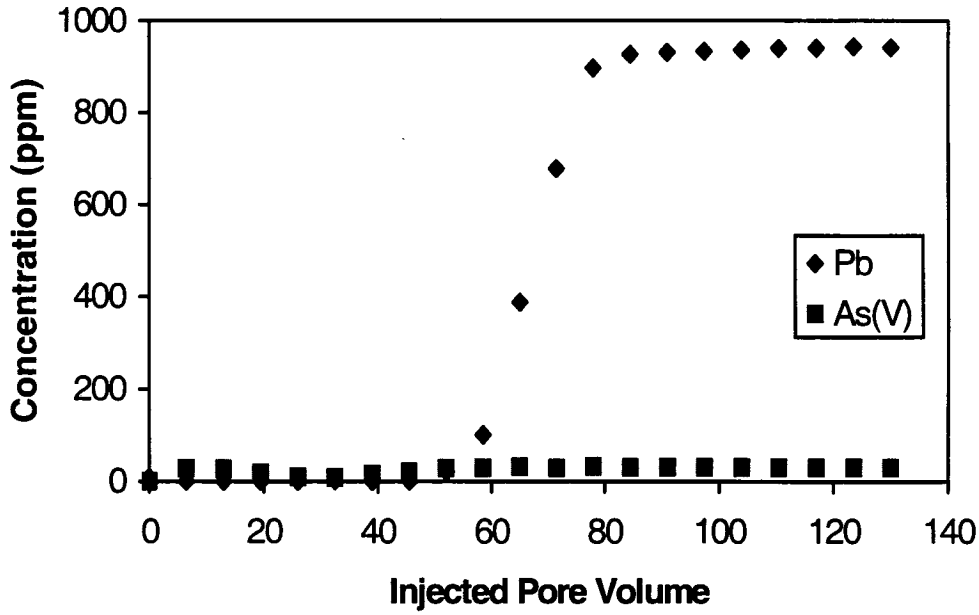

Figure 6.70. Breakthrough behavior of Run 31(flow rate 120ml/hr, As(V) 1.05 ppm , Pb (1000ppm), pH 7.0

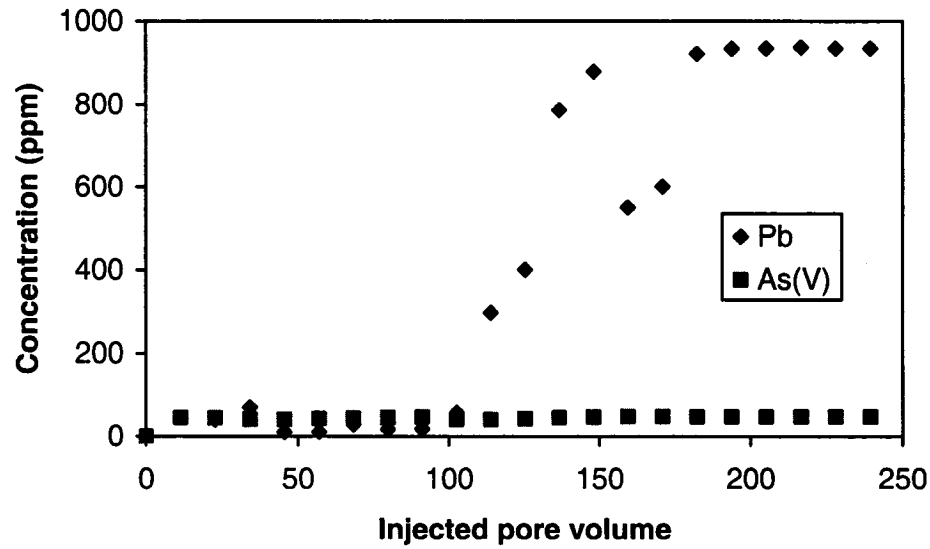

Figure 6.71 Breakthrough behavior of Run 32(flow rate 132ml/hr, As(V) 47.02 ppm , Pb (1000ppm), pH 7.3

At a concentration to 47.04 ppm of As (V) anions (Run 32), an additional 30 pore volumes of pore breakthrough interval of the Lead contaminant was observed compared to Run 31. An injection of 250 pore volumes of the bulk phase resulted in negligible reduction of Arsenate anions. Although As (V) anions existed as mono-valent anions at this pH level, the presence of lead ions deterred the interaction between the substrate and the arsenic contaminant. Lead ions, which are divalent, were immobilized on the nucleophilic sites of the adsorbent. The number of such sites per unit mass of adsorbent is sensitive to the pH of the bulk phase and this perhaps explains the increase observed in pore volume breakthrough in Run 32 compared to the earlier run. An increase of 0.3 pH units in Run 32 may have enhanced its removal capacity significantly.

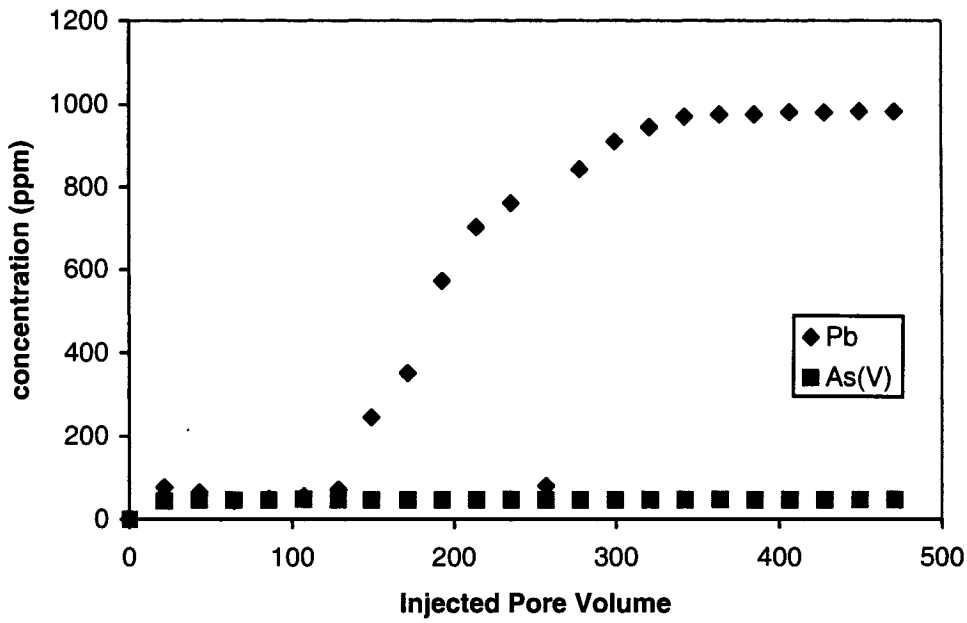

Figure 6.72 Breakthrough behavior of Run 33 (flow rate 390ml/hr, As(V) 47.02 ppm , Pb (1000ppm), pH 8.04

The functions imposed on Run 33 included an increase of flow rate to 6.5 ml/min and in the pH of the medium to 8.04. The breakthrough of Lead ions was observed after an injection of 100 pore volumes. A higher pH led to in an increase in breakthrough time, as

evident in comparison to Run 32. The removal of arsenate anions in the conditions of this run was negligible.

The reduction of arsenate ions to 0.342 ppm further characterized its abatement behavior at a pH value of 7.13. There was no significant removal of Arsenate ions from the bulk phase. In addition, a considerable decrease in breakthrough time was observed. The breakthrough was observed after injection of 40 pore volumes. In this run, a significant reduction of number of adsorption sites (as compared to Run 33) possibly played a role in abatement of pore volume breakthrough of the cation.

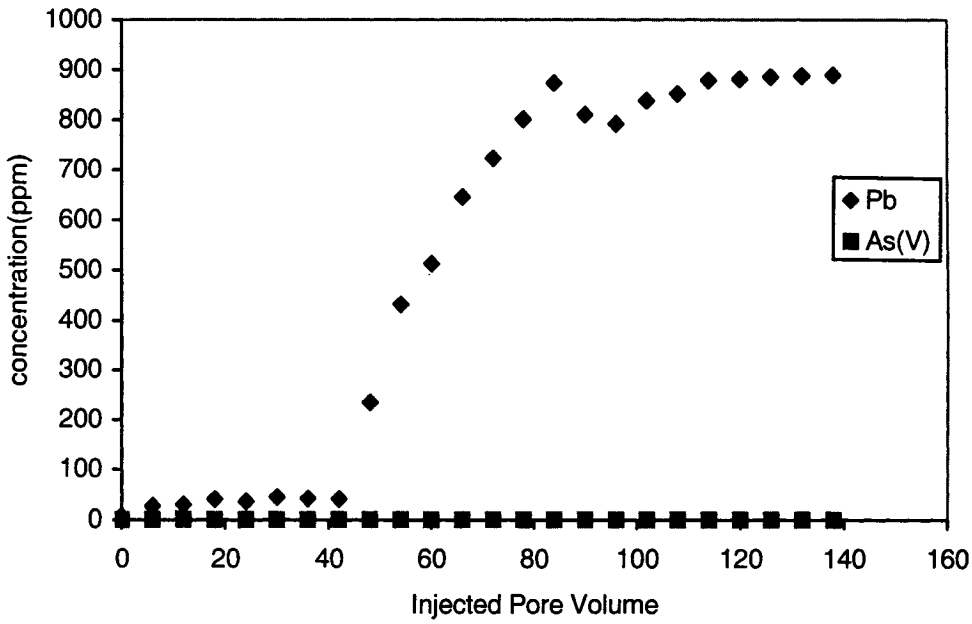

Figure 6.73. Breakthrough behavior of Run 34 (flow rate 120ml/hr, As(V) 0.342 ppm , Pb (1000ppm), pH 7.13

Runs 35 through 39 described the effects of pH in a range from 2 to 11. It was observed that with increase of pH of the bulk phase, the pore volume breakthrough of the cation was significantly enhanced. Runs 36 and 37 with the exception of initial arsenic concentrations were identical in every other respect. However, the pore volume

breakthrough values of lead ions displayed a variance of magnitude of 10 pore volumes. The effect of initial concentration of arsenic species may not have been a determining factor on pore volume breakthrough interval. Instead, the heterogeneity of the adsorbent may have been the main reason for the resulting discrepancies.

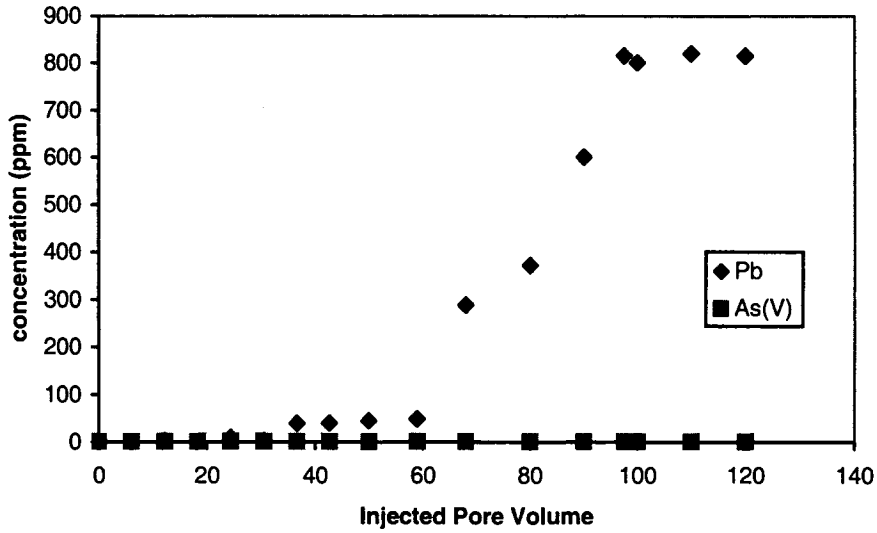

Figure 6.74. Breakthrough behavior of Run 35 (flow rate 120ml/hr, As(V) 0.485 ppm , Pb (1000ppm), pH 11.0

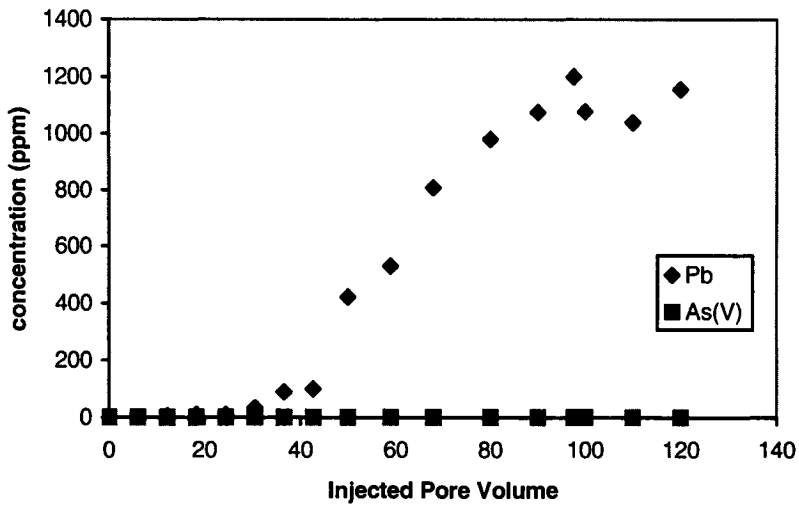

Figure 6.75. Breakthrough behavior of Run 36(flow rate 120ml/hr, As(V) 0.328 ppm , Pb (1000ppm), pH 3.95

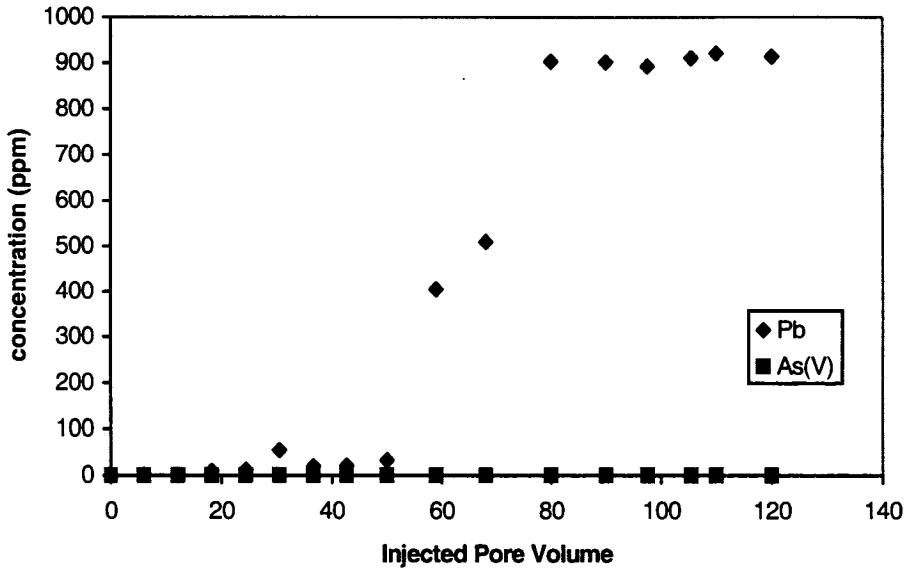

Figure 6.76. Breakthrough behavior of Run 37(flow rate 120ml/hr, As(V) 1.00 ppm , Pb (1000ppm), pH 3.95

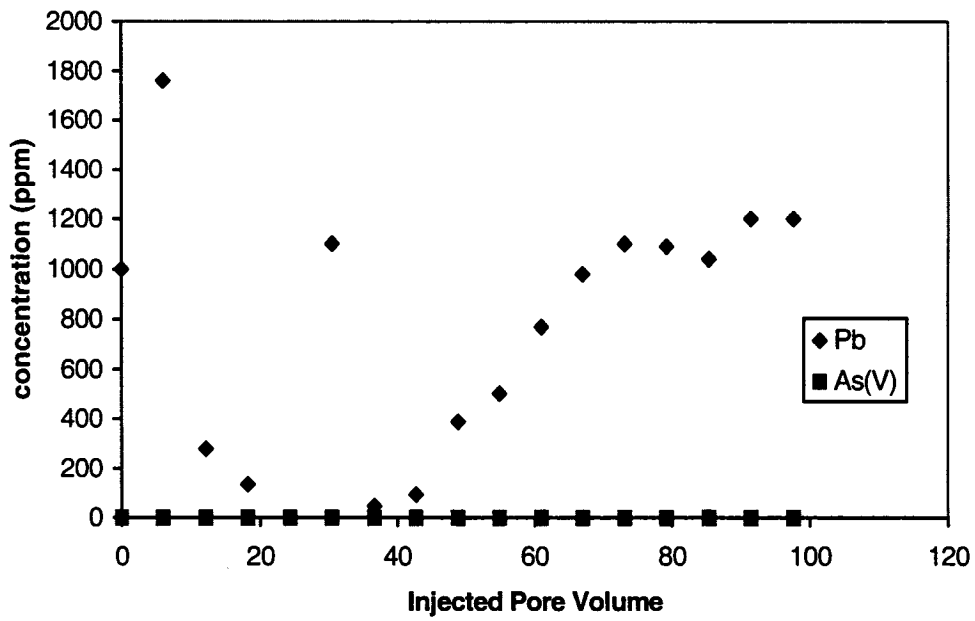

Figure 6.77. Breakthrough behavior of Run 38(flow rate 120ml/hr, As(V) 1.00 ppm , Pb (1000ppm), pH 2.00

Figure 6.77 shows the breakthrough behavior observed for a1000 ppm lead solution in a mobile phase at pH 2. The protonated substrate, susceptible to adsorption of the lead ions, appears to have resulted in an early pore volume breakthrough. Strong repulsions between the heavy metal ions and the adsorbent may have prevented early breakthrough of the contaminants. However, after an injection of 40 pore volumes, complete removal of the heavier ions was observed. At pH of 2, there was no appreciable removal of arsenate anions either by adsorption or precipitation. This may be attributed to the lack of ionization of the arsenate molecules. The fundamental correlation between static and dynamic tests lay in the usage of ultimate adsorption capacities at various pH levels to determine breakthrough intervals in dynamic runs. (The procedure is explicitly explained in the numerical section of the chapter.) No static tests at pH level of 2.00 was conducted.

At pH 4, the breakthrough was observed after 20 hours for lead ions. However, at this pH level, no appreciable reduction of arsenate anions was observed. It is likely that significant adsorption of the lead ions may have inhibited the electrostatic attractions between the arsenate anions and the adsorbent. The heavier immobile lead ions prevented adsorption of the lighter mobile anions. This may be the cause of low adsorptivity of the penta-valent anions.

6.4 Numerical Studies of Multi-component species

Removal of lead and arsenic ions from both industrial and municipal water is of extreme importance for disposal standards. Some types of fish scale (Atlantic Cod and Shouari) are capable of effectively adsorbing metal ions through either ion exchange or chemisorption or both. The removal of Arsenic ions from the bulk phase involves a complex mechanism. It includes electrostatic binding and complex formation with lead and calcium ions in the solution. The complex formation of the lead and calcium ions is competitive with respect to chemisorption on the negatively charged substrate. A model case involving two types of adsorption sites and two species of ions is being studied using the numerical model based on the theory of pore diffusion. The feasibility of

predicting the sorption behavior for multi-component influent stream is based upon the complexation constants of the components with the sorption sites. The influence of pH of the influent, effect of presence of competing ions, concentration of the components and flow characteristics is being studied with respect to sorption behavior.

6.4.1 Introduction to numerical solutions

In order to validate experimental studies, an appropriate numerical model is required. Initially, three different models from the literature were selected for this task. They include surface excess model (Sircar, 1985), entrapment model (Ali and Islam, 1998), and the pore diffusion model (Lee and Weber, 1969).

Surface excess is based on the theory of the difference between the actual adsorption extent of one component and the amount of the component that would be present in the adsorbed phase. The disadvantage of the surface excess model was the lack of sensitivity to pH conditions.

The central concept behind the theory of entrapment is the representation of both the particle and pore size distributions by partitioning the porous medium at any cross section to pluggable and non pluggable pathways. This hypothetical division involves the representation of the two branches formed in such a way that one is of smaller pores that can eventually be plugged completely. On the other hand, the non pluggable pathways cannot be completely plugged because as the pore diameter is reduced through solid deposition, the local speed becomes high enough to entrain deposits out of the pore phase. However, in the adsorption system of fish scales and inorganic ions, it is identified that the precipitation of the charged particles has not been studied. In the 'pore diffusion model,' diffusion is assumed to occur in the fluid phase with a distributed adsorption along the pore walls. There is a three-way division of the bed volume, and the contaminant diffusion occurs in the internal void fraction α, (Weber and Chakroborti, 1974). Turning to the physics behind the process, the conditions relating ε and α, it works

as follows. Consider the scenario where internal void fraction (α) is zero. In such a case, there is no possibility for the cation to enter the particle and hence there is no adsorption within the particle. There is, however, significant mass transfer to the adsorbent from the bulk solution. If the internal solid fraction is negligible (as observed in fish scales due to high pore volumes), the relative distribution between intraparticle pore volume to external voidage attaches specific importance of adsorption in relation to pore diffusivity. If α is higher than ε, internal adsorption is very large due a high proportion of the cations entering the pore phase. If the concentration of the cations in the pore phase and the adsorbate is higher than the concentration of the cations in the void spaces, contaminant concentrations in the bulk phase is negligible. On the other hand, if internal adsorption is negligible, concentration of the cations in the bulk phase, remains at steady state with respect to large time intervals. Thus in modeling the diffusivity equation, a proper choice of the values of internal porosity and external voidage is of extreme importance.

Chimera et al. (1978) reported that adsorption equilibrium constants increased, while diffusivities in a micropore decreased at lower temperatures for rare gases and hydrocarbons. Further, (Saito and Foley, 1991) noted that the pore diffusion model is an useful technique to simulate adsorption data of noble gases on zeolite structures. Guin (1995) studied the diffusional characteristics of asphaltenes into different pore sizes of heterogeneous catalysts. He observed experimentally, that pore diffusional access often limits the overall rates of adsorption. Wakao (2001) demonstrated that the value of pore diffusion coefficient is inversely proportional to the pressure applied in an activated carbon-methanol system.

The pore diffusion model is able to accommodate the adsorption phenomenon with an adsorbent related to high porosity. A high porosity in the model is accommodated by pore and surface diffusion. The effect of adsorption based on chemisorption and ion exchange is also correlated to the equation. Each specific component's interaction between their bulk and adsorbed phases is well described by the model. In relation to fish scales as an

adsorbent, the assumptions considered are that the particles are spherical in shape and are homogenous in size. Each spherical particle has a well-defined pore in which the contaminants diffuse and are adsorbed on the internal walls of the pore. The adsorption is visualized by the assumption that the functional groups that facilitate the process are oriented within the internal walls of each sphere. Adsorption at the surface of the sphere may be assumed to be negligible because of a constant contaminant concentration (x_s). The thin film, that encapsulates each particle due to saturation of the medium by deionised water before addition of the contaminant solution, acts as a resistance to mass transfer of the solute between the bulk phase and the surface of the adsorbent. An important factor that is also being considered is that the adsorption process is isothermal in nature.

The pore diffusion model is applicable to isothermal fixed bed adsorption columns. The internal porosity of the adsorbent is a very important parameter for adsorption behavior. The orientation of the functional groups in the adsorbent are assumed to exist on the internal walls of each pore. The degree of adsorption of each component depends on the complexation constants of each ion to a specific site, presence of competing ions and the pH of the influent solution. The effects of flow rates and concentration of the contaminants to adsorption behavior will be studied using the model.

6.4.2 Theory

In modeling a fixed bed adsorption column, the following equations are considered. They include:

1. The concentration of adsorbate in the external voids of the bed as fluid passes through the column.
2. An equation that describes the diffusion process within the pellets.
3. A model that couples the first two equations in terms of a film resistance engulfing the particles.

4. The charge balance of the system is maintained by keeping the total charge of the contaminant ions and protons (involved in model) constant. It is assumed that besides the contaminant ions and protons, there is no interaction of other ions with substrate.

In case of Equation 6.7, it is assumed that the contaminant solution passes through the bed in plug flow. For the pore model, Lee and Weber (1969) presented the following equation:

$$v\,\partial y/\partial z + \partial y/\partial t = -\left(A/\rho\varepsilon\right)\left(\alpha/1-\varepsilon\right)k_f(y - x_s) \tag{6.7}$$

The adsorbent presents A cm^2 of external surface area per cc of bed and v the velocity of the ion. Assuming that each internal pore has a uniform diameter and that there are no bottlenecks, the fraction of the area represented by the pore spaces is $\alpha/(1-\varepsilon)$. This is the only fraction, which is effective for diffusion of adsorbate into the pores, and therefore this factor appears on the right hand side of the equation 6.7. ρ is liquid density (gmol/cc). The terms k_f (gmol per cm^2,s)and x_s (mole fraction) represent mass transfer coefficients and concentration of contaminant at the film encapsulating the adsorbent respectively.

The rate of mass transfer between the bulk of the fluid and the outer surface of the adsorbent is expressed as a driving force between these two regions and the concentration gradient at the surface of the pellet. For the pore model, the equation is written in the following form as described by Lee and Weber (1969).

$$\left(D_p\rho\frac{1}{(1-x)} + \rho_a\frac{Ds}{\alpha}\frac{dw}{dx}\right) = k_f(y - x_s)\frac{1}{1-y} \tag{6.8}$$

Substituting Equation 6.8 in Equation 6.7 we get:

$$v\left(\frac{\partial y}{\partial z}\right)+\frac{\partial y}{\partial t}=-A\frac{1}{\rho\varepsilon}\left(\frac{\alpha}{1-\varepsilon}\right)\left(\rho\frac{D_p}{1.0}+\rho_a\frac{D_s}{\alpha}\frac{dw}{dx}\right) \tag{6.9}$$

Due to bulk diffusion effects, the values of x and y are much smaller than unity. Therefore the factors (1-x) and (1-y) are approximately equal to unity. Knowing the flow rate, a concentration profile with respect to y, t and z can be determined. The boundary conditions that can be incorporated are

At t=0, y=0 (6.10)

Z=0, $V_p1 + V_v1 = V$ for t>0 (6.11)

If V moles of a cation is moving through a column per unit time,

V_{p1} = x * (V_p, total molar flow rate through pores) (6.12)

V_{v1} = y* (V_v, total molar flow rate through the voids) (6.13)

$V_p/V_v = (\alpha/\varepsilon)$ (6.14)

Equation 6.14 illustrates the fact that the ratio of total molar flow in external voids to internal pores is equal to the ratio of external voidage to internal porosity. In other words, the total molar flow rate is inversely proportional to the path of flow resistance. Thus V_{p1} and V_{v1}, are time dependent, and their sum includes the total amount of cations in pore phase, bulks phase and adsorbed phase. However, due to diffusion of contaminants from bulk phase to pore phase, y is assumed to be equal to x, after equilibrium is attained. In other words pore phase and bulk phase assume identical concentrations of the contaminant. An important feature with pore diffusion that needs to be addressed is that the ions are immobilized in the adsorbed phase. Thus the ions in sorbed phase in

equilibrium with bulk phase include the net accumulation of the contaminants already adsorbed at earlier time intervals.

$$\text{Then } \left(V = x\left(\frac{\alpha}{\varepsilon}\right)V_v + y(V_v\ ) - W\ \right) \tag{6.16}$$

or,

$$V = xV_v((\alpha/\varepsilon)+1) - W \tag{6.17}$$

W is moles of contaminant adsorbed per unit time in 1/19 mass of adsorbent in column.

A relationship between y and x is established. It is also considered that the adsorption process is instantaneous and the mole fraction of the cation concentration in the pore phase (x) is the equilibrium concentration after adsorption. At equilibrium, it may be assumed that concentrations of pore and void phase are identical and no accumulation of contaminants in pore phase is possible.

For all practical purposes, the experimental models relating w and x, are expected to be non linear. Therefore the isotherms can be interpreted (Weber and Chakrovorti, 1974) as:

$$w = \left(\frac{1-\varepsilon}{\rho_a} \right)\left[(Q_m - 1\ )\rho x - d\rho^2 x^2\right]\frac{1}{[1+d\rho x]} \tag{6.18}$$

where w is moles of ion adsorbed per unit mass of adsorbent

If the value of ρx is small, then ρ^2x^2 are negligible. This is especially appropriate because ρ is very close to unity and x is very small when compared to unity.

Equation 6.18 can be modified to in Equation 6.19 as:

$$w = \left(\frac{1-\varepsilon}{\rho_a}\right)\left[(Q_m d - 1\ )\rho x\ \right]\frac{1}{[1+d\rho x]} \tag{6.19}$$

Differentiating w with respect to x,

$$\frac{dw}{dx} = \frac{(1-\varepsilon)}{\rho_a}(Q_m d - 1)\left[\rho(1+d\rho x) - d\rho^2 x\right]\frac{1}{(1+d\rho x)^2} \tag{6.20}$$

Substituting Equation 6.20 in Equation 6.9,

$$v\left(\frac{\partial y}{\partial z}\right) + \frac{\partial y}{\partial t} = -\left(\frac{A}{\rho\varepsilon}\right)\left(\frac{\alpha}{1-\varepsilon}\right)\left[\begin{array}{l} D_p \dfrac{\rho}{1-x} + \\ \rho_a \dfrac{D_s}{\alpha}\left[\left[\dfrac{1-\varepsilon}{\rho_a}\right](Q_m d - 1)\left[\rho(1+d\rho x) - d\rho^2 x\left(\dfrac{1}{1+d\rho x}\right)^2\right]\right] \end{array}\right] \tag{6.21}$$

Solving Equation 6.16 and Equation 6.21 simultaneously, the mass balance for the adsorbate in external voids can be solved with respect to both x and y. In other words, the total amount of cations in the pore phase is directly related to adsorption in internal sites of the pore. The metal binding mechanism in adsorption may involve different processes such as complexation, coordination, electrostatic attraction or ion exchange. It is on the basis of chemisorption that a Langmuir type isotherm may be chosen for numerical purposes. Often the prediction of sorption equilibrium is complicated by the presence of several sorbed ions, requiring the use of multi-component isotherm models. This is especially relevant when the sorption of one ion influences the binding of the other species, as is the case when different cations compete for the same binding site.

The pH is another parameter that has a significant effect on metal binding. Most cations adsorb better in an alkaline medium. This is largely due to a lowered competition by protons for the same binding sites that the cations use. The modeling of this effect is rendered more difficult in the case where the adsorbent contains several acidic groups active in metal adsorption. The pH values, site quantities and the binding constants for the cations must be identified for those specific sites. However, in case of arsenic species, it is assumed that the adsorption occurs at predominantly calcium sites which are composed of carbonate and phosphate functional groups.

After determining the above values, a multicomponent isotherm for one binding site and formation of 1:1 adsorbate/sorbent complexes have been described (Buffle, 1988).
These isotherms were adapted for the case of multi site and multi ion adsorption for various valences. Since adsorption by Atlantic Cod scales is largely a combination of chemisorption and an ion exchange mechanism, the equation of cation M of the charge j sorbing to a binding site B is expressed as:

$$jB^{-} + M^{j+} \Leftrightarrow j\left(M_{1/j}B\right)$$

$$K_{MB} = [M_{1/j}B]^{j}/[M^{j+}][\,B]^{j} \qquad (6.22)$$

Assuming all activity coefficients equal to unity (in case of an ideal behavior), the subscript MB on the left hand side of the above equation refers to the binding site with respect to cation M. The left term K_{MB} in the above equation is defined as the equilibrium constant of the species M with respect to site type B. It is also to be observed that the term $M_{1/j}B$ has been chose instead of MB_j because it implies that a number of bonds equal to charge j of the cation have to be broken for the release of a j valent ion. Thus the dissociation reaction is of the order j and not of the order one as this would as this would be the case of a MB_j species. Accordingly, the former version should be preferred over the latter when specific complexation instead of nonspecific electrostatic attraction is the binding mechanism. It is also assumed that secondary interactions (electrostatic attractions, hydrogen bonding, etc.) are negligible and that there is no other influence of the other cations than competition for the same binding sites, (Schiewer and Volesky, 1996). For the reaction of the ion M^{j+} in a system with n cations and m binding sites, it follows from Equation 6.23:

$$w = \sum_{k=1}^{m}\left[M_{i/j}B\right] = \sum_{k=1}^{m} B' K_{MB}[M]^{1/j} \Big/ \left(1 + \sum_{h=1}^{n} K_{MB}[M]^{1/j}\right) \qquad (6.23)$$

The binding sites in Atlantic cod scale (with respect to lead) are believed to be composed of carbonyl (signified by C) and amide groups (denoted by S). The model also includes two sites, ^{t}Ca and ^{t}Ph groups, (carbonate and phosphorous) for arsenic sorption. In a system of two metal ions consisting of Pb and As, Equation 6.23 is reduced to

$$w(Pb) = {}^{t}C \left({}^{C1}K[{}^{1}M]\right)^{1/2} / \left(1 + {}^{CH}K[H] + \left({}^{C1}K[{}^{1}M]\right)^{1/2} + \left({}^{C2}K[{}^{2}M]\right)^{-1/1}\right) + {}^{t}S \left({}^{S1}K[{}^{1}M]\right)^{1/2} / \left(1 + {}^{SH}K[H] + \left({}^{S1}K[{}^{1}M]\right)^{1/2} + \left({}^{S2}K[{}^{2}M]\right)^{-1/1}\right) \quad (6.24)$$

$$w(As) = {}^{t}Ca \left({}^{C2}K[{}^{2}M]\right)^{-1} / \left(1 + {}^{CH}K[H] + \left({}^{C1}K[{}^{1}M]\right)^{1/2} + \left({}^{C2}K[{}^{2}M]\right)^{-1/1}\right) + {}^{t}Ph \left({}^{S2}K[{}^{2}M]\right)^{-1} / \left(1 + {}^{SH}K[H] + \left({}^{S1}K[{}^{1}M]\right)^{1/2} + \left({}^{S2}K[{}^{2}M]\right)^{-1/1}\right) \quad (6.25)$$

$$[H] + b[M] = \text{constant (where b is valency of metal ion)} \quad (6.26)$$

(Total charge balance)

It is to be noted that the concentrations in the pore phase are expressed as moles per liter. In order to maintain the charge balance in the bulk phase, the cation, anion and proton concentrations vary that are incorporated into the model. However the sum of total variables with respect to time is constant. To predict final concentrations from initial conditions, a numerical code will be developed based on all the model equations described above. Overall, the initial solute concentration in the bulk phase is considered to be sum of the final concentration and the amount of the solute adsorbed per unit mass of the adsorbent. Pore diffusion theory considers the adsorbent to be a sink where the adsorbate is accumulated due to adsorption (Weber and Chakroborti, 1974)

The values of d1 and d2 are calculated earlier. Appropriate values are coupled in the dynamic system with respect to respective pH and initial concentration of the contaminants.

Note: Let it be assumed that the equilibrium constants of As species with respect to the adsorbent are identical to the sorption coefficients in single component dynamic Runs 11-24.

Let us also assume that Dp and Ds are dependent on flow rate and porosity parameters
K11= 1000 L per mmole, ^{CH}K[H]= 1000 L per mmole (Schiewer and Volesky,1995)
K12= 1000 L per mmole, ^{SH}K[H]=1000L per mmole (Schiewer and Volesky, 1996)
^{t}C = 1.20E-03 moles per g, ^{t} Ca= 0.4 E-03 moles per g
^{t}S = 0.52E-03 moles per g, ^{t} P= 0.1 E-03 moles per g
Also it is assumed that equilibrium coeeficient of lead is identical for all cases.

The values of Q_{m1} and $Q_{m2}$are considered from Tables 6.1 and 6.2 respectively. It is assumed that maximum adsorption capacity of lead is dependent on pH and amount of arsenic in the multi-component phase. In the model, Q_{m1} and $Q_{m2}$are in units g mol adsorbed per cc of adsorbent. The significant assumption considered in modeling of combined effect of lead and arsenic ions is that the adsorption activities of lead species occur at the amide and carbonyl sites of the polymer. The sorption behavior of Arsenic species in presence of lead ions is insignificant and assumed to occur exclusively at the carbonate and phosphate sites. It is also assumed that significant presence of lead ions will hinder anion exchange of arsenic species with calcium sites. The parametric assumptions are meant to simulate the combined single-component conditions of lead and arsenic species. Lack of adequate studies of the mechanisms involved in the process can be supplemented by coupling certain conditions in single phases to observe if match fitting is possible. If match fitting is observed then it can be concluded that barring competitive interference of removal of the contaminants, the mechanisms comply with the trends assumed in single component runs. However on the negative side, if match fitting is not observed, future studies on reaction mechanisms need to be documented. Only then the model may display significant correlations between experimental and

numerical results. Otherwise, in case of single component runs, the match fitting provided in numerous cases is no path to foresight of the actual sorption mechanisms.

6.5 Numerical Results

The forcing parameters (parameters coupled into the model by trial) were identical for single-component runs of lead and arsenic species. In both Figures 6.76 and 6.77, the breakthrough intervals determined by numerical simulations were smaller than the values observed by experimental runs. Thus, in order to validate the experimental runs by numerical methods, it was of utmost importance to thoroughly characterize the heterogeneous adsorbent.

The breakthrough delay observed in experimental procedures may be attributed to the complexation mechanisms in the bulk phase. That may not be exclusively an adsorption phenomenon. The calcium ions released into the bulk phase may either act as a competitor with lead ions or may allow the lead ions to form complexes with the carbonates and phosphates. The complex formation or competition of calcium ions (or both) may be controlled by the pH of the bulk phase. It is also possible that the calcium ions may be initially adsorbed on the substrate followed by an ion exchange mechanism with lead.

Table 6.5 in the following page displays both the experimental (determined) and enforced coefficients invoked in the dynamic runs for runs 24-38.

Table 6.5 Physical model parameters for numerical simulations of multi component runs

Note: It is assumed that the adsorption coefficients of arsenic are identical for all sites on the substrate at a set of specific parameters.

Run	Flow rate (ml/hr)	Poro sity (Φ)	pH of bulk solution	Initial Conc (ppm)	Amount Adsorbent (g)	K21 (L/mmol)	K22 (L/mmol)	Dp cm^2 per hr	Ds cm^2 per hr
25	120.0	0.83	7.7	41.22	61.54	1.00	1.00	100	80
26	390.0	0.83	7.7	82.22	61.54	1E-07	1E-07	100	100
27	165.0	0.82	9.25	82.76	66.87	5.0	5.0	100	100
28	120.0	0.82	9.25	42.22	66.87	10.0	10.0	20000	500
29	120.0	0.81	2.0	0.5	69.44	50.0	50.0	70.0	500
30	337.2	0.81	11.5	1.000	69.44	8E-07	8E-07	60000	500
31	120.0	0.81	7.0	1.050	69.44	6E-04	6E-04	45	45
32	132.0	0.82	7.3	47.02	67.13	2E-06	2E-06	250	500
33	390.0	0.80	8.04	47.02	75.01	2E-07	2E-07	500	500
34	120.0	0.87	7.13	0.342	46.76	2E-07	2E-07	100	500
35	120.0	0.86	11.0	0.485	50.31	2E-04	2E-04	500	500
36	120.0	0.86	3.95	0.328	50.31	90.0	90.0	300	300
37	120.0	0.86	3.95	1.000	50.31	90.0	90.0	300	300
38	120.0	0.86	2.00	1.000	50.31	1E-06	1E-06	300	300

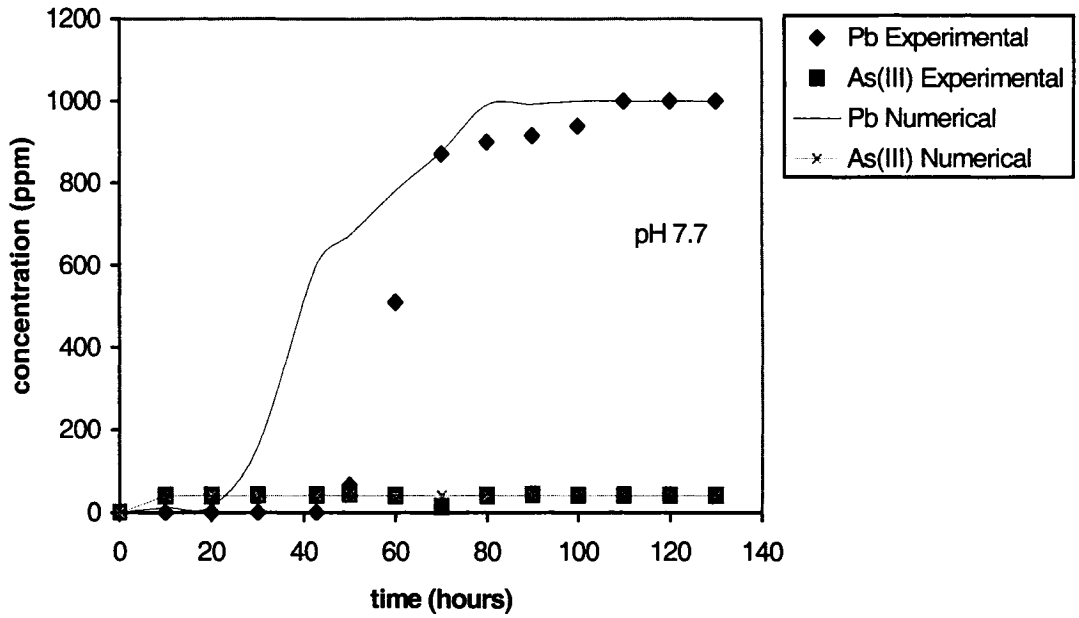

Figure 6.78 Comparison of experimental and numerical run (Run 25)

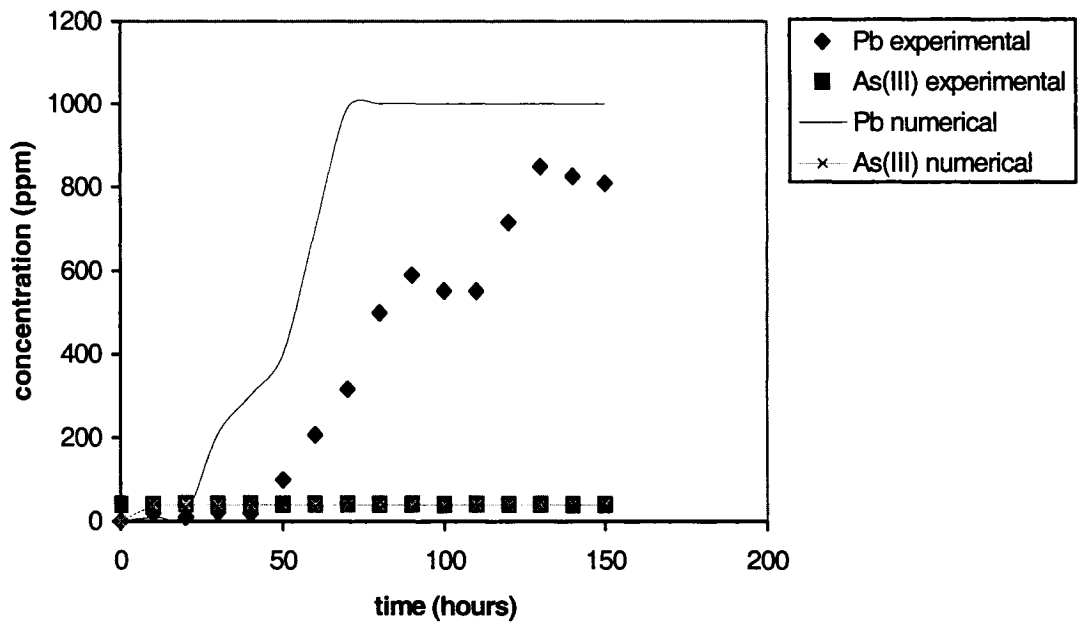

Figure 6.79. Comparison of numerical and experimental run (run 28)

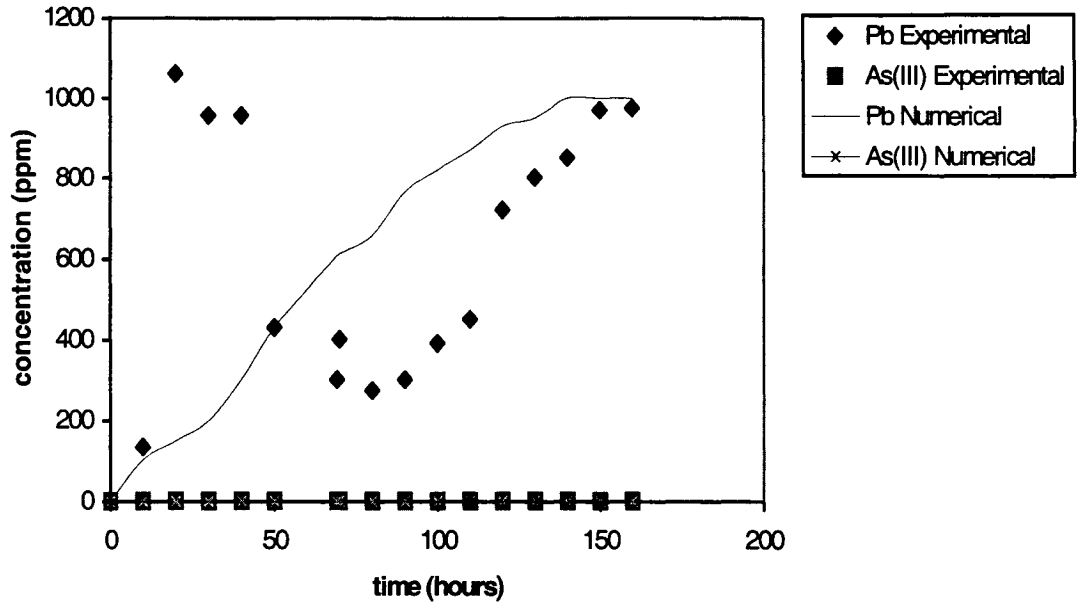

Figure 6.80. Comparison of experiment and numerical run (Run 29)

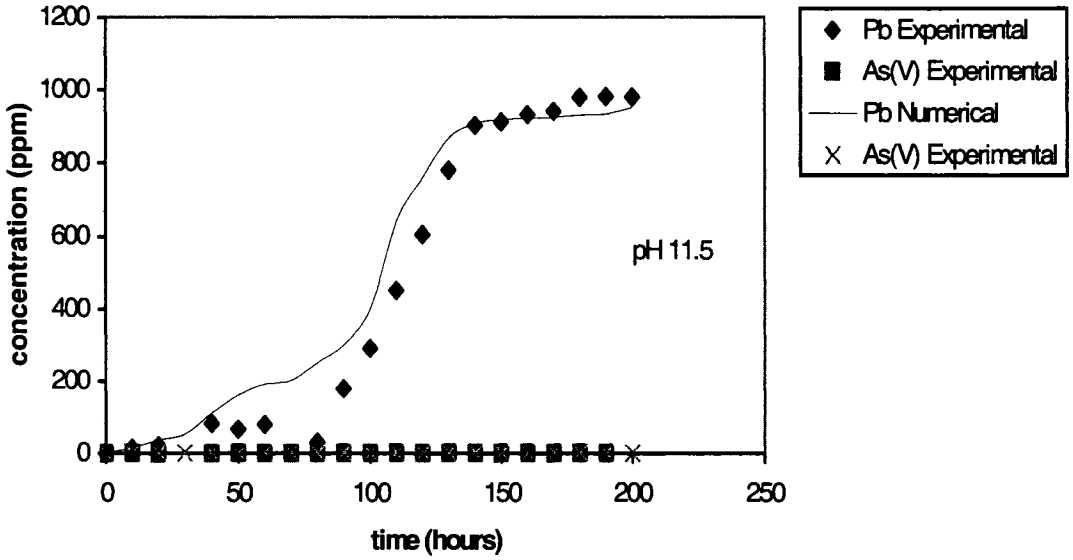

Figure 6.81. Comparison of numerical and experimental run (Run 30)

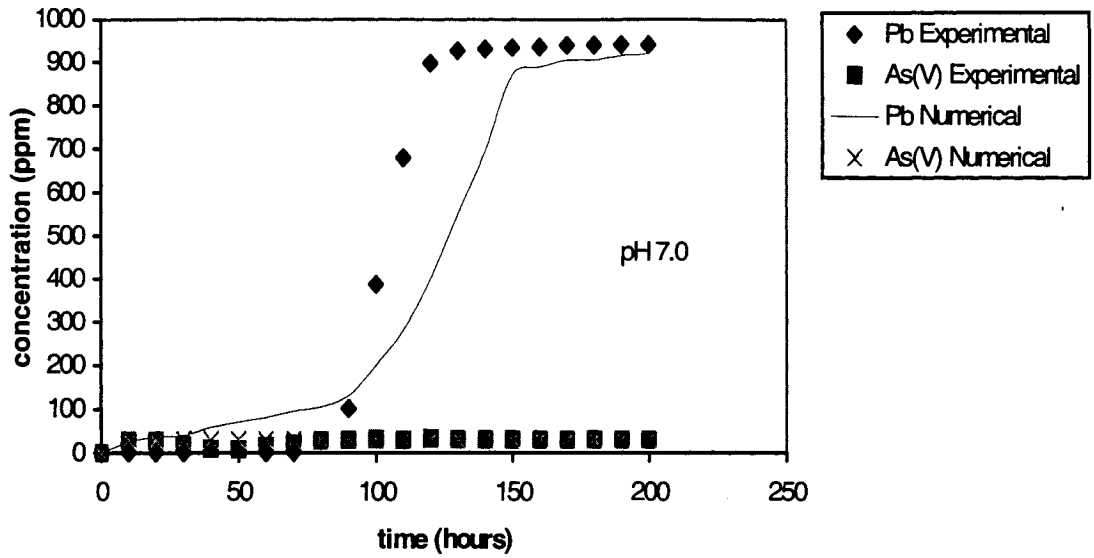

Figure 6.82. Comparison of numerical and experimental run (Run 31)

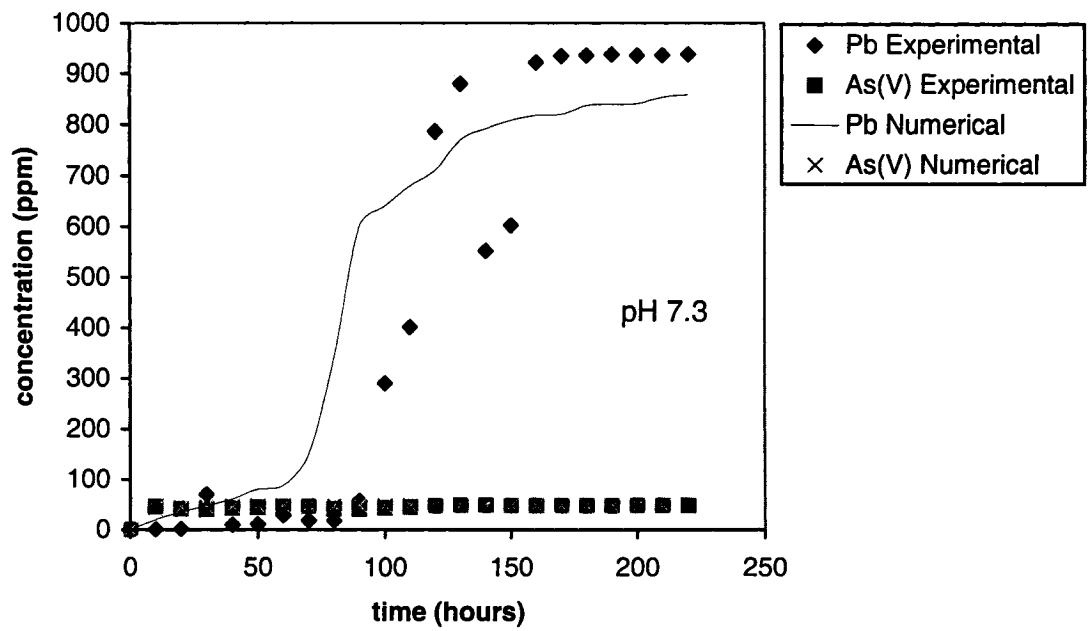

Figure 6.83. Comparison of numerical and experimental run (Run 32)

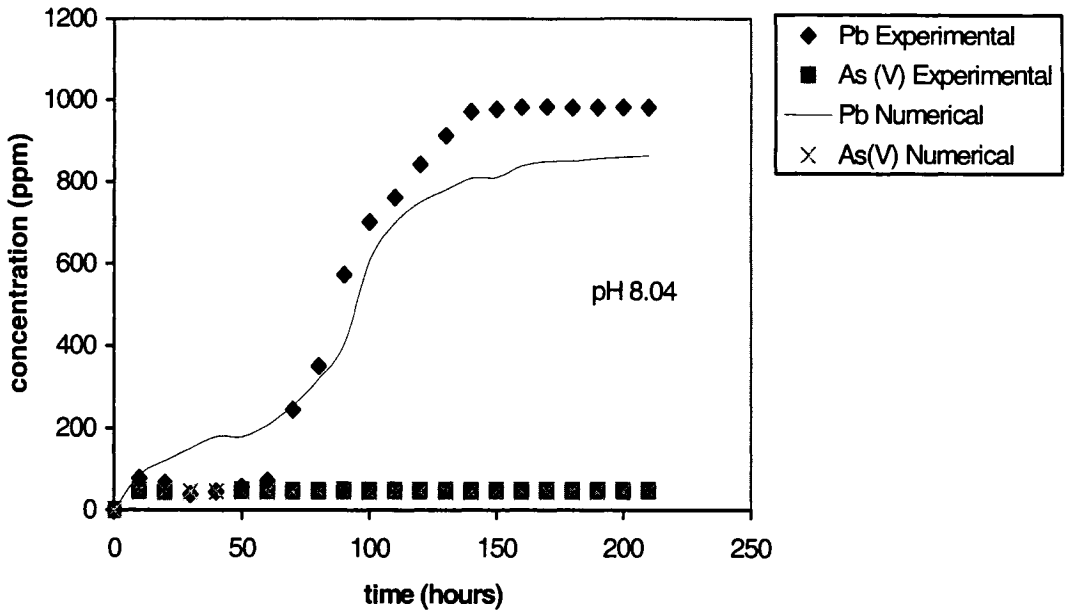

Figure 6.84. Comparison of numerical and experimental run (Run 33)

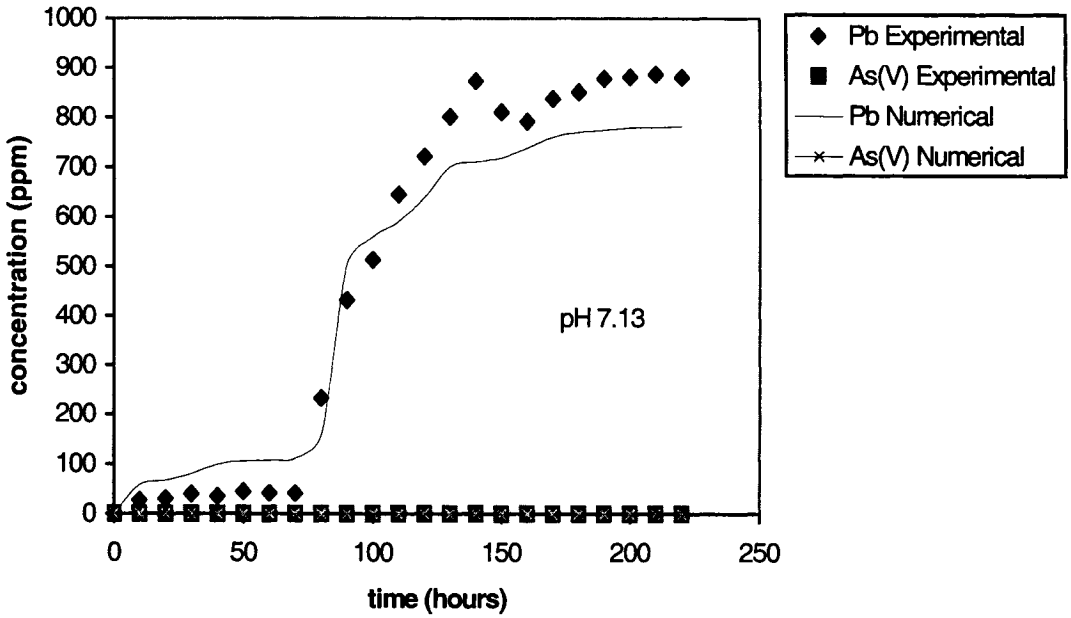

Figure 6.85. Comparison of numerical and experimental run (Run 34)

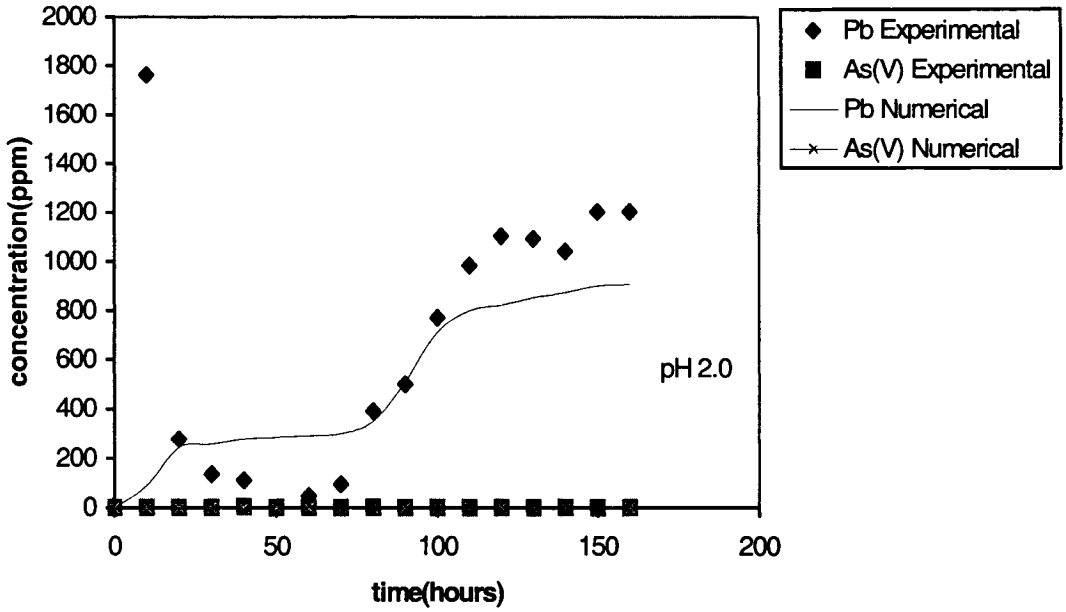

Figure 6.86 Comparison of numerical and experimental run (Run 38)

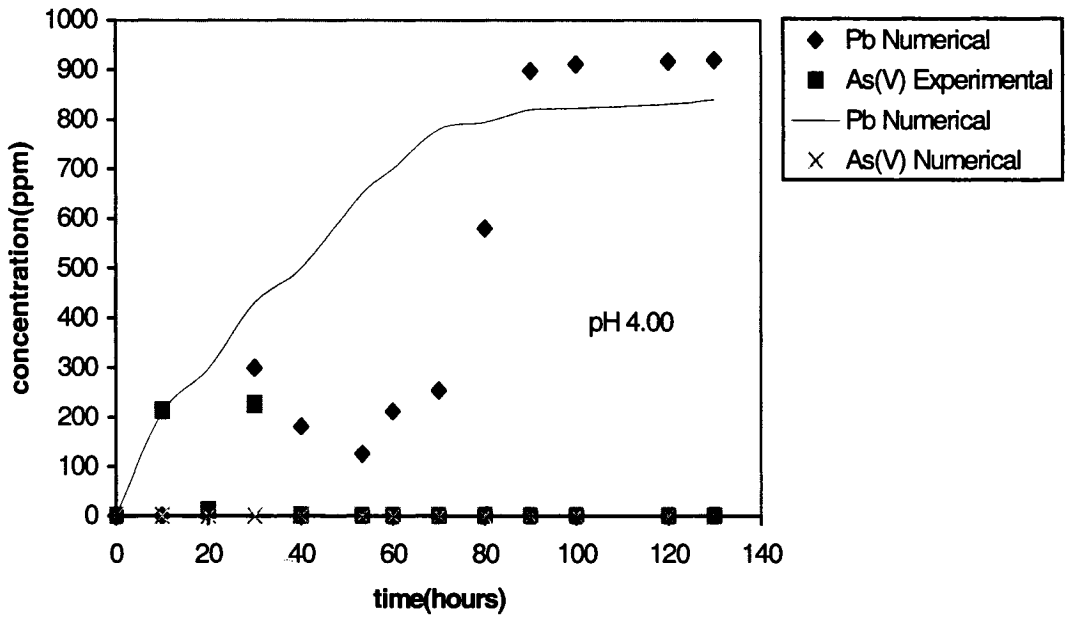

Figure 6.87 Comparison of numerical and experimental run (Run 37)

6.6 Summary of the Numerical Results

The numerical runs were conducted to simulate the experimental results of the dynamic column tests. The model was tested for each dynamic run using the physical model parameters obtained from experimental observations. The remaining parameters were coupled into the code to fit the experimental data. This has become a science in itself, known as the parameter estimation problem (Rice, 1982).

The numerical simulations illustrate considerable discrepancies with the experimental runs. The problem lies not in the logical development of the model but in the lack of complete understanding of the chemical nature of the substrate. The accuracy of the model does not depend only on the mathematical formula used and on the determined constants but also on the reliability of the independent variables that are fed into the model (Scheiwer and Volesky, 1995).

The relevance of calcium (carbonate and phosphate, combined mass of 37 percent) is largely ignored in the model. It is not clearly understood if the calcium ions at low pH values compete with lead ions on the substrate or act as sites for ion exchange (assumed for numerical purposes) mechanism. It has also not been quantitatively estimated the extent of complex formation of lead carbonates and phosphates. The lead ions interact largely covalently with the adsorbent, while the arsenic ions are influenced by electrostatic forces on the substrate. The presence of co-ions (nitrate and chloride) has been ignored in development of the numerical code. But several researchers have observed that anionic effect is dominant below pH value of 3 in the bulk phase. However, since the effect of adsorption of arsenic is negligible, compliance between experimental and numerical runs is achieved by coupling the low adsorption coefficients of arsenic with the high adsorption coefficients of lead ions. The concentration of lead ions is significantly higher than arsenic. When the adsorption of arsenic anions is considered in a multi-component phase, the lead ions were assumed to adsorb on calcium sites. Overall, the numerical results for Figures 6.74-6.85 do not validate the experimental runs. It

indicates that besides ion exchange, several other mechanisms do influence the sorption process. It needs to be investigated whether the interaction mechanism of lead on calcium sites is ion exchange behavior or predominantly precipitation. At high pH (alkaline medium) the lead ions may interact with each specific functional group with a varying mechanism. Hence, since the total number of sites is a critical factor in overall sorption behavior, the importance in quantifying the sites is extremely significant.

6.7 Sensitivity analysis

The purpose of this analysis is to study the effects of different parameters on the performance of dynamic columns. Varying each of the parameters, while maintaining the other conditions constant, is the aim of the study. The varied parameters are porosity, kinetic adsorption coefficients, ultimate adsorption capacities, flow rates and total number of adsorption sites. The analysis is conducted with parameters of run 1. Varying its values and maintaining the rest constant, the effects of each parameter are analyzed.

6.7.1 Effects of internal porosity and external voidage

The effect of porosity is illustrated in Figure 6.88. It is revealed that internal porosity has a profound effect on the adsorption behavior in a dynamic column. The breakthrough occurs earlier for the medium with lower internal porosity. The lesser the internal porosity, fewer ions are able to diffuse through the internal pores resulting in lower adsorptivities.

6.7.2 Effects of mobility of the Lead cation

Figure 6.89 displays the effect of mobility of the cations with respect to time intervals. The higher the mobility, the medium is saturated earlier. The adsorption coefficient of the medium for both the types of sites is considered to be 0.003 millimoles per liter.

6.7.3 Effects of adsorption coefficient on breakthrough interval

Figure 6.90 illustrates the effect of adsorption coefficients on a dynamic column. The higher the value of adsorption coefficient, the breakthrough interval is delayed. The breakthrough curve becomes steeper. One important feature is the figure does not display the rate of saturation of the medium.

6.7.4 Effects of maximum adsorption capacity on breakthrough interval

Figure 6.91 depicts that the factor Q_m is insensitive to the numerical model.

6.7.5 Effect of number of adsorption sites per unit mass of adsorbent

Figure 6.92 displays the impact of number of adsorption sites on breakthrough interval of the adsorbent. The breakthrough curve becomes steeper and the column is saturated earlier for higher values of the coupled parameter.

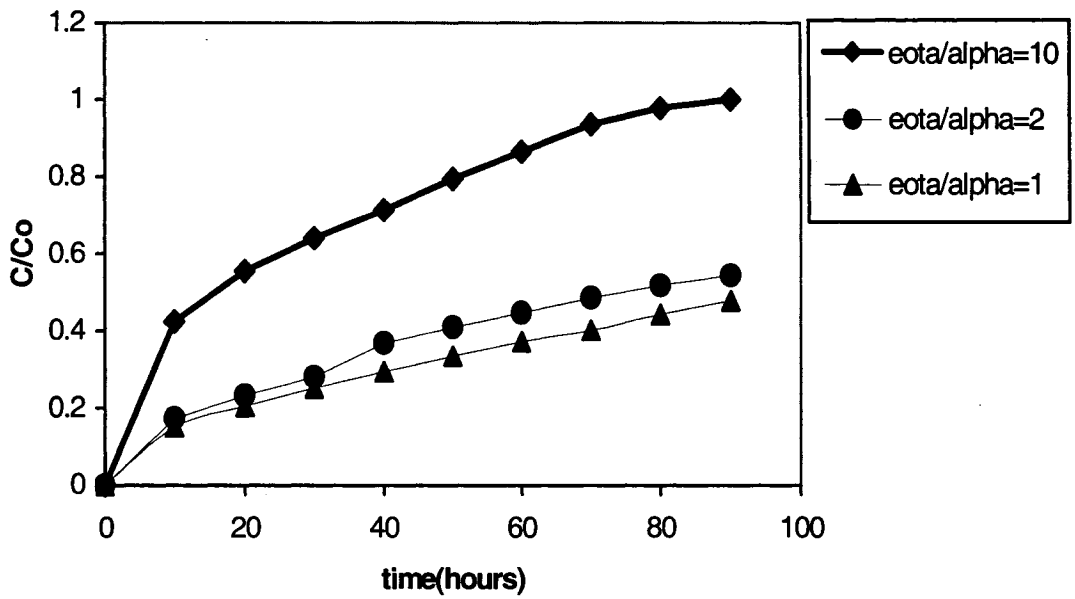

Figure 6.88 Effects of ratio of internal porosity to external voidage on breakthrough time (Note: The total porosity in each case is constant)

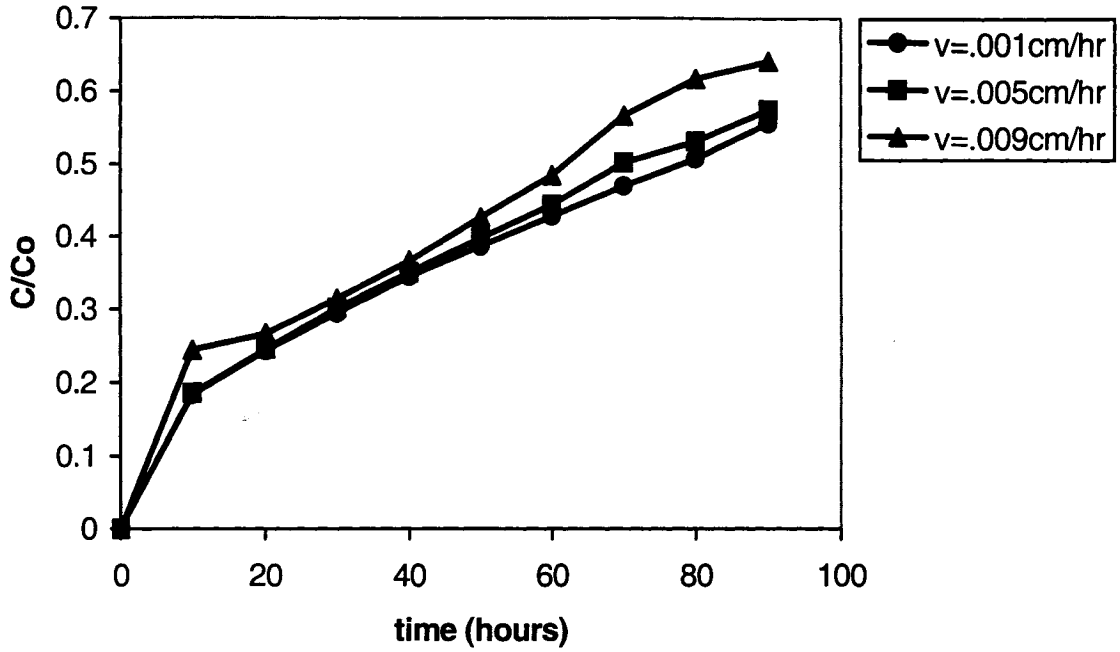

Figure 6.89. Effect of mobility of cations on breakthrough interval (identical porosities)

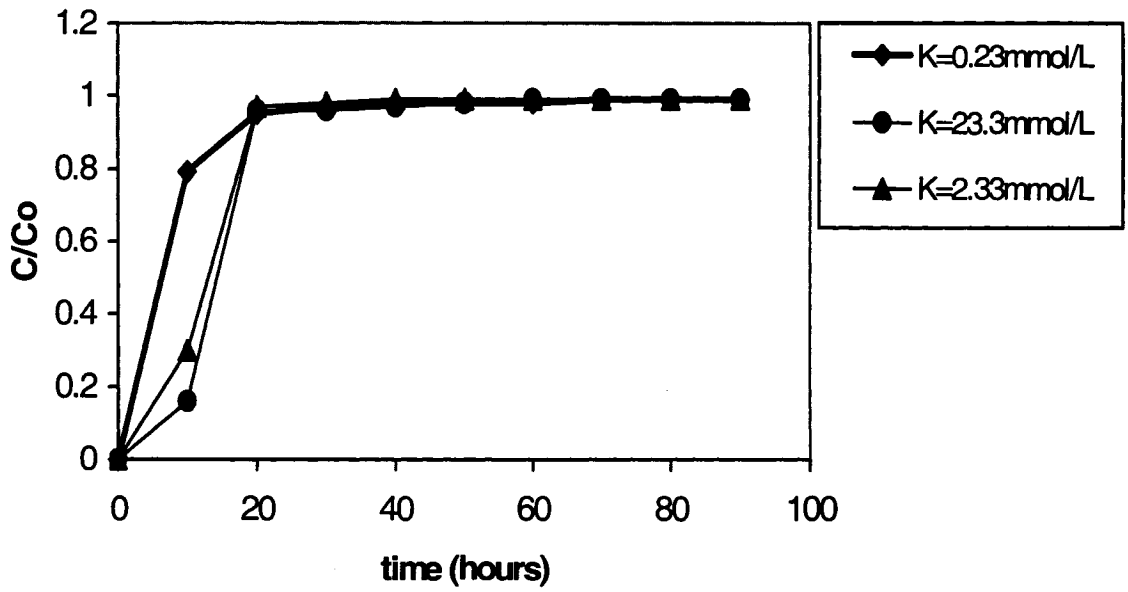

Figure 6.90 Effect of adsorption coefficient on breakthrough interval

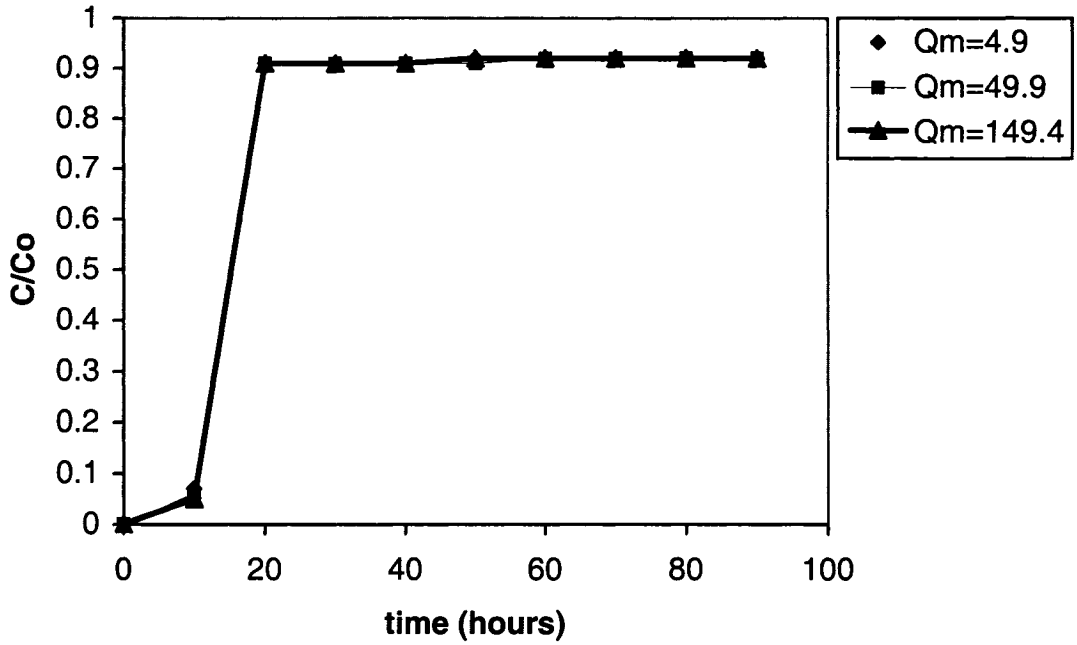

Figure 6.91 Effect of breakthrough interval on ultimate adsorption capacity (mg/g)

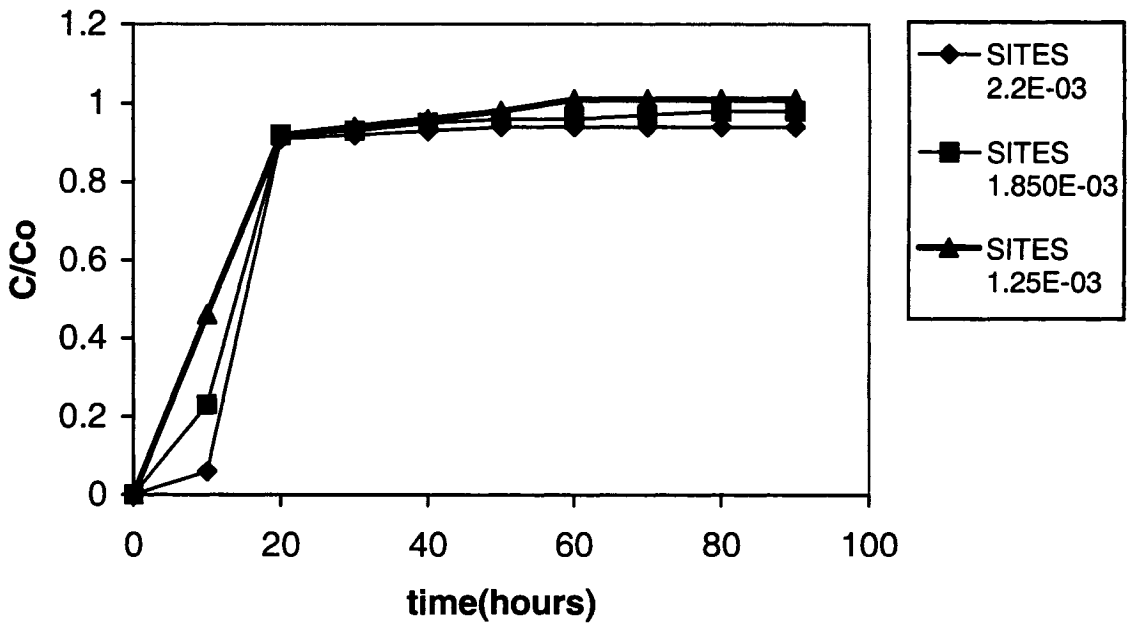

Figure 6.92 Effect of breakthrough interval on total number of adsorption sites (moles/g)

Chapter 7

7 SURFACE CHEMISTRY OF FISH SCALE

Summary

In the present study, the applicability of fish scales as a sorbent material for the solid phase extraction of environmental inorganic contaminants, such as lead ions, was investigated, and the degree of heterogeneity of the adsorbent was evaluated using SEM and NMR techniques. These analyses provided an understanding of the structure of the fish scale, and a number of factors related to the underlying adsorption mechanism were predicted.

7.1 Tests

The original Cod scale was collected from the Fisherman's Market at Bedford, Nova Scotia, Canada. It was rinsed with distilled water to remove weakly associated sodium ions that may interfere with the over all adsorption phenomenon. A portion of the scales was pulverized to a size of 37-40 micron. To test the adsorption of lead ions, an un pulverized portion was immersed in a solution of lead ions at 1000 ppm for adsorption studies.

To analyze the elements present in the fish scale, an ultimate analysis was conducted at Philip Analytical Services, Bedford. The substrate used for determining the cation exchange and anion exchange capacities is Atlantic Salmon scale. The exchange capacity is determined by 'Methods of Soil Analysis' at Agvise Laboratories, Northwood, North Dakota , USA. The ultimate batch adsorption capacity of the Atlantic Salmon Scale is determined in Department of Mineral Resources Laboratory, Dalhousie University, Nova Scotia , Canada. Structural studies of the fish scale by Scanning Electron Microscope

(SEM) methods were performed at the Department of Metallurgy of Dalhousie University. All NMR experiments were carried out at the Atlantic Region Magnetic Resonance Centre, Department of Chemistry, Dalhousie University, on a Bruker AMX-400 NMR spectrometer. The spectra was obtained using a Bruker 4 mm magic-angle spinning triple-resonance probe with a MAS spinning rate of 10 kHz. Both ^{13}C and ^{31}P spectra were obtained using cross-polarization as well as high-power proton decoupling. The contact time in each case was 5 ms and a recycle delay of 10 s was employed. For the ^{31}P spectrum, 32 transients were accumulated, whereas 5512 were accumulated for the ^{13}C spectrum. Carbon chemical shifts were referenced with respect to tetramethylsilane (TMS) at 0 ppm by using adamantane as a secondary reference. This was achieved by setting the highest frequency peak of the adamantane carbon spectrum to 38.6 ppm. Similarly, phosphorus chemical shifts were referenced to 85% H_3PO_4 (aq.) at 0 ppm by using ammonium dihydrogen phosphate (ADP) as a secondary reference. This was attained by setting the phosphorus signal of ADP to 0.8 ppm.

7.2 Results and Discussion

The foremost priority in determining the structure of the fish scale is to conduct a study of its substrate by Scanning Electron Microscope (SEM) methods. The SEM system belongs to the Department of Material Science of Dalhousie University, Halifax, Nova Scotia. The SEM techniques are conducted and it is determined that other elements (besides regular elements of Carbon, Hydrogen, Nitrogen and Oxygen) consisted of Calcium and Phosphorous. The relative concentrations of these two elements are in the ratio of 78 to 22 respectively.

7.2.1 Structural Analysis

The ultimate analysis results for the composition of fish scale are displayed in Table 7.1. The amounts of carbon, hydrogen and nitrogen detected are consistent with organic material, and the high level of ash suggests a significant inorganic component. The molar ratio of carbon to nitrogen (3.6:1) in fish scale is remarkably similar to the 3.7:1 ratio

calculated from a typical elemental composition for a protein (Lehninger, 1970) and is much less than that given by the formulae for the amino sugar subunits of chitin (8:1) and chitosan (6:1).

Table 7.1. Elemental Analysis of Atlantic Cod Fish Scale

Analyte	Units (% Wt)	Molar Ratio
Carbon	26.0	1.0
Hydrogen	4.6	2.1
Nitrogen	8.4	0.28
Oxygen	23.2	0.67
Ash	37.8	-

Ash signifies a mixture of various oxides including calcium, magnesium and phosphorous. Table 7.2 displays the physical and chemical properties of Atlantic Salmon and Cod scale.

Table 7.2: Physical and chemical characteristics of Fish Scale

Properties of the Biomass	Numerical values
Cation Exchange Capacity (Salmon scale)	180 milliequivalent per kilogram of adsorbent
Anion Exchange Capacity (Salmon Scale)(pH 7.0)	55.8 milliequivalent per kilogram of adsorbent
Maximum Adsorption Capacity (Salmon Scale)	262.4 milliequivalent of lead per kilo gram of adsorbent
Zero point charge calculated from equations 3.61 and 3.62	6.8
Surface Charge of Atlantic Cod scale	$8.48 * 10^2$ Coloumbs per unit gram of adsorbent
Inorganic content in Atlantic Cod Scale	37.8%

Note: Zero point charge= $-(pk_1^{int}+pk_2^{int})/2$ [page 65]

From Table 7.2, it can be inferred that maximum adsorption capacity is higher than cation exchange capacity in case of Atlantic Salmon scales. Thus besides cation exchange, chemisorption, precipitation and coordinate linkage mechanisms are associated with removal of lead contaminant.

7.3 Scanning Electron Microscope (SEM) Techniques

In addition to the regular elements of carbon, hydrogen, nitrogen and oxygen as components of fish scale, SEM analysis identified calcium and phosphorus in a ratio of 78 to 22. This ratio is based on the mass of each element.

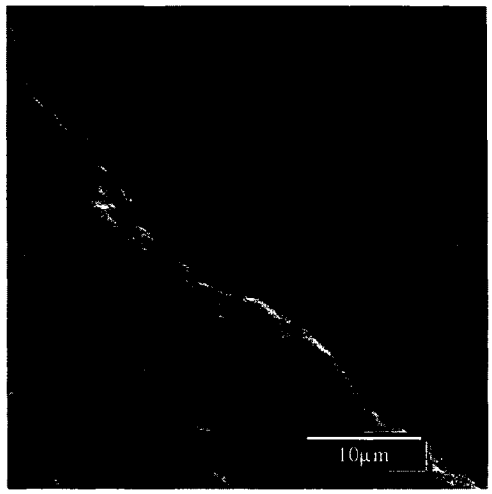

Figure 7.1 1558X magnification of substrate (fish scale)

At 1558X magnification (Figure 7.1), the non-planar nature of the fish scale is apparent, whereas at a 317X magnification (Figure 7. 2) reveals an extensive 'ridge-like' network. The network consists of 'tooth shaped' features. The 'features' when closely analysed,

confirm that they consist of calcium and phosphorous. An interesting pattern emerges at 79X magnification (Figure 7.3). In this view, the substrate of the fish scale, which adheres to the body of the animal, is displayed along with a small portion twisted from the side of the substrate that contacts the aqueous phase. There is no trace of ridges on the body side, yet there is ample distribution of the ridges on its opposite side. Another view at 158X magnification (Figure 7.4) further demonstrates that the substrate is extensively covered with the 'ridges'. Examination of a specific lobe at 317X magnification shows that the lobe consists of a 'bundle of ropes' that is neatly tied together (Figure 7. 5). The SEM study confirmed the presence of lead and arsenic ions adsorbed on the substrate.

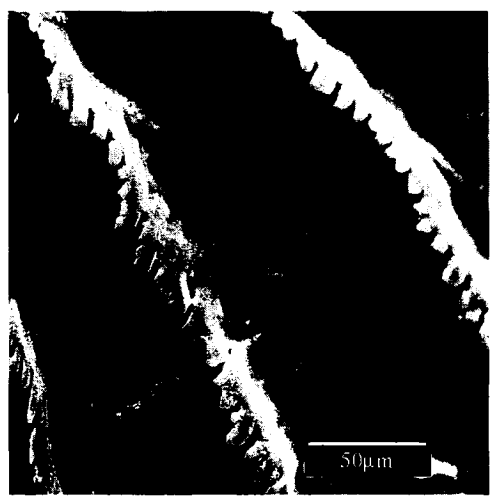

Figure 7.2 317X magnification of substrate (fish scale)

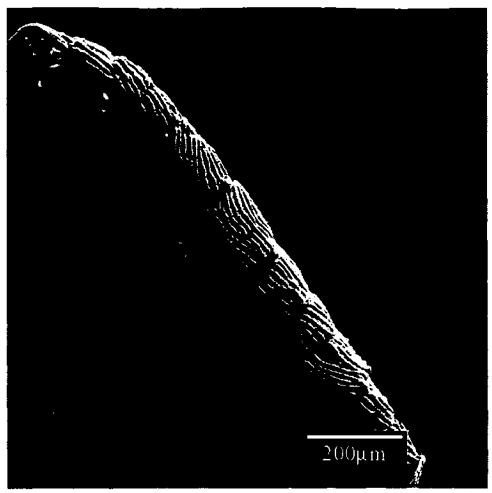

Figure 7.3. 79X magnification of substrate (fish scale)

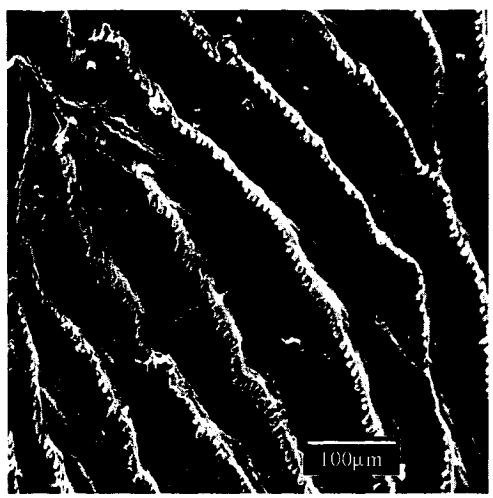

Figure 7.4 158Xmagnification of substrate (fish scale)

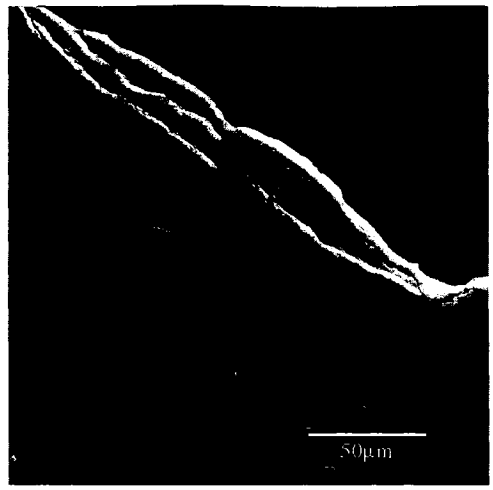

Figure 7.5 317X magnification on lobes of the substrate of Figure 7.2

7.4 Nuclear Magnetic Resonance (NMR) Analysis

The solid-state ^{13}C NMR spectrum of Cod fish scale is displayed in Figure 7.6a. The spectrum shows prominent resonances for carbonyl carbons (δ 168-180 ppm) and aliphatic carbons (δ 12-66 ppm), as well as less intense resonances around δ 130 and 158 ppm, attributed to aromatic carbons. The ^{31}P NMR spectrum of scale showed only a single resonance peak at 2.8 ppm (Figure 7.6b).

Polysaccharide is not detected in the sample; no signal characteristic of anomeric carbons is observed near δ 100 ppm in the ^{13}C NMR spectrum. On the other hand, the overall appearance of the spectrum is similar to the spectra of structural proteins, such as collagen (Saitô and Tabeta, 1984) and silk fibroin (Saitô et al., 1984), suggesting protein as the major organic component of fish scale. A general structure of protein is shown in Figure 7.7. The range of chemical shifts of the signals within the region for aliphatic carbons is consistent with resonances expected for the α-carbons of amino acid residues in the protein, the carbons attached to oxygen in alcohols, and carbons in hydrophobic

side chains of amino acids. The presence of amino acids possessing non-polar side chains is consistent with the hydrophobic nature of Cod scale and its low solubility in water.

The chemical shift of the ^{13}C resonance assigned to carbonyl groups is very similar to that observed in other proteins (Saitô and Tabeta, 1984; Saitô et al., 1984) and therefore corresponds to amide carbonyls in the protein backbone and carboxyl groups in the side chains of aspartic and glutamic acid residues. The very high intensity of the carbonyl resonance, however, suggests the presence of another species containing carbon that resonates at a similar chemical shift. When the fish scale was treated with dilute aqueous HCl, an approximately 20% loss of mass was observed, suggesting the conversion of carbonate ion to carbon dioxide. Carbonate ion could be associated with the calcium detected by SEM and contribute to the intensity of the carbonyl resonance in the ^{13}C-NMR spectrum. For example, the carbon chemical shift of solid calcium carbonate (limestone) has been measured by Skála and Rohovec (Skála and Rohovec, 1998) in range between 166 and 169 ppm, consistent with this interpretation.

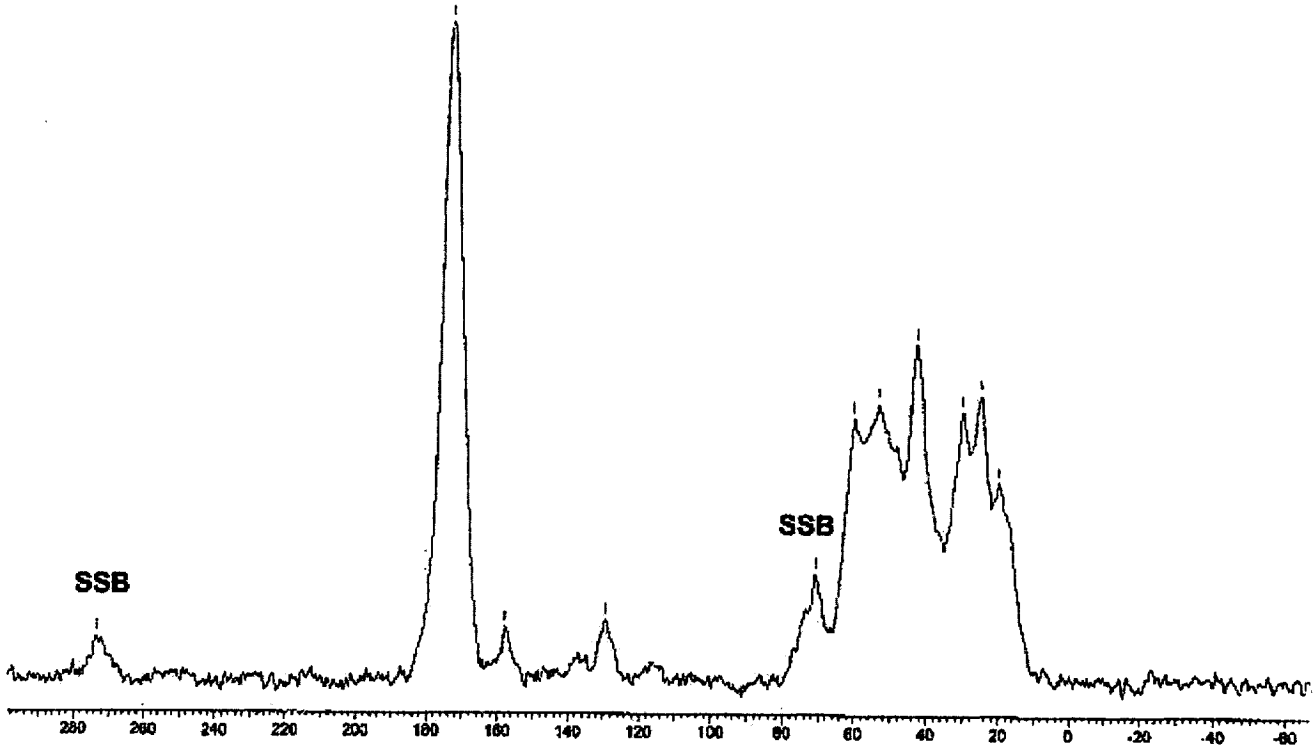

Figure7.6 (a). ^{13}C CP/MAS spectrum of the pulverized Cod scale sample. The peaks denoted by "SSB" are spinning sidebands. The spectrum represents the accumulation of 5512 scans.

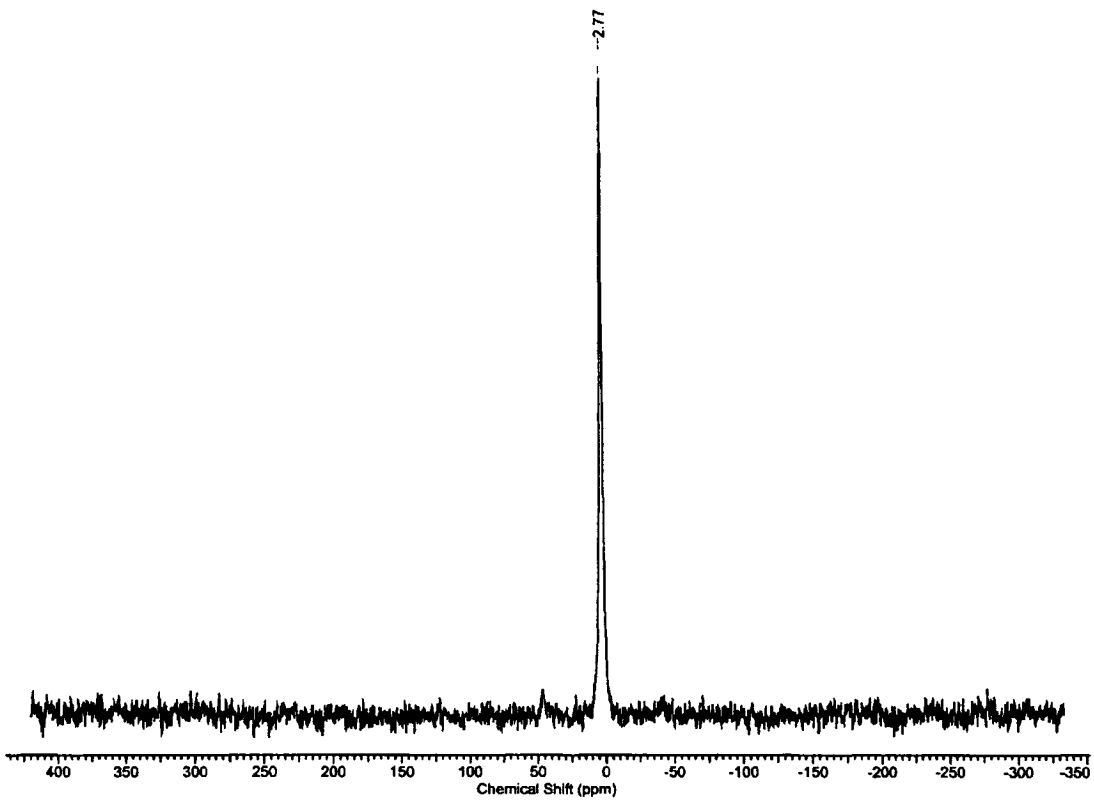

Figure7.6 (b). ^{31}P NMR spectrum of the pulverized Cod scale sample. The peak denotes the existence of phosphate by NMR method

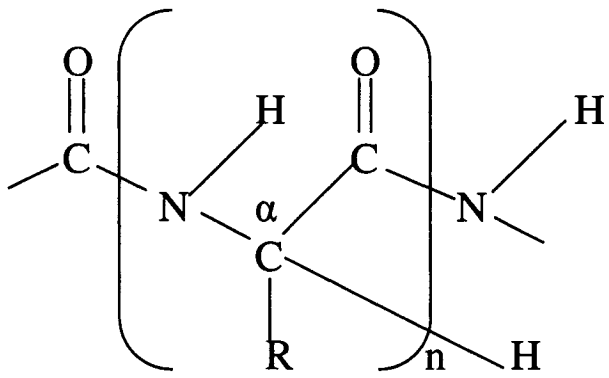

Figure 7.7. A general structure (proposed) of protein showing the α-carbon and R for the various side-chain structures of the amino acid residues

The phosphorus indicated by SEM was confirmed by a strong resonance in the ^{31}P NMR spectrum with a chemical shift of 2.8 ppm. The absence of spinning sidebands in the spectrum also indicates a small chemical shielding anisotropy associated with this species. These results are consistent with the presence of orthophosphate in the sample and furthermore show a striking similarity with the ^{31}P NMR spectrum obtained in the study by Turner et al. (Turner et al., 1986) for calcium phosphate. These workers measured phosphorus chemical shifts and anisotropies in a series of orthophosphates using a number of different cations. For the calcium cation, they measured an isotropic shift of +3.0 ppm and a negligibly small anisotropy, in very close agreement with what was observed for the fish scale sample.

Collectively, the NMR, SEM and ultimate analysis data collected in this study suggest that the Cod fish scale is a composite consisting of protein, calcium carbonate, and calcium phosphate. Like chitin, which also possesses amide groups (Figure 7.8), strong hydrogen bonding between water molecules and nitrogen sites within the biopolymer is a main factor behind swelling of fish scales.

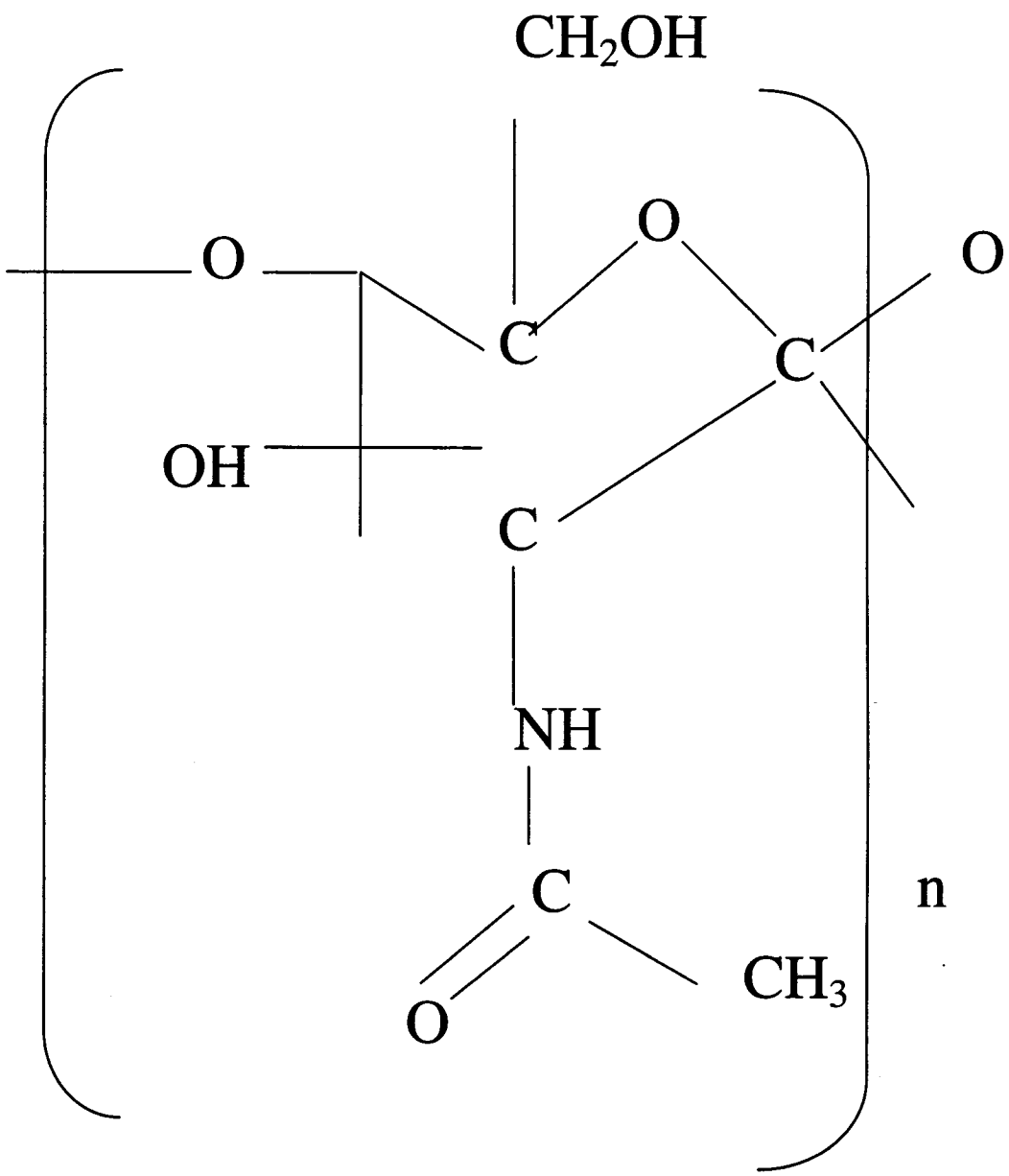

Figure 7.8 Molecular structure of Chitin (Rhee et al., 1998)

7.5 Characterization of Fish Scale

Information on adsorbent material

This thesis illustrates the use of two types of fish scale:

1. Atlantic Cod scale
2. Shouairi scale

Atlantic Cod scale

Atlantic Cod scale is the scale of Atlantic Cod fish. This fish, *Gadus morhua* is one of 59 species of Atlantic Cod fish. The Cod family is the most numerous and best represented of fishes in the Canadian area. It is a deep-sea fish, commonly known as Atlantic ground fish because they generally feed and dwell near the bottom. The 'ground' of the sea- make up about half of Atlantic Canada's total catches of all saltwater species (Fisheries and Oceans Canada, 2002).

In understanding the nature of adsorption of metal ions and Arsenic anions it is necessary to study a set of physical characteristics of the substrate. They include:

- Porosity of the Adsorbent.
- Point of Zero charge.
- Specific surface area of the adsorbent.

Saturating the medium with deionised water and then measuring the total amount of water entrapped in the column measures the porosity of the adsorbent. In the experimental runs the porosity varied from 0.7-0.9. It will be determined numerically the effect of porosity of the metal ion on its adsorption behavior.

7.6 Adsorption Mechanism of Metals and Arsenic on Fish scale

The objective of this study is to understand and analyze both the cationic and anionic binding capacity of the Atlantic Cod scale. The sorption of anions such as Chromium (VI) and Arsenic is highly dependant on the pH of the bulk phase (Bailey et al., 1999). In acidic environment, the protonated sites initiate electrostatic attraction with the anions in the bulk phase. Infra Red and Ultra violet spectral studies confirm the phenomenon of electrostatic attraction of anions and protonated sites (Fu et al., 1997). XPS (X ray Photoelectron Spectroscopic) studies (Dambies et al., 2001) provide identification of the sorption sites involved and the forms of the species adsorbed. Dabson and McQuillan (1999) have reported that adsorption of Cr (VI) does indeed occur on amine functional groups of Chitosan. It has also been observed that binding of any metal on a bio-adsorbent may be a combination of both covalent and ionic bonding (Krishnamurthy and Harris, 1960).

In relation to adsorption of metals such as Lead, Cobalt, Arsenic and Zinc, the term 'metal-organic' is used to describe structural configurations in which the metal is bonded to the Fish scales by either of the following ways:

(i) Carbon Atoms yielding organo-metallic complexes.

(ii) Carboxylic groups producing salts of organic acids
Electron-donating atoms such as Oxygen, Nitrogen, Sulfur and Phosphorus forming coordination complexes.

(iii) Π- electron donating arrangements such as Carbonyl, Aromatic and Olefin groups.

Salts of heavy metal ions display varying degrees of acidity when dissolved in water. This observation is explained by the effect of reaction of the metal ion with solvent water, which is termed 'hydrolysis'.

$$M^{n+} + H_2O \dashrightarrow MOH^{(n-1)+} + H^+ \quad (7.1)$$

(Duggar et.al., 1964)

The adsorption behavior of hydrolysable metal ions at the solid/water interface is strongly pH dependant and is characterized by a general agreement between the hydrolysis of the aqueous metal ions and their enhanced adsorption and charge reversal properties. Models used to describe the phenomena, include ion exchange and the specific adsorption of certain species, are compared to a second model in which all the species of a hydrolysable metal ion are considered as potential adsorbates. In this second model, the lower charged hydrated complexes have favorable free energies for the adsorption process.

High molecular weight organics such as fish scales are of low solubility and have functional groups consisting mainly of amino, carbonyl, hydroxyl and carboxyl groups.
The role of fish scale in reducing heavy metal concentration has been linked to the presence of functional groups that are nucleophilic in nature (Mustafiz et al., 2003). All these types of functional groups may either generate a surface charge that governs electrostatic adsorption, or may form direct bonds (Saxby, 1969). The composite structure also consists of Calcium carbonate that disassociates in an acidic medium to form Calcium ions. It has been noted that released ions like Ca^{2+} adsorb on the substrate, giving it a positive charge (Driehaus et al., 1995). At low pH values, presence of Ca^{2+} ions enhance the removal of anions and acts as a competiting ion in reduction of heavy metal cations from the bulk phase.

7.6.1 Ion exchange Model at pH >p_{zpc}

The ion exchange model is useful for conceptually interpreting the removal of aqueous metal ions by the Fish Scale substrate. In aqueous dispersions the Calcium Carbonate species become hydrated resulting in formation of hydroxyl groups (pH >6.8). At an alkaline phase, the protons from the substrate are removed, resulting in formation of nucleophilic sites at carbonyl and amide positions in the Figure 7.7. The R group in the figure signifies a long chain alkyl group that consists of hydroxyl, carboxyl, amino, aromatic and hydrogen groups. It can be interpreted that perhaps the main interaction in adsorption between the metal cations and fish scale is attributed to the coordinate bonding of the cations with the Nitrogen sites in position 3. The functional groups in the alkyl chain R may also substitute the protons with the metal ions.

Equation 7.2 illustrates the proton exchange mechanism for metal ions M^{n+} (Duggar et al., 1964).

$$m(S\text{-}OH) + M^{n+} \dashrightarrow (S\text{-}O)_m M^{(n-m)+} + mH^{+} \qquad (7.2)$$

At position (1) in Figure 2.34, the π electron cloud shift towards the Oxygen atom results in a partial negative charge on the Oxygen atom. The Lead ions undergo electrostatic attraction to the partially negative charged Oxygen atoms.

In case of anion X, the reaction mechanism may be defined as:

$$\equiv Ca\text{-}OH + XH \dashrightarrow Ca\text{-}X + H_2O \qquad (7.3)$$

A review of the efficiency of common coagulants to remove Arsenic from water has indicated that it can be effectively removed by lime at pH higher than 10.5 (Trace Inorganic Substances Research Committee, 1988). However, the removal of the anions at

pH values above p_{zpc} is hindered by electrostatic repulsions between the deprotonated sites and the anions.

7.6.2 Ion Exchange Model at pH< p_{zpc}

The partially negative charged Oxygen atoms of the Carbonyl groups electrostatically attract the protons

$$m(C\text{-}O^{-}H^{+}) + M^{n+} \longrightarrow C\text{-}O_m M^{(n-m)+} + H^{+} \quad (7.4)$$

At R alkyl group, the Carboxyl, amino and hydroxyl groups undergo protonation to form positively charged substrates. The anions are electrostatically attracted to the protonated surfaces. However, the proton exchange theory is not entirely satisfactory because it is a constant surface charge model. It cannot explain the charge reversal when hydrolysis occurs. The only way in which the observations could be explained is that n>m in equation 7.2 and that n/m is a function of pH.

Equation 7.4 may be written in an equivalent way that gives a different mechanistic interpretation, namely

$$S] + M^{n+} \longleftrightarrow S] M(OH)_m{}^{(n-m)+}(H_2O)_x + mH^{+} \quad (7.5)$$

In other words, adsorption of hydrated, hydrolyzed species is an alternative model with same stoichiometry. It can be illustrated that uptake of metals may be described by equation 7.5. Thus ion exchange and adsorption models are difficult to differentiate experimentally and to some extent both the models may be applied.

The binding strength of a metal ion to the fish scale depends on the nature of the metal. If a divalent metal ion interacts with the fish scale, two equivalent functional groups of the

adsorbent will bind with the metal ion (Rendelman, 1978). It is highly possible in long-chain isomers, that metal ions are bonded to bonded to functional groups from an adjacent chain. Cross linking of polymers lead to decrease in porosity of the adsorbent (Gonzalzez et al., 2001). Overall the binding strength of a metal ion on Atlantic Cod scale is dependant on properties such as the ionic radius or first hydrolysis constant (Martell and Hanock, 1996). These correlations provide insights into the governing factors behind complex formation with the functional groups and may allow for prediction of unknown products.

7.7 Factors affecting uptake of metals

Rahmani and Sternberg (1999) observed that several factors affect the uptake of metal ions. These include:

- Nature and amount of biomass
- Prior treatment
- The metal species to be removed
- Competing metal ions
- Flow rate of the effluent

7.8 Nature and amount of biomass

Over the past few years, biosorption research has focused on the use of readily available material for the accumulation of metal ions (Schewer, 1999). In particular, the excellent metal binding capability of marine organisms has been investigated in numerous biosorption studies (Holan et al., 1993). Chitosan, an aminopolysaccharide isolated from crab and lobster shells is known to bind metal ions (Yang and Zall, 1994). Recent preliminary studies in our laboratory (Mustafiz, 2002) have indicated that over 90% of heavy metal ions (e.g., lead) are adsorbed by the scales of *Gadus morhua*, one of the 59 species of Atlantic Cod fish. At present, however, there is no evidence to indicate

whether Atlantic Cod fish scales are composed of chitin (the insoluble raw material processed to chitosan) or other biopolymers.

Separation of ionic species by membrane substrates strongly depends on pore size and the charge on the substrate (Tsuru et al 1991a, 1991b; Peeters et al., 1998). A membrane with small pore sizes effectively retains ionic species, and the pore diffusivities of ions diminish with increasing ionic radii of both metal ions and molecular species. The pH of the bulk phase is an important parameter for removing heavy metal ions. At high pH values (>7), the substrate is substantially negatively charged due to deprotonation of ionisable groups on its surface, and the negatively charged surface has a strong affinity for heavy metal cations. The presence of nucleophilic groups, such as hydroxyl, amino, and carboxylate, is highly advantageous for sorption mechanisms (Dronnet et al., 1997), and results in covalent, hydrogen and electrostatic bonding between the cations in the bulk phase and the nucleophilic sites on the adsorbed phase (Sarwar and Islam, 1997).

7.9 Pre-Treatment

An adsorbent such as fish scale must be pretreated in order to achieve the desired results. The first important task should comprise of rinsing the fish scales with distilled water to remove the sodium ions from its substrate. The sodium ions are highly electrostatic in nature and they may occupy the negatively charged sites on the adsorbate. This reduces the removal efficiency of heavier metals (Schiewer et al., 2000). The biomass (fish scales) is then dried to expel the moisture and pulverized to a smaller size. The larger the extent of pulverization, the higher the surface area available for adsorption. However, extreme reduction of the particle size may destroy some of the functional groups that are associated with adsorption. The adsorbent may then be treated with an acid or an alkali in order to charge the substrate either positively or negatively.

7.10 Metal Species to be removed

Monovalent metal cations in an aqueous phase are largely electrostatic in nature. Such cations like sodium contribute to high ionic strengths that reduce the binding capacity of heavy metals to adsorbents (Schiewer, 1999). Sodium will not be bound covalently and therefore it may not compete for covalent binding of metals by the adsorbent (Stumm and Morgan, 1996).

It has been long accepted that the adsorption of most divalent and trivalent metals increases with increasing pH (Holan et al., 1993). This has been explained as an effect of reduced competition with protons for the existing binding sites (Schiewer and Volesky, 1995). In case of arsenic species, some investigators have reported favorable adsorption of As(III) versus As(V) (Lackovic et al., 2000), while others have reported a more favorable adsorption of As(V) against As(III) (Su et al., 2001). Differences in the relative ease of adsorption of a specific Arsenic species may be attributed to the nature of the adsorbent, water chemistry and pH of the bulk phase (Su et al., 1997). Adsorption and co-precipitation of arsenite and arsenate species on Fe (III) oxides have been investigated (Melitas et al., 2002). They reported that an Arsenate ion uptake is accompanied via a ligand exchange that replaces the hydroxyl ions on the surface by Arsenate ions. Given the rapidity of surface complex formation, the slow approach to sorptive equilibrium (often requiring days to reach) has been attributed to the slow diffusion of arsenic species through porous substrates (Fuller et al., 1993). Overall it may be assumed at this moment the most important factor in removal of the Arsenic species is the pH and concentration of the bulk phase. Another distinct feature that will be proved during the proceedings of this research is that adsorption of arsenic species is dominated by electrostatic behavior, which is in contrast to removal characteristics of heavy metals.

7.11 Competing metal ions

Certain metal ions such as Copper display similar removal efficiencies for equimolar binary systems consisting of Cu (II) /Cd (II). It has also been reported that Cu^{2+} ions form complexes with solid sites on a bio-adsorbent that favor adsorption if the effect of competing salts is decreased (Reddad et al., 2003). As the concentrations of the three competing ions Ni (II), Cd (II) and Zn (II) is increased, the adsorption efficiency of Cu (II) remains undisturbed. However, the adsorptive capacity of Cd (II) decreases rapidly as the concentration of both the ions is increased in equimolar proportions. The results illustrate that with increasing adsorbate to site ratio, elements with larger adsorption coefficients remain unaffected by the change in ratio. With fewer sites available, the competition is strong and therefore the element with weaker adsorption coefficient remains highly affected. Several values predict a stability trend for organic metal complexes of Pb>Cu>Ni>Zn>Cd (Sposito et al., 1981).

Selectivity between metals resulted in the following metal affinities based upon their distribution coefficients. Overall the adsorptive capacities of the metals are different for each ion and competitive adsorption is reflected by the relative affinity of each ion for the specific functional group.

The adsorbent material may be either homogeneous or heterogeneous by nature. The number of different functional groups attached to its substrate reflects the degree of heterogeneity of the material. It may be feasible that a specific ion will interact strongly with a specific site on substrate and yet adsorb weakly to another site of the same material. Thus the number of specific sites and equilibrium constants of each ion with respect to each sites the determining factor of removal of metal contaminants in an aqueous phase.

7.12 Effect of Flow rate

The purpose of conducting dynamic studies is to establish data on a dynamic column that will determine the effectiveness of the adsorbents, as predicted from the isotherms that will be applicable in column studies. Batch reactors cannot provide scale up data to be used for flow columns (Lee and Davis, 2001). The major parameter that is lacking from static test runs is the breakthrough time interval. The breakthrough capacity of the column is different for each pollutant and data obtained from dynamic runs reflect the affinity of a adsorbent for a specific contaminant.

If the influent flow rate is high, the amount of contaminants exposed is proportonately high resulting in earlier saturation of the adsorbent. However, if the site available to the contaminant ratio is high, the breakthrough interval will be delayed. It has been demonstrated that at laminar flow levels, the breakthrough interval is proportional to flow rate (Coskuner and Bentsen, 1987).

Overall, at higher feed rates, the breakthrough time intervals are very low and they tend to converge to a minimum value. This minimum value should correspond to the flooding velocity of the column.

Chapter 8

8 SCALE-UP DESIGN PROCEDURES

8.1 Introduction

The following procedure in ascending order is the ultimate guiding factor to improved methods for analyzing a complex physical and chemical phenomenon (Farouq Ali et al., 1987) :

1. Mathematical models;
2. Un-scaled experimental models;
3. Numerical and unscaled experimental models;
4. Scaled experimental models;
5. Experimental, numerical and scaled models.

One should strive to develop numerical models that can predict behavior of a scaled model. Scaled physical models have been reported to be more desirable than numerical simulations (Farouq Ali et al., 1987). This is largely applicable for recovery methods where phase equilibrium and gravitational forces are significant factors. A chemical process such as adsorption may require a specific set of scaling criteria that requires a comprehensive description of diffusion, dispersion and retardation mechanisms. Types of adsorbent-contaminant system, model geometry, pressure drop, flow rate, time factor, etc are different depending on the type of scaling criteria used. Each approach has its unique advantages and disadvantages (Bansal and Islam, 1994). In a specific scaling option, chemical processes may offer the most challenges, as conventional techniques fail to scale the most relevant chemical phenomena (Islam and Farouq Ali, 1990).

8.2 Theory

When mass transfer occurs, it involves transport of mass of a component from bulk phase to the adsorbed phase through a stagnant film encapsulating an adsorbent particle. It is assumed that the phases are in equilibrium to each other at the actual points of contact of the interface (Sherwood et al., 1975). Therefore, the flux equations may be expressed as

$$N_{ijk} = k_{ikj}\, a_{ik}\, \Phi\, S_j\, (\rho_j\, C_{ij} - \rho_j\, C_{ij}^{i}) \qquad (8.1)$$

N_{ijk}= Mass Transfer rate of component j in or out of i phase through ik interface.
k_{ikj}= Local Mass Transfer Coefficient of component j in i phase through ik interface
C_{ij}^{i}=mole fraction of component j in i phase along the interface
C_{ij}= mole fraction of component j in i phase.
L= length of the field or model
D = dispersion parameter

A correlation for the mass transfer coefficient multiplied by interfacial area for the contaminant phase may be applied as follows:

$$k_{ikj}\, a_{ik} = c_l\, (k_o\, p_o^2\, D_{oj})\, (\Phi\, S_o\, \mu_o\, L^2)^{-1} \qquad (8.2)$$

Martin et al. (1981) originally developed the equation 8.2. This equation was first applied for case of carbon dioxide/ oil system as a function of velocity of the liquid phase, diffusion, cross sectional area, thickness of the experimental cell and molar flux. In the expression 8.2, the Darcy's law is incorporated and the equation couples $k_{ikj}\, a_{ik}$ with pressure, diffusion, saturation, length and permeability of the system. c_l is an experimentally determined parameter. The number of variables considered above is adequate for scaling analysis (Islam and Farouq Ali, 1990).

In the present study, preference is attached to dynamic phenomena of mass transfer. The above equation displays that the rate of mass transfer in the model is inversely proportional to the square of the length of the model. The important aspect of mass transfer in this application is that it includes chemisorption, precipitation and ion exchange as feasible mechanisms in the system.

For a specific process, the significant parameters to be satisfied may be selected. The subset below is chosen includes same porous media, same pressure drops, geometric similarity and same temperature. The subset below is not chosen randomly but after considering the various physical and chemical interactions possible.

The subset consists of the following dimensionless groups.

$$H/L,\ W/L,\ A_{inj}/R^2,\ (\Phi\ \mu\ L^2)\ /(t\ k\ p),\ (\mu\ D/\ K\ p),\ (d\ V\ \rho/\ \mu) \tag{8.3}$$

This approach has the advantage that all properties depending on pressure and composition are accurately scaled. The relative permeabilities will be properly scaled when the porosity of the prototype and the model is identical.

The height of the experimental column is 20 cm and the internal diameter is 3.83 cm.

The height of the prototype is 20 m, then

$$H_{field} / H_{lab} = 100=a \tag{8.4}$$

The diameter of the prototype is 383 cm.

if,

$$\Phi_{lab}\ \mu_{lab}\ (L_{lab})^2 / t_{lab}\ K_{lab}\ p_{lab} = \Phi_{field}\ \mu_{field}\ (100 * L_{lab})^2 / t_{field}\ K_{field}\ p_{field} \tag{8.5}$$

then,

$$t_{field} / t_{lab} = (100*100)\, K_{lab}\, p_{lab} / K_{field}\, p_{field} \quad (8.6)$$

For a model reduced in length by a scaling factor 'a' and employing the same fluids as the prototype, p, K must be same (Islam and Farouq Ali, 1990).

Equation 8.6 is then reduced to-

$$t_{field} / t_{lab} = a^2 \quad (8.7)$$

where

$$K_{lab}\, p_{lab} = K_{field}\, p_{field} \quad (8.8)$$

Considering the significance of Reynolds number,

$$(Re)_{field} = (Re)_{lab} \quad (8.9)$$

$$100*V_{field} = V_{lab} \quad (8.10)$$

Thus from equation 8.10, the field velocity has to operate at 100 times lower than laboratory scale.

if,

$$(A_{inj})_{lab} / (A_{inj})_{field} = 1/a^2 \quad (8.11)$$

then,

$$Q_{field} = V_{field} * A_{field} \quad (8.12)$$

and,

$$Q_{field} = (V_{lab}/100) * (100)^2 * A_{lab} \quad (8.13)$$

or,

$$Q_{field} = 100 * Q_{lab} \quad (8.14)$$

if,

$$(k1/k2)_{lab} = (k1/k2)_{field} \quad (8.15)$$

From equation 8.2,

$$k_{field} = 1/((100)^2 * (L_{lab})^2) \quad (8.16)$$

or,

$$k_{field} = 1/(100)^2 * k_{lab} \quad (8.17)$$

Thus adsorption coefficient in field is $(1/100)^2$ lower than in lab.

The scale up design studies can be categorized into two sub- groups:

1. Conversion of laboratory results into field results based on the prototype features,
2. Numerical scale up studies.

Table 8.1 displays the operating conditions of both model and prototype

Table 8.1. Dimensional operating conditions in the model and prototype

	Model	**Prototype**
Height (cm)	H	a*H
Length (cm)	L	a*L
Flow rate (cc per day)	Q	a*Q
Velocity (cm per day)	V	V/a
Time (day)	T	a*a*t

The term 'a' is defined in equation 8.4.

The groups that are satisfied in this subset are:

I. $D_{lab} V_{lab} = D_{field} V_{field}$

II. $H_{lab} / L_{lab} = H_{field} / L_{field}$

III. $A_{inj\ lab} / L_{lab}^2 = A_{inj\ field} / L_{field}^2$

IV. $Q_{field} = Q_{lab} * a$

V. $\mu_{lab} D^*_{lab} / K_{lab} p_{lab} = \mu_{field} D^*_{field} / K_{field} p_{field}$

The limitations of this subset are that it does not allow scaling of gravitational and dispersive forces.

The groups not satisfied include:

I. $H_{lab} / (\Phi d_p L)_{lab}^{0.5} = H_{field} / (\Phi d_p L)_{field}^{0.5}$

II. $A_{injlab} / L_{lab} (\Phi d_p)_{lab} = A_{inj\ field} / L_{lab} (\Phi d_p)_{field}$

(d_p is mean particle diameter of the adsorbent)

8.3. Conversion of laboratory results into field results based on the prototype features

Equation 8.7 illustrates that by selecting a set of dimensionless groups; the residence time in laboratory may be scaled to field time by a factor of a^2. Therefore the experimental

results in a dynamic column if reflected in field conditions will require effluent profiles with respect to field time intervals. The experimental runs (multi-component) are scaled to field time conditions and illustrated in the following figures 8.1-8.10.

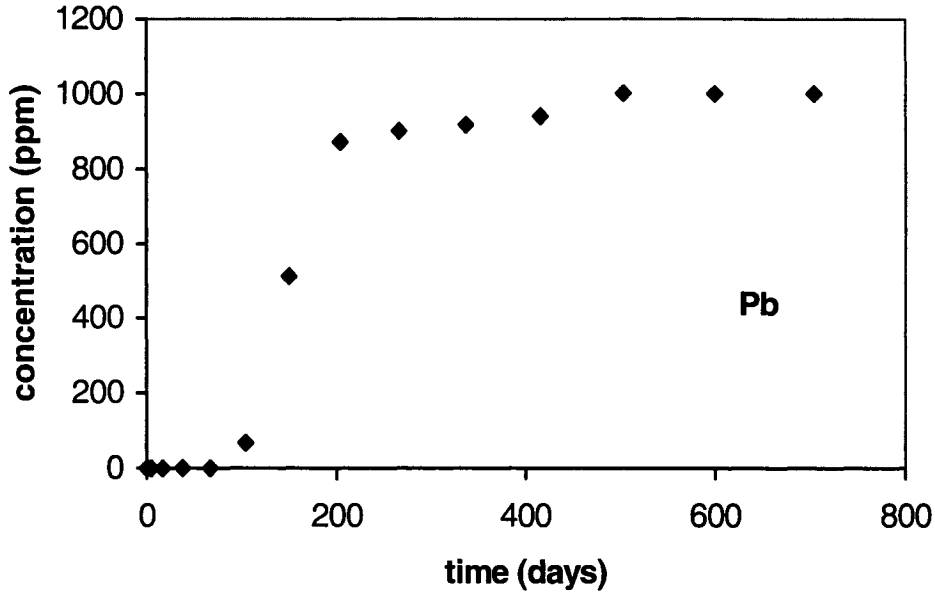

Figure 8.1. Scaled up concentration profile to field conditions (pH 7.7)(Run 25)

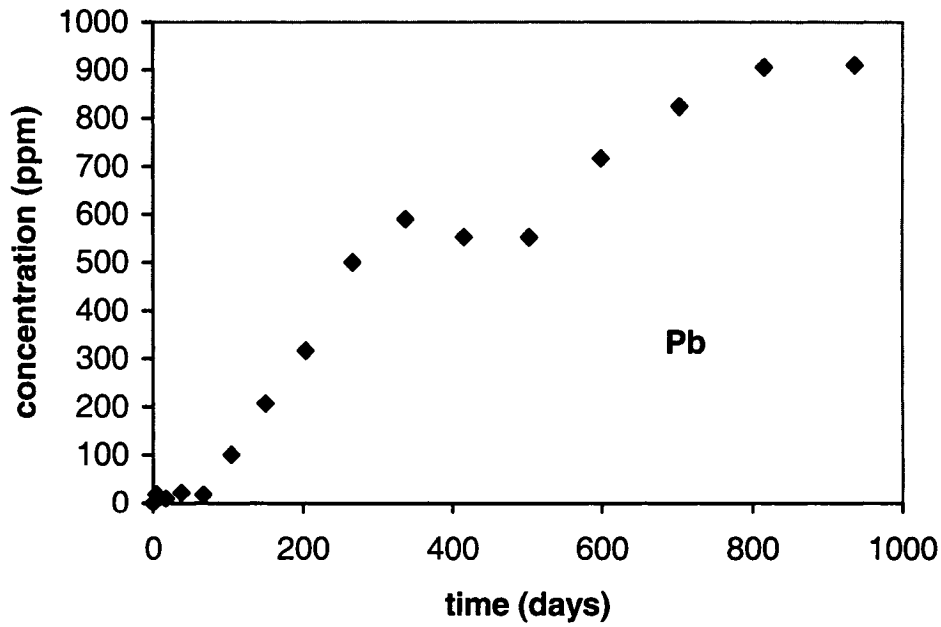

Figure 8.2. Scaled up concentration profile to field conditions (pH 7.7)(Run 26)

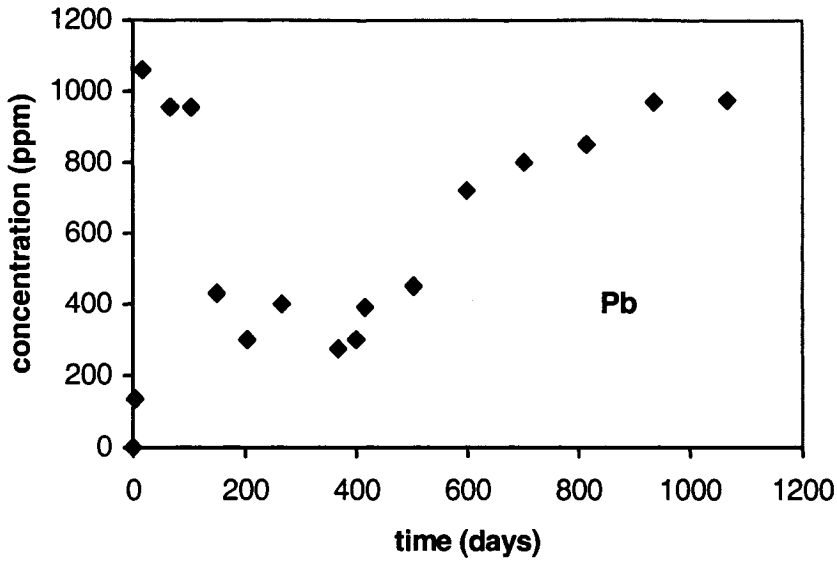

Figure 8.3. Scaled up concentration profile to field conditions (pH 2)(Run 29)

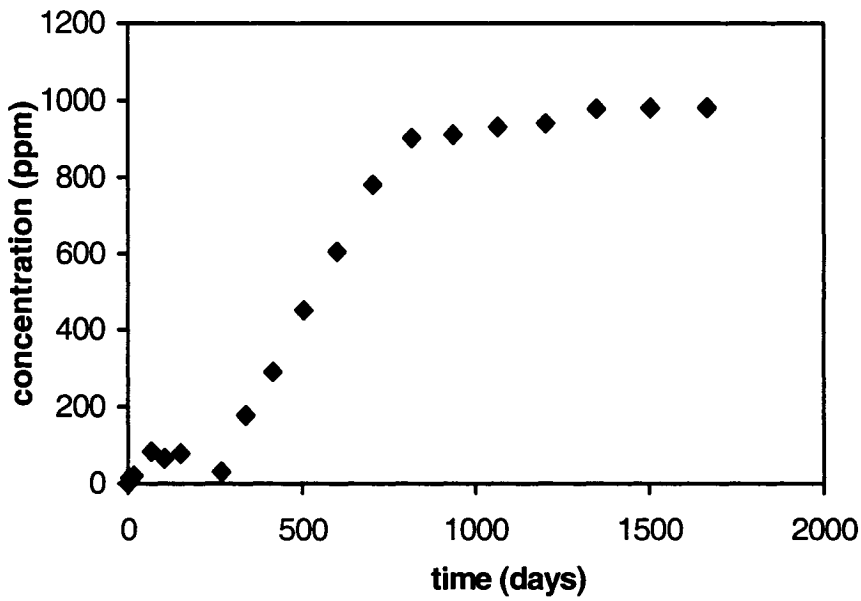

Figure 8.4. Scaled up concentration profile to field conditions (pH 11.5) (Run 30)

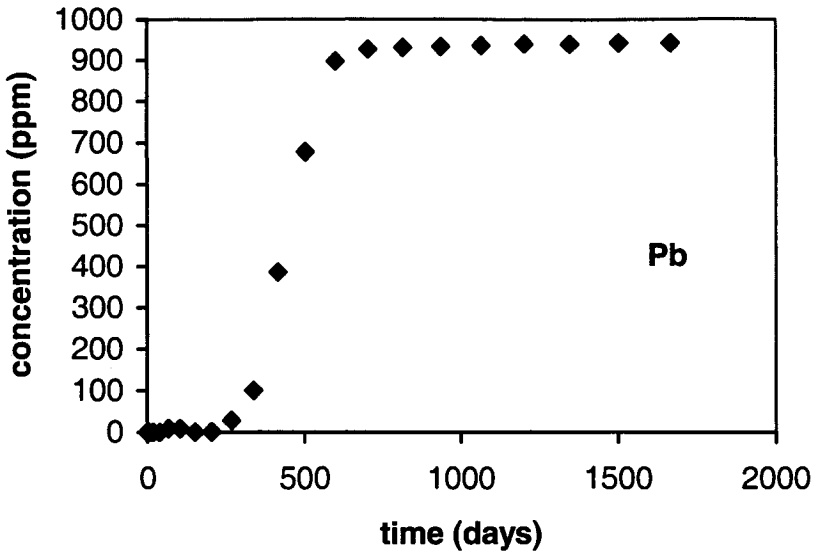

Figure 8.5. Scaled up concentration profile to field conditions (pH 7.0)(Run 31)

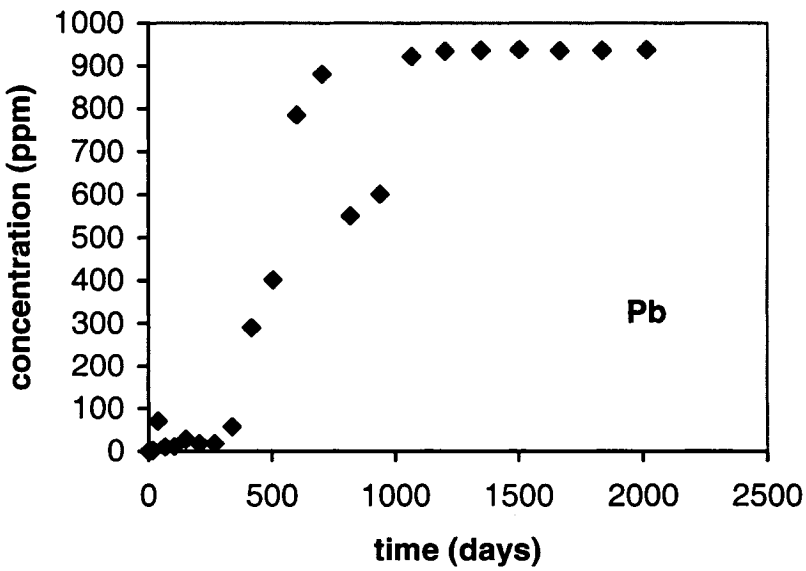

Figure 8.6. Scaled up concentration profile to field conditions (pH 7.3)(Run 32)

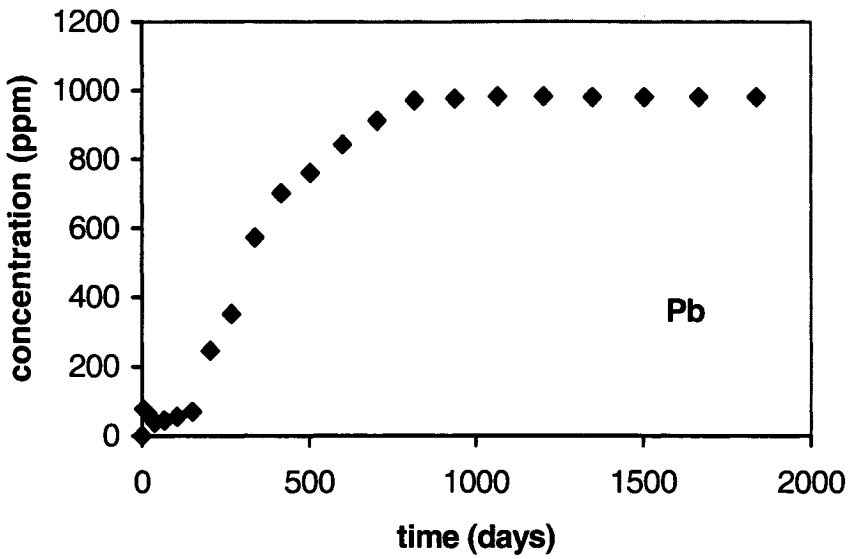

Figure 8.7. Scaled up concentration profile to field conditions (pH 8.04)(Run 33)

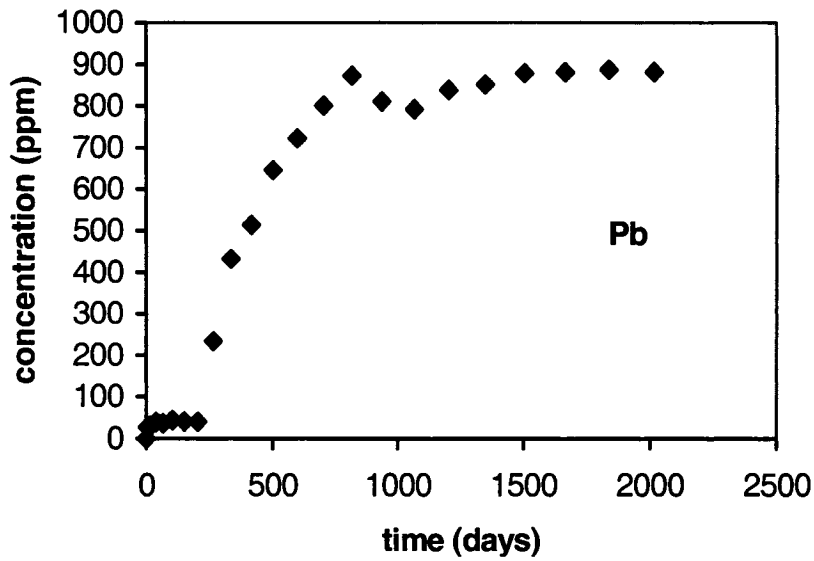

Figure 8.8. Scaled up concentration profile to field conditions (pH 7.13)(Run 34)

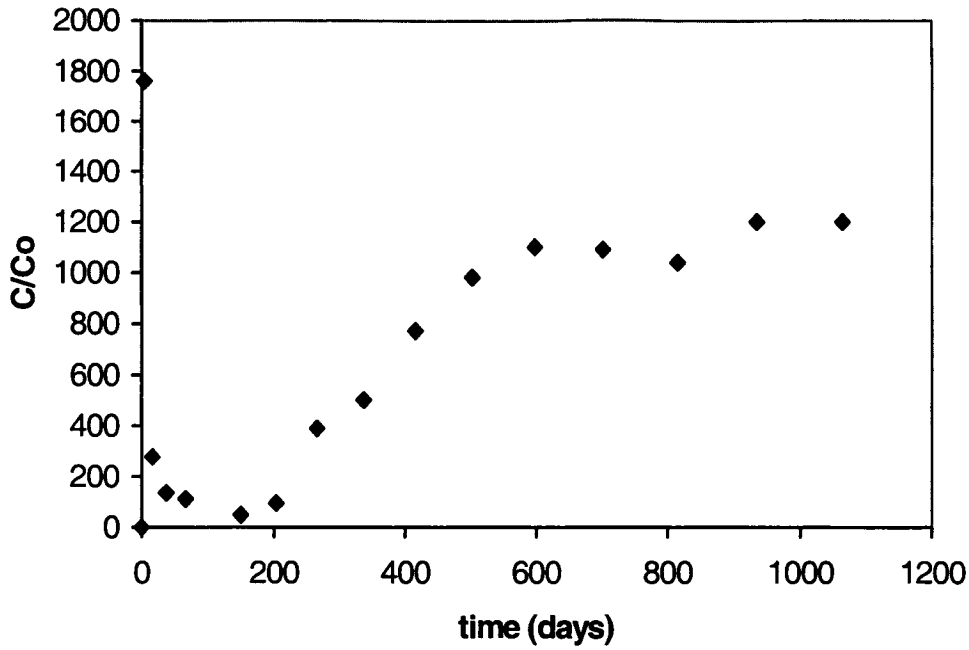

Figure 8.9. Scaled up concentration profile to field conditions (pH 2)(Run 38)

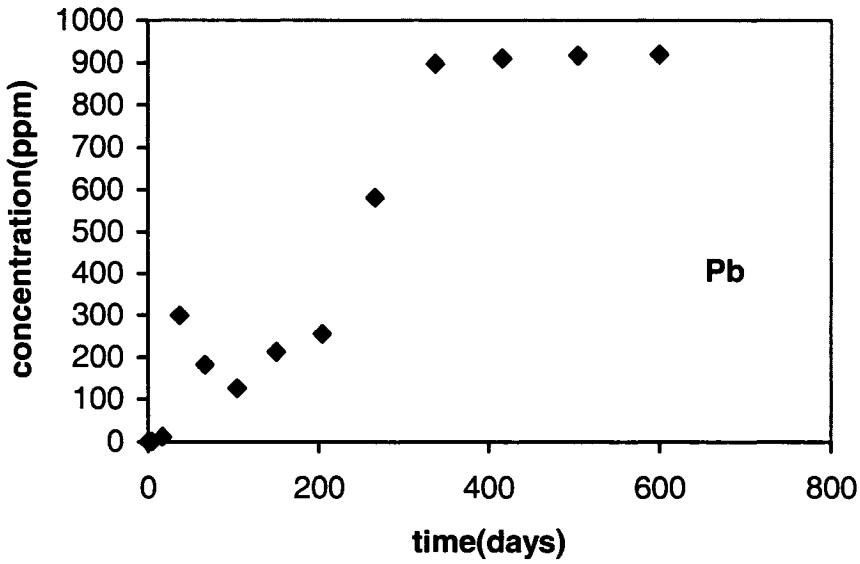

Figure 8.10. Scaled up concentration profile to field conditions (pH 3.95)(Run 37)

8.4. Conversion of field results into numerical results based on the prototype features

Numerical solutions with respect to field conditions are offered on the basis of pore velocity, flow rates, adsorption coefficients and amount of adsorbent. The aspect ratio of the dynamic column is also considered for scale up operations. However, the limiting factor to the numerical results is the lack of a comprehensive model that satisfies the overall mechanism of biosorption between the adsorbent and the contaminant phase. The results are displayed in the Figures 8.11-8.20. The numerical solutions displayed early breakthrough profiles in all the cases. The feature of an early breakthrough can be correlated to the inadequate knowledge of adsorption mechanisms in all the cases. It has been assumed that mass transfer rate that supposedly includes chemisorption, precipitation and ion exchange is a^2 times faster in model than in prototype. However, it remains to be investigated if the rates of all the mechanisms can be identically scaled from model conditions. In the scaled up numerical runs, the adsorption coefficients are considered to be smaller than the model by 10,000. ominance of precipitation in scaling criteria can lead to permeability change in the prototype (Krumrine et al., 1985). A decrease in permeability of the prototype is correlated to proportionate decrease in pore velocity of the fluid phase in the medium. However, it is observed numerically that the effect of velocity of the cation did not adversely affect the breakthrough behavior of the system (Figures 8.11 and 8.12). Figures 8.13-8.16 displays that breakthrough intervals are affected by increase of dispersion coefficient of the contaminant. The amount of adsorbent available is directly linked to the porosity of the medium. The porosity parameter remains unchanged for both prototype and model conditions and its effect illustrates (Figures 8.17 and 8.18) that its effect induces an early breakthrough behavior in case of Figure 8.18. A higher flow rate with respect to Figure 8.17 should have resulted in the reverse situation. The following numerical runs are conducted by invoking a dispersion parameter of 1000 times the value in the model for each case.

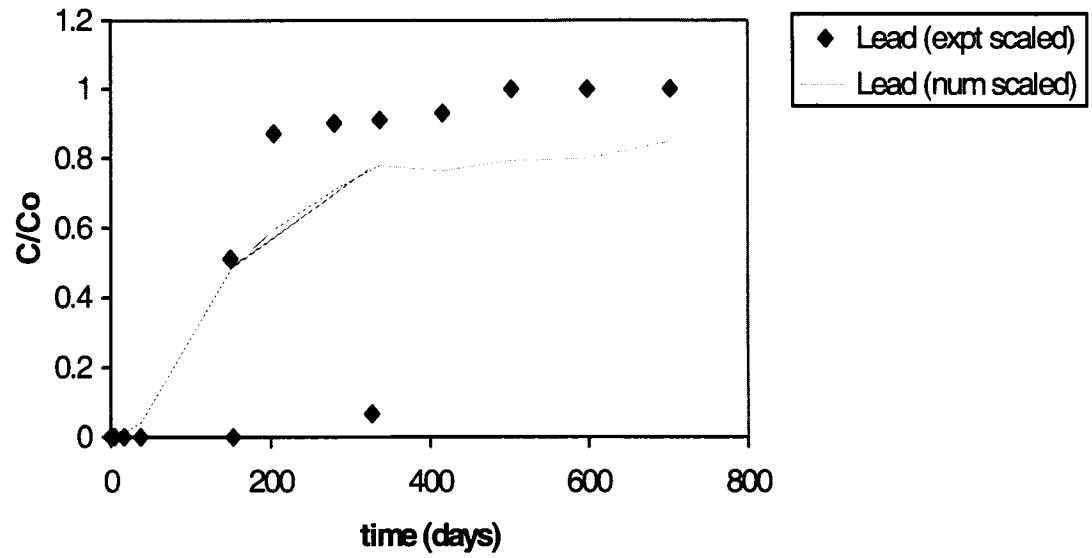

Figure 8.11. Numerically Scaled up concentration profile with respect to field conditions (Run25)

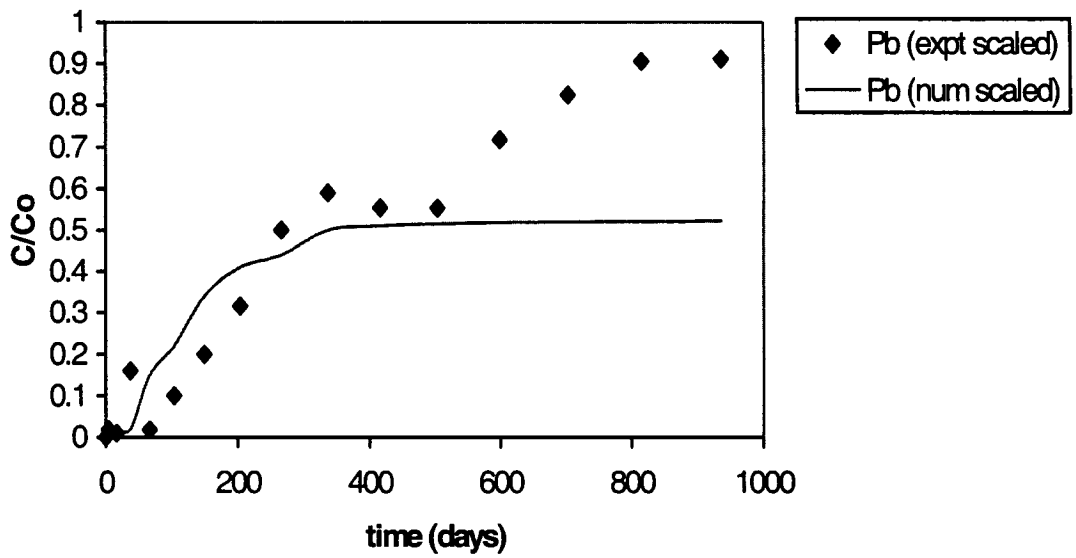

Figure 8.12. Numerically Scaled up concentration profile with respect to field conditions (Run 26)

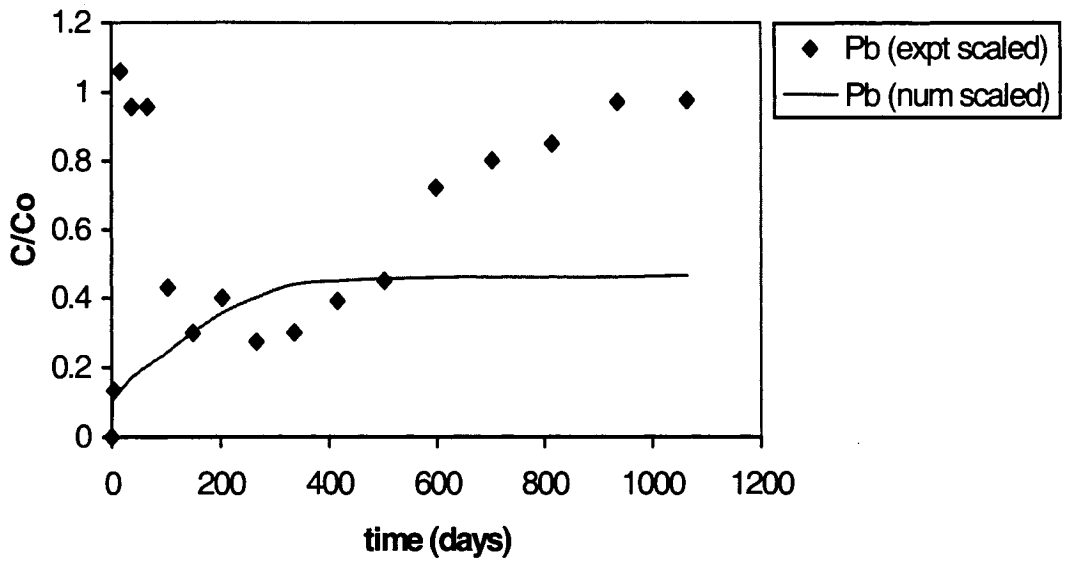

Figure 8.13 Numerically Scaled up concentration profile with respect to field conditions (Run 29)

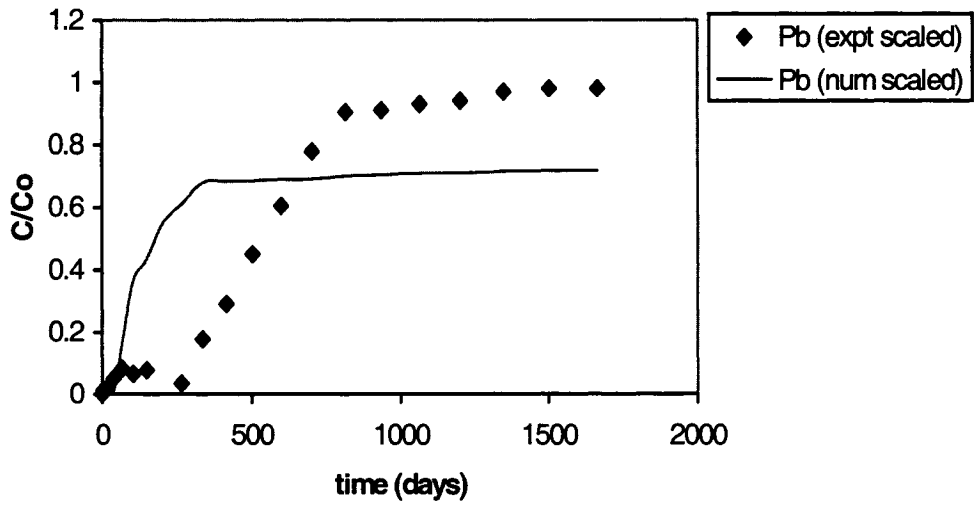

Figure 8.14 Numerically Scaled up concentration profile with respect to field conditions (Run 30)

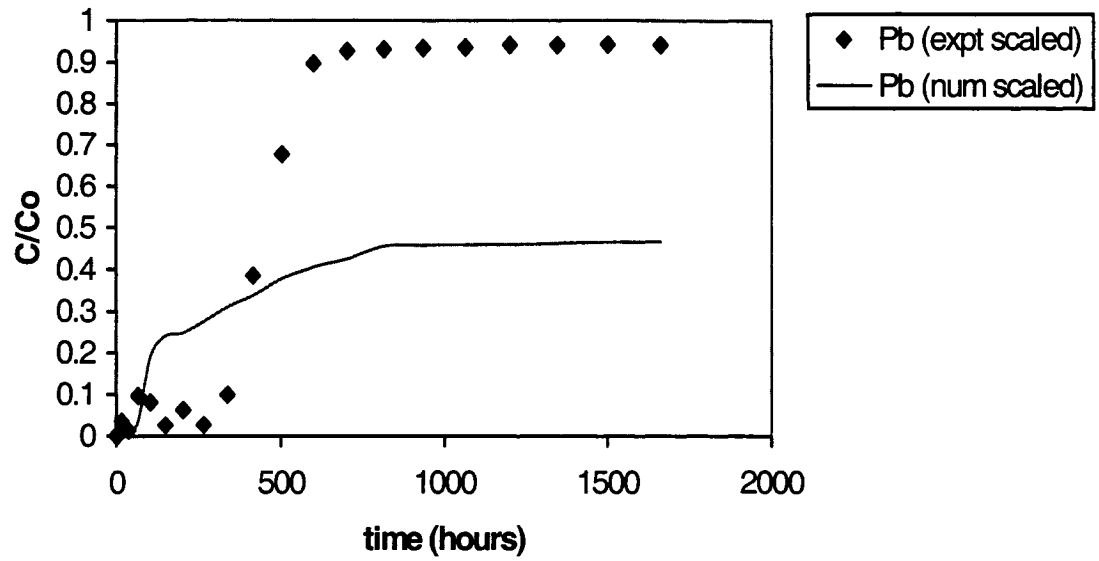

Figure 8.15 Numerically Scaled up concentration profile with respect to field conditions (Run 31)

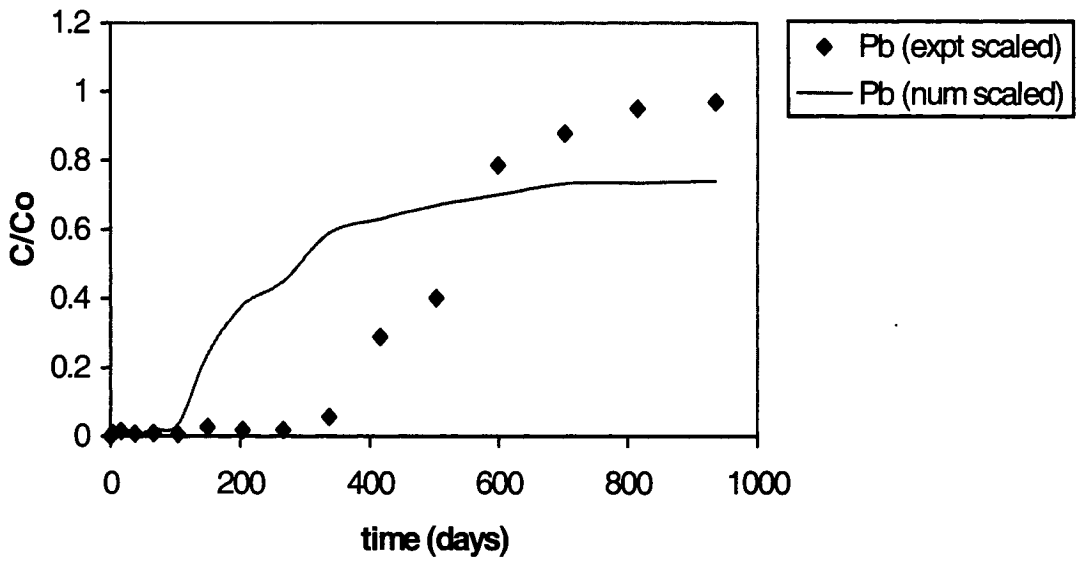

Figure 8.16 Numerically Scaled up concentration profile with respect to field conditions (Run 32)

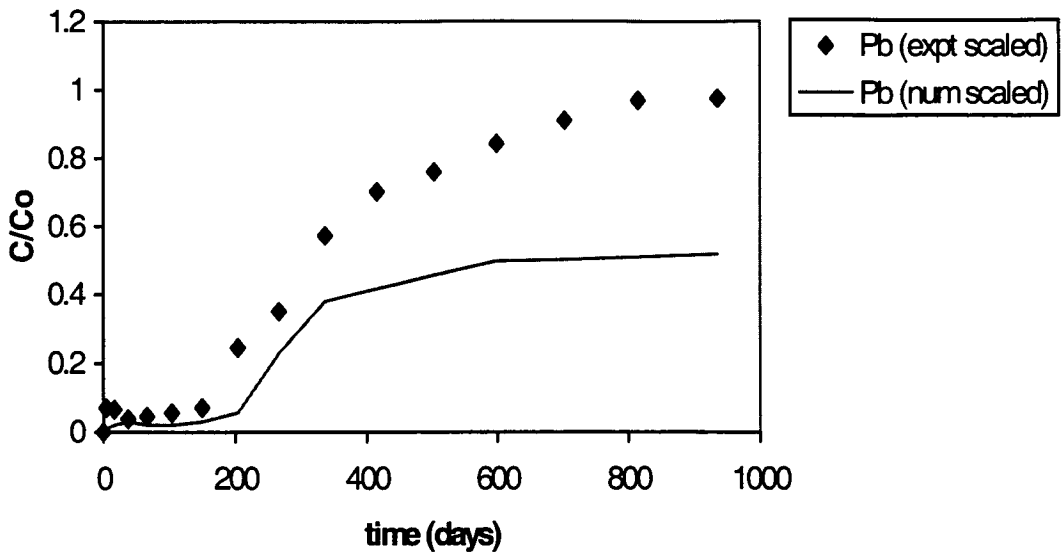

Figure 8.17 Numerically Scaled up concentration profile with respect to field conditions (Run 33)

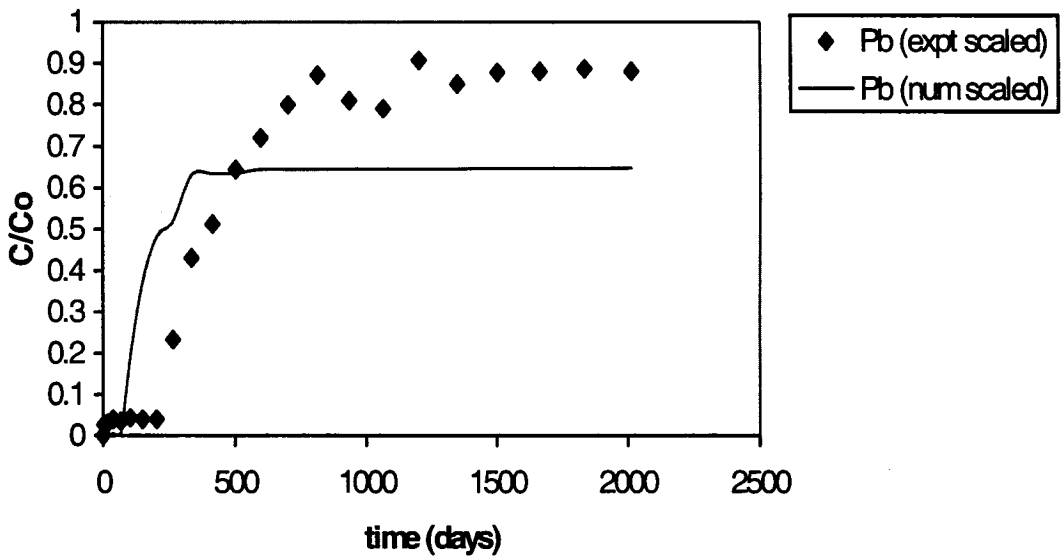

Figure 8.18 Numerically Scaled up concentration profile with respect to field conditions (Run 34)

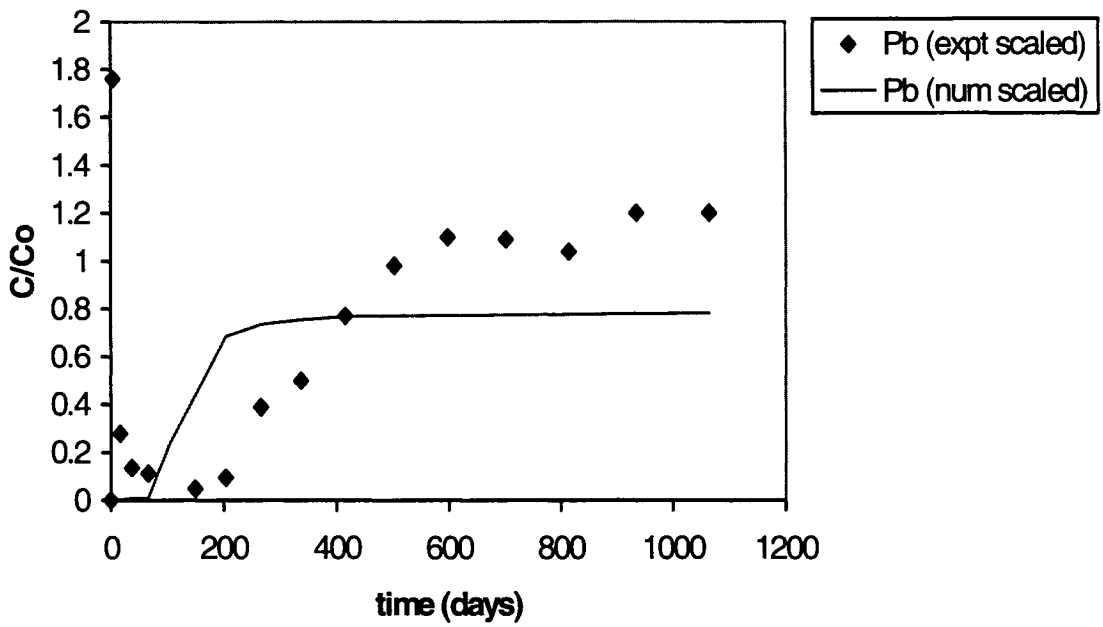

Figure 8.19 Numerically Scaled up concentration profile with respect to field conditions (Run 37)

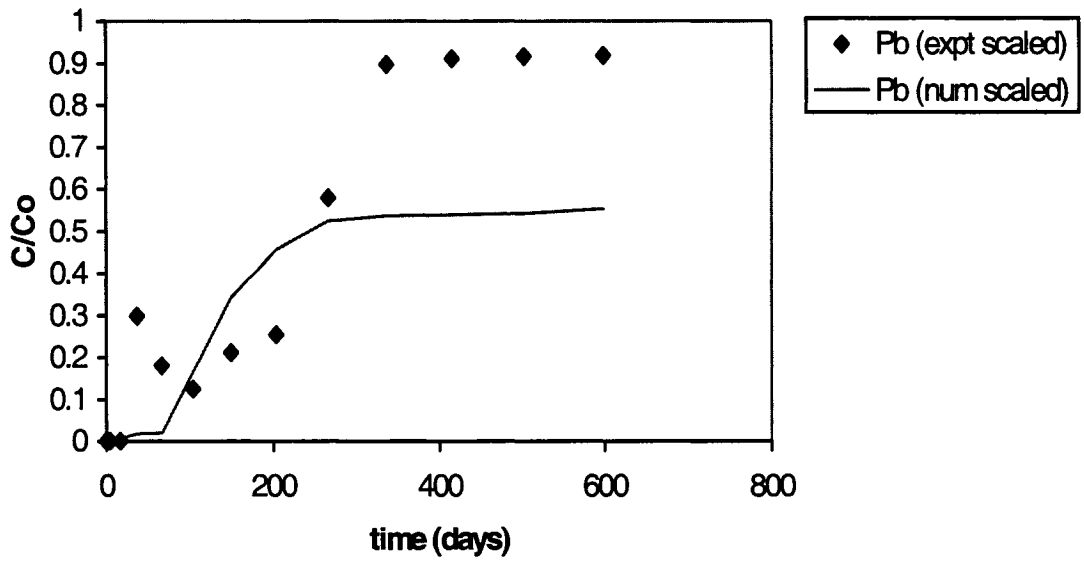

Figure 8.20 Numerically Scaled up concentration profile with respect to field conditions (Run 38)

Chapter 9

9 CONCLUSIONS AND RECOMMENDATIONS

9.1 Conclusions

In this study, the bindings of both cations and anions to fish scales were investigated in detail. Most experiments were conducted with Atlantic Cod, some of them carried out using Shouairi fish scales, and a final set of batch of tests was carried out using Atlantic Salmon scales. A series of experimental runs were performed to characterize the adsorbent and the adsorption equilibrium of Pb (II), As (III) and As (V) ions onto the substrate in pH range of 4-11. These data have been utilized in applying a pore diffusion model to predict both cationic and anionic adsorption onto the bioadsorbent. Based on the experimental, spectroscopic and numerical studies conducted as part of this dissertation, the following conclusions can be made.

1. The SEM analysis shows the presence of significant amount of calcium and phosphorus in the scale material. The NMR technique confirms the heterogeneity and the long chain nature of the adsorbent. The substrate of the fish scale is composed of carbonyl, amide, alkyl and other functional groups. The existence of a series of functional groups and the heterogeneity of the fish scale bear a profound effect on the sorption phenomena.

2. The cationic exchange capacity of Atlantic Salmon scales was determined using the standard method of soil analysis. The cationic exchange capacity correlated with maximum adsorption capacity, confirming unusually high adsorptive capacity of fish scales.

3. The heterogeneity of the fish scale structure can pose a challenging question to the study of adsorption of the metal ions. The heterorganic nature inhibits the

effect of repeatability of experimental work. The adsorption mechanism is clearly a non-linear phenomenon and un-scaled experimental studies offer limited scope to the proper understanding of the reaction mechanism(s). In this study, both experimental and numerical investigations, along with scale-up procedures for plant designs helped develop an engineering approach. Further scientific studies are recommended for in-depth understanding of the mechanisms behind the extremely heterogeneous adsorption process.

4. The studies conducted demonstrated that the adsorption behavior is a combination of ion exchange, electrostatic forces, chemisorption and coordinate bonding mechanisms. The two dominant mechanisms behind the abatement of inorganic constituents with respect to fish scales were found to be adsorption and the complexation mechanism. Adsorption results for multi-component systems (Pb (II)/As (III) and Pb (II)/As (V)) indicate that removal of Pb (II) is not affected by the arsenic species. The removal of the lead and arsenic species is strongly dependant on the pH of the bulk phase. At acidic ranges, As (V) species are strongly adsorbed to protonated substrates and lead species display stronger affinity to the adsorbent at higher pH ranges (7-11). The speciation of both As (III) and As (V) species are highly dependant on pH of the bulk phase. As (III) remains in undissassociated form at a pH range of 4-9. This explains the low adsorption behavior of the species at the specified range.

5. The breakthrough capacities of the metals during column tests are different for each metal ion. The experimental data based on flow rate, pH of the bulk phase, adsorbent dosage and porosity have a significant impact on breakthrough behavior. The most dominant reason behind this behavior was found to be adsorption, followed by complexation mechanisms and finally dispersive forces.

6. The use of the pore diffusion and the surface excess model helped elucidate mechanisms behind experimental studies. After achieving reasonable agreement between experimental and numerical results, a number of sensitivity analyses was performed. The sensitivity analysis illustrates that the adsorption of the contaminants is influenced by the number of adsorption sites per unit mass of adsorbent, local adsorption coefficients and flow rates of the effluent streams.

7. Initial scaled-up design studies were conducted for proper application of a subset that includes all the necessary dimensionless groups. The role of different forces such as dispersive, gravitational and mass transfer reflects the choice of a subset that fits appropriately to the field conditions. In order to improve the agreement between scaled-up experimental results and numerical modeling results of the scaled-up model, the dispersion coefficient in the field had to be significantly different from laboratory values. This is in conformance with conventional dimensional analysis of dispersive phenomena.

9.2. Recommendations

The following recommendations can be made in order to advance knowledge in this topic.

1. Fish scale characterization should be carried out thoroughly. In addition to measuring macroscopic properties, such as ion exchange capacity, detailed spectroscopic studies (NMR, X-Ray photoelectron emission, etc.) should be carried out in order to investigate the nature of reaction mechanisms with the substrate, i.e., ion exchange, chemisorption, cross linkage and precipitation. This will help one quantify contributions of various mechanisms

2. A further improvement of the newly developed numerical code should be performed. The improved model should incorporate all features of the reaction mechanisms involved in the process. The current models include only the ion exchange mechanism.

3. A scaled-up experimental model should be developed in order to study the role of various scaling groups proposed in this work. This will help validate some of the hypotheses proposed in relation to the role various mechanisms involved. The scaled up model does not have to be full scale or a pilot scale. A mid-scale model will be sufficient to determine the scaling laws involving various scaling groups.

4. Further developments are recommended for advancing the numerical code in order to be suitable for full-scale plant design. This can be accomplished only after the scaling laws are validated through the Recommendation 3 above.

Chapter 10

10 REFERENCES

Aderhold, D., Williams, C. J. and Edyveen, R. G. J., (1996) The removal of heavy metal ions by seaweeds and their derivatives, Bioresource Technology, vol. 58, pp. 1-6

Ahmed, F.A. (2001) An overview of arsenic removal technologies in Bangladesh and India, Proceedings, BUET-UNU International Workshop on Technologies for Arsenic Removal from Drinking Water, Dhaka, Bangladesh, May 5-7, pp. 251-269

Akthar, N. N., Sastry, K. S. and Mohan, P. M., (1996) Biosorption of silver ions by processed *Aspergillus niger* biomass, Biometals, vol. 9, pp. 21-28

Alam, M.G.M., Tokunaga, S. and Maekawa, T., (2001) Extraction of arsenic in a synthetic arsenic contaminated soil using phosphate, Chemosphere, vol. 43, pp. 1035-1041

Al-Awadhy, F., Abou-Kassem, J.H. and Islam, M.R., (2004) Modeling of Sulfur Plugging in Carbonate Oil Reservoirs, Energy Sources, vol.25, No.6, pp.107-115

Ali, M. and Islam, M.R., (1998) The Effect of Asphaltene Precipitation on Carbonate Rock Permeability: An experimental and numerical approach, SPE 38856, SPE Production & Facilities, August

Allen, T. (1987) Particle size measurement, 3rd Edition, Chapman and Hall Ltd., London, England

Alves, M., Gonzalez, C., Guedas de Carvalho, R., Castanheira, J.M., Sol Periera, M. and Vasconcelos L.A.T., (1993) Chromium removal in tannery waste waters 'polishing' by Pinus Silverstris bar, Water Research, vol.27, No.8, pp. 133-138

Alves, M. M., Gonzalez Beca C. G., Guedes de Carvalho R., Castanheira, J. M., Sol Pereira, M.C. and Vasconcelos L. A. T., (1993) Chromium removal in tannery wastewaters 'polishing' by Pinus sylverstris bar, Water research, vol. 27, No. 8, pp. 133-1338

Anderson, M.A., Ferguson, J.F. and Gavis, J., (1976). Arsenate Adsorption on Amorphous Aluminium Hydroxide, Journal of Colloid Interface Science, vol. 54, pp. 391-399

Apak, R., Tutem, E., Hugul, M. and Hizal, J., (1998) Heavy Metal Cation Retention by Unconventional Sorbents (Red Muds and Fly Ashes), Water Resources, vol. 32, No. 2, pp. 430-440

Apak, V. and Unseren, E., (1987) Treatment of wastewater and effluents with solid industrial wastes for the adsorptive removal of heavy metal contaminants, In flocculation in biotechnology and separation systems (Edited by Attia Y. A.), pp. 765-771, Elsvier Amsterdam

Avery, S.V. and Tobin, J.M., (1992) Mechanisms of Strontium uptake by laboratory and brewing strain of *Saccharomyces cervisiae*, Applied Environmental Microbiology, vol. 58, pp. 3883-3889

Ayala, J., Blanco, F., Garcia, P., Rodriguez, P. and Sancho, J., (1998) Asturian fly ash as a heavy metals removal material, Fuel, vol. 77, No. 11, pp. 1147-1154

AWWA Committee (1993) Research need for inorganic Contaminants, Journal of American Water Work Association, vol. 85, pp. 106-113

Bailey, R.P., Bennett, T. and Benjamin, M.M., (1992) Sorption onto and Recovery of Cr (VI) Using Iron-Oxide-Coated Sand, Water Science and Technology, vol. 26, No. 5-6, pp. 1239-1244

Bailey, S.E., Olin, T.J., Bricka, R.M. and Adrian, D.D., (1999). A review of potentially low-cost sorbents for heavy metals, Water Research, vol. 33, No. 11, pp. 2469-2479

Bajpai, S. and Chaudhuri, M., (1999) Removal of arsenic from ground water by manganese dioxide-coated sand, Journal of Environmental Engineering, vol. 125, No. 8, pp. 782-784

Bansal, A. and Islam, M.R., (1994) Scaled Model Studies of Heavy Oil recovery from an Alaskan Reservoir Using Gravity – Assisted Gas Injection, Journal of Canadian Petroleum Technology, vol. 3, pp. 52-62

Bear, J., Tsang, C., and Marsily, G., (1993) Flow and Contaminant Transport in Fractured Rock, Academic Press, San Diego, pp 49-51

Berkeley, R.C.W., (1979) Chitin, Chitosan and their Degradative Enzymes, Microbial Polysaccharides, eds. R.C.W. Berkeley, C.W. Gooday and D.C. Elwood, 205-236. Academic Press, New York

Beveridge, T. J. and Murray, R. G. E., (1980) Sites of metal deposition in the cell wall of *Bacillus subtilis*, Journal of Bacteriology, vol. 141, pp. 876-887

Bickerstaff, G., (2002) Universtiy of Paisley, Department of Biological Sciences, Sturcture and Function of Macromolecules [online] Available:(http://www-biol.paisley.ac.uk/courses/stfunmac/glossary/collagen.html) [June 29, 2002]

Black, J.G., (1999) Microbiology Principles and Explorations. Fourth Edition, John Wiley and Sons, Inc., Toronto, pp. 146

Bockris, J. and Reddy, A.K., (1970) Modern Electrochemistry, Volume 2, Plenum, New York.

Borwankar, R.P. and Wasan, D.T., (1986) Dynamic interfacial tensions in acidic crude oil/caustic systems, American Institute of Chemical Engineers Journal, vol. 32, No. 3, pp. 455-465

Bryant, P.S., Peterson, J.N., Lee, J.M. and Brouns, T.M., (1992) Sorption of heavy metals by untreated red fir sawdust, Applied Biochemistry and Biotechnology, vol. 34-35, pp. 777-788

Buffle, J., (1988) *Complexation reactions in aquatic systems: An analytical approach:* ", Ellis Harwood Ltd; Chichester, UK

Cadena, F., Rizvi, R. and Peters, R.W., (1990) Feasibility Studies for the Removal of Heavy Metals form Solution using Tailored Bentonite, Hazardous and Industrial Wastes, proceedings of the 22nd Mid-Atlantic Industrial Waste Conference, Drexel University, pp. 77-94

Carrillo, A. and Drever, J.I., (1998) Adsorption of arsenic by natural aquifer material in the San Antonio-El Triunfo mining area, Baja California, Mexico, Environmental Geology, vol. 35 pp. 251-257

Chaalal, O. and Islam, M.R., (2001) Integrated Management of Radioactive Strontium Contamination in Aqueous Stream Systems, Journal of Environmental Management, vol.61, pp.51-59

Chen, X.H., Gosset, T. and Thevenot, D.R., (1990) Batch Copper Ion Binding and Exchange Properties of Peat, Water Research, vol. 24, No. 12, 1463-1471

Chimera, K., Suzuki, M. and Kawazoe, K., (1978) Adsorption rates on Molecular Sieving Carbon by Chromatography, AIChE J., vol.24, No.2, pp.5-12

Chong, K.H, and Volesky, B., (1995) Desorption of 2-metal biosorption equilibria by Langmuir type isotherms, Journal of Biotechnology and Bioengineering, vol.47, pp.451-460

Christophi, C.A. and Axe, L., (2000) Competition of Cd, Cu and Pb adsorption on goethite, Journal of Environmental Engineering, vol. 126, No. 1, pp. 66-74

Cole, C., (2001) Informal discussion in Mineral and Mining laboratories, Dalhousie University, Halifax, Canada

Corapcioglu M.O. and Huang C.P., (1987) The Surface Acidity of and Characterization of Commercial Activated Carbons, Carbon, vol.25, 569-578

Coskuner, G. and Bentsen, R., (1987) Prediction of Instability for Miscible displacements in a Hele Shaw cell, Rev.de.1' IFP, vol.42, No.2, pp. 151-162

Crusberg, T. C., Biomineralization of heavy metals within fungal mycelia: A new technology for bioremediation of hazardous wastes, EPA grant no. R823341 [online] Available:http://es.epa.gov/ncer_abstracts/grants/95/engineering/engcrusb.html [July 2, 2002]

Dabson, K.D. and McQuillan, A., (1999) Study of Mechanism of Cr (VI). Journal of Spectrochemistry. Acta, Part A 55A, pp.1395-1405

Dahi, E. (1997) Environmental Chemistry of Arsenic, paper presented at ITN-Bangladesh Training Course on Water Supply and Waste Management, ITN Center, BUET, August 9-12

Dambies, L., Guimon, C., Yiacoumi, S. and Guibal, E., (2001) Characterization of Metal Ion Interactions with Chitosan by X-Ray Photoelectron Spectroscopy, Colloids and Surfaces, No.177, pp.203-214

Desborough, G.A., (1995) Acetic acid leachability of Lead from clinoptilolite-rich rocks that extracted heavy metals from polluted drainage water in Colorado, Gelogical Survey (Preliminary Report) open-file report, pp. 95-49

Diamadopolous, E., Ioannids, S. and Sakellaropoulos, G., (1993) As (V) removal from aqueous solutions by fly ash, Water Resources, vol.27, No.12, pp.1773-1777

Driehaus, W., Seith, R. and Jekel, M., (1995) Oxidation of Aresenate (III) with Manganese Oxides in water Treatment, Water Resources, vol.29, No.1, pp.297-305

Dronnet, V.M., Renard, C.M.G., Axelos, M.A.V. and Thibault, J.F., (1997). Binding of Divalent metal ions by sugar beet pulp, *Carbohydrate polymers*, vol.34, pp.73-82

Dugger, D., Stanton, L.J., Irby, B., McConnell, W., Cummings, W. and Maatmaan, R., (1964) Exchange of twenty metal ions with the weak acidic silanol groups of silica gel, Journal of Physical Chemistry, 68, pp. 757-760

Durrant, P. and Durrant, B., (1964) Introduction to Advanced Inorganic Chemistry, Longmans, first edition, pp 748

Eckenfelder, Jr., W.W., (2000) Coagulation, Precipitation and metals removal, Industrial Water Pollution Control, third edition, pp. 138-156

Esalah, J., Weber, M. and Vera. J., (2000) Removal of Lead, Cadmium and Zinc from Aqueous solutions by Precipitation with Sodium Di-(n-Octyl) Phosphinate, Canadian Journal of Chemical Engineering, vol.78, pp. 948-954

Environment Canada, (1998) Status Report on Water Pollution Control, pp. 23-24

Farouq Ali, S.M., Redford, D.A. and Islam, M.R., (1987) Scaling Laws for Enhanced Oil Recovery Experiments, China-Canada Joint Technical Conference on Heavy Oil Recovery, Zhou Zhou City, China

Faust, S.D. and Aly, O.M., Chemistry of water treatment (2^{nd} Edition), Lewis publisher, 1999, pp. 143

Fazal, M.A. and Kawaci, T., (2001) Extent and severity of ground water arsenic contamination in -Bangladesh, International water resources association, Water International, vol. 26, No. 3, pp. 370-379

Ferguson, J. F. and Davis, J., (1972) A review of arsenic cycle in natural waters, Journal of Water Resources, vol. 6, pp. 1259-1274

Fisheries and Oceans Canada, (2002) Sentinel Fisheries Program, Cod [online] Available:
http://www.osl.gc.ca/en/peches-sentinelles/morue.htm [June 29, 2002]

Fisheries and Oceans Canada, (2002) Underwater World, Atlantic Groundfish [online] Available:
http://www.dfo-mpo.gc.ca/zone/underwater_sous-marin/atlantic_ground/aground-fonda_e.htm [July 1, 2002]

Fleming, S., Furness, R.W. and Davies, I.M., (2000) Contemporary patterns and historical rates of increase of mercury contamination in different marine food chains, International Council for the Exploration of the Sea (ICES CM), theme session on temporal and spatial trends in the distribution of contaminants and their biological effects in the ICES area, S/02

Frank, P. and Clifford, D., (1986) As (III) Oxidation and Removal from Drinking Water, USEPA Project Summary 600/S2-86/021

Frost, R.R. and Griffin, R.A., (1977) Effect of pH on adsorption of arsenic and selenium from landfill leachate by clay minerals, Soil Society of America, vol.41, pp. 51-57

Freeland, G.N., Hoskinson, R.M. and Mayfield, R.J., (1974) Adsorption of Mercury for aqueous solutions by polyethylenimine-modified wool fibers. Environmental Science and Technology, vol. 8, No. 10, pp. 943-944

Fuller, C.C., Davis, J.A. and Waychunas, G.A., (1993) Surface Chemistry of ferrihydrite: Part II, Kinetics of arsenate adsorption and co-precipitation. Geochim. Cosmochim. Acta, vol.57, pp. 2271-2282

Galer, G.M., Delmas, R. and Loos-Neskovic., (1997) Decontamination of arsenic-containing aqueous solutions using inorganic sorbents, The royal society of chemistry, pp. 187

Gao, S., Walker, W., Dahlgren, R. and Bold, J., (1997) Simultaneous sorption of Cd, Cu, Ni, Zn, Pb and Cr on soils treated with sewage sludge supernatant, Water, Air Soil Pollution vol.93, pp.331-335

Ghimire, K.N., Inoue, K., Makino, K. and Miyajima, T., (2002) Adsorptive removal of arsenic using orange juice residue, Separation Science and Technology, vol.37, No.12, pp.2785-2799

Gonzalez, M.P., Mattusch, J., Einickie, W. and Wennrich, R., (2001) Sorption on natural solids for arsenic removal, Chemical Engineering Journal, vol.81, pp.187-195

Gupta, S.K. and Chen, K.Y., (1978) Arsenic removal by adsorption, Journal of Water Pollution Control Federation, vol. 50, pp. 493-506

Greenpeace, (2000) Ghazieh coast another Lebanese industrial disaster zone
Available:
http://www.greenpeacemed.org.mt/020500.html [June 29, 2002]

Guibal, E., Roulph, C. and Cloirec, P. L., (1995) Infrared spectroscopic study of uranyl biosorption by fungal biomass and materials of biological origin, Environmental Science and Technology, vol. 29, No. 10, pp. 2496-2503

Guin, J., "Hindered diffusion of Asphaltenes at specific Temperature and Pressure." DOE GRANT NO: DE-FG22-95PC95221

Hafez, N., Abdel-Razek, A.S. and Hafez, M.B., (1997) Accumulation of some heavy metals on *Aspergillus flavus*, Journal of Chemical Technology and Biotechnology, vol. 68, pp. 19-22

Haferl, S., Poulikakos, D. and Zhao, Z., (2001) Employing scanning force for Microscopy to investigate the free surfaces of liquid microstructures and their wetting behavior on smooth surfaces: Gathered Experiences, Experimental Heat Transfer, vol.14, No. 1, pp.1-25

Hall, K.R., Eagleton, L.C., Acrivos, A. and Vermevlem, T., (1966) Industrial Engineering Chemistry Fundamentals, vol.5, pp. 212

Hayes, K.F. and Leckie, J.O., (1987) Modeling Ionic strength on Cation Adsorption at Hydrous Oxide / Solution Interfaces, Journal of Colloid Interface Sciences, No.115, pp.564-572

Healy, T.W., Murray , D.J. and Fuerstenau, D.W., (1968) The Adsorption of Aqueous Metal on Colloidal Hydrous Manganese Oxides, Advances in Chemical Series, No 79, ACS, Washington D.C, pp.74-81

Hill, C. G. J., (1977) *An introduction to Chemical Engineering kinetics and Reactor Design*, John Wiley & Sons: NY

Hodgson, T.D., (1970) Properties of cellulose acetate membrane towards ions in aqueous solutions, Desalination, vol. 8, pp.99-103

Holan, Z.R., Volesky, B. and Prasteyo, I., (1993) Biosorption of Cadmium by Biomass of Marine Algae, Biotechnology Progress, vol.41, pp.819-825

Hsien, T.Y. and Rorrer, G.L., (1995) Effects of acylation and crosslinking on the material properties and Cadmium ion adsorption capacity of porous chitosan beads, Separation Science and Technology, vol. 30, No. 12, pp. 2455-2475

Huang, C.P., (1981) The surface acidity of hydrous solids. In adsorption of Inorganics at Solid-Liquid Interfaces, eds. M.A. Anderson and A.J. Rubin pp. 183-217. Ann Arbour Science, Ann Arbour, MI

Huang, A. Y. and Novosad, J. J., (1986) Modeling of adsorption of foam forming surfactants in porous media, Fundamentals of adsorption, Engineering Foundation, New York

Huang, J.G. and Liu, J.C., (1997) Enhanced removal of As (V) from water with iron-coated spent catalyst, Separation Science and technology, vol.32, pp. 1557-1569

Islam, M.R. and Chakma, A., (1990) Simulation of Activated Carbon Adsorbers used in gas plants, Gas Separation and Purification, vol.4, No.2, pp.103-108

Islam, M.R. and Chakma, A., (1991) Mathematical Modeling of enhanced oil recovery by alkaline solutions in presence of co-surfactant and polymer, Journal of Petroleum Science and Engineering, vol.5, No.2, pp.105-126

Islam, M.R. and Farouq Ali, S.M., (1990) New Scaling criteria for chemical flooding experiments, Journal of Canadian Petroleum Technology, vol.29, No.1, pp.29-36

Islam, M.R. and Wellington, S.L., (2001) Past, present, and future trends in petroleum research, SPE, paper no. 68799

Jang, L. K., Nguyen, D. and Geesy, G. G., (1995) Effect of pH on the absorption of Cu(II) by alginate gel, Water Research, vol. 29, No. 1, pp. 315-321

Jekel, M. R., (1994) Removal of Arsenic in Drinking Water Treatment: Arsenic in the Environment, Part I: Cycling and Characterization, Nriagu, J. O. ed., Wiley Interscience, New York

Jordan, R. Zur., (1994) Adsorption von Arsen an Tonminerale, naturliche Eisenverbindungen, Sande und Tone, Ph.D. Thesis, University of Munich, Germany

Kapoor, A. and Viraraghavan, T., (1996) Treatment of metal industrial wastewater by fly ash and cement fixation, Journal of Environmental Engineering, American Society of Civil Engineers, vol. 122, No. 3, pp. 243-244

Kapoor, A. and Viraraghavan, T., (1998) Biosorption of heavy metals on *Aspergillus niger*: Effect of pretreatment, Bioresource Technology, 63, 109-113

Kartinen, E. O. and Martin, C.J., (1995) A review of Arsenic removal processes. Desalination, vol. 103, No. 1-2, pp. 79-88

Kertman, S.V., Kertman, G.M. and Chibrikova, Z.S., (1993) Peat as a heavy metal sorbent, Journal of Applied Chemistry, Russia vol. 66, No. 2, pp. 511-515

Kim, K. S. and Choi, H. C., (1998) Characteristics of adsorption of rice-hull activated Carbon, vol. 38, No. 4-5, pp. 95-101

Kleiv, R.A. and Sandvik, K.L., (2000) Using tailings as heavy metal adsorbents – The effect of buffering capacity, Minerals Engineering, vol. 13, No. 7, pp. 719-728

Krishnamurthy, K.V. and Harris, G.M., (1960) The Chemistry of Metal Oxalo X complexes, Chemical Reviews, pp.213-246

Krumrine, P.H., Mayer, E.H. and Brock, G.F., (1985) Scale formation during Alkaline Flooding, SPE/DOE 12761, presented in Tulsa, Oklahoma, April 1984

Kurita, K., Koyama, Y. and Taniguchi, A., (1986) Studies on Chitin. IX. crosslinking of water-soluble chitin and evaluation of the products as adsorbents for Cupric ion, Journal of Applied Polymer Science, vol. 31, No. 5, pp. 1169-1176

Lackovic, J., A., Nikolaidis, N., P. and Dobbs, G., M., (2000) Inorganic Arsenic Removal by Zero-Valent Iron, Environmental Engineering Science, vol.17, No. 1, pp. 29-39

LaGrega M.D., Buckingham P.L. and Evans J.C., (1994) Hazardous waste management, McGraw-Hill, New York, pp. 408

Lee, S.M. and Davis, A.P., (2001) Removal of Cu (II) and Cd (II) from Aqueous Solution by Seafood Processing Waste Sludge, Water Resources, vol. 35, No.2, pp.534-540

Lee, R.G. and Weber, T.W., (1969) Isothermal Adsorption in fixed Beds, Canadian Journal of Chemical Engineering, vol.47, pp.54-57

Lehninger, A.L. (1970). Biochemistry; The molecular basis of Cell Structure and Function, Worth Publishers, New York, pp.55-56

Leppert, D., (1990) Heavy metal sorption with clinoptilolite zeolite: alternatives for treating contaminated soil and water, Mining Engineering, vol. 42, No. 6, pp. 604-608

Li, L.Y., (2003) Multi-component of heavy metal contaminants adsorptivity and compatibility onto variable charge clay mineral, Clay Science, vol.12, pp.73-80

Lide, D., (1991) Handbook of Chemistry and Physics, *CRC Press*, 10-180

Lindberg, J., Sterneland, J., Johansson, P.O. and Gustafsoon, J.P., (1997) Spodic material for in situ treatment of arsenic in ground water, Groundwater monitoring & remediation, vol. 17, pp. 125-130

Lin. Z. and Puls, R.W., (2000) Adsorption, desorption and oxidation of arsenic affected by clay minerals and aging process, Environmental Geology, vol.39, No.7, pp.753-759

Low, K.S., Lee, C.K., Cheong, F.Y. and Lim, G.S., (1993) Enhancement effect of dye-coating on the sorption of Copper by moss, Journal of Environmental Science and Health, part-A, vol. 28, No. 8, pp. 1689-1704

Mannhardt, K., Schramm, L.L. and Novosad, J.J., (1990) Effect of rock type and brine composition on adsorption of two foam forming surfactants, Society of Petroleum Engineers 20463, New Orleans, September, 23-26

Martell, A. and Hanock, R.D., (1996) Metal Complexes in Aqueous solutions, Plenum: New York

Martin, J.M., Combarnous., M. and Charpentier, J.C., (1981) Mass Transfer and Phase Distribution for two phase flow through Porous Media, Chemical Engineering Communications, vol.2, pp.269-280

Masri, M.S. and Friedman, M., (1974) Effect of chemical modification of wool on metal ion binding, Journal of Applied Polymer Science, vol. 18, pp. 2367-2377

Masri, M.S., Reuter, F.W. and Friedman, M., (1974) Binding of Metal Cations by natural substances, Journal of Applied Polymer Science, vol. 18, pp. 675-681

Matheickal, J. T. and Yu, Q., (1999) Biosorption of Lead (II) and Copper (II) from aqueous solution by pretreated biomass of Australian marine algae, Bioresource Technology, vol. 69, pp. 223-229

Mathews, A.P. and Weber, W.J., Jr., (1977) Effects of external mass transfer and intraparticle diffusion on adsorption in slurry reactors, Symposium Series, American Institute of Chemical Engineers Journal, vol. 73, No. 166, pp. 91-98

Mathews, A.P. and Zayas I., (1986) Particle size and shape effects on adsorption rate parameters, Journal of Environmental Engineering, vol. 115, No. 1, pp. 41-55

McKay, G., Bino, M. J. and Altamemi, A. R., (1985) The adsorption of various pollutants from aqueous solution on to activated carbon, Water research, vol. 19, pp. 491-495

Melitas, N., Wang, J., Conklin, M., O'Day, P. and Farrell, J., (2002) Understanding soluble arsenate removal kinetics by zero-valent iron media, Environmental Science and Technology, vol.36, No.9, pp.2074-2081

Miles, M., Bush, B. and Johnson, K., "Nuclear Science and Technology: Fusion devices", Naval and Air Warfare Center, Weapons Division, China Lake, California, Report Number: A020513, September 1995

Montgomery, J., M., *Water Treatment Principles and Design,* John Wiley & Sons, Inc. NewYork, 1985, pp. 174-197.

Mo, S.C., Choi, D.S. and Robinson, J.W., (1988) A study of the uptake by duckweed of aluminium, copper and lead from aqueous solution, Journal of Environmental Science and Health, vol. 23, No. 2, pp. 139-156

Morrison, R. and Boyd, R., (1960) Organic Chemistry, Allyn and Bacon Inc, Amsterdam

Mustafiz, S., (2002) A novel method for heavy metal removal from aqueous streams, MASc Thesis, Department of Civil Engineering, Dalhousie University, Halifax, NS, Canada

Mustafiz, S., Bjorndalen, N., Kelly, D., Tango, M. and Islam, M.R. (2003) The Application of Fish Scales in Removing Heavy Metals from Energy- Produced Waste streams: The Role of Microbes, Energy Sources, vol.25, No.9, pp.905-915

Namasivayam, C. and Senthilkumar, S., (1998) Removal of As (V) from aqueous solution using industrial solid waste: Adsorption rate and equilibrium studies, Industrial and engineering chemistry research, vol. 37, No. 12, pp. 4816

Niu, H., Xu, X.S. and Wang, J.H., (1993) Removal of Lead from aqueous solutions by penicillium biomass, Biotechnology and Bioengineering, vol. 42, pp. 785-787

Niu, H., Volesky, B. and Gomes, N., (1999) Enhancement of gold-cyanide biosorption by L-cysteine, International Biohydrometullurgy Symposium, El Escorial, Spain, June 20-23

Niu, H. and Volesky, B., (2001) Biosorption of metal complexes, International Biohydromettalurgy Symposium, Brazil

Orhan, Y. and Buyukgungor, H., (1993) The removal of heavy metals by using agriculture wastes, Water Science and Technology, vol. 28, No. 2, pp. 247-255

Park, J.K., Jin, Y.B. and Chang, H. N., (1999) Reusable biosorbents in capsules from *Zoogloea ramigera* cells for Cadmium removal, Biotechnology and Bioengineering, vol. 63, No. 1, pp. 116-121

Pearson, R.G., (1990) Hard and Soft Acids and Bases- The Evolution of a Chemical Concept, Coordination Chemistry Review, vol. 100, pp. 403-425

Peeters, J.M.M., Boom, J.P., Mulder, M.H.V. and Strathmann, H., (1998) Retention Measurements of Nano Filtration membranes with Electrolyte Solutions, Journal of Membrane Science, vol.145, pp.199-203

Petersen, J.N., Davison, B.H., Scott, C.D. and Blankinship, S.L., (1991) Size changes associated with metal adsorption onto modified bone gelatin beads, Biotechnology and Bioengineering, vol. 38, pp. 923-928

Pierce, M.L. and Moore, C.B., (1982) Effect of pH on adsorption of arsenic on goethite, Water Resources, vol.16, pp.1247-1253

Pontius, F.W., Brown, K.G. and Chen, C.J., (1994) Health implications of arsenic in drinking water, Journal of American Water Works Association, vol. 86, pp. 52-63

Pradas, E. G., Sanchez, M. V., Cruz, F. C., Viciana, M. S. and Perez, M. F., (1994) Adsorption of Cadmium and Zinc from aqueous solution on natural and activated bentonite, Journal of Chemical Technology and Biotechnology, vol.59, pp.289-295

Rahaman, S., (2003) Experimental and Numerical Studies of Arsenic Adsorption on various Natural Adsorbents, MASc Thesis, Department of Civil Engineering, Dalhousie University, Halifax, NS, Canada

Rahmani, G.N.H. and Sternberg, S.P.K., (1999) Bioremoval of lead from water using *Lemna minor*, Journal of Bioresources,vol.70, pp.225-230

Randall, J.M., Bermann, R.L., Garrett, V. and Waiss Jr., A.C., (1974) Use of bark to remove heavy metal ions from waste solutions, Forest Products Journal, vol. 24, No. 9, pp. 80-84

Randall, J.M., Hautala, E. and McDonald, G., (1978) Binding of heavy metal ions by formaldehyde-polymerized peanut skins, Journal of Applied Polymer Science, vol. 22, No. 2, pp. 379-387

Raven, K.P., Jain, A. and Loeppert, R.H., (1998) Arsenite and arsenate adsorption on ferrihydrite: Kinetics, equilibrium, and adsorption envelopes, Environmental Science and technology, vol.32, pp. 344-349

Reddad, Z., Gerente, C., Andres, Y., Thibault, J.F. and Le Cloirec, P., (2003) Adsorption by a natural polysaccharide in MF membrane reactor: experimental analysis and modeling, Water Research, vol.37, pp.3983-3991

Rendelman, J.A. (1978). Interaction of Metal ions with Pectic Chains, Food Chemistry, vol.3, pp.127-161

Rhee, J., Jung, M. and Paeng, K.J., (1998), Evaluation of Chitin and Chitosan as a Sorbent for Preconcentration of Phenol and Chlorophenols in Water, Analytical Sciences, vol.14, pp.1089-1092

Rice, R., (1982) Approximate solutions for Batch, Packed Tube and Radial Flow Adsorbers-Comparison with Experiment, Journal of Chemical Engineering Science, vol.37, No.1, pp.83-91

Roy, D., Greenlaw, P.N. and Shane, B.S., (1993) Adsorption of heavy metals by green algae and ground rice hulls, Journal of Environmental Science and Health, part A, vol. 28, No. 1, pp. 37-50

Sabadell, J.E. and Krach, R.J., (1975) Adsorption of heavy metals from wastewater and sludge on forest residuals and forest produce waste, Water's interface with energy, air, and solids, presented at the 2nd National conference on complete water reuse, Chicago, IL, May 4-8

Said, O.B., Shalmor, M.B. and Egila, J.N., (1992) A note on the binding of Nickel and Copper ions by cellulosic materials, Bioresource Technology, vol. 43, pp. 63-65

Saito, A. and Foley, H., (1991) Curvature and Parametric Sensitivity in models for Adsorption in Micropores, American Institute of Chemical Engineers Journal, vol.37, No.3, pp. 70-75

Saito, H. and Tabeta, R., (1984) A High-Resolution C-NMR Study of Collagen like and Collagen Fibrils in Solid State studied by Cross-Polarization-Magic Angle Spinning Method. Manifestation of Conformational –Dependent ^{13}C chemical shifts and Application to conformational characterization, Biopolymers, vol.23, pp. 2279-2297

Saito, H., Tabeta, R., Asakura, T., Iwanaga, Y., Shoji, A., Ozaki, T. and Ando, I., (1984) High –Resolution C-NMR study of Silk Fibroin in the Solid State by the Cross-Polarization-magic Angle Spinning Method, Conformational Characterization of Silk I and Silk II type forms of Bombyx mori Fibroin by the conformational-Dependant ^{13}C chemical shifts, Macromolecules, vol. 17, pp. 1405-1412

Salinas, E., Orellando, M.E., Rezza, I., Martinez, L., Marchesvky, E. and Tosetti, M.S., (2000) Removal of Cadmium and Lead from dilute aqueous solutions by *Rhodotorula rubra*, Bioresource Technology, vol. 72, pp. 107-112

Santiago, I., Worland, V.P., Cazares-Rivera, E. and Cadena, F., (1992) Adsorption of hexavalent Chromium onto tailored zeolites. presened at the 47th Purdue industrial waste conference, Chelsea, MI., pp. 669-710

Sarwar, M. and Islam, M. R., (1997) A non-Fickian surface excess model for chemical transport through fractured porous media, Journal of Chemical Engineering Communications, vol.60, pp.1-34

Saxby, J.D., (1969) Effects of electrostatic adsorption of colloids, Rev. Pure Applied Chemistry, vol.19, pp.131-135

Say, R., Denizli, A., Arica, J. and M.Y., (2001) Biosorption of Cadmium(II), Lead(II) and Copper(II) with the filamentous fungus *Phanerochaete chrysosporium*, Bioresource Technology, vol.76, pp.67-70

Schiewer, S., (1999) Modeling complexation and electrostatic attraction in heavy metal biosorption by Saragassum biomass, Journal of Applied Phycology, vol.11, pp.79-87

Schiewer, S. and Volesky, B., (1995) Mathematical evaluation of the experimental and modeling errors in biosorption, Biotechnology Techniques, vol.9, No.11, pp. 845-848

Schiewer, S. and Volesky, B., (1996) Modeling Multi-metal ion exchange in Biosorption, Environmental, Science and Technology, vol.30, pp. 2921-2927

Schiewer, S. and Wong, M.H., (2000) Ionic strengths in biosorption of metals by marine algae, Chemosphere, vol.41, pp.271-282

Science News, (2001) Arsenic pollution disrupts hormone, vol. 159, No. 11, pp. 164

Seco, A., Marzal, P. and Gabaldon, C., (1997) Adsorption of heavy metals from aqueous solutions onto activated Carbon in single Cu and Ni systems and in binary Cu-Ni, Cu-Cd and Cu-Zn systems. Journal of Chemical Technology and Biotechnology, vol.68, pp.23-30

Seidel, A., Waypa, J. and Elimelech, M., (2001) Role of charge exclusion in removal of Arsenic from water by a negatively charged porous nanofiltration membrane, Environmental Engineering Science, vol.18, No.2, pp.105-113

Sharma. C., Gupta, G.S., Prasad, G. and Rupainwar, D.C., (1990) Use of Wollastonite in the Removal of Ni (II) from aqueous solutions, Water Air and Soil Pollution, vol. 49, pp. 69-79

Sharma, D.C. and Foster, C.F., (1993) Removal of hexavalent Chromium using sphagnum moss peat, Water Research, vol. 27, No. 7, pp. 1201-1208

Sherwood, TK., Pigford, R.I, and Wilke, C.R., Mass Transfer, McGraw Hill, Inc, New York, 1975

Shiskowski, D.M. and Viraraghavan, T., (1993) Removal of Chromium from wastewater by peat filters, Journal of Environmental Science and Health, part A, vol. 28, pp. 967-981

Shukla, S.R. and Sakhardande, V.D., (1992) Column studies on metal ion removal by dyed cellulosic materials, Journal of Applied Polymer Science, vol. 44, pp. 903-910

Sircar, S., (1985) Excess properties and thermodynamics of multi-component gas adsorption Journal of Chemical Society, Faraday Transactions, vol.81, pp.1527-1540

Skala, R., and Rohovec, J., (1998) Magic angle spinning magnetic resonance spectroscopy of shocked limestone from Steinheim Crater, Proceedings 61 st Meteoritical Society Meeting, Dublin, Ireland

Song, F.Y. and Islam, M.R., (1994) a Effect of salinity of rock type on adsorption behavior of surfactants as applied in cleaning of Petroleum contaminants, Journal of Petroleum Science and Engineering, April, pp.321-326

Song, F.Y. and Islam, M.R., (1994) b A new mathematical model and experimental validation of multicomponent adsorption, Society of Petroleum Engineers 27838, Presented at the 9th symposium on improved oil recovery, April 17-20, Oklahoma, USA

Speigler, K.S. and Kedem, O., (1966) Thermodynamics of Hyperfiltration (reverse osmosis): Criteria for efficient membranes, Desalination, vol.1, pp.311-317

Spostio, G., Holtzclaw, K.W. and LeVesque-Madore, C.S., (1979) Cupric ion complexation by fulvic acid extracted from sewage sludge-soil mixture, Soil Science Society of America Journal, vol.43, pp.1148-1155

Spostio, G., Holtzclaw, K.W. and LeVesque-Madore, C.S., (1981) Trace metal complexation by fulvic acid extracted from sewage sludge-soil mixture, Soil Science Society of America Journal, vol.45, pp.465-468

Srivastava, S.K., Singh, A.K. and Sharma, A., (1994) Studies on the uptake of Lead and Zinc by lignin obtained from black liquor – A paper industry waste material, Environmental Technology, vol. 15, pp. 353-361

Stumm, W. and Morgan, J.J., (1996) Aquatic Chemistry, Wiley-Interscience, New York

Su, C. and Puls, R.W., (2001) Arsenate and arsenite removal by Zero-Valent Iron: Kinetics, Redox transformation and implications for in-situ ground water remediation, Environment, Science and Technology, vol.35, No.7, pp.1487-1492

Subramanian K.S., Viraraghavan, T., Phommavong, T. and Tanjore, S., (1997) Manganese green sand for removal of arsenic in drinking water, Water quality research journal of Canada, vol. 125, pp. 87-98

Suvanich, V., Ghaedian, R., Chanamai, R., Decker, E. A. and McClements, D. J., (1998) Prediction of Proximate fish composition from ultrasonic properties: Catfish, Cod, Flounder, Mackerel and Salmon, Journal of Food Science, vol. 63, No. 6, pp. 966-968

Tare, V., Chaudhari, S. and Jawed, M., (1992) Comparative Evaluation of soluble and insoluble xanthate process for heavy metal removal from wastewaters, Water Science and Technology, vol. 26, No.1, pp. 237-246

The State of Queensland, Department of Primary Industries, (2002) Fisheries and aquaculture, Spangled emperor (yellow sweetlip)
Available:
http://www.dpi.qld.gov.au/fishweb/2469.html [July 10, 2002]

Thirunavukkarasu, O.S., Viraraghavan, T., Subramaniann, K.S., Chaalal, O. and Islam, M.R., (2005) Arsenic removal in drinking water-Impacts and novel removal technologies, Energy Sources, vol.27, No.1, pp.209-219

Tobin, J. M., Cooper, D. G. and Neufeld, R. J., (1990) Investigation of the mechanism of metal uptake by denatured *Rhizopus arrhizus* biomass, Enzyme and Microbial Technology, vol. 12, pp. 591-595

Toft, P., Tobin, R.S., Meek, M.E. and Wood, G.C., (1990) Guidelines for Canadian drinking water quality, Coping with the guidelines in the 1990s, Proceedings, Fourth National Conference on Drinking Water, Toronto, Ontario, Canada, R.S. Tobin and W.J. Robertson (eds), pp. 1-9

Tokunaga, S., Hakuta, T. and Wasay, S. A., (1999) Treatment of waters containing hazardous anions using rare earth based materials, Journal of the national institute of materials and chemical research, vol. 76, pp. 291-334

Tsuru, T., Nakao, S. and Kimura., S., (1991a) Calculations of ion rejection by extended Nernst-Planck Equation with reversed charged osmosis membranes for single and mixed electrolyte solutions, Journal of Chemical Engineering, Japan, vol.24, pp.511-517

Tsuru, T., Urairi, M., Nakao, S. and Kimura, S., (1991b) Reverse Osmosis of single and mixed electrolytes with charged membranes: experiments and analysis, Journal of Chemical Engineering, Japan, vol.24, pp. 518-523

Turner, G.L., Smith, K.A., Kirpatrick, J. and Oldfield, E., (1986) Structure and Cation effects on Phosphorous-31 NMR chemical shifts and Chemical-shift Anisotropies of Orthophosphates, Journal of Magnetic Resonance, vol.70, pp. 408-415

Vazquez, G., Antorrena, G., Gonzalez, J. and Doval, M.D., (1994) Adsorption of heavy metal ions by chemically modified *pinus pinaster* bark, Bioresource Technology, vol. 48, pp. 251-255

Vera, G. and Vera, J., (2003) Peculiarities of the thermodynamics of electrolyte solutions: A critical discussion, Canadian Journal of Chemical Engineering, vol. 81, pp.70-79

Viraraghavan, T. and Kapoor, A., (1994) Adsorption of Mercury from wastewater by bentonite, Applied Clay Science, vol. 9, pp. 31-49

Volesky, B., (1990) Biosorption of heavy metals, CRC Press, Bocca Raton, USA

Volesky, B., (1999) Biosorption for the Next Century, International Biohydrometullurgy Symposium, El Escorial, Spain, June 20-23

Volesky, B., (2003) Sorption and Biosorption, Chapter 6, Sorption equilibrium: Evaluation of biosorption performance, First Edition, p.108
Available :
http://ww2.mcgill.ca/biosorption/publication/book/6.1-4w%28103-16%29 [September 11, 2004]

Volesky, B. and Prasetyo, I., (1994) Cadmium removal in a biosorption column, Biotechnology and Bioengineering, vol. 43, pp. 1010-1015

Wakao, N., (2001) A proposal of numerical model for pressure swing adsorption based on pore diffusion, Journal of Chemical Engineering of Japan, vol.34, pp.1-10

Wasiuddin, N.M., Tango, M., and Islam, M.R., (2002) A novel method for arsenic removal at low concentrations, Energy Sources, vol. 24, pp. 1031-1041

Waypa, J.J., Elimelech, M. and Hering, J.G., (1997) Arsenic removal by RO and NF membranes, Journal of American Water Works Association, vol.89, pp.102-104

Weber, T. and Chakrovorti, R., (1974) Pore and solid diffusion models for fixed bed adsorbers, American Institute of Chemical Engineers Journal, vol. 20, No.2, pp.228-237

Wilson, M.W. and Edyvean, R.G., (1994) Biosorption for the Removal of heavy metals from industrial wastewaters, Institution of Chemical Engineers Symposium Series, Environmental Biotechnolgy, pp. 89-91

Woolson, E.A. and Kearney, P., (1977) Characterization of Arsenic compounds formed by Daphina magna and Tetraselius chuii from inorganic arsenate, Environmental Health Perspective, vol. 19, pp. 73-77

Worstell, A., (2004) Improved fixed bed reactor performance with capital expenditure, Chemical Engineering Progress, vol.1, pp.51-57

Xu, H., Allard, B. and Grimvall, A., (1988) Influence of pH and organic substance of the adsorption of As (V) on geologic materials, Water, Air and Science Pollution, vol. 40, pp. 293-305

Yadava, K.P., Tyagi, B.S. and Singh, V.N., (1991) Effect of temperature on the removal of Lead (II) by adsorption on China clay and Woolastonite, Journal of Chemical Technology and Biotechnology, vol. 51, pp. 47-60

Yallay, B., Kramer, T.A. and Vermace, M.E., (1999) Removal of toxic metals using powdered activated alumina and ultra-filtartion membranes, Hazardous and industrial wastes-Proceedings of the Mid-Atlantic Industrial waste conference, Lancaster, PA USA, Technomic publ. Co Inc, pp. 125-132

Yang, J. and Volesky, B., (1999) Cadmium biosorption rate in Protonated Sargassum Biomass, Environmental Science and Technology, vol.33, pp.751-757

Yang, T.C. and Zall, R.R., (1984) Adsorption by natural polymers generated from sea-food processing wastes, Industrial Engineering Chemistry, vol.23, pp.168-172

Yun, Y., Niu, H. and Volesky, B., (2003) Effects of impurities on metal biosorption, International Biohydromettalurgy Symposium, Brazil